Universidade do Minho
Escola de Engenharia

Luís Luciano Gouveia Correia

Durability and long-term behaviour of RC slabs strengthened in flexure with prestressed CFRP laminate strips

December, 2018

Durability and long-term behaviour of RC slabs strengthened in flexure with prestressed CFRP laminate strips
Luís Luciano Gouveia Correia
UMinho | 2018

FCT Fundação para a Ciência e a Tecnologia
MINISTÉRIO DA CIÊNCIA, TECNOLOGIA E ENSINO SUPERIOR
POPH QUALIFICAR É CRESCER
QREN QUADRO DE REFERÊNCIA ESTRATÉGICO NACIONAL
GOVERNO DA REPÚBLICA PORTUGUESA
UNIÃO EUROPEIA Fundo Social Europeu

Universidade do Minho
Escola de Engenharia

Luís Luciano Gouveia Correia

Durability and long-term behaviour of RC slabs strengthened in flexure with prestressed CFRP laminate strips

Doctorate Thesis in Civil Engineering

Work conducted under supervision of
Professor Doctor José Sena Cruz
Professor Doctor Paulo Macedo França

December, 2018

STATEMENT OF INTEGRITY

I HEREBY DECLARE HAVING CONDUCTED MY THESIS WITH INTEGRITY. I CONFIRM THAT I HAVE NOT USED PLAGIARISM OR ANY FORM OF FALSIFICATION OF RESULTS IN THE PROCESS OF THE THESIS ELABORATION.

I FURTHER DECLARE THAT I HAVE FULLY ACKNOWLEDGE THE CODE OF ETHICAL CONDUCT OF THE UNIVERSITY OF MINHO.

FULL NAME: Luís Luciano Gouveia Correia

University of Minho,

Luís Luciano Gouveia Correia

(SIGNATURE)

"FOR WHAT IT'S WORTH; IT'S NEVER TOO LATE, OR IN MY CASE, TOO EARLY TO BE WHOEVER YOU WANT TO BE. THERE'S NO TIME LIMIT, STOP WHENEVER YOU WANT. YOU CAN CHANGE OR STAY THE SAME, THERE ARE NO RULES TO THIS THING. WE CAN MAKE THE BEST OR THE WORST OF IT. I HOPE YOU MAKE THE BEST OF IT. AND I HOPE YOU SEE THINGS THAT STARTLE YOU. I HOPE YOU FEEL THINGS YOU'VE NEVER FELT BEFORE. I HOPE YOU MEET PEOPLE WITH A DIFFERENT POINT OF VIEW. I HOPE YOU LIVE A LIFE YOU'RE PROUD OF. IF YOU'RE NOT, I HOPE YOU HAVE THE COURAGE TO START ALL OVER AGAIN."

– **F. Scott Fitzgerald**

TO THE FAMILY THAT WE ARE BUILDING TOGUETHER
L. S. C.

Acknowledgments

The research has been carried out at the Civil Engineering Department of University of Minho, Portugal, under the supervision of Professor José Sena-Cruz and co-supervision of Professor Paulo Macedo França. This work was financially supported by the Portuguese Foundation for the Science and Technology (FCT) under the grant number SFRH/BD/98309/2013, which is gratefully acknowledged. This study would not have existed without the financial support of this institution. Additionally, this work was also incorporated in a research project FRPreDur with the reference number PTDC/ECM-EST/2424/2012, supported by FEDER funds through the Operational Program for Competitiveness Factors – COMPETE and FCT.

First, I would like to express my deepest gratitude to Professor Jose Sena-Cruz, for his support, constructive comments, guidance and friendship. Over the last years Professor Sena-Cruz has constantly shown great character, wisdom, honesty, high work capacity and dedication to others. He is, undoubtedly, one of the best acquaintances that I've made during the development of this work. I would also show my appreciation to my co-supervisor Professor Paulo França, for his assistance, time and support.

Also, I would like to thank Professor Cristina Barris, Professor Eduardo Pereira, and Dr. Julien Michels. Their positive and productive collaboration was fundamental to the development of this research work. I would like to acknowledge their willingness, enthusiasm, scientific knowledge and time.

I would like to sincerely thank all the staff of the Civil Engineering Department of the University of Minho and the staff of the Structural Laboratory of the University of Minho. I am especially grateful for the experience and assistance provided by António Matos and Marco Peixoto. Also, I would like to acknowledge the Institute for Sustainability and Innovation in Structural Engineering (ISISE) for providing the facilities and resources to develop this thesis.

I could not forget to thank all the companies that have been involved supporting and contributing for the development of this work, mainly: S&P Clever Reinforcement Ibérica Lda., Casais – Engenharia & Construção S.A., Artecanter - Indústria de Transformação de Granitos, Lda., Tecnipor

- Gomes & Taveira Lda., Vialam – Indústrias Metalúrgicas e Metalomecânicas, Lda., Novo Modelo Europa, S.A.

I want to thank my peers Andrea Benedetti, Christoph de Sousa, Fabio Panella, Filipe Ribeiro, Giulia Marchiori, Gonçalo Escusa, João Almeida, José Granja, Mário Coelho, Patrícia Silva, Pedro Fernandes, Ricardo Cruz, and Sérgio Soares, for all the hours spent discussing each other's works, for all the support and positive energy.

I would like to express my gratitude to my father Ramiro and mother Angelina who have dedicated their adult life to raise their children with the tools to prosper and were always present, with love and unconditional support; and to my brother Hélder for the support, kindness and motivation. I would also like to thank another family member, Professor Sílvio Fernandes who has been present since I've started my journey as a college student and have always gave me the best advices, support and knowledge that I needed.

Most of all, I would like to dedicate this work to my soulmate, Sílvia. I couldn't express in words the level of appreciation that I feel for you. Thank you for your support, kindness, love, dedication, loyalty and strength. The family we are building gives me tremendous joy and, every day, I am thankful for having your company.

Finally, I would like to take the opportunity to pay tribute to Tiago Teixeira, who welcomed me when I first arrived at University of Minho. Tiago Teixeira exuded kindness, generosity, respect, humility, passion, humanity and insight. At work he always presented himself with positive mindset, unmeasured strength, strong character, flawless logic and a great sense of humour. My dearest friend passed away on May 4th of 2015, but his energy was always present throughout the development of this doctoral thesis.

Abstract

The Externally Bonded Reinforcement (EBR) technique using Carbon Fibre Reinforced Polymers (CFRP) has been commonly used to strengthen reinforced concrete (RC) structures in flexure. The use of prestressed CFRP material offers several advantages well-reported in the literature. However, the experience with strengthening reinforced concrete using prestressed EBR-CFRP solutions is still limited. Some concerns regarding the efficiency of the technique still exist, especially the durability and the long-term behaviour.

The present PhD thesis aimed to give insights on two main literature gaps of prestressed EBR CFRP systems in RC structures, mainly: (i) durability and (ii) long-term performance. Thereby, the underlying main objective was to test, analyse and evaluate the durability, short and long-term structural behaviour of RC elements strengthened in flexure with pre-stressed CFRP laminates under various specific environmental conditions, load conditions and chemical degradation. For that purpose, an experimental program was carried out with thirty RC slabs. The effect of the anchorage system, level of prestress, CFRP laminate geometry and concrete surface preparation on the short-term flexural response were the main studied parameters. The durability and long-term performance were studied by exposing sixteen strengthened RC slabs to a sustained loading and to four distinct environmental conditions for approximately 8 months After the exposure period the slabs were monotonically tested up to failure by using a four-point bending test configuration. Additionally, large scale pull-out tests were carried out to assess the bond behaviour of the mechanical anchorage (MA) plate used on the strengthening of the slabs.

Results show a better short-term flexural performance on slabs with prestressed laminates using the MA system and with the sandblasted surface preparation. The environmental conditions and sustained loading, separately or combined, led in general to small losses of performance and ductility. The pull-out tests showed that, at room temperature (20 °C), the mechanical anchorage provided adequate compressive stress of the CFRP laminate to the concrete substrate, and that it is highly influenced by high temperature (60°C and 80 °C).

Lastly, numerical simulations were developed to better understand the observations in the tests carried out on the main experimental campaign with strengthened slabs. Good correlations have been found between the experimental results and numerical modelling. Subsequently, these models were used on a parametric study that intended to investigate the influence of different parameters affecting the behaviour of the slabs, namely the prestress level and the CFRP geometry.

Resumo

A técnica EBR (Externally Bonded Reinforcement) com recurso a compósitos de CFRP (Carbon Fibre Reinforced Polymers) tem sido utilizada no reforço à flexão de estruturas de betão armado. O uso de CFRP pré-esforçado acumula as vantagens da técnica EBR com as do pré-esforço externo. Contudo, o conhecimento neste tópico é ainda limitado, especialmente nas áreas da durabilidade e do comportamento a longo prazo.

A presente tese de doutoramento pretende contribuir para o aumento do conhecimento da durabilidade e comportamento a longo prazo de estruturas de betão armado reforçadas com laminados de CFRP pré-esforçados segundo a técnica EBR. O principal objetivo consistiu em avaliar o efeito de diferentes condições ambientais, de carregamento e químicas no comportamento a curto e longo prazo e na durabilidade de lajes de betão armado reforçadas com laminados de CFRP pré-esforçados segundo a técnica EBR. A influência do tipo de ancoragem, nível de pré-esforço, geometria do laminado de CFRP e tratamento de superfície do betão no comportamento a curto prazo foi estudada através de testes de flexão à rotura. A durabilidade e comportamento a longo prazo foram avaliados através da exposição de dezasseis lajes a um carregamento gravítico e a quatro condições ambientais distintas durante oito meses. No final destas ações, todas as lajes foram ensaiadas até à rotura segundo uma configuração de ensaio de quatro pontos de carga. Adicionalmente, realizaram-se ensaios de arranque direto de forma a avaliar o comportamento da ligação da ancoragem mecânica (MA) utilizada no reforço das lajes.

Os resultados obtidos mostram um melhor comportamento a curto prazo nas lajes que foram pré-esforçadas com laminados de CFRP, com o sistema de ancoragem MA e cuja superfície do betão foi tratada com jato de areia. Em geral, o carregamento gravítico e as condições ambientais conduziram a pequenas perdas na eficiência e ductilidade das lajes. Com os ensaios de arranque direto verificou-se que, à temperatura ambiente, a ancoragem mecânica permitiu o aproveitamento total da capacidade do laminado de CFRP. Todavia, verificou-se que o comportamento deste sistema é seriamente influenciado na presença de temperas elevadas.

Adicionalmente, simulações numéricas foram desenvolvidas para uma melhor compreensão dos resultados obtidos na campanha experimental principal. Existe uma boa concordância entre os resultados numéricos e os resultados experimentais. Com base nestes modelos numéricos, realizou-se um estudo paramétrico com o intuito de investigar a influência de diferentes parâmetros no comportamento das lajes, nomeadamente o nível de pré-esforço e a geometria do laminado de CFRP.

Keywords

Reinforced concrete structures

Anchorage systems

Prestressing

CFRP laminate strips

EBR technique

Durability

Long-term behaviour

Bond behaviour

Numerical modelling

Table of contents

List of Tables

List of Figures

List of abbreviations and symbols

Abbreviations

ACI	American Concrete Institute
$Ca(OH)_2$	Calcium hydroxide
CB	Concrete Batch
CFRP	Carbon fibre reinforced polymer
CNR	National Research Council
CoV	Coefficient of Variation
CTE	Coefficient of thermal expansion
CW	Chloride water
DMA	Dynamic mechanical analysis
EBR	Externally bonded reinforcement
EBRIG	Externally bonded reinforcement in Grooves
EBROG	Externally bonded reinforcement on Grooves
Empa	Swiss Federal Laboratories for Material Science and Technology
EN	European Norm
FEM	Finite element method
FIB	International Federation for Structural Concrete
FRP	Fibre reinforced polymers
FT-RH	Freeze-thaw cycling under 90% of relative humidity
FT-WI	Freeze-thaw cycling with water immersion
GA	Gradient anchorage (system)
GFRP	Glass fibre reinforced polymer
IR	Infra-red (radiation)
ISIS	Intelligent Sensing for Innovative Structures
ISO	International Organization for Standardization
JSCE	Japan Society of Civil Engineers
KOH	Potassium hydroxide

LNEC	Portuguese National Laboratory of Civil Engineering
LVDT	Linear variable differential transducer
MA	Mechanical anchorage (system)
MFCM	Multidirectional fixed crack model
MF-EBR	Mechanically fastened and externally bonded reinforcement
NaCl	Sodium chloride
NaOH	Sodium hydroxide
NP	Portuguese Norm
NSM	Near-surface mounted
OFSS	Optical fibre strain sensor
RC	Reinforced concrete
REF	Reference conditions (laboratory premises)
RH	Relative humidity
RILEM	International Union of Laboratories and Experts in Construction Materials, Systems and Structures
SG	Strain gauge
SIA	Swiss Engineering and Architects Association
TSCM	Total strain-based crack model
TW	Tap water (immersion)
UV	Ultra-violet (radiation)
WD	Wet and dry cycles

Symbols

Latin upper-case letters

A'_s	Area of the top (compression) reinforcement
A	Area of the corresponding element mesh
A_f	Cross-section area of the CFRP reinforcement
$E_c; E_{cm}$	Modulus of elasticity of concrete
E_f	Modulus of elasticity of CFRP reinforcement

E_K	Elasticity of a Hookean spring (Kelvin Model)
E_M	Elasticity of a Hookean spring (Maxwell Model)
E_s	Modulus of elasticity of steel reinforcement
F	Applied Force; Total Force
F_{cr}	Total load at cracking
F_{max}	Peak load
F_p	Prestress force
F_y	Total load at steel yielding
FC	Confidence factor
$G_{f,exp}$	Fracture energy (obtained experimentally)
$G_{f,th1}$; $G_{f,th2}$	Predicted fracture energy
G_f	Fracture energy
G_{f0}	Base value of fracture energy
I_R	Roughness factor
K_I	Stiffness of the elastic phase
K_{II}	Stiffness of the cracked phase
$M_{ffd,2}$	Expected bending moment at mid-span section (intermediate debonding)
M_{ffd}	Expected bending moment at mid-span section (end anchorage failure)
M_{max}	Ultimate bending moment at mid-span section
$P_{deb,ave}$	Average debonding load (obtained experimentally)
$P_{deb,exp}$	Expected debonding load
$P_{deb,th}$	Predicted average debonding load
P_{deb}	Debonding load
P_{res}	Residual (pull-out) load
P_u	Ultimate (pull-out) load
R_a	Arithmetic average of absolute values of surface roughness
R_p	Maximum peak height on surface roughness measurements
R_q	Root mean squared of surface roughness

R_t	Maximum height of the profile on surface roughness measurements
R_v	Maximum valley depth on surface roughness measurements
S	Time-dependent factor
T	Test temperature
T_{deb}	Temperature in the bonded length during the debonding process
T_g	Glass transition temperature
T_L	Torque level
T_u	Temperature in the anchorage region at failure
VD	Percentage of visible damage

Latin lower-case letters

b	Width of the concrete element
b_f	Width of the laminate strip
d	Effective depth of section
f_{bd}	Design bond strength between the FRP and concrete
$f_c; f_{cm}$	Average compressive strength of concrete
f_{ctm}	Average tensile strength of concrete
$f_f; f_{fu}$	Tensile strength of CFRP reinforcement
f_{ffd}	Ultimate design strength (end anchorage failure)
$f_{ffd,2}$	Ultimate design strength (intermediate debonding)
f_u	Ultimate stress of steel reinforcement
f_y	Yield stress of steel reinforcement
h	Crack band-width
k_b	Geometrical corrective factor
k_G	Corrective factor that considers the bonding system
k_q	Coefficient that considers the load distribution
k_R	Roughness corrective factor

$l_{ed}; l_e$	Optimal/effective bond length
l_m	Evaluation length on surface roughness measurements
n	Parameter (governs the descending branch on a bond-slip model)
$\bar{s}; s_0$	Slip at the maximum shear stress
$s_{i+1/2}$	Slip of the CFRP laminate at the mean "$i + 1/2$" location
$s_{u,1}$	Slip at failure registered at the loaded-end
$s_{u,2}$	Slip at failure registered at the mid-end
$s_u; s_f$	Interface slip at full debonding
t_f	Thickness of the laminate strip
$w_f; w$	Width of the laminate strip
$z(x)$	Profile height at position x

Greek letters

$\Delta\bar{\varepsilon}_{f,i}$	Relative strain variation due to short-term prestress loss
β_w	Geometrical factor
$\gamma_{f,d}$	Partial factor
$\gamma_{R,d}$	Corrective factor
Γ_{Fd}	Design fracture energy of the strip/concrete interface
$\Delta\delta_{c,env}$	Mid-span displacement growth after the environmental exposure (10 days)
$\Delta F_{p,i}$	Absolute value of the short-term prestress loss
δ	Mid-span displacement
$\delta_{c,CREEP}$	Mid-span displacement due to creep
$\delta_{c,ela}$	Instantaneous mid-span displacement (gravity load)
$\delta_{c,rec}$	Mid-span displacement after unloading the creep weight
$\delta_{c,ult}$	Maximum mid-span displacement during gravity loading
δ_{cr}	Mid-span displacement at cracking
δ_{max}	Mid-span displacement at peak load
δ_y	Mid-span displacement at steel yielding

$\varepsilon_{fdd,2}$	Expected strain in the CFRP laminate (intermediate debonding)
$\varepsilon_{i+1/2}$	Laminate strain at "$i + 1/2$" location
ε_c	Strain in the concrete
ε_{c1}	Strain in the concrete at the peak stress
ε_{fdd}	Expected strain in the CFRP laminate (end anchorage failure)
ε_i	Laminate strain at "i" location
$\varepsilon_{max}; \varepsilon_u$	Maximum Strain in the CFRP laminate
η	Ratio between the average debonding load (obtained experimentally) and the predicted debonding load
η_K	Dynamic viscosity of a Newtonian dashpot (Kelvin Model)
η_M	Dynamic viscosity of a Newtonian dashpot (Maxwell Model)
μ_F	Efficiency parameter (load)
μ_δ	Ductility parameter (mid-span displacement)
μ_φ	Ductility parameter (mid-span curvature)
$\overline{\mu_F}$	Normalized Efficiency parameter (load)
$\overline{\mu_\delta}$	Ductility parameter (mid-span displacement)
ρ'	Compression reinforcement ratio
$\rho_{l,eq}$	Equivalent longitudinal reinforcement ratio
ρ_l	Longitudinal reinforcement ratio
$\sigma_{f,max}$	Maximum stress in the CFRP laminate during the monotonic test
$\sigma_{f,u}$	Tensile strength of the CFRP laminate
σ_L	Compressive stress
σ_L	Maximum tensile Stress in the laminate
$\bar{\tau}$	Maximum shear stress
$\tau_{i+1/2}$	Mean bond shear stress between two consecutive strain gauges
τ_{max}	Peak value of the bond shear stress
φ_{cr}	Mid-span curvature at cracking
φ_{max}	Mid-span curvature at peak load
$\varphi_{t\infty}$	Long term creep coefficient
φ_{ult}	Creep coefficient based on the period of loading

φ_y	Mid-span curvature at steel yielding

CHAPTER 1

INTRODUCTION

1.1 Strengthening with prestressed FRP materials

Nowadays, Fibre Reinforced Polymer (FRP) materials and related strengthening techniques are well-known and used by the construction industry [1–12]. In the context of retrofitting Reinforced Concrete (RC) structures, Carbon FRP materials (CFRP) are mostly used due to their intrinsic properties - among the other FRPs, CFRPs present higher strength, stiffness and fatigue life, and are less susceptible against aggressive environments and creep rupture [6–9]. From different attempts, two main strengthening techniques have been developed [6–9,13–18]: (i) the Externally Bonded Reinforcement (EBR), and (ii) the Near-Surface Mounted (NSM). The EBR technique consists of gluing the FRP laminate on the tensile face of the RC element to be strengthened; whereas in the NSM technique the FRP strip or bar is inserted onto a groove previously cut in the concrete cover, and then is bonded to concrete with an appropriate groove filler. Epoxy adhesives are typically used as bonding agent in the EBR and the NSM techniques due to superior bond performance compared with other materials (e.g. cementitious materials).

Typically, the EBR technique is used on RC elements to improve the flexural and shear resistance, to control the cracking process and to increase the concrete confinement [19]. Despite the advantages of this technique, the strengthening performance of the EBR technique depends significantly on the resistance of the concrete cover. Normally, the concrete cover is the most degraded concrete region on the structure due to its great exposure to environmental conditions, such as temperature variations and moisture [19]. Consequently, premature failure of the strengthening system may occur before the full use of the ultimate mechanical capacity of the FRP material. In fact, the bond behaviour between FRP and concrete is generally a critical issue as it is shown by the significant number of studies found in the literature for both EBR [11,13,14,20–27] and NSM [11,13–18] techniques. In order to avoid this premature failure, several solutions were developed [19]: anchorage systems composed of steel plates bolted in the ends of the FRP; the use of strapping with FRP fabric; and the use of FRP anchor spikes. Alternatively, other techniques like the (i) Mechanically Fastened and Externally Bonded Reinforcement (MF-EBR), the (ii) Externally Bonded Reinforcement on Grooves (EBROG) technique and the (iii) Externally Bonded Reinforcement in Grooves (EBRIG) were developed to avoid premature failure. In the MF-EBR technique the FRP material is applied similarly to the EBR technique, but is also fixed against the

concrete element with prestressed bolts [19,28–30]. In the EBROG technique, several grooves are cut in the tension surface of the RC element instead of the conventional surface preparation (sandblasting, grinding, brushing and bush hammering) and the FRP material is applied over the grooves [31,32]. Finally, in the EBRIG, the concrete surface is prepared as if it was the EBROG or the NSM technique (with longitudinal grooves on the tension surface) and the FRP sheets is applied (wet-lay-up application) on top of the tensile surface and inside the concrete grooves as shown in **Figure 1.1e** [31]. The five abovementioned strengthening techniques (EBR, NSM, MF-EBR, EBROG and EBRIG) are presented in **Figure 1.1**.

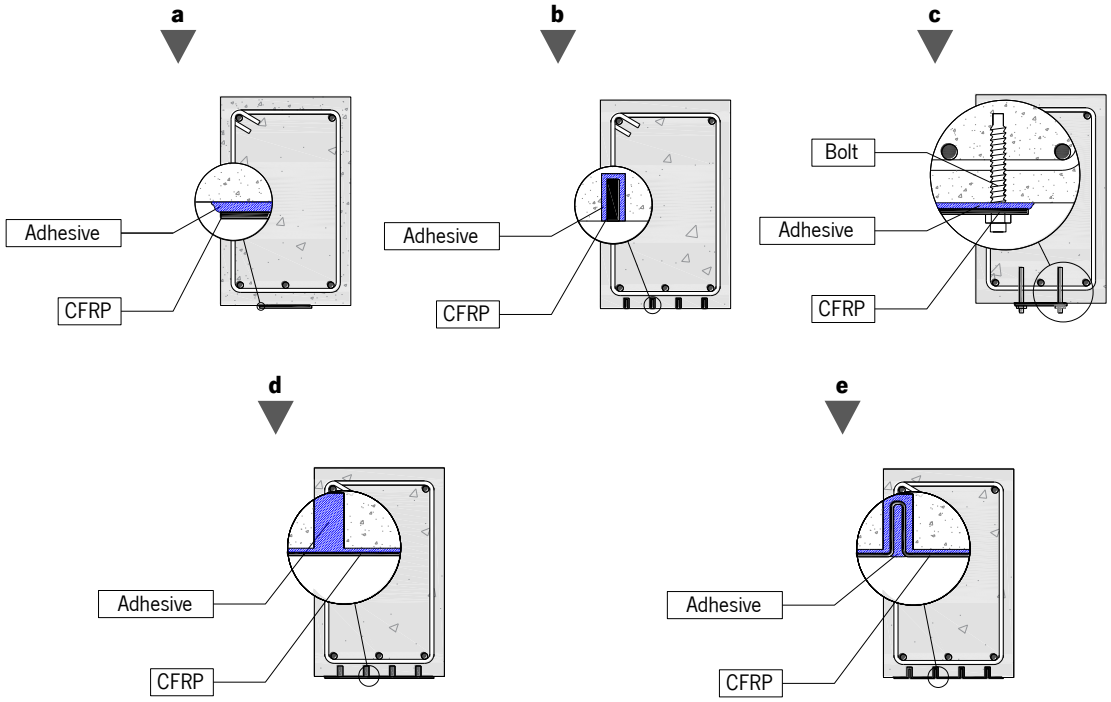

Figure 1.1: Strengthening techniques: (a) EBR; (b) NSM; (c) MF-EBR; (d) EBROG; and (e) EBRIG.

When compared with the EBR technique, the techniques NSM, MF-EBR, EBROG and EBRIG present several advantages, already reported in the literature [3,4,12,19,30,31]. The NSM presents greater bond surface which induces a better anchorage capacity and the confinement effect of the grooves makes this technique less susceptible to premature debonding [3,12,33]. The MF-EBR technique combines the advantages of the EBR technique with the fasteners from this technique, which improves the bond between components (FRP and concrete) and might avoid premature debonding

and increase the specimen's ductility [19,28–30]. The EBROG and the EBRIG uses the concrete groves to allow the interfacial stresses (developed between the FRP and concrete surface) to be transferred to the underlying concrete layers [31]. Nonetheless, a lot of research on RC elements strengthened with FRP materials using the EBR technique has been done in recent past years, and this solution has been used in many real cases with increasing knowledge and confidence due to easy application and lower labour skills level [1,11,25,27,34]. Several approaches for the design of EBR strengthening have been developed over the last two decades [35–37]. Currently, in the scope of the design and execution of the EBR technique, there are several reference documents worldwide such as:

- Italian design recommendations, CNR [6];
- American Concrete Institute, ACI440.2R-08 [7];
- International Federation for Structural Concrete, FIB Bulletin 14 [38];
- Swiss design recommendations, SIA 166 [39];
- Concrete Society, Technical Report N°55 [40];
- Japan Society of Civil Engineers, JSCE-CES41 [41];
- Canadian design recommendations, ISIS-4 [42].

Although the load bearing capacity of an RC member can be improved with an EBR strengthening, a very large number of research studies have clearly demonstrated that the ultimate failure at a structural level occurs with the debonding of the FRP [11]. Moreover, in most cases, failure is observed when the FRP material is in-between of 20-30% of its ultimate tensile strength [43]. In some specific cases, the use of prestressed FRP materials for strengthening RC structures is convenient or even required. This technique presents several positive aspects since it combines the benefits of passive EBR FRP systems with the advantages associated with external prestressing, mainly [23]: (i) use of non-corrosive materials; (ii) deflection reduction; (iii) crack widths reduction and the onset of cracking is delayed (typically this is not the case of existing structures); (iv) internal steel reinforcement strains are relieved; (v) higher fatigue failure resistance; (vi) more efficient use of the concrete and FRP; (vii) opposes stresses due to both dead and live loads; (viii) reduction of risk of premature debonding failure between the FRP and concrete; (x) ultimate capacity can be

further increased; (xi) it can be worked as a substitute of internal prestress that has been lost; and (xii) shear capacity is increased by the longitudinal stresses induced by prestressed FRP laminates.

Laminates [43–55], sheets [54,56–62] and bars [47,56] are the most common prestressed FRP shapes, the former being the most prominent. Several systems have been proposed to induce a prestress in the FRP and can be divided in three categories [23]: (i) cambered prestressing systems; (ii) prestressing against an external support; and, (iii) prestressing against the element to be strengthened. These three methods are presented in **Figure 1.2**. In the first technique, shown in **Figure 1.2a**, the RC element is cambered using hydraulic jacks. Subsequently, the FRP strip is fixed against the bottom tensile face. The FRP strip is indirectly prestressed once bonded to the concrete surface, when the hydraulic jacks are removed, and the initial camber deflection is released. In the two remaining methods, the FRP strip is directly prestressed. Prestressing against an external support, shown in **Figure 1.2b**, requires an independent and external reaction steel frame that prestresses the FRP strip before fixing it against the RC element. The external support is removed when the FRP strip is fully bonded to the RC element, and the prestress is transferred to the concrete. The last method, shown in **Figure 1.2c**, is the most common method. Specific anchors are bonded to the FRP strip ends, while other set of anchors are fixed to the RC element. Prestress is applied when the strip anchors are pulled with hydraulic jacks that react against the anchors mounted on the RC element. Once the FRP strip is fully bonded to the RC element, temporary elements are removed [11,23].

In spite of each one having advantages and disadvantages [23], the last method - systems that apply the prestressing against the element to be strengthened - has known so far the biggest success. Special end-anchorage systems are required at the ends of the prestressed FRP element to transfer the high shear stress developed from the reinforcement into the concrete substrate, in order to avoid a premature FRP peeling-off failure. Several anchorage devices can be already found in the literature, and can be classified into [25,63,64]: (i) U-jacked anchors [56,65–70], (ii) mechanically fastened metallic anchors [34,71–75], (iii) FRP anchors [29,76–81] and (iv) gradient anchorage [64,82–84].

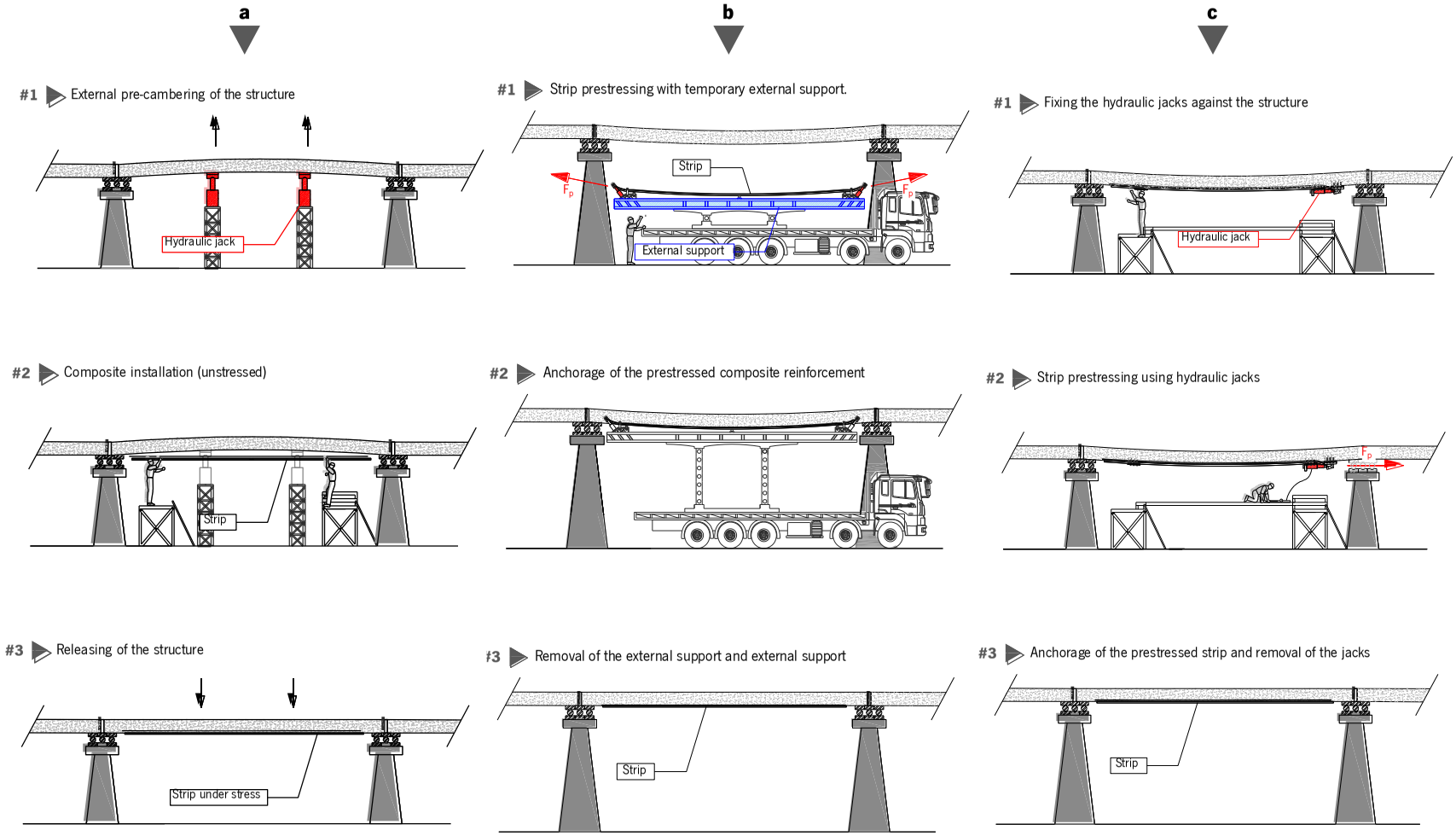

Figure 1.2: Different types of prestressing of an existing RC construction: (a) Cambered prestressing; (b) Prestressing against an external support; and (c) Prestressing against the structure (Adapted from [11,23,85]).

The U-jacked anchors consist of wrapping the prestressed FRP strip with FRP sheets to form a U, as shown in **Figure 1.3**. Additionally, the use of these FRP straps alone will enhance the shear capacity of the section. Prestressing the FRP strip still requires temporary metallic anchors that are bonded to the CFRP ends. The FRP U-straps are fixed against the strengthened RC element after the prestress application and, once all elements are bonded, the temporary metallic anchors are cut off [56,69,70].

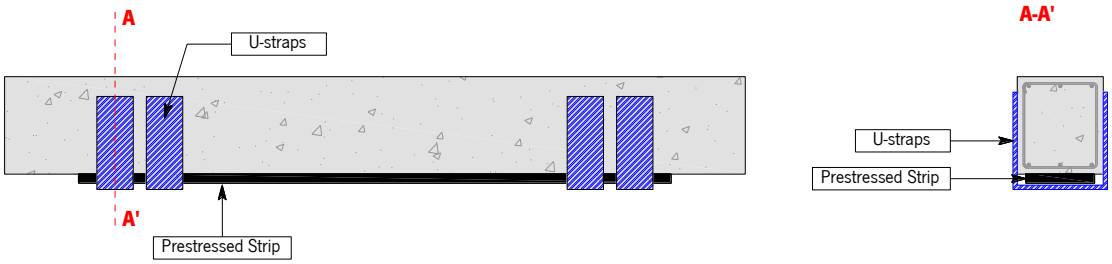

Figure 1.3: RC element strengthened with prestressed FRP strip using U-jacked anchors.

The mechanically fastened metallic anchors, also known as metallic anchors, are typically composed by metallic plates that are fastened against the concrete subtract at the ends of the FRP strip. The metallic anchors are very efficient, being capable of reaching the FRP's maximum tensile capacity in many studies [49,71–75,86]. An RC element strengthened with prestressed FRP strip using metallic anchors is illustrated in **Figure 1.4**. Additional information regarding the mechanically fastened metallic anchors is given in Chapter 2 (Section 2.2.3).

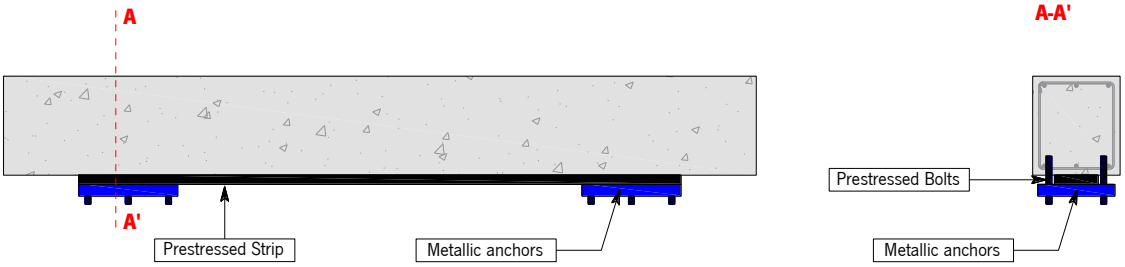

Figure 1.4: RC element strengthened with prestressed FRP strip using mechanically fastened metallic anchors.

The FRP anchors are a non-metallic alternative to the previous type of anchors. This type of anchorage system uses FRP spike anchors that are used to fix the prestressed FRP against the concrete element. Typically, the FRP spike anchors are composed of wet (precured) and dry fibres. After the concrete surface preparation, several holes are drilled to accommodate these FRP spikes.

During the strengthening, the wet (precured) fibres of the FRP spike anchors are inserted in the previously drilled holes (filled with a mortar/epoxy adhesive) and the dry fibres are spread (fan out) over and around the FRP strengthening, as shown in **Figure 1.5** [29,76–81].

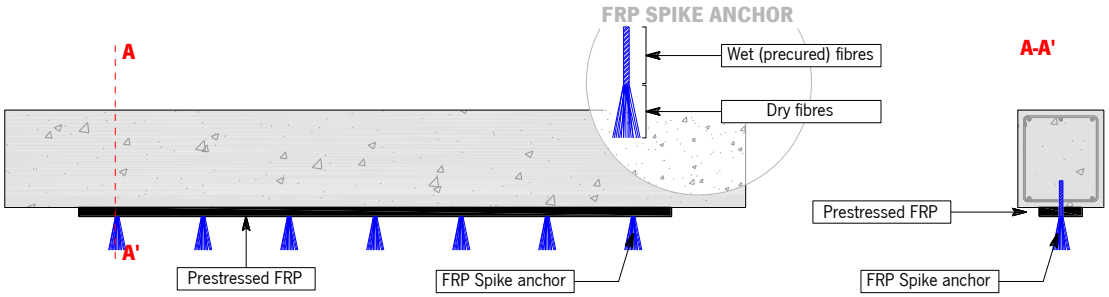

Figure 1.5: RC element strengthened with prestressed FRP strip using FRP spike anchors.

The gradient anchorage was developed at EMPA (Swiss Federal Laboratories for Materials Science and Technology) and is unique for laminate strips [87]. The concept of the anchorage consists on gradually reducing the prestress force towards the FRP ends. As a result, there is a greater development length of the prestressing force (F_p in **Figure 1.6**) and, consequently, the occurring shear stresses are within the limitations of the shear strength of concrete [64,82–84]. The application technique is based on the adhesive's ability to cure faster at higher temperatures [87,88]. Additional information regarding the gradient anchorage system is given in Chapter 2 (Section 2.2.3).

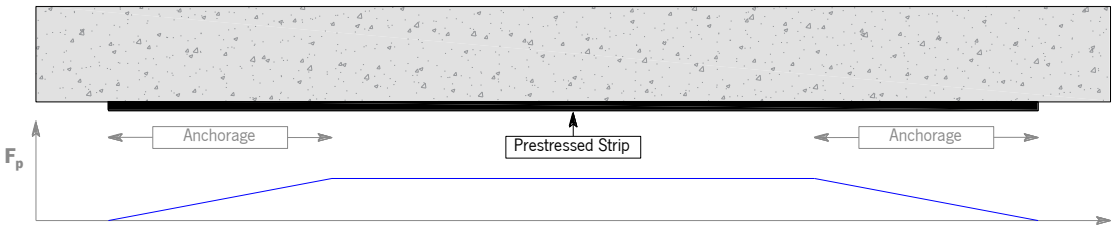

Figure 1.6: RC element strengthened with prestressed FRP strip using a gradient anchorage.

Up to now, the majority of the studies focus on the development/improvement of the prestressing systems as well as the structural behaviour in terms of serviceability and ultimate resistance of the strengthened elements. In 2001, El-Hacha *et al.* [89] developed a state-of-the-art article concerning prestressed fibre reinforced polymer laminates for strengthening structures. More recently, in 2015, Aslam *et al.* [90] made a contribution on the same topic with the state-of-the-art article review

entitled: “Strengthening of RC beams using prestressed fibre reinforced polymers”. The later document [90] covers the flexural behaviour of strengthened RC beams using prestressed FRPs, using the externally bonded reinforcement (EBR), near surface mounted (NSM), and post-tensioned techniques (EPT). Moreover, in 2016, the RILEM Technical Committee 234-DCU [11] published a state-of-the-art report on the design procedures for the use of composites in strengthening of RC structures. This report includes an overview on the state-of-the-art in prestressing systems for the structural retrofitting of reinforced concrete structures using fibre reinforced polymers. The doctoral thesis of França [34] and Czaderski [87] should also be referred in the present section due to the relevant work developed on the prestress of concrete members, externally bonded with mechanically fastened and gradient anchorages, respectively. In this context, in the scope of the present thesis it was decided not to develop an extensive review, especially on the short-term behaviour of RC members strengthened with prestressed CFRP laminates since the previously referred documents give the actual state-of-the-art of this topic. However, a short literature review on the durability and long-term performance of RC members strengthened with prestressed CFRP laminates is presented, since these topics were not included in the above-mentioned publications. In fact, the durability and long-term behaviour have been appointed as one of the open issues on the study of prestressed FRP systems, to which further research and development is needed [11].

1.2 Durability

Other industrial sectors (e.g. automotive, marine and aerospace) have been showing successful use of FRPs and epoxy adhesives for mass production of mechanical and structural components. However, these results do not find direct translation into civil infrastructures applications, mainly because there are critical differences in loading, environmental exposures and the specific types of material/processes used in these applications [5,91,92]. Several authors [3,4,93] have defined durability of a structural element strengthened with composite materials as its ability to resist cracking, abrasion, delamination, chemical degradation, oxidation, and other external agents that, for a specific period of time and under certain loading and environmental conditions, damages the structural element. There are several factors that influence the durability of such strengthening systems, such as: (i) environmental exposure conditions; (ii) type of FRP strengthening system; (iii) curing and installation quality; and (iv) maintenance quality [4,93]. It should be highlighted that the

research of the durability of structural elements strengthened with composite materials, should consider the study of the degradation mechanisms that occur at the individual materials, interfaces between them, and possible synergies [3,4]. The degradation mechanism consists of the sequence of physical, mechanical, or chemical changes that lead to the alteration of the mechanical properties of the material/structure in a harmful way. The degradation mechanisms occur when the material/structure is exposed to a degradation factor, such as moisture, temperature, UV radiation, marine environments, freeze-thaw cycling, or fire [3,4,94].

Four different materials compose a RC structure with externally-bonded fibre reinforced polymer (EB-FRP): concrete, steel reinforcement, FRP reinforcement, and epoxy adhesive. Significant research on the durability of concrete and steel reinforcement has been developed over the last decades [95–98]. However, the existing knowledge on this topic regarding FRP reinforcement and bonding agents is limited when compared with the concrete and steel materials. The following section includes the main findings reported in previous studies about the durability of the CFRP reinforcement, on the bonding agent (epoxy adhesive) and FRP-concrete interfaces.

1.2.1 Carbon FRP reinforcement, epoxy adhesive and FRP/concrete interface

According to the ISIS Manual no. 8 [92], the main factors in terms of durability of FRP are: (i) the effect of moisture, (ii) marine environments, (iii) alkalinity, (iv) high and low temperatures, (v) freeze and thaw cycles and (vi) ultra-violet radiation. These factors are included in the following literature review.

1.2.1.1 Carbon FRP reinforcement

Marine and wet environments have been appointed as two of the most severe degradation factors for reinforce concrete structures [92]. FRP materials do not exhibit corrosion and are well-suited to be used in such environments. However, FRP materials are subjectable to potential harmful effects of these environments. The effect of the marine environment on CFRP has been quite studied over the last years [3,99,100] and, there is a reduction on the mechanical properties of the CFRP material when subjected to the effect of salt solutions (used to simulate the exposure to sea water and de-icing salts). Although there is a decrease on CFRP strength after the exposure to salt-water

environments, several authors have concluded that the strength reduction is higher when the composite is immersed in water without salt [3,99,100]. In fact, it is known that hot and humid environments can influence of the FRP performance [101]. FRP materials consists of a large number of non-metallic fibres bundled in a resin matrix. The carbon fibres do not absorb moisture and, apparently, are not affected by moisture [92]. However, the resin matrix absorbs moisture and, consequently, suffers plasticization simultaneously with swelling. The plasticization of the matrix is a consequence of interruption of Van Der Waals bonds between the polymetric chains, which ultimately leads to the reduction of the glass transition temperature (T_g), matrix stiffness and strength [102,103]. The degradation of the FRP with moisture can be amplified when constant stress or elevated temperature are also present [101,103].The stress state installed in the FRP can cause microcracking in the resin matrix and, consequently, promote the moisture diffusion [92]. As referred before, moisture decreases the resin matrix glass transition temperature which, aligned with high temperatures, leads to an even higher decrease in the matrix dominated strength and stiffness [103]. The influence of high temperatures on the mechanical properties of FRPs is well documented in the literature [103]. The polymer matrices typically used in CFRP composites decomposes over the temperature range of about 350 °C to 600 °C [104]. According to ISIS [92] CFRPs have great resistance to thermal cycles in service temperature, however the different thermal expansion between the matrix (coefficient of thermal expansion, CTE, of $60\times10^{-6}\ K^{-1}$ [105]) and the carbon fibres (CTE of $1\times10^{-6}\ K^{-1}$ [106]) might cause microcracking in the matrix and, consequently, might accelerate other degradation mechanisms.

According to ISIS [92] the tensile strength of the unidirectional FRP decreases within a range of -10 °C to -40 °C. Freeze-thaw cycles might increase the microcracking in the FRP and, consequently, affect the strength, stiffness, moisture absorption and alkalinity resistance. The literature review carried out by Reed and Golda [107] on the effect of cryogenic temperatures on unidirectional composites should be mentioned. Their study summarized the experimental results gathered over four decades on the cryogenic properties of composite laminate plates with the reinforcement fibres of boron, alumina, aramid, S-glass, E-glass and carbon (high modulus and medium modulus). Although the majority of the CFRP plates were produced for airspace applications, it is noteworthy that in more than 30 studies, there was little variability between tests

carried out at room temperature (between 19 °C and 22 °C) and at cryogenic temperatures (between -195 °C and -270 °C). The review concluded that the CFRP plates have the best behaviour for temperature below -250 °C and for fatigue loading at cryogenic temperatures.

Micelli *et al.* [108] studied the effect of accelerated aging on five types of GFRP (glass FRP) and CFRP rods. These specimens were subjected to (i) alkaline simulated concrete pore solution at 60 °C; and to (ii) an environmental exposure that included 200 freeze-thaw cycles (ranging from -18 °C to 4 °C), 600 high temperature cycles (ranging from 16 °C to 49 °C), and 480 humidity cycles (ranging from 60% to 100% of relative humidity) on three distinct temperatures (16 °C, 27 °C and 38 °C). The later environmental condition also included UV radiation and was designed to simulate all four seasons of the year. The alkali environment (1.6 g/l of $Ca(OH)_2$; 14.0 g/l of KOH;10.0 g/l of $NaOH$) had a pH that varied between 13.0 and 12.6 during the 42 day-period of exposure. The CFRP specimens had a good retention of mechanical properties and, after the 42-day exposure, the maximum reduction on the tensile strength, modulus of elasticity and ultimate strain was equal to 8%, 7.5% and 7.4%, respectively. The synergy between moisture, high temperature, freeze-thaw cycles and UV radiation lead to a neglectable reduction on the tensile properties (reduction in the tensile strength of 1.2%).

Cabral-Fonseca [99] studied the durability of three commercial types of CFRP laminate strips with a long-term exposure to (i) condensation at 40 °C, (ii) full-immersion in demineralized water, (iii) full-immersion in salt-water (35 g/l of NaCl), (iv) full-immersion in alkaline solutions, and (v) UV radiation with humidity. The CFRP laminate specimens were subjected to environments (i), (ii), (iii) and (iv) for a period of 18 months, and to environment (v) for a period of 83 days. The immersion in demineralised water, in salt-water and in alkaline water was carried out at 23 °C, 40 °C and 60 °C. Results show a clear decrease on the mechanical properties of specimens fully-immersed in demineralized water, being the lowest values of flexural strength observed on specimens submitted to the highest temperature level (reduction of 32-11% depending on the type of CFRP laminate). The highest reduction on the flexural strength of the CFRP specimens fully-immersed on salt-water was also observed for the temperature of 60 °C (reduction of 47%, 31% and 1% depending on the type of CFRP laminate). The alkaline solution (118 g/l of $CaOH_2$; 4.0 g/l of KOH; 0.9 g/l of $NaOH$) used by Cabral-Fonseca *et al.* [99] caused the highest variation of mass and greatest

reduction on the flexural strength (compared with salt-water and demineralised water). The synergy between alkaline solution and high temperature (60 °C) produced a reduction on the flexural strength close to 44%. It is noteworthy to mentioned that in two types of CFRP strips, the attack of the alkaline solution led to the extraction of the polymetric matrix to the point that it was impossible to perform the flexural tests. In contrast, the 2000-hour exposition to ultraviolet radiation led to a degradation on the CFRP surface, but no reduction on the flexural strength.

The durability of CFRP laminates was recently studied by Silva [3]. The program included 72 samples, that were submitted to (i) full-immersion in tap water, (ii) full-immersion in salt-water (35 g/l of NaCl), (iii) wet-dry cycles on salt-water (35 g/l of NaCl), (iv) thermal cycles and (v) freeze-thaw cycles. For each environment, two exposure periods were considered: 240 days and 480 days for environments (i), (ii), and (iii); 120 days and 240 days for environments (iv) and (v). After an exposure of 480 days to immersion in tap water, a reduction of 3% on the CFRP laminate's tensile strength and elastic modulus was observed, with respect to the reference values. The highest degradation (reduction on the elastic modulus and tensile strength) was observed after the 480-day exposure to wet-dry cycles on salt-water. The wet-dry cycles led to a reduction of 7.3% and 2.0%, respectively, on the tensile strength and elastic modulus, after 480 days. At the end of the same period, a reduction of 7.1% and 1.3% in the tensile strength and elastic modulus, respectively, was reported for CFRP specimens exposed to full-immersion on salt-water (at 20 °C). The experimental study developed by Silva [3] on the durability of a CFRP strip included freeze-thaw cycles (between -18 °C and 20 °C, for a period up to 240 days) and two sets of thermal cycles: (i) 240-day period of thermal cycles that ranged between -15 °C and 60 °C; and (ii) 180-day period of thermal cycles that ranged between 20 °C and 80 °C. Results showed no significant changes on the stiffness, tensile strength or ultimate strain of the CFRP strip laminate, after the exposure to freeze-thaw cycles or both thermal cycles.

1.2.1.2 Epoxy adhesive

Like the FRP matrix, epoxy adhesives are susceptible to moisture absorption, which has deleterious effects on its mechanical properties. Lin and Chen [109] performed an experimental study on moisture absorption, desorption and reabsorption of an epoxy adhesive. The authors concluded that the moisture diffusion in epoxy systems is influenced by the hydrothermal conditions, the

specimen's thickness and hydrothermal history. From the three studied processes, reabsorption is fastest, and absorption is the slowest. In this study [109] the mechanical properties of the adhesive were also evaluated after the reabsorption process, for which a decrease of 42% in the elastic modulus and a reduction of 54% in the tensile strength was observed.

Silva [3] carried out ageing tests on epoxy adhesive samples. The environmental conditions and exposure duration were the same used on the CFRP's durability investigation, mentioned in the previous sub-section. The study included the dynamic mechanical analysis (DMA) and monotonic tensile tests up to failure. From all the environmental conditions studied, full-immersion on water presented the greatest reduction on the mechanical properties of the epoxy adhesive. After the exposure period of 480 days, Silva [3] reported a reduction on the adhesive's T_g (about 14%, based on onset of the glass transition of the storage modulus), tensile strength (38%) and elastic modulus (47%), when compared with the reference specimens (kept in laboratory environment - average temperature of 20 °C and average relative humidity (RH) of 55% - for 480 days). During the same period, two different sets of adhesive samples were submitted to wet-dry cycles and full-immersion to salt-water (35 g/l of NaCl) at 20 °C. A reduction on the adhesive's T_g (6%), tensile strength (21%) and elastic modulus (22%), was observed on specimens exposed to wet-dry cycles. The full-immersion to salt-water also produced a reduction on the adhesive's glass transition temperature (21% reduction after 250 days of exposure), on its tensile strength (reduction of 26% and 28% after 250 days and 480 days of exposure, respectively) and tensile modulus (reduction of 29% and 35% after 250 days and 480 days of exposure, respectively). Results also show a reduction of 23% on the glass transition temperature of the epoxy adhesive after 240 days of exposure to freeze-thaw, mainly because the low temperatures interrupted the curing process. After the freeze-thaw cycling, the tensile strength and elastic modulus decreased 22% and 23%, respectively. In contrast, thermal cycles (between -15 °C and 60 °C; and between 20 °C and 80 °C, as above mentioned) improved the mechanical characteristics of the adhesive samples. When compared with the un-aged specimens, there was an increase on the tensile strength (in between 18% and 50%, depending on the type of thermal cycle and exposition time), elastic modulus (between 5% and 25%, depending on the type of thermal cycle and exposition time), and ultimate strain (between 8% and 31%, depending on the type of thermal cycle and exposition time). The post-curing process occurs when

temperatures higher than the ones experienced during the first curing and, according to Silva [3], this process improved the mechanical properties of the epoxy adhesive.

Savvilotidou *et al.* [110,111] evaluated the physical and mechanical behaviours of epoxy adhesive specimens in dry and wet environments, during an aging period of up to two years. The wet environments included full-immersion in demineralized water (at 13 °C, 30 °C and 50 °C) and full-immersion in alkaline water with the pH ≈ 13 (at 13 °C, 30 °C and 50 °C). The water uptake led to a reduction of 23% on the adhesive's glass transition temperature. The authors reported, for the temperatures of 13 °C, 30 °C and 50 °C, a reduction of 20%, 30% and 47%, respectively, on the elastic modulus and a reduction of 18%, 24% and 37%, respectively, on the tensile strength. The immersion in alkaline water resulted in reductions of mechanical properties similar to those obtained after immersion in demineralized water. Using Arrhenius law, the authors predicted a retention of about 70% of elastic modulus and strength, after a period of 100 years (bridge service life time), at a 10 °C reference temperature.

Sousa *et al.* [112] investigated the durability of an epoxy adhesive, using the following environmental conditions: (i) immersion in water at 20 °C and 40 °C; (ii) immersion in salt-water (35 g/l of NaCl) at 20 °C and 40 °C; (iii) continuous condensation environment at 40 °C and 100% of relative humidity; and (iv) outdoor Mediterranean climate, with average RH of 83% (winter) and 58% (summer), average monthly temperature ranging from 11 °C to 24 °C and ultraviolet radiation. Epoxy specimens were kept under environmental conditions (i) and (ii) for 2 years and on environmental conditions (iii) and (iv) for 1 year. The experimental study included evaluation of the media diffusion (water uptake), the viscoelastic behaviour (dynamic mechanical analysis), the flexural behaviour, and the plane shear behaviour. The authors reported the highest reduction on the flexural properties of 24% and 30% in the strength and E-modulus, respectively, after the 2-years-period of immersion in water at 40 °C. The same environmental conditions led to a reduction on the adhesive's T_g of about 20% and a decrease on the shear modulus of 43%, after 1 year. A reduction of 11% and 6% on the flexural modulus and strength, respectively, was reported on the epoxy specimens immersed on salt-water for 2 years. The salt-water also produced changes in the polymer structures which led to a 10% decrease on its glass transition temperature. The UV radiation, relative humidity and temperature of the outdoor environment (Mediterranean climate)

was measured during the one-year aging period. The average monthly UV radiation ranged between 10428 kJ/m² and 27690 kJ/m². Dynamic mechanical analysis presented negligible changes in the adhesive's T_g (2% reduction). The authors also reported a 13% decrease on the shear modulus and a 7% increase on the shear strength. Post cure phenomena was appointed as the most probable cause for the shear strength increase.

Yang et al. [113] studied the durability of an ambient cured epoxy (during 30 days at 23 °C and 30% relative humidity) when subjected to full-immersion: (i) in deionized water at 23 °C, 37.8 °C, and 60 °C; (ii) in salt water (50 g/l NaCl solution) at 23 °C and (iii) alkaline immersion at 23 °C. After a 24-month period, the immersion in alkaline water caused the highest degradation in the tensile strength (reduction of 43%, 36% and 53% for specimens immersed in deionized water at 23 °C, salt solution and alkaline solution, respectively) and in the elastic modulus (reduction of 36%, 30% and 50% for specimens immersed in deionized water at 23 °C, salt solution and alkaline solution, respectively). It is noteworthy to mentioned that the influence of temperature was included in their experimental programme and that after being subjected to immersion in deionized water at 60°C, the retention in tensile strength and elastic modulus at the end of the 2-year period was 31%.

The effect of low-temperature curing on the physical properties of a commercial cold-curing epoxy adhesive was investigated by Moussa *et al.* [114]. The curing process of the epoxy adhesive was carried out at low (5 °C, 10 °C) and high (70 °C) temperatures and constant relative humidity (50%). The authors concluded that low temperatures should be avoided during the application of strengthening systems. The conclusion was fundamented on the fact that low temperatures increased substantially the time of curing: at high temperatures full curing was attained after a few hours (3.73h, 2.42h, 2.05h, and 1.58h for 35 °C, 45 °C, 50 °C, and 60 °C, respectively); at 10°C, 90% of curing required three days; whereas 70% was attained after 1 day at 5 °C. The authors also realised that curing the epoxy adhesive at low temperatures (5 °C and 10 °C) would produce a high decrease on their glass transition temperature. It should be noted that some adhesive suppliers already state in their technical datasheets not to apply these materials at low temperatures (below 8 °C) [115,116].

Frigione *et al.* [117,118] studied the effect of different environmental conditions on the curing behaviour and flexural properties of two epoxy adhesives. After being cured for 20 days at room temperature, adhesive specimens were aged (i) in a freezer at -20 °C, (ii) in a climatic chamber at 18-26 °C (dry, dark and inert to atmosphere), and (iii) in an outdoor environment (Salerno, Italy). The aging lasted two years for the first two environments, and three years for the outdoor environment. The mechanical properties of the adhesives exposed to the UV radiation (and temperature oscillations) of the outdoor environment, did not differ from their initial values. There is still a great deal of uncertainty associated with the current testing methodology, regarding the study of the UV radiation effects. Furthermore, in outdoor exposure, it is not always clear if the changes in the composite materials can be attributed solely to the ultraviolet radiation or to the synergy of UV and other agents (such as moisture and temperature) [119].

1.2.1.3 FRP/Concrete interface

Typically epoxy bonded joints used in bridge construction are sealed in order to prevent exposure to degradation agents such as UV radiation and moisture. However, during the long service life of bridges, up to 100 years, an initially sealed joint may start leaking, exposing the joint to moisture and other degradation agents. Moreover, the epoxy-based joint might be exposed to concrete pore water solution with high pH (close to 12.5) [110,111].

Choi *et al.* [120] performed three-point bending tests to evaluate the bond behaviour between CFRP and concrete, using the EBR technique. The durability of the composite system was assessed through various environmental exposure conditions: (i) immersion in tap water at temperatures of 30 °C, 40 °C, 50 °C and 60 °C; (ii) immersion in alkali solution with a pH of 11.5 (at 50 °C); (iii) immersion in chloride solution at 50 °C; (iv) cyclic exposure to UV light (using UV reflector lamps) and immersion in tap water at 50 °C; and (v) outdoor exposure to the brackish water on the Matanzas River, in Florida. The experimental program included five CFRP systems (4 wet lay-up and 1 precured laminate) and the exposition to the abovementioned environments had a duration of 18 months. The precured CFRP specimens subjected to the 18-month water immersion at 30 °C, 40 °C, 50 °C and 60 °C showed a reduction on the failure load of 33%, 45%, 57%, and 67%, respectively, when compared with the control specimens (also tested after 18 months). In fact, the precured CFRP laminate showed the largest losses in failure load when submitted to chloride

solution immersion (reduction of 71%), alkali solution immersion (reduction of 63%) and to the synergy between artificial UV radiation and water immersion at 50 °C (reduction of 54%). The failure mode changed from adhesive on the control specimens to interlaminar composite failure. The authors justified this behaviour with the durability of the resin used for precuring the CFRP laminate strip (by the supplier), which was lower than the durability of the epoxy resin used for bonding the CFRP laminate strip to concrete. The wet lay-up systems presented higher durability (reduction in the flexural strength between 10% and 40%, depending on the type of CFRP system and environmental condition) and adhesive or adhesive/interfacial failure.

Lai *et al.* [121] studied the effects of exposing externally-bonded CFRP-concrete beams to water immersion at 25 °C, 40 °C and 60 °C. Pull-out tests were performed after 5, 15, 30 and 50 weeks. Results show a decrease on the shear strength of 8% and 21% for the temperatures of 40 °C and 60 °C, whereas the immersion on water at 25 °C lead to a negligible variation on the shear strength (5% increase).

Kabir [122] investigated the durability of the bond between the external CFRP reinforcement and concrete when exposed to temperature cycles, wet-dry cycles and outdoor environments, for a period of up to 18 months. Each wet-dry cycle had the duration of 2 weeks, being the first wetting followed by 1 week drying. Pull-off tests were performed at ages of 1, 6, 12 and 18 months on specimens exposed to wet-dry cycles and the results show no specific degradation trend. Over the aging period, the results show variation on the bond strength ranging from -5% to 15%, when compared with control specimens.

Mohammadi *et al.* [123] studied the effect of immersion on alkali solution (pH≈13) at temperatures of 23 °C, 40 °C and 60 °C on the CFRP-concrete bond strength, when using the EBR and EBROG methods. Single-shear tests were conducted after 125 days of aging. Results show a significant reduction in the EBR bond strength regardless of the temperature (reduction of 23%, 21% and 23% for temperatures of 23 °C, 40 °C and 60 °C, respectively). Additionally, the failure mode on EBR specimens changed from concrete delamination in laboratory premises to concrete-epoxy interface separation in the alkaline solution.

Several other authors [124–127] have also studied the influence of moisture on the interface of externally-bonded carbon fibre reinforced polymer (EB-CFRP) laminates. In general, results show a reduction on the bond strength in the presence of moisture, typically due to the water uptake of the epoxy adhesive and, consequently, plasticization and hydrolysis phenomena.

Literature [119,128–133] shows that the exposure to freeze-thaw cycles might be crucial to the epoxy-based bond between concrete and CFRP. Low temperatures might cause matrix hardening / microcracking and fibre-matrix degradation. The fracture energy of the CFRP-concrete bond decreases with the number of freeze-thaw cycles. Also, the synergy between salt-water and freeze-thaw cycles can result in an accelerated degradation, due to the formation and expansion of the salt. Yun and Wu [130] investigated the effect of freeze-thaw cycles on the bond interface between concrete and CFRP, using water with 40 g/l of NaCl. Each cycle presented a duration of 4 hours and temperatures that varied between -18 °C and 4 °C. After an exposure period that lasted 17, 33, 50 and 67 cycles, single-lap shear tests were carried out. The main conclusion states that the damage on the CFRP-concrete bond increased with the number of cycles mainly because the freeze-thaw process reduces the concrete strength and stiffness. Subramaniam *et al.* [131] also studied the durability of CFRP-concrete joints when submitted to freeze-thaw cycling (water without NaCl). Each specimen was subjected to two cycles of freezing and thawing per day, for a period of 50 days, 100 days and 150 days. The temperature ranged between -18°C and 5°C. Single lap shear showed a reduction of 8%, 12% and 17% after 100, 200 and 300 freeze-thaw cycles, respectively.

Pan *et al.* [132] studied the effects of freeze-thaw cycles in water without NaCl and 90% RH on the behaviour of the bond between the CFRP and concrete. Each freeze-thaw cycle had a duration of 24 hours: for 10 hours the temperature was kept at -20 °C, followed by a (2 hours) heating up to 30 °C that was succeeded by a 10-hour period at 30 °C and another 2-hour period where the temperature was reduced to the initial -20 °C. Single-lap shear tests were carried out at the end of 30, 60 and 90 days to evaluate the fracture energy, bond stress, interfacial stiffness and load capacity of the CFRP-concrete bonded joint. Results show a more severe degradation on specimens exposed to freeze-thaw cycling with water immersion (FT-WI) than on specimens exposed to freeze-thaw cycling under 90% RH (FT-RH). The FT-RH conditions change the failure mode from concrete cohesive failure (average load capacity, P_u, of 17.0 kN; average fracture energy, G_f, of 0.95 N/mm;

and effective bond length, L_e, of 143 mm) to adhesive/concrete interfacial debonding (after 90 days, P_u = 14.8 kN; G_f = 0.72 N/mm; and L_e = 145 mm), whereas FT-WI did not change the failure mode due to severe degradation of the concrete (after 90 days, P_u = 12.6 kN; G_f = 0.52 N/mm; and L_e = 183 mm).

Harmanci *et al.* [133] presented an experimental investigation on the durability and long-term behaviour of the gradient anchorage (GA). Ten specimens (for lap-shear tests) were subjected to four different scenarios: (i) reference tests (no aging), (ii) carbonated concrete, (iii) freeze thaw cycles and (iv) the combination of the last two environments. After 120 freeze-thaw cycles (2 cycles/day, ranging between -15 °C and 25 °C), there was a reduction in the ultimate strength of the gradient anchorage, determined from lap-shear tests, of nearly 30%. The freeze-thaw cycles also changed the failure mode. Conventional mixed failure was obtained for reference specimens and specimens with carbonated concrete, whereas specimens subjected to freeze-thaw cycles presented a failure surface that lies exclusively between the epoxy-concrete interface.

A research work carried out by Firmo *et al.* [134] has shown interesting results regarding the bond between concrete and CFRP strengthening system at elevated temperatures. The experimental campaign included double-lap shear tests on concrete blocks with externally-bonded CFRP laminates with epoxy adhesive. The tests were carried out with the temperature levels of 20 °C, 55 °C, 90 °C and 120 °C. Firmo *et al.* [134] concluded that the effective bond length consistently increased with temperature and, simultaneously, the bond strength decreases (14%, 71% and 76% when compared with ambient temperature, for the temperatures of 55 °C, 90 °C and 120 °C, respectively). Also, at elevated temperatures, the axial strains along the CFRP laminate presented almost a linear distribution, which was a consequence of the softening of the interface (the test temperatures surpassed the adhesive's glass transition temperature). It is noteworthy to mentioned that Firmo *et al.* [117] also tested specimens with a mechanical anchorage in the ends of the CFRP strip. Although no information about the normal stress at the mechanical anchorage was given, results showed that the use of the mechanical anchorages led to more uniform axial strain distribution and provided significantly higher bond strength (between 56% and 139%, depending on the temperature level). At room temperature specimens with the mechanical anchorage presented

shear failure of the concrete block at the anchorage zone, whereas, at elevated temperatures, failure was caused by the progressive slip of the CFRP system under the anchorage plate.

The UV radiation effect was not independently studied in any of the abovementioned research works. The ultraviolet (UV) radiation has wavelengths between 290 nm and 400 nm. Most polymers have bond dissociations energies about the UV radiation wavelengths and, when exposed to natural sunlight, present surface degradation (to a depth of about ten micrometres) [103,119]. It should be noted that when an EB-CFRP joint is exposed to UV radiation, only the exposed areas are damaged (typically the CFRP). Additionally, protective coating is commonly applied on the CFRP surface to protect it from direct ultraviolet exposure [135].

1.2.2 Prestressed FRP system

According to Michels *et al.* [63] the durability is one key aspect in structural engineering. The durability of RC structures strengthened with prestressed CFRP laminates is still an open issue, and, although there is plenty of research on the durability of each composing material (CFRP reinforcements, epoxy adhesives, concrete and steel), the behaviour of these composite system (RC element / epoxy adhesive / CFRP laminate strip) should be further investigated. As referred in Section 1.2.1, some environments might not produce great degradation on the properties of each material but might influence the interaction between of them.

Over the last decades several studies have focused on the durability of RC elements strengthened with non-prestressed FRP laminates (e.g. Cromwell *et al.* [136]; Toutanji *et al.* [137]), however, the effects of environmental exposure on RC elements strengthened with prestressed EBR CFRP laminates is still scarce. In fact, during the literature search, only two studies were found on the durability of RC elements strengthened with prestressed EBR CFRP composites by El-Hacha *et al.* [59,60].

El-Hacha *et al.* [59,60] studied the effect of room (22 °C) and low temperatures (-28 °C) combined with sustained load on prestressed CFRP RC beams. The study included eight prestressed EBR beams, four per studied temperature: (i) one unstrengthened control beam, (ii) one strengthened beam, (iii) one strengthened beam subjected to its own weight for one year and (iv) one strengthened beam subjected to sustained load (50% of the strengthened beam capacity) for one

year. The following main conclusions were obtained: (i) the strengthening produced a considerable enhancement in stiffness and strength; (ii) the isolated effect of sustained load had no impact on the beams ultimate strength; (iii) the combined effect of sustained load and low temperatures reduced the ultimate strength of the beams by 8%.

1.3 Long-term behaviour

In the context of the present thesis, the long-term behaviour concept is associated to the evolution of the performance of the structure during its service life. The long-term performance of a composite system (RC element/epoxy adhesive/CFRP laminate strip) might be influenced by phenomena such as creep, shrinkage or relaxation of each of the components of the system, or interaction between them [11]. Silva [3] presented a state-of-the-art review on the time-dependent behaviour of RC elements strengthened with CFRP materials. The revision included (i) basic concepts of creep and relaxation, (ii) the principles of linearity of the materials (superposition principle and homogeneity), and, (iii) rheological models for the simulation of creep.

In this section, a brief literature review on the long-term behaviour of RC elements prestressed with externally bonded FRP elements will be presented. The section is divided in two sub-section. Section 1.3.1 presents a summary on the creep, shrinkage, and relaxation of composite materials, whereas in Section 1.3.2 a brief state-of-the-art review on the long-term behaviour of RC structures prestressed with FRP laminates is presented.

1.3.1 Carbon FRP reinforcement, epoxy adhesive and FRP/concrete interface

The long-term performance of the concrete (creep and shrinkage) has been studied over the last decades and, nowadays, there is deep a knowledge on the area, consolidated by a comprehensive number of reports, papers and books [3,11,138,139]. In contrast, the information on the long-term behaviour of FRP and epoxy adhesives is limited. The present section provides a short compilation of the available information on creep, shrinkage and relaxation of Carbon FRP reinforcement, epoxy adhesives and FRP/concrete interface.

1.3.1.1 Carbon FRP reinforcement

Typically, FRP materials present lower stress relaxation than steel strands. The type of fibre, volume of fibre, stress history, temperature and humidity are the main parameters that influence the relaxation and creep of FRP's. The FRP relaxation is primarily related to the relaxation of the matrix resin and straightening of the fibres [3,11]. Wang *et al.* [140] performed relaxation tests on CFRP sheets, which were subjected to three sustained deformation levels (40%, 48% and 56% of the CFRP strength obtained in static tests). After a period of 2.500 h, the authors observed a relaxation loss raging between 2.2% and 6.6%. According to Dolan *et al.* [141] the carbon fibres exhibit no relaxation. Moreover, the CFRP laminates possess high percentage of fibre content and the manufacturing procedure avoids eccentricities along each fibre. Consequently, the relaxation of CFRP laminates is not a relevant effect for its long-term performance.

Ascione *et al.* [142] performed a research program on creep in CFRP laminates under various stress levels that varied between 15% and 75% of the characteristic tensile strength for a period of 500 days. The authors concluded that the strain variation during the test were limited (1.4% - 1.9% of the initial strain) due to the high volumetric fraction of fibres and high modulus of elasticity. Also, the creep evolution is mainly governed by the matrix behaviour and is more pronounced in CFRP composites with low volume of fibres [143].

1.3.1.2 Epoxy adhesive

A volumetric shrinkage between 2% and 7% is typically observed during the curing of an epoxy-based adhesive. When the adhesive is completely cured, the shrinkage coefficient variation becomes negligible to the point that the long-term behaviour is only creep-dependent [11]. In fact, epoxy-based adhesives exhibit relevant creep deformation when subjected to constant load. Additionally, the creep evolution of adhesives is highly influenced by level of applied stress and by the environmental conditions, such as temperature and humidity [3,11,144–146]. The creep behaviour of epoxy adhesives is frequently modelled using rheological models. **Figure 1.7** presents the three most used rheological models: (i) Maxwell model, (ii) Kelvin model, and (iii) Burger's model. Typically, these models are illustrated by means of Newtonian dashpots and Hookean springs that replicate, respectively, the viscous and elastic components of the adhesive's response. The Maxwell model (see **Figure 1.7a**) is a 2-parameter model that combines a spring with E_M

elasticity and a dashpot with η_M dynamic viscosity, in series. The Kelvin model is also a 2-parameter model that combines a spring with E_K elasticity and a dashpot with η_K dynamic viscosity, in parallel. The Burgers model is a 4-parameter model that results from the combination of the Maxwell model with the Kelvin model. The common configuration is depicted in **Figure 1.7c** as a combination in series of the Maxwell and Kelvin's models, but in alternative it can be presented as two Maxwell models in parallel. It is possible to generate other models like the generalized Kelvin model (several Kevin model connected in series) or the generalized Maxwell model (several Maxwell models connected in parallel).

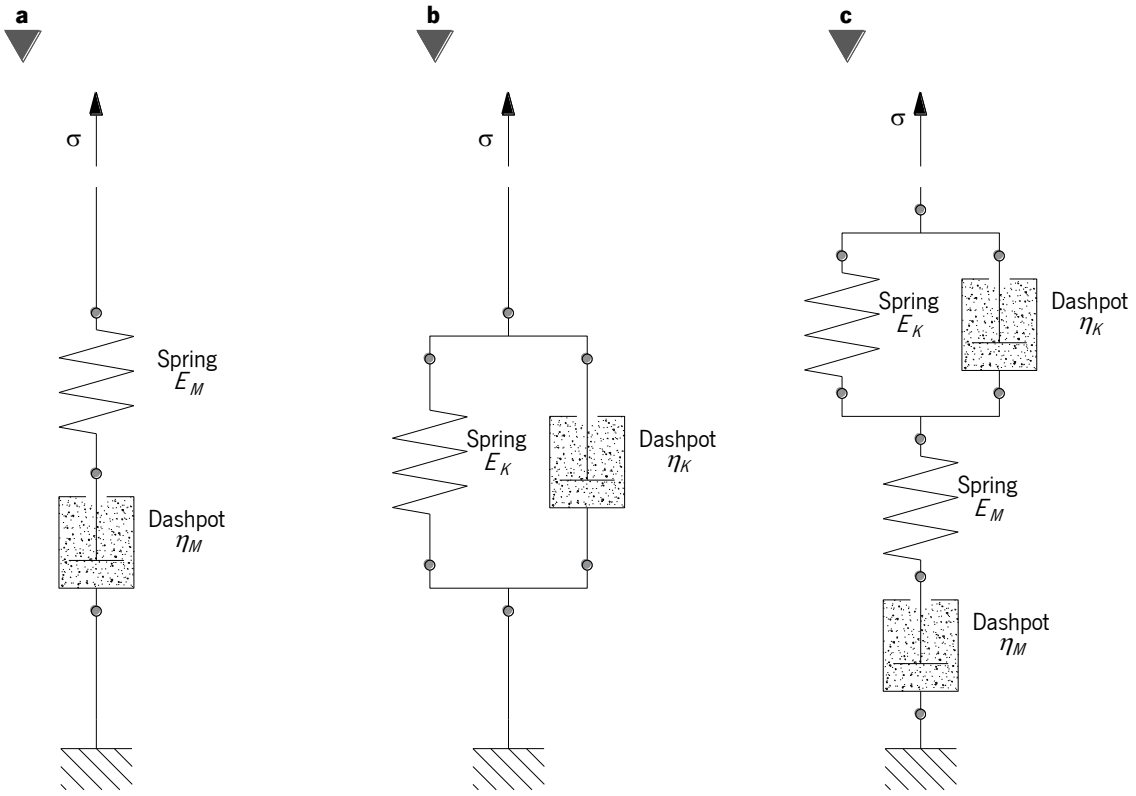

Figure 1.7: Rheological models: (a) Maxwell model; (b) Kelvin model; and (c) Burgers model (adapted from [11]).

Majda and Skrodzewicz [147] developed an experimental investigation on the creep behaviour of an epoxy adhesive. The experimental campaign included four levels of constant value of stress (33%, 43%, 54% and 65% of the ultimate tensile strength – 40 MPa), at a constant temperature of 22 °C, in order to determine the parameters of rheological models for the adhesive. The test results showed nonlinearity of creep strains for the two highest stress levels (57% and 65% of the ultimate

tensile strength). Using a nonlinear regression analysis, Majda and Skrodzewicz [147] were able to quantify the rheological properties and obtain a good fitting (Burger's model) to the experimental results. The authors also concluded that the stress level has a significant impact on the parameters of the Burger's model.

Costa and Barros [145] presented an experimental and analytical investigation on the tensile creep behaviour of an epoxy-based adhesive. Creep tests were carried out using three different load levels (20%, 40% and 60% of the adhesive's tensile strength), which were applied after 3 days of curing and kept for a period of 1000 h, in a climatic chamber with a constant temperature of 20 °C and 60% of relative humidity. The adhesive presented a linear viscoelastic behaviour for all the stress levels tested. During the creep tests the adhesive endured a deformation level that was two times higher than the ultimate strain measured on the material characterization (0.3%). As referred by Costa and Barros [145], the abovementioned observation indices that the epoxy is able of reorganizing its internal structure to continuously withstand more deformation without rupturing. The authors were also able to successfully obtain creep strain and creep modulus curves using the Burger's model in agreement with the experimental results.

Silva *et al.* [148] also presented an experimental and analytical study comprising tensile creep tests on an epoxy-based adhesive. The experimental program included: (i) adhesive specimens subjected to two stress levels (30% and 40% of the adhesive's tensile strength) for a predefined initial age (7 days of curing); and (ii) adhesive specimens subjected to equal stress level (30% of the adhesive's tensile strength) loaded at different loading age (1, 2, 3 and 7 days of curing). Based on the experimental results, the authors confirmed the viability of the principles of homogeneity and superposition on the epoxy adhesive. Also, specimens subjected to sustained stress at the earlier ages exhibit larger creep strains (creep coefficient of 4.1, 2.1, 1.9 and 1.3 for specimens loaded at 1, 2, 3 and 7 days of age, respectively). The Burger's model was used on the analytical analysis of the adhesive but, for specimens tested at early stages (when curing reactions are occurring), the model could not successfully simulate the creep recovery. Silva *et al.* [148] proposed a new framework, based on the generalized Kelvin model, for which a good fit to the experimental results of the creep tests was achieved.

1.3.1.3 FRP/Concrete interface

Meshgin *et al.* [47] presented an experimental and analytical study on the creep behaviour of epoxy at the interface between concrete and FRP. The experimental component of the study was composed by nine specimens subjected to constant shear stress for up to nine months period. The sustained load was applied after 1 and 7 days of curing. Results show that most of the creep deformation develops within relatively short period of time compared to the long creep period of concrete. Also, specimens subjected to the shear creep tests with 1 day of curing presented higher creep deformation than specimens loaded after 7 days of curing. Meshgin *et al.* [47] also stated that the magnitude of the sustained shear stress is a relevant factor and, when high shear stress was applied, unexpected failure (tertiary creep) occurred.

1.3.2 Prestressed FRP system

The knowledge on the long-term behaviour of RC structures strengthened with FRP reinforcements is fundamental for the acceptance of the EBR FRP systems on the construction industry. The works carried out over the last decade on this subject present an interesting feedback regarding the long-term behaviour and durability of the RC structures strengthened with CFRP, when the EBR technique is used.

Diab *et al.* [149] presented an experimental work on the short and long-term behaviour of prestressed FRP sheet anchorages. The experimental program included seven beams with prestressed FRP sheets with a prestress level that varied from 16.7% to 33.3% of the ultimate tensile strength. These specimens were kept in an outdoor environment, where the temperature varied between 7 °C and 30 °C, for a period of twenty months. Based on the strain measurements on the FRP sheet over the long-term test, the authors observed that the temperature did produce a significant effect on the middle span deflection of the beam and a negligible effect on the anchorage zones. Creep of the adhesive layer was considered the main reason for the observed prestress losses at the effective bond length (anchorage zone), whereas creep of the concrete and changes in the temperature were appointed responsible for the prestress losses beyond the effective bond length.

Michels *et al.* [64] presented long-term measurements on a 2.4 m long RC beam strengthened with a prestressed CFRP strip with gradient anchorage. A mean prestrain of 0.55% was measured in the middle part of the strip and the slab was kept in a laboratory environment. Over the period of 13 years, the level of prestrain only dropped from 0.55% to 0.51%, most likely due to creep of the concrete.

Czaderski and Meier [150] recently presented the results on two long-term monitoring campaigns: (i) a 47-year long monitoring campaign on a concrete beam with an epoxy bonded steel plate and (ii) a 20-year monitoring campaign on a road bridge with epoxy bonded CFRP strip. Regarding the first long-term monitoring campaign, in 1970 the strengthened RC beam was loaded using a four-point bending test with a constant load of 60 kN (30 kN in each load point), which represents 87% of the mean value of the failure load. The authors state that after 47 years, the beam is still in a good condition, despite some corrosion at the surface of the steel plate. The main creep occurs in the concrete in the compression zone and almost no creep takes place in the adhesive layer. Moreover, results show that the long-term high loading did not influence the externally bonded steel strips negatively. The second long-term monitoring campaign presented by Czaderski and Meier [150] reports a 20-year long monitoring on RC slab strengthened with CFRP strips. The strengthening was conducted in 1996 due to higher road loads and chloride contaminated concrete. Over the last 20 years, structural expansions and contractions due to the temperature seasonal variation (in between -10 °C and 25 °C) were observed. However, a visual inspection showed that the externally bonded CFRP laminates are still in good condition, despite the air humidity and foggy weather that is common in the outdoor environment where the slab is located.

1.4 Summary and research significance

The research works presented and discussed above have shown the significance of the durability on the performance of materials like CFRP and epoxy adhesives, and the interface between them. The number of available experimental data is particularly significant on water-based environments (e.g. wet-dry cycles or immersion on tap/deionized, salt-water and alkaline water), where, typically, specimens (material samples or composite specimens designed to test the bond between materials) are also exposed to high (up to 60 °C) or low (e.g. freeze-thaw cycles) temperatures. In

fact, from the experimental works above-mentioned, the synergy between immersion in water and high temperature is responsible for the highest reduction on the mechanical properties of both materials and on the interface strength. However, it should be noted that these research studies present differences in the type of materials, manufacturing process (e.g. curing time, temperature, and humidity), and exposure conditions (e.g. duration, temperature range, relative humidity, and salt concentration), which inevitably led to a non-negligible result dispersion. In general, CFRP materials present high durability in all the environments, except on alkali environment. The plasticization is a consequence of the water uptake, commonly observed on epoxy adhesives, which lead to a significant reduction on their mechanical properties and glass transition temperature. Results show that this phenomenon is lower on salt-water than on tap or demineralized, since water uptake is lower due to the osmotic effect present on environments with higher salt concentration (e.g. salt-water). Several research works have shown a direct relation between the durability of the epoxy adhesive and the epoxy-based bond between CFRP and concrete. The reduction on the mechanical properties of the epoxy tend to reduce the bond strength. Temperature is another key factor on the durability of epoxy adhesives and epoxy-based interfaces. The heating can improve the adhesive's mechanical properties due to post-curing phenomenon; however, tests have shown that testing epoxy samples and epoxy-based joints at high temperatures results in a significant reduction on the mechanical properties and bond strength/stiffness, respectively, especially, when exceeding the corresponding T_g's .

The long-term behaviour of CFRP, bonding agent and interface between materials were also considered on the literature review, for which a general conclusion could be observed. The relaxation and creep observed on the CFRP material can be neglected, mainly because, in general, CFRP materials have high fibre content. However, epoxy adhesives present a significant creep behaviour which is higher when the loading is applied in the early ages.

Despite the recent research developments on the durability and long-term behaviour of prestressed RC elements with FRPs, the effects of environmental exposure such as immersion in water, immersion in salt-water or wet/dry cycles with water, which may be considered critical on RC elements strengthened with prestressed EBR CFRP laminates, have not yet been addressed by the scientific community. Therefore, the present thesis serves as a contribution to this research gap.

1.5 Objectives

The present research work aims to give insights on two main literature gaps of prestressed EBR CFRP systems in reinforced concrete structures, mainly: (i) durability and (ii) long-term performance. The main objective of the research conducted in this thesis was to test, analyse and evaluate the durability, short and long-term structural behaviour of RC elements strengthened in flexure with pre-stressed CFRP laminates under various specific environmental conditions, load conditions and chemical degradation. In order to fulfil this goal two different anchorage systems were used: (i) the mechanical anchorage (MA) and (ii) the gradient anchorage (GA). With the development of this research work, it is expected a relevant contribution to the existing knowledge on this subject. It is also expected that the research derived from this thesis will constitute a valuable contribution for the definition and development of design guidelines, as to better accounting for the durability and long-term behaviour of RC members strengthened with prestressed CFRP laminate strips. The detailed objectives of the present thesis are as follows:

- To assess the influence of the CFRP strip geometry, prestrain level, surface preparation and anchorage system on the flexural response of RC slabs strengthened with EBR prestressed CFRP laminates strips;
- To assess the influence of different environmental conditions on the durability of RC slabs strengthened with prestressed CFRP laminates according to EBR technique. It includes the study on the effect of moisture, chlorides, and wet-dry cycling on both anchorage systems;
- To assess the short-term and long-term prestress losses for both anchorage systems: the Mechanical Anchorage (MA) system and the Gradient Anchorage (GA) system. In the same topic, it is a goal to study of the effect of different environmental conditions on the prestress losses;
- To assess of the creep effect on RC slabs strengthened with EBR prestressed CFRP laminates strips, and identification of the critical environmental conditions that might accelerate this effect;
- To assess the bond behaviour of the mechanical anchorage and study the influence of the CFRP strip geometry, level of transverse compression and temperature on the anchorage' performance;

- To extend the analysis of the experimental campaign with analytical formulations;
- Development of finite element analyses to simulate the experimental results obtained with RC slabs strengthened with EBR prestressed CFRP laminates strips for a better understanding the observed phenomena in the tests and extend the studies carried out.

This doctoral thesis was developed in the scope of the research project FRPreDur – "Short and long-term structural behaviour of concrete elements flexurally strengthened with prestressed CFRP laminates" (PTDC/ECM-EST/2424/2012) – funded by the Portuguese Foundation for Science and Technology (FCT). The overall research methodology is presented in **Figure 1.8**, and it incorporates three main tasks: (i) state-of-the-art review; (ii) experimental programme; (iii) numerical simulations.

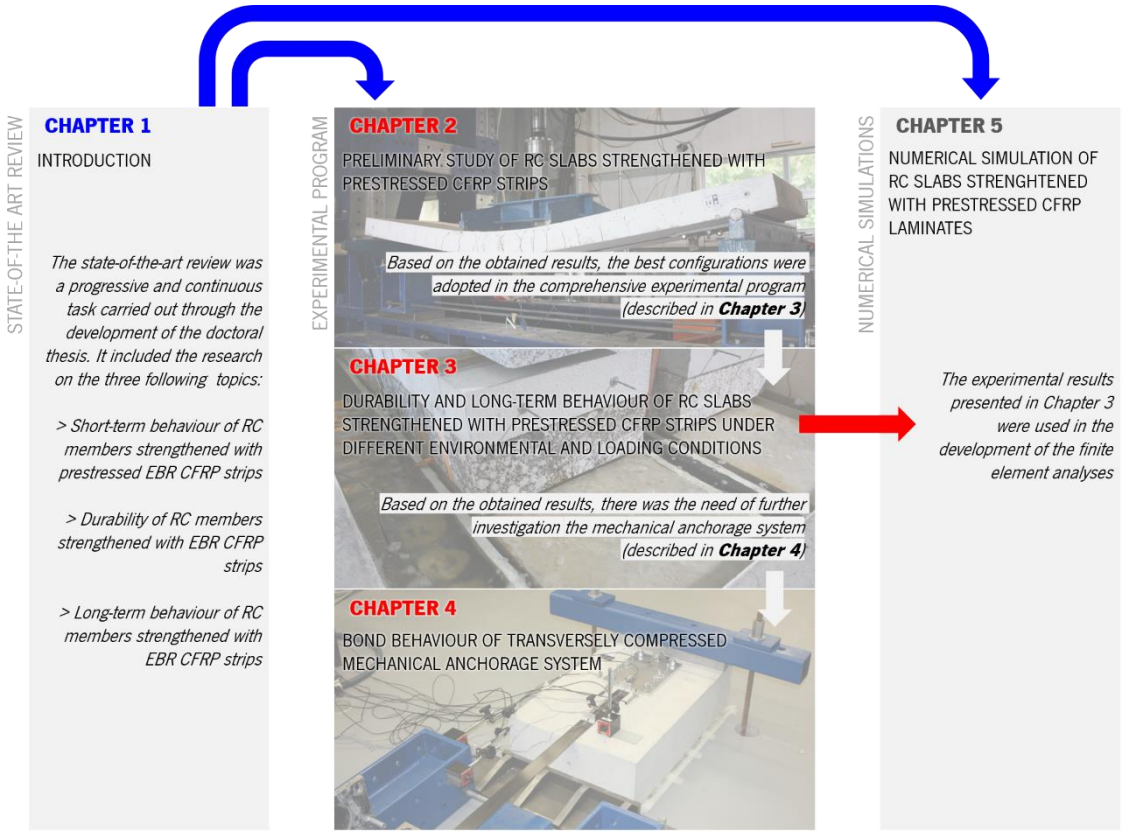

Figure 1.8: Research Methodology.

1.6 List of Publications

Several outcomes were obtained in the scope of the present doctoral thesis. The present section lists the main publications already published and under preparation.

Book (Editor)

1. Sena-Cruz, J.; Correia, L. (2015) "3º Seminário sobre o projeto de reforço de estruturas de betão com FRP's" http://hdl.handle.net/1822/37934

Papers published in ISI International Journals

1. Correia, L.; Teixeira, T.; Michels, J.; Almeida, J.; Sena-Cruz, J. (2015) "Flexural behaviour of RC slabs strengthened with prestressed CFRP strips using different anchorage systems", *Composites Part B: Engineering*, 81: 158-170. https://doi.org/10.1016/j.compositesb.2015.07.011
2. Sena-Cruz, J.; Michels, J.; Harmanci, Y.; Correia, L. (2015) "Flexural strengthening of RC slabs with prestressed CFRP strips using different anchorage systems", *Polymers*, 7: 2100-2118. https://doi.org/10.3390/polym7101502
3. Correia, L.; Sena-Cruz, J.; Michels, J.; França, P.; Pereira, E.; Escusa, G. (2017) "Durability of RC slabs strengthened with prestressed CFRP laminate strips under different environmental and loading conditions", *Composites Part B: Engineering*, 125: 71-88. https://doi.org/10.1016/j.compositesb.2017.05.047
4. Barris, C.; Correia, L.; Sena-Cruz, J. (2018) "Experimental study on the bond behaviour of a transversely compressed mechanical anchorage system for externally bonded reinforcement", *Composite Structures*, 200: 217-228. https://doi.org/10.1016/j.compstruct.2018.05.084.
5. Correia, L.; Barris, C.; França, P.; Sena-Cruz, J. (2018) "Effect of temperature on bond behavior of externally-bonded fiber-reinforced polymers with mechanical end anchorage system", *Journal of Composites for Construction* [Paper resubmitted on 12/02/2018 (Under Review Process)]
6. Correia, L.; Sena-Cruz, J.; Michels, J.; França, P. "Numerical simulation of RC slabs strengthened with prestressed CFRP strips using different anchorage systems" [Paper under preparation]
7. Correia, L.; Sena-Cruz, J.; Michels, J.; França, P. "An Experimental and Numerical study on the creep behaviour of RC slabs strengthened with prestressed CFRP strips under different environmental conditions" [Paper under preparation]

Papers published in National Journals

1. Correia, L.; Sena-Cruz, J.; Michels, J.; França, P. (2015) "Reforço à flexão de lajes de betão armado com laminados de CFRP pré-esforçados usando distintos métodos de ancoragem", *Revista de Engenharia Civil*, 51: 5-22. http://www.civil.uminho.pt/revista/artigos/n51/pag.5-22.pdf

Papers published in International Conferences

1. Correia, L.; Teixeira, T.; Sena-Cruz, J.; Michels, J. (2014) "Flexural strengthening of RC slabs with prestressed CFRP strips using different anchorage systems", *CICE2014 - The 7th International Conference on FRP Composites in Civil Engineering*, Vancover, Canada, 20-22 August 2014.
2. Sena-Cruz, J.; Correia, L.; Teixeira, T.; Michels; J. (2014). "Flexural strengthening of RC slabs with prestressed CFRP strips: serviceability and ultimate load state behaviour", *CBPAT - 1º Congresso Brasileiro de patologia das construções*, Foz do Iguaçu, Brazil, 21-23 May 2014.
3. Fernandes, P.; Silva, P. Correia, P.; Sena-Cruz, J. (2015) "Durability of an epoxy adhesive and a CFRP laminate under different exposure conditions", *SMAR2015 - The Third Conference on Smart Monitoring, Assessment and Rehabilitation of Structures*, Antalya, Turkey, 7-9 September 2015.
4. Sena-Cruz, J.; Correia, L.; Escusa, G.; Pereira, E.; Michels, J.; França, P. (2016) "Effect of distinct environmental actions on the durability of RC slabs strengthened with prestressed CFRP laminate strips", *SEMC2016 - Structural Engineering, Mechanics and Computation*, Cape Town, South Africa, 5-7 September 2016.
5. Sena-Cruz, J.; Correia, L.; Escusa, G.; Michels, J.; França, P. (2016) "Durability of RC slabs strengthened with prestressed CFRP laminate strips", *ACMBS - 7th International Conference on Advanced Composite Materials in Bridges and Structures*, Vancouver, Canada, 24-26 August 2016.
6. Barris, C.; Correia, L.; Sena-Cruz, J. (2017) "Experimental study on the bond behaviour of a transversely compressed mechanical anchorage system for externally bonded reinforcement", *APFIS2017 - 6th Asia-Pacific Conference on FRP in Structures*, Singapore, 19-21 July 2017.
7. Sena-Cruz, J.; Michels, J.; Correia, L.; Harmanci, Y.; Silva, P.; Gallego, J.; Fernandes, P.; Czaderski, C.; França, P. (2017) "Recent contributions from UMinho and Empa on durability issues of flexural strengthening of RC slab with EB CFRP laminates", *SMAR 2017 - Fourth International Conference on Smart Monitoring, Assessment and Rehabilitation of Civil Structures*, Zurich, Switzerland, 13-15 September 2017.
8. Sena-Cruz, J.; Correia, L.; França, P.; Michels, J. (2017) "Short and long-term behaviour of RC slabs strengthened with prestressed CFRP laminate strips", *39th IABSE Symposium – Engineering the Future*, Vancouver, Canada, 21-23 September 2017.

9. Sena-Cruz, J.; Correia, L.; Barris, C. (2018) "Behaviour of metallic anchorage plates for prestressing CFRP laminates under room and elevated temperatures", *IABSE/Spring 2018*, Kuala Lumpur, Malaysia, 25-27 April 2018.
10. Correia, L.; Barris, C.; Sena-Cruz, J. (2018) "Temperature effect on the bond behaviour of a transversely compressed mechanical anchorage system", *CICE 2018 - The 8th International Conference on FRP Composites in Civil Engineering*, Paris, France, 17-19 July 2018.

Papers published in National Conferences

1. Teixeira, T.; Correia, L.; Sena-Cruz, J.; Michels, J. (2014) "Reforço à flexão de lajes de betão armado com laminados de CFRP pré-esforçados: comportamento em estado limite último e de utilização", *JPEE - 5as Jornadas Portuguesas de Engenharia de Estruturas*, Lisbon, 26-28 November 2014.
2. Correia, L.; Sena-Cruz, J.; Michels, J.; França, P.; Teixeira, T. (2015) "Comportamento de lajes pré-esforçadas", *3º Seminário sobre o Projeto de Reforço de Estruturas de Betão com FRP's (SPREB-FRP 2015)*, University of Minho, Guimarães, 18 September 2015.
3. Fernandes, P.; Silva, P.; Correia, L.; Sena-Cruz, J. (2015) "Durabilidade de um adesivo epóxi e um laminado de CFRP expostos a distintas condições ambientais." *3º Seminário sobre o Projeto de Reforço de Estruturas de Betão com FRP's (SPREB-FRP 2015)*, University of Minho, Guimarães, 18 September 2015.
4. Correia, L.; Sena-Cruz, J.; França, P.; Michels, J.; Escusa, G.; Pereira, E. (2016) "Efeito de distintas condições ambientes na durabilidade de lajes de betão armado reforçadas com laminados de CFRP pré-esforçados", *BE2016 - Encontro Nacional Betão Estrutural*, Coimbra, 2-4 November 2016.
5. Sena-Cruz, J.; Correia, L.; Barris, C. (2018) "Efeito da temperatura no comportamento de ancoragens mecânicas para confinamento transversal de FRP" *BE2018 - Encontro Nacional Betão Estrutural*, Lisbon, 7-9 November 2018 [Under Review Process].
6. Correia, L.; Sena-Cruz, J.; França, P. (2018) "Estudos numéricos de lajes de betão armado reforçadas à flexão com laminados de CFRP pré-esforçados" *BE2018 - Encontro Nacional Betão Estrutural*, Lisbon, 7-9 November 2018 [Under Review Process].

1.7 Outline

The conducted scientific research work described in this thesis is organized in six chapters. The present Chapter 1 contains a brief introduction and review of the available literature and current understandings about the subjects covered in this research work. Then, it enumerates the main

objectives of the work, publications already developed and ends with the contents summary of each chapter of this thesis.

Chapter 2 presents the description, results and analysis of an experimental work of reinforced concrete slabs strengthened with prestressed CFRP laminates, using the mechanical anchorage (MA) system and the gradient anchorage (GA) system. This experimental work is composed of fourteen full-scale slabs with a total length of 2600 mm. The laminate geometry, level of prestress, surface preparation were the studied parameters. Some of the slabs were not strengthened to provide reference slabs. Based on the obtained results, the best configurations were adopted in the comprehensive experimental program developed to achieve the main objective of this thesis.

Chapter 3 includes the comprehensive experimental programme developed to achieve the main objective of this thesis. The monitoring of prestress losses, the mid-span vertical displacement and CFRP strain due to a creep loading, and the effect of four environmental actions were the main parameters studied. A total of twenty full-scale slabs compose this experimental campaign, which ended with a monotonic test up to failure. The obtained results were presented and discussed with reference to the relevant literature.

Chapter 4 presents another experimental campaign, composed of twenty-four large scale pull-out specimens. Each specimen intended to study the bond behaviour of the mechanical anchorage used on the prestressing of the aforementioned slabs. The studied parameters included the laminate geometry, the level of confinement stress, and temperature. The results were presented, compared with the existing literature and discussed.

Chapter 5 shows the developed numerical simulations used to further analyse the results obtained in Chapter 3. The selection of the constitutive material models for each constitutive material are elaborated in detail. The performance of these simulations was compared with experimental results. Using the calibrated models, further studies were performed.

Although the conclusions are included in each chapter, a summary of the work carried out is presented in Chapter 6. It is also presented the research needs for future work to be followed.

1.8 References

[1] Bakis CE, Bank LC, Brown VL, Cosenza E, Davalos JF, Lesko JJ, et al. Fiber-Reinforced Polymer Composites for Construction—State-of-the-Art Review. J Compos Constr 2002. doi:10.1061/(ASCE)1090-0268(2002)6:2(73).

[2] Zoghi M, editor. The International Handbook of FRP Composites in Civil Engineering. CRC Press; 2013.

[3] Silva PM da. Time-dependent behaviour and durability of RC slabs strengthened with NSM CFRP strips. University of Minho, 2017.

[4] Fernandes P. Bond behaviour of NSM CFRP-concrete systems: durability and quality control. University of Minho, 2016.

[5] FIB. Externally bonded FRP reinforcement for RC structures. 2001. doi:10.1016/0262-5075(85)90032-6.

[6] CNR. Guide for the design and construction of externally bonded FRP systems for strengthening existing structures. 2013.

[7] ACI 440.2R-08. Guide for the design and construction of externally bonded FRP systems for strengthening existing structures. 2008.

[8] Oehlers DJ, Seracino R, Smith ST. Design handbook for RC structures retrofitted with FRP and metal plates: beams and slabs HB 305-2008. Sydney: Standards Australia; 2018.

[9] CAN/CSA-S6-06. Canadian highway bridge design code. Ontario: National Standard of Canada; 2006.

[10] Juvandes LFP. Reforço e Reabilitação de Estruturas de Betão Usando Materiais Compósitos de " CFRP ". Luís Filipe Pereira Juvandes 1999.

[11] Pellegrino C, Sena-Cruz J. Design Procedures for the Use of Composites in Strengthening of Reinforced Concrete Structures: State-of-the-Art Report of the RILEM Technical Committee 234-DUC. 2016. doi:10.1007/978-94-017-7336-2.

[12] Sena-Cruz J. Strengthening of concrete structures with near-surface mounted CFRP laminate strips. University of Minho, 2004.

[13] Bilotta A, Ceroni F, Di Ludovico M, Nigro E, Pecce M, Manfredi G. Bond Efficiency of EBR and NSM FRP Systems for Strengthening Concrete Members. J Compos Constr 2011;15:757–72. doi:10.1061/(ASCE)CC.1943-5614.0000204.

[14] Seracino R, Raizal Saifulnaz MR, Oehlers DJ. Generic Debonding Resistance of EB and NSM Plate-to-Concrete Joints. J Compos Constr 2007;11:62–70. doi:10.1061/(ASCE)1090-0268(2007)11:1(62).

[15] Sena-Cruz JM, Barros JAO. Bond between Near-surface mounted carbond-fiber reinfroced polymer laminate strips and concrete. J Compos Constr 2004;8:519–27.

[16] De Lorenzis L, Teng JG. Near-surface mounted FRP reinforcement: An emerging technique for strengthening structures. Compos Part B Eng 2007;38:119–43. doi:10.1016/j.compositesb.2006.08.003.

[17] Coelho MRF, Sena-Cruz JM, Neves LAC. A review on the bond behavior of FRP NSM systems in concrete. Constr Build Mater 2015;93:1157–69. doi:10.1016/j.conbuildmat.2015.05.010.

[18] Ceroni F, Pecce M, Bilotta A, Nigro E. Bond behavior of FRP NSM systems in concrete elements. Compos Part B Eng 2012;43:99–109. doi:10.1016/j.compositesb.2011.10.017.

[19] Sena-Cruz JM, Barros JAO, Coelho MRF, Silva LFFT. Efficiency of different techniques in flexural strengthening of RC beams under monotonic and fatigue loading. Constr Build Mater 2012. doi:10.1016/j.conbuildmat.2011.10.044.

[20] Mazzotti C, Savoia M, Ferracuti B. A new single-shear set-up for stable debonding of FRP-concrete joints. Constr Build Mater 2009;23:1529–37. doi:10.1016/j.conbuildmat.2008.04.003.

[21] Chen J, Teng J. Anchorage Strength Models for FRP and Steel Plates. J Struct Eng 2001;127:784–91.

[22] Ceroni F, Pecce M. Evaluation of Bond Strength in Concrete Elements Externally Reinforced with CFRP Sheets and Anchoring Devices. J Compos Constr 2010. doi:10.1061/(ASCE)CC.1943-5614.0000118.

[23] El-Hacha R, Wight R, Green MF. Prestressed fibre-reinforced polymer laminates for strengthening structures. Prog Struct Eng Mater 2001;3:111–21. doi:10.1002/pse.76.

[24] Oehlers DJ, Visintin P, Lucas W. Fundamental mechanics governing FRP-retrofitted RC beams with anchored and prestressed FRP plates. J Compos Constr 2016;20:04015072. doi:10.1061/(ASCE)CC.

[25] Kalfat R, Smith ST. Anchorage devices used to improve the performance of reinforced concrete beams retrofitted with FRP composites : state-of-the-art review. J Compos Constr 2013;17:14–33. doi:10.1061/(ASCE)CC.1943-5614.0000276.

[26] Iovinella I, Prota A, Mazzotti C. Influence of surface roughness on the bond of FRP laminates to concrete. Constr Build Mater 2013. doi:10.1016/j.conbuildmat.2012.09.112.

[27] Mazzotti C, Bilotta A, Carloni C, Ceroni F, D'Antino T, Nigro E, et al. Bond between EBR FRP and concrete. In: Pellegrino C, Sena-Cruz J, editors. Des. Proced. Use Compos. Strength. Reinf. Concr. Struct. State-of-the-Art Rep. RILEM Tech. Comm. 234-DUC, Dordrecht: Springer Netherlands; 2016, p. 39–96. doi:10.1007/978-94-017-7336-2_3.

[28] Sena-Cruz J, Barros J, Coelho M. Bond between Concrete and Multi-Directional CFRP Laminates. Adv Mater Res 2010;133–134:917–22. doi:10.4028/www.scientific.net/AMR.133-134.917.

[29] Micelli F, Rizzo A, Galati D. Anchorage of composite laminates in RC flexural beams. Struct Concr 2010;11:117–26. doi:10.1680/stco.2010.11.3.117.

[30] Bank LC, Arora D. Analysis of RC beams strengthened with mechanically fastened FRP (MF-FRP) strips. Compos Struct 2007;79:180–91. doi:10.1016/J.COMPSTRUCT.2005.12.001.

[31] Mostofinejad D, Shameli SM. Externally bonded reinforcement in grooves (EBRIG) technique to postpone debonding of FRP sheets in strengthened concrete beams. Constr Build Mater 2013;38:751–8. doi:10.1016/J.CONBUILDMAT.2012.09.030.

[32] Mostofinejad D, Mahmoudabadi E. Grooving as Alternative Method of Surface Preparation to Postpone Debonding of FRP Laminates in Concrete Beams. J Compos Constr 2010. doi:10.1061/(ASCE)CC.1943-5614.0000117.

[33] Fernandes P, Granja JL, Benedetti A, Sena-Cruz J, Azenha M. Quality control and monitoring of NSM CFRP systems: E-modulus evolution of epoxy adhesive and its relation to the pull-out force. Compos Part B Eng 2015;75:95–103. doi:10.1016/J.COMPOSITESB.2015.01.021.

[34] França PM. Reinforced Concrete Beams Strenghtened with Prestressed CFRP Laminates. Lisbon Technical University - Instituto superior técnico (IST), 2007.

[35] Chaallal O, Nollet M-J, Perraton D. Strengthening of reinforced concrete beams with externally bonded fiber-reinforced-plastic plates: design guidelines for shear and flexure. Can J Civ Eng 1998;25:692–704. doi:10.1139/l98-008.

[36] Triantafillou TC, Antonopoulos CP. DESIGN OF CONCRETE FLEXURAL MEMBERS STRENGTHENED IN SHEAR WITH FRP. J Compos Constr 2000. doi:10.1061/(ASCE)1090-0268(2000)4:4(198).

[37] Sami R, Tarek H, Nahla H. Design recommendations for the use of FRP for reinforcement and strengthening of concrete structures. Prog Struct Eng Mater 2003;5:16–28. doi:10.1002/pse.139.

[38] International Federation for Structural Concrete (fib). Externally bonded FRP reinforcement for RC structures. Lausanne, Switzerland: 2001.

[39] Schweizer Ingenieur-und Architektenverein, (SIA). Klebebewehrungen (Externally Bonded Reinforcements). Zürich, Switzerland: 2004.

[40] TR55. Design guidance for strengthening concrete structures using fibre composite materials, Third Edition. Technical Report No. 55. UK: 2012.

[41] JSCE-CES41. RECOMMENDATIONS FOR UPGRADING OF CONCRETE STRUCTURES WITH USE OF CONTINUOUS FIBER SHEETS. Japan: 2001.

[42] ISIS Manual No. 4. Strengthening Reinforced Concrete Structures with Externally-bonded Fibre Reinforced Polymers. Canada: 2001.

[43] Motavalli M, Czaderski C, Pfyl-Lang K. Prestressed CFRP for Strengthening of Reinforced Concrete Structures: Recent Developments at Empa, Switzerland. J Compos Constr 2011. doi:10.1061/(ASCE)CC.1943-5614.0000125.

[44] Kotynia R, Walendziak R, Stoecklin I, Meier U. RC Slabs Strengthened with Prestressed and Gradually Anchored CFRP Strips under Monotonic and Cyclic Loading. J Compos Constr 2011. doi:10.1061/(ASCE)CC.1943-5614.0000081.

[45] Quantrill RJ, Hollaway LC. The flexural rehabilitation of reinforced concrete beams by the use of prestressed advanced composite plates. Compos Sci Technol 1998. doi:10.1016/S0266-3538(98)00002-5.

[46] Bryan PE, Green MF. Low temperature behaviour of CFRP prestressed concrete beams. Can J Civ Eng 1996.

[47] Meshgin P, Choi KK, Reda Taha MM. Experimental and analytical investigations of creep of epoxy adhesive at the concrete-FRP interfaces. Int J Adhes Adhes 2009. doi:10.1016/j.ijadhadh.2008.01.003.

[48] Mukherjee A, Rai GL. Performance of reinforced concrete beams externally prestressed with fiber composites. Constr Build Mater 2009. doi:10.1016/j.conbuildmat.2008.03.008.

[49] Yang D-S, Park S-K, Neale KW. Flexural behaviour of reinforced concrete beams strengthened with prestressed carbon composites. Compos Struct 2009;88:497–508. doi:10.1016/J.COMPSTRUCT.2008.05.016.

[50] Aram MR, Czadersk C, Motavalli M. Effects of Gradually Anchored Prestressed CFRP Strips Bonded on Prestressed Concrete Beams. J Compos Constr 2008;12:25–34.

[51] Woo SK, Nam JW, Kim JHJ, Han SH, Byun KJ. Suggestion of flexural capacity evaluation and prediction of prestressed CFRP strengthened design. Eng Struct 2008. doi:10.1016/j.engstruct.2008.06.013.

[52] Czaderski C, Motavalli M. 40-Year-old full-scale concrete bridge girder strengthened with prestressed CFRP plates anchored using gradient method. Compos Part B Eng 2007. doi:10.1016/j.compositesb.2006.11.003.

[53] Kim JHJ, Shi C, Bizindavyi L, Green MF. Applying Prestressed CFRP Sheets to Restore Prestress Losses in Prestressed Concrete Beams. ACI Spec Publ 2007;245:105–22.

[54] Svecova D, Razaqpur AG. Flexural behavior of concrete beams reinforced with carbon fiber-reinforced polymer (CFRP) prestressed prisms. ACI Struct J 2000.

[55] J. M. Lees, C. J. Burgoyne. Experimental study of influence of bond on flexural behavior of concrete beams pretensioned with aramid fiber reinforced plastics. Aci Struct J 1999.

[56] Kim YJ, Green MF, Fallis GJ. Repair of Bridge Girder Damaged by Impact Loads with Prestressed CFRP Sheets. J Bridg Eng 2008. doi:10.1061/(ASCE)1084-0702(2008)13:1(15).

[57] Kim YJ, Shi C, Green MF. Ductility and Cracking Behavior of Prestressed Concrete Beams Strengthened with Prestressed CFRP Sheets. J Compos Constr 2008. doi:10.1061/(ASCE)1090-0268(2008)12:3(274).

[58] Kim YJ, Green MF, Fallis GJ, Wight G, Eden R. Damaged Bridge Girder Strengthening. Concr Int 2006.

[59] El-Hacha R, Wight RG, Green MF. Prestressed Carbon Fiber Reinforced Polymer Sheets for Strengthening Concrete Beams at Room and Low Temperatures. J Compos Constr 2004. doi:10.1061/(ASCE)1090-0268(2004)8:1(3).

[60] El-Hacha R, Wight RG, Green MF. Flexural behaviour of concrete beams strengthened with prestressed carbon fibre reinforced polymer sheets subjected to sustained loading and low temperature. Can J Civ Eng 2004;31:239–52. doi:10.1139/l03-091.

[61] Wu ZS, Iwashita K, Hayashi K, Higuchi T, Murakami S, Koseki Y. Strengthening prestressed-concrete girders with externally prestressed PBO fiber reinforced polymer sheets. J Reinf Plast Compos 2003. doi:10.1177/0731684403035572.

[62] Wight RG, Green MF, Erki M-A. Prestressed FRP Sheets for Poststrengthening Reinforced Concrete Beams. J Compos Constr 2001. doi:10.1061/(ASCE)1090-0268(2001)5:4(214).

[63] Michels J, Barros J, Costa I, Sena-Cruz J, Czaderski C, Giacomin G, et al. Prestressed FRP Systems. In: Pellegrino C, Sena-Cruz J, editors. Des. Proced. Use Compos. Strength. Reinf. Concr. Struct. State-of-the-Art Rep. RILEM Tech. Comm. 234-DUC, Dordrecht: Springer Netherlands; 2016, p. 263–301. doi:10.1007/978-94-017-7336-2_7.

[64] Michels J, Sena-Cruz JJ, Czaderski C, Motavalli M. Structural Strengthening with Prestressed CFRP Strips with Gradient Anchorage. J Compos Constr 2013;17:651–61. doi:10.1061/(ASCE)CC.1943-5614.0000372.

[65] Smith ST, Teng JG. Shear-Bending Interaction in Debonding Failures of FRP-Plated RC Beams. Adv Struct Eng 2003;6:183–99. doi:10.1260/136943303322419214.

[66] Al-Amery R, Al-Mahaidi R. Coupled flexural–shear retrofitting of RC beams using CFRP straps. Compos Struct 2006;75:457–64. doi:10.1016/J.COMPSTRUCT.2006.04.037.

[67] Pham HB, Al-Mahaidi R. Prediction Models for Debonding Failure Loads of Carbon Fiber Reinforced Polymer Retrofitted Reinforced Concrete Beams. J Compos Constr 2006. doi:10.1061/(ASCE)1090-0268(2006)10:1(48).

[68] Yalim B, Kalayci AS, Mirmiran A. Performance of FRP-Strengthened RC Beams with Different Concrete Surface Profiles. J Compos Constr 2008. doi:10.1061/(ASCE)1090-0268(2008)12:6(626).

[69] Kim Y, Wight R, Green M. Flexural Strengthening of RC Beams with Prestressed CFRP Sheets: Using Nonmetallic Anchor Systems. J Compos Constr 2008;12:44–52. doi:https://doi.org/10.1061/(ASCE)1090-0268(2008)12:1(44).

[70] Kim Y, Wight R, Green M. Flexural strengthening of RC beams with prestressed CFRP sheets: Development of nonmetallic anchor systems. J Compos Constr 2008. doi:10.1061/(asce)1090-0268(2008)12:1(35).

[71] Garden HN, Hollaway LC. An experimental study of the influence of plate end anchorage of carbon fibre composite plates used to strengthen reinforced concrete beams. Compos

Struct 1998;42:175–88. doi:10.1016/S0263-8223(98)00070-1.

[72] Spadea G, Bencardino F, Swamy RN. Structural Behavior of Composite RC Beams with Externally Bonded CFRP. J Compos Constr 1998. doi:10.1061/(ASCE)1090-0268(1998)2:3(132).

[73] Jensen AP, Petersen CG, Poulsen E, Ottosen C, Thorsen T. On the anchorage to concrete of sika carbodur CFRP strips. Congr. Creat. with Concr., London.: Thomas Telford London.; 1999.

[74] Duthinh D, Starnes M. Strengthening of reinforced concrete beams with carbon FRP. Compos Constr 2001;I:493–498.

[75] Wu Y-F, Huang Y. Hybrid Bonding of FRP to Reinforced Concrete Structures. J Compos Constr 2008. doi:10.1061/(ASCE)1090-0268(2008)12:3(266).

[76] Lam L, Teng JG. Strength of RC Cantilever Slabs Bonded with GFRP Strips. J Compos Constr 2001. doi:10.1061/(ASCE)1090-0268(2001)5:4(221).

[77] Eshwar N, Ibell TJ, Nanni A. Effectiveness of CFRP Strengthening on Curved Soffit RC Beams. Adv Struct Eng 2005;8:55–68. doi:10.1260/1369433053749607.

[78] Zhang HW, Smith ST. Influence of FRP anchor fan configuration and dowel angle on anchoring FRP plates. Compos Part B Eng 2012;43:3516–27. doi:10.1016/J.COMPOSITESB.2011.11.072.

[79] Zhang HW, Smith ST. FRP-to-concrete joint assemblages anchored with multiple FRP anchors. Compos Struct 2012;94:403–14. doi:10.1016/J.COMPSTRUCT.2011.07.025.

[80] Zhang HW, Smith ST, Kim SJ. Optimisation of carbon and glass FRP anchor design. Constr Build Mater 2012;32:1–12. doi:10.1016/J.CONBUILDMAT.2010.11.100.

[81] Smith ST. Strengthening of concrete, metallic and timber construction materials with FRP composites. Adv. FRP Compos. Civ. Eng. Proc., 5th Int. Conf. FRP Compos. Civ. Eng. CICE 2010, Beijing: Tsinghue University Press; 2010.

[82] Michels J, Sena-Cruz J, Christen R, Czaderski C, Motavalli M. Mechanical performance of

cold-curing epoxy adhesives after different mixing and curing procedures. Compos Part B Eng 2016;98:434–43. doi:10.1016/j.compositesb.2016.05.054.

[83] Meier U, St¨ocklin I. A novel carbon fibre reinforced polymer (CFRP) system for post-strengthening. Int. Conf. Concr. Repair Rehabil. Retrofit., Cape Town, South Africa: 2005.

[84] Kim P, Meier H, Meier U. Anchorage device for high-performance fiber composite cables. EP19950914260, 1994.

[85] Wight R. Strengthening concrete beams with prestressed fibre reinforced polymer sheets. Queen's University, 1998.

[86] Barris C, Correia L, Sena-Cruz J. Experimental study on the bond behaviour of a transversely compressed mechanical anchorage system for externally bonded reinforcement. Compos Struct 2018;200:217–28. doi:10.1016/J.COMPSTRUCT.2018.05.084.

[87] Czaderski C. Strengthening of reinforced concrete members by prestressed, externally bonded reinforcement with gradient anchorage. ETH ZURICH, 2012.

[88] Michels J, Czaderski C, El-Hacha R, Brönnimann R, Motavalli M. Temporary bond strength of partly cured epoxy adhesive for anchoring prestressed CFRP strips on concrete. Compos Struct 2012;94:2667–76. doi:10.1016/J.COMPSTRUCT.2012.03.037.

[89] El-Hacha R, Elbadry M. Strengthening Concrete Beams with Externally Prestressed Carbon Fiber Composite Cables: Experimental Investigation. PTI J 2006;4:53–70.

[90] Aslam M, Shafigh P, Jumaat MZ, Shah SNR. Strengthening of RC beams using prestressed fiber reinforced polymers – A review. Constr Build Mater 2015;82:235–56. doi:10.1016/J.CONBUILDMAT.2015.02.051.

[91] Liao K, Schultheisz CR, Hunston DL, Brinson LC. Long-term durability of fiber-reinforced polymer-matrix composite materials for infrastructure applications: A review. J Adv Mater 1998.

[92] ISIS Manual No. 8. Durability of FRP Composites for Construction. 2006.

[93] Karbhari VM, Ghosh K. Comparative durability evaluation of ambient temperature cured

externally bonded CFRP and GFRP composite systems for repair of bridges. Compos Part A Appl Sci Manuf 2009;40:1353–63. doi:10.1016/J.COMPOSITESA.2009.01.011.

[94] Ferreira RM. Avaliação dos ensaios de durabilidade do betão. Univerity of Minho, 2010.

[95] Shi X, Xie N, Fortune K, Gong J. Durability of steel reinforced concrete in chloride environments: An overview. Constr Build Mater 2012. doi:10.1016/j.conbuildmat.2011.12.038.

[96] ACI 201. 201.2R-08 Guide to Durable Concrete. Concrete 2008. doi:9780870312847.

[97] Mehta PK, Monteiro PJM. Concrete: microstructure, properties, and materials. 2006. doi:10.1036/0071462899.

[98] Richardson MG. Fundamentals of durable reinforced concrete. 2003. doi:10.1007/s13398-014-0173-7.2.

[99] Cabral-Fonseca S, Nunes JP, Rodrigues MP, Eusébio MI. Durability of carbon fibre reinforced polymer laminates used to reinforced concrete structures. Sci Eng Compos Mater 2011;18:201–7. doi:https://doi.org/10.1515/SECM.2011.041.

[100] Grace NF. Concrete repair with CFRP. Concr Int 2004;26:45–51.

[101] Soutis C, Turkmen D. Moisture and Temperature Effects of the Compressive Failure of CFRP Unidirectional Laminates. J Compos Mater 1997;31:832–49. doi:10.1177/002199839703100805.

[102] Browning C, Husman G, Whitney J. Moisture Effects in Epoxy Matrix Composites - AFML-TR-77-17. OHIO: 1977.

[103] Bank LC, Gentry TR, Barkatt A. Accelerated Test Methods to Determine the Long-Term Behavior of FRP Composite Structures: Environmental Effects. J Reinf Plast Compos 1995;14:559–87. doi:10.1177/073168449501400602.

[104] Mouritz A, Gibson A. Fire Properties of Polymer Composite Materials. Netherlands: Springer, Dordrecht; 2006. doi:https://doi.org/10.1007/978-1-4020-5356-6.

[105] Brinson HF, Brinson LC. Polymer engineering science and viscoelasticity: An introduction.

2008. doi:10.1007/978-0-387-73861-1.

[106] Carolin A. Carbon Fibre Reinforced Polymers for Strengthening of Structural Elements. 2003.

[107] Reed RP, Golda M. Cryogenic properties of unidirectional composites. Cryogenics (Guildf) 1994. doi:10.1016/0011-2275(94)90077-9.

[108] Micelli F, Nanni A. Durability of FRP rods for concrete structures. Constr Build Mater 2004. doi:10.1016/j.conbuildmat.2004.04.012.

[109] Lin YC, Chen X. Moisture sorption–desorption–resorption characteristics and its effect on the mechanical behavior of the epoxy system. Polymer (Guildf) 2005;46:11994–2003. doi:10.1016/J.POLYMER.2005.10.002.

[110] Savvilotidou M, Vassilopoulos AP, Frigione M, Keller T. Development of physical and mechanical properties of a cold-curing structural adhesive in a wet bridge environment. Constr Build Mater 2017;144:115–24. doi:10.1016/J.CONBUILDMAT.2017.03.145.

[111] Savvilotidou M, Vassilopoulos AP, Frigione M, Keller T. Effects of aging in dry environment on physical and mechanical properties of a cold-curing structural epoxy adhesive for bridge construction. Constr Build Mater 2017;140:552–61. doi:10.1016/J.CONBUILDMAT.2017.02.063.

[112] Sousa JM, Correia JR, Cabral-Fonseca S. Durability of an epoxy adhesive used in civil structural applications. Constr Build Mater 2018. doi:10.1016/j.conbuildmat.2017.11.168.

[113] Yang Q, Xian G, Karbhari VM. Hygrothermal ageing of an epoxy adhesive used in FRP strengthening of concrete. J Appl Polym Sci 2008. doi:10.1002/app.27287.

[114] Moussa O, Vassilopoulos AP, Keller T. Effects of low-temperature curing on physical behavior of cold-curing epoxy adhesives in bridge construction. Int J Adhes Adhes 2012. doi:10.1016/j.ijadhadh.2011.09.001.

[115] S&P. Resin 220 epoxy adhesive, technical datasheet. Seewen, Switzerland: 2013.

[116] Sika. Sikadur®-30 PRODUCT DATA SHEET. Dublin, Ireland: 2017.

[117] Frigione M, Naddeo C, Acierno D. Cold-curing epoxy resins: Aging and environmental effects. I-Thermal properties. J Polym Eng 2001. doi:10.1515/POLYENG.2001.21.1.23.

[118] Frigione M, Naddeo C, Acierno D. Cold-curing epoxy resins: Aging and environmental effects. II-mechanical properties. J Polym Eng 2001. doi:10.1515/POLYENG.2001.21.4.349.

[119] Karbhari VM, Chin JW, Hunston D, Benmokrane B, Juska T, Morgan R, et al. Durability gap analysis for fiber-reinforced polymer composites in civil infrastructure. J Compos Constr 2003. doi:10.1061/(ASCE)1090-0268(2003)7:3(238).

[120] Choi S, Gartner AL, Etten N Van, Hamilton HR, Douglas EP. Durability of Concrete Beams Externally Reinforced with CFRP Composites Exposed to Various Environments. J Compos Constr 2012. doi:10.1061/(ASCE)CC.1943-5614.0000233.

[121] Lai WL, Kou SC, Poon CS, Tsang WF, Lai CC. Effects of elevated water temperatures on interfacial delaminations, failure modes and shear strength in externally-bonded CFRP-concrete beams using infrared thermography, gray-scale images and direct shear test. Constr Build Mater 2009;23:3152–60. doi:10.1016/J.CONBUILDMAT.2009.06.012.

[122] Kabir MI, Shrestha R, Samali B. Effects of applied environmental conditions on the pull-out strengths of CFRP-concrete bond. Constr Build Mater 2016;114:817–30. doi:10.1016/J.CONBUILDMAT.2016.03.195.

[123] Mahdie M, Davood M, Majid B. Effects of Surface Preparation Method on FRP-Concrete Bond Strength under Alkaline Conditions. J Compos Constr 2017;21. doi:10.1061/(ASCE)CC.1943-5614.0000786.

[124] Francesca C, Antonio B, Vittorio G, Antonio O. Effects of Environmental Conditioning on the Bond Behavior of FRP and FRCM Systems Applied to Concrete Elements. J Eng Mech 2018;144. doi:10.1061/(ASCE)EM.1943-7889.0001375.

[125] Karbhari VM, Engineer M. Effect of Environmental Exposure on the External Strengthening of Concrete with Composites-Short Term Bond Durability. J Reinf Plast Compos 1996;15:1194–216. doi:10.1177/073168449601501202.

[126] Karbhari VM, Engineer M, Eckel DA. On the durability of composite rehabilitation schemes for concrete: Use of a peel test. J Mater Sci 1997. doi:10.1023/A:1018591619404.

[127] Benzarti K, Chataigner S, Quiertant M, Marty C, Aubagnac C. Accelerated ageing behaviour of the adhesive bond between concrete specimens and CFRP overlays. Constr Build Mater 2011. doi:10.1016/j.conbuildmat.2010.08.003.

[128] Li H, Xian G, Lin Q, Zhang H. Freeze-thaw resistance of unidirectional-fiber-reinforced epoxy composites. J Appl Polym Sci 2012. doi:10.1002/app.34870.

[129] Chajes MJ, Thomson TA, Farschman CA. Durability of concrete beams externally reinforced with composite fabrics. Constr Build Mater 1995. doi:10.1016/0950-0618(95)00006-2.

[130] Yun Y, Wu YF. Durability of CFRP-concrete joints under freeze-thaw cycling. Cold Reg Sci Technol 2011. doi:10.1016/j.coldregions.2010.11.008.

[131] Subramaniam K V., Ali-Ahmad M, Ghosn M. Freeze-thaw degradation of FRP-concrete interface: Impact on cohesive fracture response. Eng Fract Mech 2008. doi:10.1016/j.engfracmech.2007.12.016.

[132] Pan Y, Xian G, Li H. Effects of Freeze-Thaw Cycles on the Behavior of the Bond between CFRP Plates and Concrete Substrates. J Compos Constr 2018;22. doi:10.1061/(ASCE)CC.1943-5614.0000846.

[133] Harmanci YE, Michels J, Czaderski C, Loser R, Chatzi E. Long-term residual anchorage resistance of gradient anchorages for prestressed CFRP strips. Compos Part B Eng 2018;139:171–84. doi:https://doi.org/10.1016/j.compositesb.2017.11.062.

[134] Firmo JP, Correia JR, Pitta D, Tiago C, Arruda MRT. Experimental characterization of the bond between externally bonded reinforcement (EBR) CFRP strips and concrete at elevated temperatures. Cem Concr Compos 2015;60:44–54. doi:https://doi.org/10.1016/j.cemconcomp.2015.02.008.

[135] Cabral-Fonseca S, Correia JR, Custódio J, Silva HM, Machado AM, Sousa J. Durability of FRP - concrete bonded joints in structural rehabilitation: A review. Int J Adhes Adhes 2018;83:153–67. doi:10.1016/J.IJADHADH.2018.02.014.

[136] Cromwell JR, Harries KA, Shahrooz BM. Environmental durability of externally bonded FRP materials intended for repair of concrete structures. Constr Build Mater 2011;25:2528–39. doi:10.1016/J.CONBUILDMAT.2010.11.096.

[137] Toutanji HA, Gómez W. Durability characteristics of concrete beams externally bonded with FRP composite sheets. Cem Concr Compos 1997;19:351–8. doi:10.1016/S0958-9465(97)00028-0.

[138] Bažant ZP. Prediction of concrete creep and shrinkage: Past, present and future. Nucl Eng Des 2001. doi:10.1016/S0029-5493(00)00299-5.

[139] Bažant ZP, Wittmann FH. Creep and shrinkage in concrete structures. Wiley Chichester; 1982.

[140] Wang W-W, Dai J-G, Harries KA, Bao Q-H. Prestress Losses and Flexural Behavior of Reinforced Concrete Beams Strengthened with Posttensioned CFRP Sheets. J Compos Constr 2012. doi:10.1061/(ASCE)CC.1943-5614.0000255.

[141] Dolan CW, Hamilton HR, Bakis CE, Nanni A. Design recommendations for concrete structures prestressed with FRP tendons. 2001. doi:10.1097/01.AOG.0000429656.01094.69.

[142] Ascione F, Berardi VP, Feo L, Giordano A. An experimental study on the long-term behavior of CFRP pultruded laminates suitable to concrete structures rehabilitation. Compos Part B Eng 2008. doi:10.1016/j.compositesb.2008.03.008.

[143] Ascione L, Berardi VP, D'Aponte A. A viscoelastic constitutive law for FRP materials. Int J Comput Methods Eng Sci Mech 2011. doi:10.1080/15502281003660211.

[144] Meyers MA, Chawla K. Mechanical behavior of materials. Cambridge university press Cambridge; 2009.

[145] Costa I, Barros J. Tensile creep of a structural epoxy adhesive: Experimental and analytical characterization. Int J Adhes Adhes 2015. doi:10.1016/j.ijadhadh.2015.02.006.

[146] Costa I, Barros J. Creep of structural adhesives: an overview. Cice 2012 2012.

[147] Majda P, Skrodzewicz J. A modified creep model of epoxy adhesive at ambient temperature. Int J Adhes Adhes 2009. doi:10.1016/j.ijadhadh.2008.07.010.

[148] Silva PP, Fernandes P, Sena-Cruz JJ, Xavier JJJ, Castro F, Soares D, et al. Effects of different environmental conditions on the mechanical characteristics of a structural epoxy. Compos Part B Eng 2016;88:55–63. doi:10.1016/J.COMPOSITESB.2015.10.036.

[149] Diab H, Wu Z, Iwashita K. Short and long-term bond performance of prestressed FRP sheet anchorages. Eng Struct 2009;31:1241–9. doi:https://doi.org/10.1016/j.engstruct.2009.01.021.

[150] Czaderski C, Meier U. EBR Strengthening Technique for Concrete, Long-Term Behaviour and Historical Survey. Polymers (Basel) 2018;10.

CHAPTER 2

PRELIMINARY STUDIES OF RC SLABS STRENGTHENED WITH PRESTRESSED CFRP STRIPS

2.1 Introduction

As stated in the previous chapter, the main objective of this thesis is to study the short and long-term behaviour and durability of reinforced concrete slabs strengthened with prestressed CFRP laminates. In this research, two anchorage systems which play key role in the success of the strengthening technique, were studied: (i) the mechanical anchorage (MA) system and (ii) the gradient anchorage (GA) system.

The geometry and materials used in the present work outcomes from the experience acquired from previous work developed at the University of Minho [1], [2]. However, due to several uncertainties, at the onset of this experimental work the influence of several other parameters like the concrete surface treatment, the laminate geometry and level of prestress on the behaviour of the prestressing system were analysed. Thus, a preliminary experimental work was carried out composed of fourteen reinforced concrete (RC) slabs. Based on the obtained results, the best configurations were adopted in the comprehensive experimental program developed to achieve the main objective of this thesis (additional details are given in Chapter 3).

In this chapter, detailed information about the specimens and test configuration, materials, prestressing and anchorage systems, and surface preparation are initially presented. Then, the obtained results are reported focusing the main aspects at service and ultimate conditions. Finally, the principal conclusions are highlighted at the end of the chapter.

Part of the work herein described has been already published in three journal papers [3]–[5] and several conference [6]–[8] papers.

2.2 Experimental programme

This preliminary experimental programme was composed of fourteen slabs, divided into two series according to the surface preparation method: in series GD, composed of ten reinforced concrete (RC) slabs, the concrete surface region where the FRP reinforcement was installed was treated by means of grinding with a stone wheel, whereas in series SB the surface preparation of the three RC slabs was performed by sand blasting. In both cases the main aim was to remove the weak concrete laitance layer and expose the aggregates of the substrate. Three slabs were used as control

specimens (GD_REF1, GD_REF_2 and SB_REF_3). Four slabs were strengthened with a simple CFRP laminate strip according to the EBR technique without any prestressing (GD_EBR_L50×1.4, GD_EBR_L50×1.2, GD_EBR_L80×1.2, and SB_EBR_L50×1.2). The remaining seven slabs were strengthened with one externally bonded prestressed CFRP laminate strip with either a mechanical anchorage (MA) or a gradient anchorage (GA). As it is shown in **Table 2.1**, all specimens are labelled with a generic denomination: X_Y_LZ, where X is the specimen series (GD or SB), Y is the type of anchorage (MA or GA, or EBR for specimens strengthened with an unstressed CFRP laminate), and Z is the cross-section geometry of the laminate strip in millimetres (L50×1.4, L50×1.2 or L80×1.2). The three control specimens are also labelled with the specimen series and a differentiator suffix (REF_1, REF_2 and REF_3). The main goal of the prestress application was to duplicate the carrying capacity of an unstrengthened slab.

Table 2.1
Experimental programme.

Specimen	**Anchorage System**	**CFRP Strip** [mm]	**Initial Strain** [%]	**Prestress Force** [kN]	**Concrete Batch**	**Surface Preparation**
Series GD						
GD_REF_1	–	–	–	–	B1	Grinding
GD_EBR_L50x1.4	–	50 × 1.4	0.00	0.00	B1	Grinding
GD_MA_L50x1.4	MA	50 × 1.4	0.40	43.1	B1	Grinding
GD_GA_L50x1.4	GA	50 × 1.4	0.41	43.9	B1	Grinding
GD_EBR_L50x1.2	–	50 × 1.2	0.00	0.00	B2	Grinding
GD_MA_L50x1.2	MA	50 × 1.2	0.42	42.2	B2	Grinding
GD_REF_2	–	–	–	–	B3	Grinding
GD_EBR_L80x1.2	–	80 × 1.2	0.00	0.00	B3	Grinding
GD_MA_L80x1.2	MA	80 × 1.2	0.40	63.1	B3	Grinding
GD_GA_L80x1.2	GA	80 × 1.2	0.41	64.1	B3	Grinding
Series SB						
SB_REF_3	–	–	–	–	B4	Sand Blasting
SB_EBR_L50x1.2	–	50 × 1.2	0.00	0.00	B4	Sand Blasting
SB_MA_L50x1.2	MA	50 × 1.2	0.42	41.6	B4	Sand Blasting
SB_GA_L50x1.2	GA	50 × 1.2	0.40	39.2	B4	Sand Blasting

Notes: GA = Gradient Anchorage; MA = Mechanical Anchorage.

2.2.1 Specimens and test configuration

The specimens' geometry and test configuration are shown in **Figure 2.1**. The slabs have a total length of 2600 mm, the rectangular cross section is 600 mm wide and 120 mm thick. The upper and lower longitudinal inner reinforcement is composed of three steel bars with a diameter of 6 mm (3Ø6) and five bars with diameter 8 mm (5Ø8), respectively. Secondary and transverse reinforcement composed by closed steel stirrups of Ø6 at 300 mm spacing is also used. Three types of CFRP laminates strips (50 × 1.2 [mm], 50 × 1.4 [mm] and 80 × 1.2 [mm]) with 2200 mm of length are used as external reinforcement. The longitudinal lower steel reinforcement (5Ø8) corresponds to a longitudinal reinforcement ratio, ρ_l, equal to 0.35%. Assuming a modulus of elasticity for steel (E_s) of 224 GPa, and a modulus of elasticity for the CFRP laminate (E_f) of 163 GPa (average values from experimental characterization, see Section 2.2.2), an equivalent longitudinal reinforcement ratio, $\rho_{l,eq}$, of 0.41%, 0.42% and 0.44% is obtained with the CFRP laminate strip of 50 × 1.2 [mm], 50 × 1.4 [mm], and 80 × 1.2 [mm], respectively.

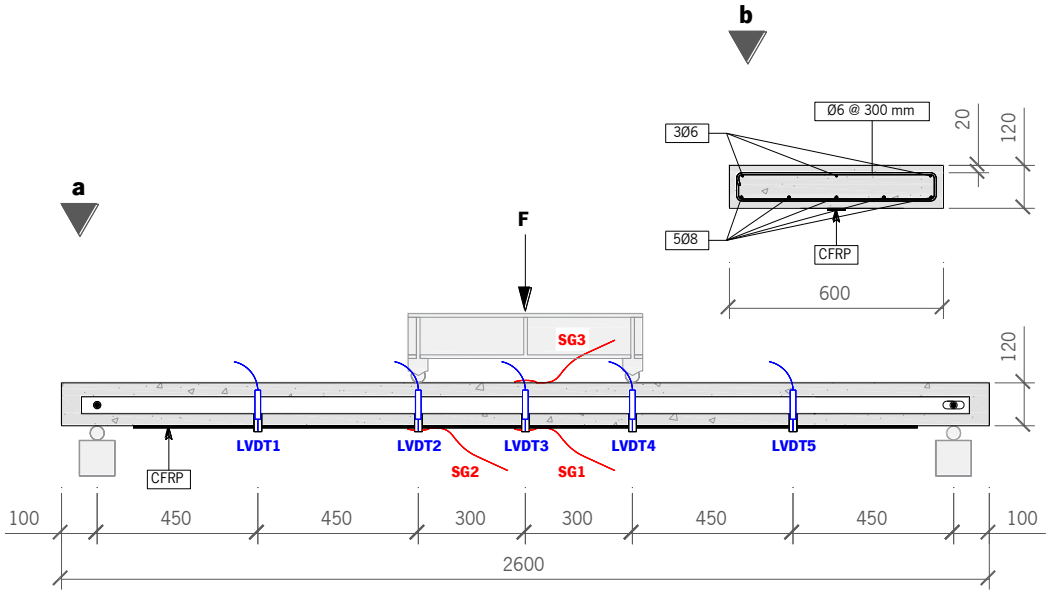

Figure 2.1: Specimen's geometry and test configuration. Note: All units are in millimetres.

In order to assess the service and ultimate behaviour of all specimens, quasi static monotonic tests up to failure were performed using a four-point bending configuration. A clear and shear spans of 2400 mm and 900 mm were adopted, respectively. The later corresponds to 9 times the effective depth. The instrumentation included 5 linear variable differential transducers (LVDT1 to LVDT5) to record the deflection along the longitudinal axis of the slab; 3 strain gauges (SG1 to SG3) with the

aim of measuring the strain in the laminate and concrete; and 1 load cell used to measure the applied load (F). **Figure 2.1** shows the position of each LVDT: three in the pure bending zone with the range of ±75 mm and a linearity error of ±0.10% and two between the supports and the applied load points with a range of ±25 mm and the same linearity error. The load cell used has a maximum measuring capacity of 200 kN and a linear error of ±0.05%. Two different strain gauge types were used: (i) two TML BFLA-5-3 strain sensors (SG1 and SG2) glued on the CFRP laminate surface at the mid-span and at the force application point; and, (ii) one TML PFL-30-11-3L strain sensor (SG3) for measuring the concrete strain at the mid-span. All tests were carried out with a servo-controlled equipment under displacement control in the actuator at a rate of 1.2 mm/min. The crack width evolution was measured during the test through a handheld USB microscope (model VEHO VMS-004 D microscope, with a native resolution of 640×480 pixels and magnification capacity up to 400×). In the present experimental program, the crack width acquisition was done with a magnification factor of 20× up to predefined applied load.

2.2.2 Materials

The material characterization included the evaluation of the mechanical properties of the materials involved in this experimental program, namely concrete, steel, CFRP laminate strip and epoxy adhesive.

Four batches (B1 to B4) were used to cast the RC slabs (see **Table 2.1**). Concrete characterization included evaluation of the modulus of elasticity (E_c) and compressive strength (f_c) through LNEC E397-1993:1993 [9] and NP EN 12390-3:2011 [10] recommendations, respectively. For each concrete batch six cylindrical specimens with 300 mm of height and 150 mm of diameter were used. **Table 2.2** shows the obtained results at the testing day. The average compressive strength of series GD was about 53 MPa, whereas for the series SB was about 40 MPa.

The tensile properties of the steel reinforcement were assessed throughout the NP EN ISO 6892-1:2012 [11] standard. A minimum of three specimens were used for each bar type. **Table 2.2** includes the modulus of elasticity (E_s) as well as the yield (f_y) and ultimate (f_u) strengths obtained from the tensile tests. The average value of the E_s was about 212 GPa and 235 GPa for the lower longitudinal steel reinforcement in series GD and SB, respectively. The steel

of the longitudinal bars and stirrups has a denomination of A400 NR SD according to the NP EN 1992-1-1:2010 [12].

Table 2.2
Material characterization (average values).

Material	Series	Modulus of elasticity [GPa]	Compressive strength [MPa]	Tensile strength [MPa]	Yield strength [MPa]	Ultimate strength [MPa]
Concrete						
Batch: B1	GD	32.2 (7.5%)	53.4 (4.3%)	–	–	–
Batch: B2	GD	32.6 (0.1%)	57.4 (3.0%)	–	–	–
Batch: B3	GD	30.7 (n.a.)	49.5 (3.1%)	–	–	–
Batch: B4	SB	30.0 (n.a.)	40.2 (0.7%)	–	–	–
Steel						
Bar type: Ø6	GD	209.5 (8.5%)	–	–	579.3 (3.3%)	669.7 (1.7%)
Bar type: Ø6	SB	206.9 (0.4%)	–	–	519.4 (6.1%)	670.2 (5.1%)
Bar type: Ø8	GD	212.8 (9.7%)	–	–	501.4 (5.9%)	593.9 (3.9%)
Bar type: Ø8	SB	235.1 (4.6%)	–	–	595.9 (4.1%)	699.0 (2.1%)
CFRP						
50×1.4 [mm]	GD	154.8 (4.6%)	–	2457.1 (1.2%)	–	–
50×1.2 [mm]	GD	167.7 (2.9%)	–	2943.5 (1.6%)	–	–
80×1.4 [mm]	GD	164.6 (0.2%)	–	2455.3 (5.0%)	–	–
50×1.2 [mm]	SB	164.0 (3.1%)	–	2374.9 (2.5%)	–	–

Note: the values between parentheses are the corresponding coefficients of variation (CoV).

The CFRP laminate strips used in the experimental work, with a trade mark CFK 150/2000 were produced by S&P Clever Reinforcement Ibérica Lda. These CFRP reinforcements consist of unidirectional carbon fibres held together by an epoxy vinyl ester resin matrix, produced by pultrusion. This type of CFRP laminate presents smooth external surface. The modulus of elasticity (E_f) and tensile strength (f_f) were obtained from tests performed according to the ISO 527-5:1997 [13] standard. Four and six samples were used for GD and SB series, respectively. The obtained values are in agreement with the information provided by the manufacturing company, i.e. E_f higher than 150 GPa and f_f higher than 2000 MPa.

The S&P Resin 220 epoxy adhesive®, produced by the same supplier as for the CFRP laminate, was used as bond agent to fix the reinforcements to the concrete substrate. In the scope of the present experimental program the epoxy adhesive was not characterized. However, in a previous experimental program the same adhesive was characterized, after 7 days of curing at 22 °C, and a Young modulus of 7.7 GPa (CoV=3.1%) and a tensile strength of 20.7 MPa (CoV=9.9%) were obtained [14].

2.2.3 Prestressing and Anchorage Systems

As referred before, two distinct end-anchorage systems were investigated: (i) the mechanical anchorage (MA) which uses steel plates at the ends of the FRP reinforcement, and (ii) the gradient anchorage (GA), which is produced by sector-wise heating of the adhesive and a step-wise releasing of the prestressed force F_p. These commercially available systems from the same supplier as for the CFRP reinforcement and adhesive, present several common and specific equipment. These are presented in **Figure 2.2**.

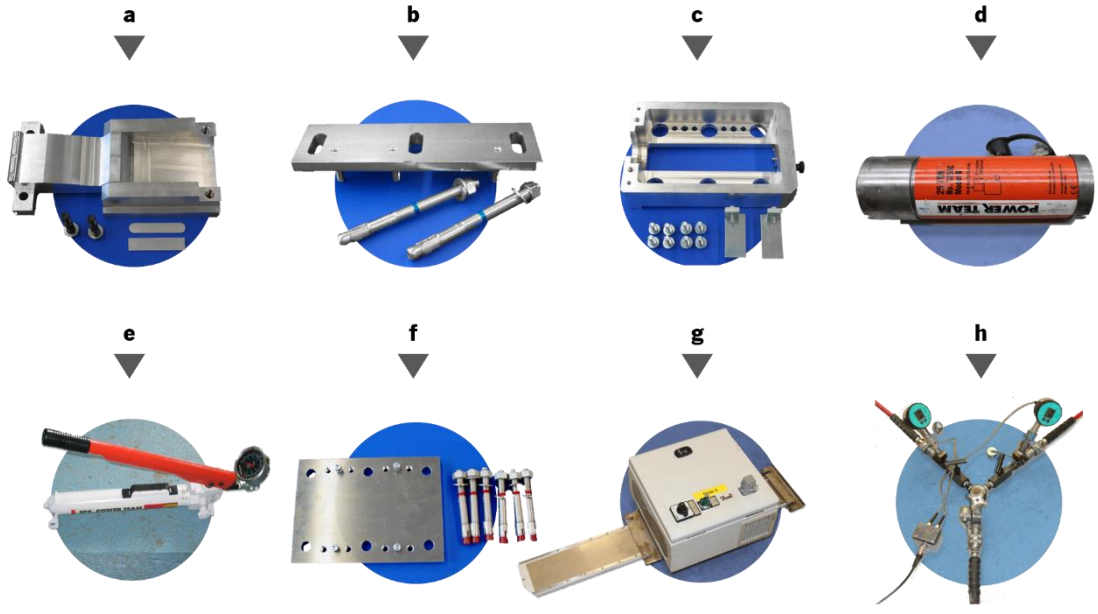

Figure 2.2: Equipment composing the anchorage systems: MA/GA - (a) clamp units; (b) guides; (c) aluminium frame; (d) hydraulic cylinder; (e) manual hydraulic pump; MA - (f) metallic anchor plate; GA - (g) heating device; (h) manometer and valves.

The MA system uses metallic anchor plates of 200 × 272 × 12 [mm] fixed with six M16 8.8 bolt anchors, guides, clamp units, aluminium frames, hydraulic cylinders, and a manual hydraulic pump. For the case of the GA system, guides, clamp units, aluminium frames, hydraulic cylinders, manometer and valves, and heating device for accelerated curing the adhesive, are required. Depending on the level of prestressing to be applied and the length of the CFRP laminate strip to be prestressed, the MA can have one or both active anchorages. In the case of the GA system both anchorages are always active due to nature of the technique. The application of these anchorage systems comprises the following main steps:

1. The first step consists on the surface preparation of concrete substrate where the strip is applied. In the present experimental program two different methods were used: (i) sand blasting (**Figure 2.3a'**) and (ii) gridding with stone wheel (**Figure 2.3a''**). Afterwards, compressive air was used to clean the treated region of the slab;
2. Several holes are drilled to accommodate temporary and permanent bolt anchors. GA system complies only temporary bolts, whereas for the case of MA system, six M16 8.8 permanent bolt anchors are used to fix each steel anchorage plate. HIT-HY 200-A® chemical bond agent was used to fix the bolts to concrete. Then, aluminium guides are placed in the right position to guide and fix the clamp units (**Figure 2.3b**);
3. The clamp units are placed in-between the guides at each extremity of the slab;
4. The epoxy adhesive is prepared according to the requirements included in producer's technical datasheet and the CFRP laminate strip is cleaned with a solvent. Then, the adhesive is applied on the surface of the CFRP laminate as well as on the concrete surface region in contact with the laminate (**Figure 2.3c**). A minimum of 2 mm of thickness of epoxy was used. The CFRP laminate strip is then placed in its final position and slightly pressed against the concrete substrate;
5. The clamping units are closed and a dynamometric key is used to tighten the screws of the clamp units with a torque of 170 N·m (**Figure 2.3d**);
6. For the case of MA system, anchors plates are slightly grinded with sandpaper and cleaned with a solvent before they are installed in their predefined location (**Figure 2.3e'**). In the case of GA, heating devices are placed in the gradient zone (**Figure 2.3e''**);

7. The aluminium frames are then placed on their predefined locations and fixed against the concrete with the anchors (**Figure 2.3f''** and (**Figure 2.3f''**) in order to accommodate the hydraulic cylinder (**Figure 2.3g'** and (**Figure 2.3g''**) for the application of the prestressing;
8. Finally, using a manual hydraulic pump, the prestress is applied to the CFRP laminate strip (**Figure 2.3h''** and (**Figure 2.3h''**).

Once the CFRP is prestressed distinct procedures are followed for the case of the MA and the GA systems. In the MA system, by applying a torque of 150 N·m in each bolt anchor of the anchor plates, it is possible to increase the transverse compression level in this region and hence reducing the probability of the CFRP laminate sliding at the ends. Afterwards, by using additional fixing screws mounted in-between the frame and the clamp units, it is possible to block the prestressing system in order to avoid prestress losses during the curing of the epoxy. The strengthening application is concluded after approximately 24 hours, since after this time span the epoxy reaches a degree of curing at least at about 90% [15] for temperatures not lower than 20 °C. In the end, the equipment is removed (fixing screws, clamp units, guides and aluminium frames) and the temporary anchors and CFRP laminate outside of the anchor plates are cut off.

The GA system uses the adhesive's ability to cure fast at high temperatures and hence to create a non-mechanical anchorage [16]. For the present specimens, a 600 mm anchorage length was used, composed of 3 sectors (50/80 mm wide and 200 mm long each). During the application of the gradient method, all specimens were monitored in terms of applied force by the hydraulic cylinders and temperature at the distinct sectors composing the heating devices. The typical evolution of the temperature, jack force and strain over time is graphically represented on **Figure 2.4** for the specimen GD_GA_L50×1.4: firstly, it begins with a plateau of 160 °C during 15 minutes, followed by an exponential decrease during 20 minutes (down to 120 °C), and finally the cooling phase. In the following sector the same heating process is carried out 10 minutes after the beginning of the cooling phase. The releasing force in each step was equal to about 1/3 of the total applied force. This released occurred 15 minutes after the initiation of the cooling phase. After the first release a slight prestrain loss in the CFRP laminate (a variation at about 1.5%) can be observed,

as depicted in **Figure 2.4a**. This variation can be justified by the lower value of the modulus of elasticity of the epoxy adhesive due to the curing process [17].

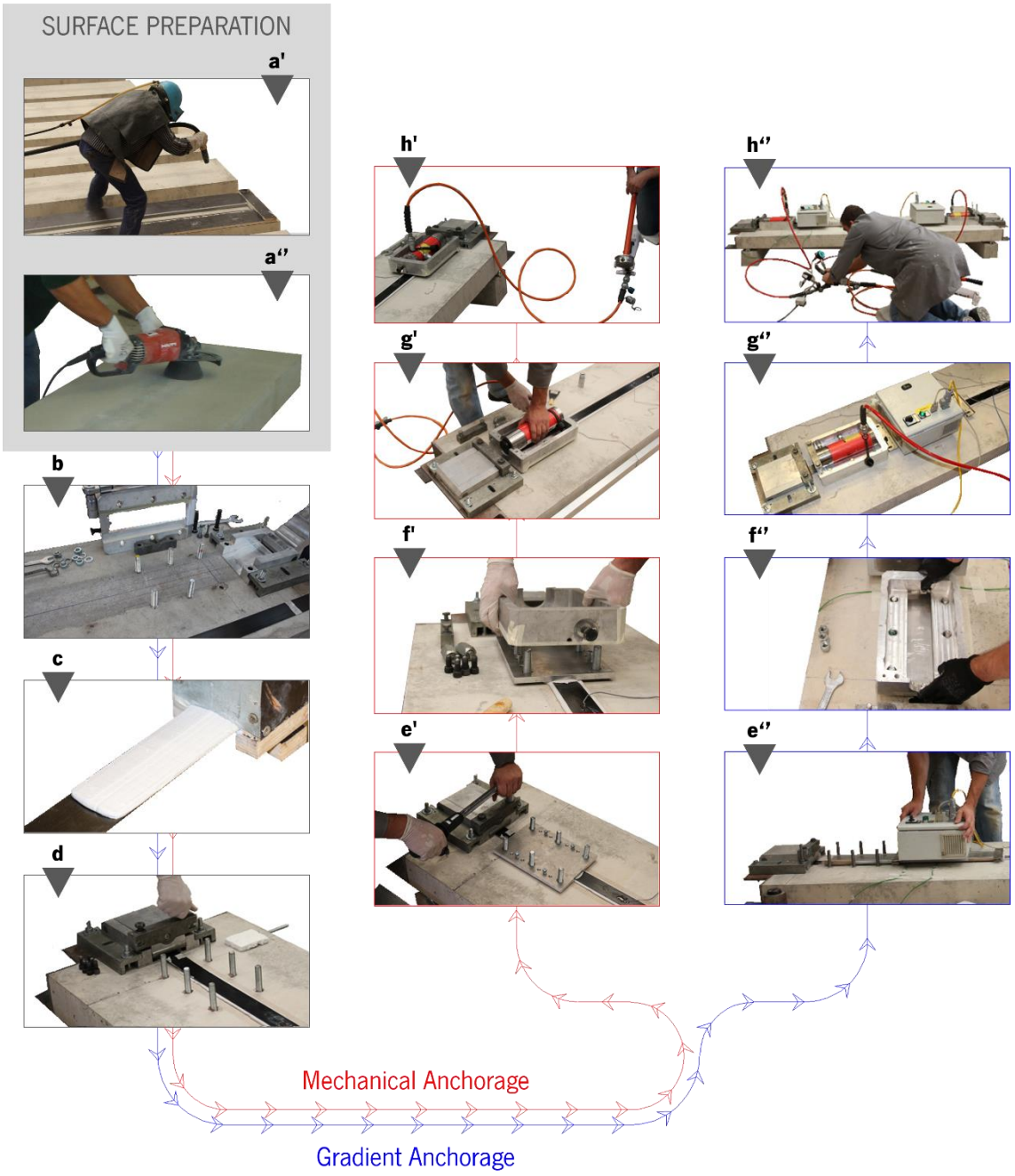

Figure 2.3: Strengthening procedures for the mechanical anchorage (red path) and gradient anchorage (blue path).

In the prestressed specimens strain gauges were used to control the prestress level. The CFRP strip was prestressed up to an average prestrain of 0.4%.**Table 2.1** highlights the values of the registered prestrain at the middle of the laminate at the end of the strengthening.

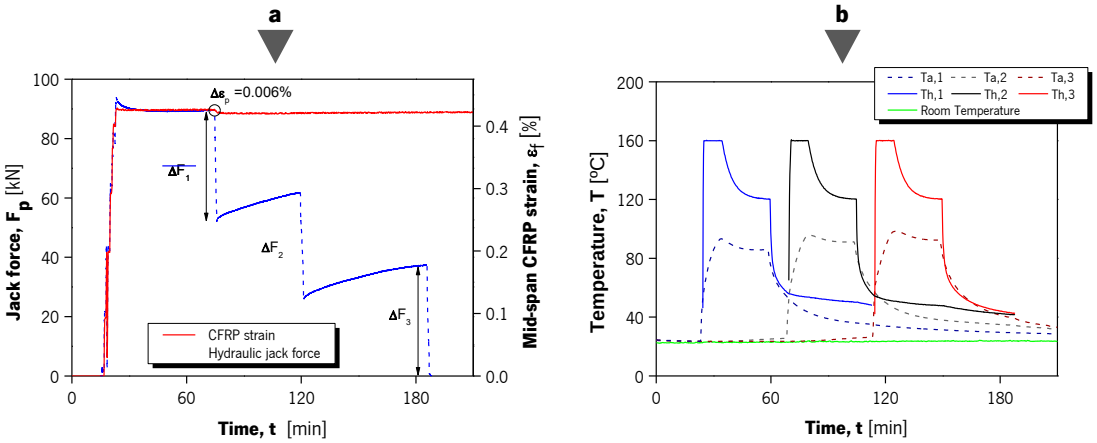

Figure 2.4: Evolution of the temperature, jack force and CFRP strain on GD_GA_L50×1.4 over time: (a) hydraulic jack force F_p and midspan CFRP strain ε_f; (b) temperature in the heating elements $T_{h,i}$ and in the epoxy adhesive $T_{a,j}$.

In contrast to the MA system where the final result (after removing the prestressing equipment, temporary anchors and excess of CFRP laminate) includes the bonded CFRP laminate strip and two metallic anchor plates, the GA system will be composed by a purely bonded CFRP strip/epoxy/concrete system. The specimens were kept in lab environment after strengthening at least one month before testing.

2.2.4 Surface preparation

Considering the two different surface treatment methodologies applied at the concrete slab surfaces and in order to allow the identification of their influence on the obtained responses, the roughness of these distinct surfaces was measured. Thus, an equipment was developed in scope of present work by Professor Eduardo Pereira, with the use of an existing laser sensor, with a resolution of 5 μm, a repeatability of 15 μm, and a linearity of 20 ±μm. The surfaces selected for the experimental characterization are representative of the three distinct types of surface treatments involved in the present research, which are the normal surface (without any treatment),

the grinded surface, and the sand blasted surface. In **Figure 2.5** it is possible to see the three different roughness of the material.

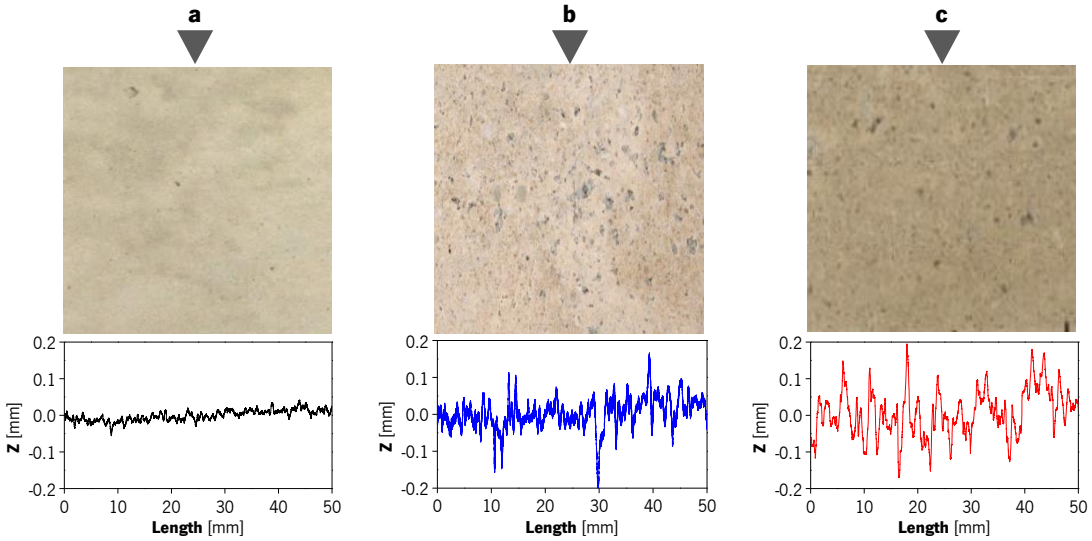

Figure 2.5: Different roughness of concrete surfaces: (a) smooth (before any treatment); (b) grinded treatment; (c) sandblasted treatment.

The laser sensor was coupled to a metallic plate, which was part of a mechanism conceived to produce a slow displacement at a constant rate, as well as to allow the displacement of the laser sensor during scanning at a parallel trajectory relatively to the scanned surface, as shown in **Figure 2.6**. The displacement rate was 0.69 mm/s and the data acquisition rate was 120 Hz, leading to consecutive readings spaced of 0.00575 mm. Representative profiles of the three different surfaces are shown in **Figure 2.5**. The representative profiles clearly distinguish the untreated surface and the treated surfaces, both the grinded and the sandblasted surfaces.

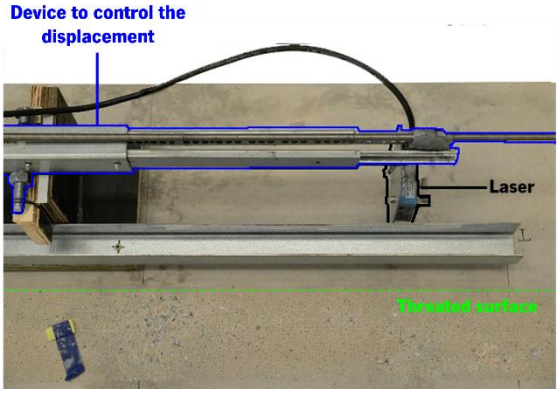

Figure 2.6: Setup details about the device used to control de displacement of the sensor.

In this work several statistical indicators were considered to characterize the surface roughness [18], especially the average roughness, R_a, and the root mean square, R_q, as well as the peak and valley values of the samples. The average roughness and the root mean square can be determined using the equations (2.1) and (2.2), respectively. In these equations l_m is the evaluation length, $z(x)$ is the profile height at position x, and n is the number of scan readings.

$$R_a = \frac{1}{l_m} \cdot \int_0^{l_m} z(x) \cdot dx \tag{2.1}$$

$$R_q = \sqrt{\frac{1}{n} \cdot \sum_{i=1}^{n} {z_i}^2} \tag{2.2}$$

The most common mathematical parameters used to characterize the roughness were computed for the three types of surfaces and are presented in **Table 2.3**. It is possible to verify that for the three different surfaces the obtained values of roughness R_a show the expected trend, increasing in a reasonable fashion when departing from the smooth surface and arriving at the sandblasted slabs.

Table 2.3
Results from the roughness assessment.

Roughness parameter [mm]	**Smooth**	**Grinded**	**Sandblasted**	
			SLAB A	SLAB B
Arithmetic average of absolute values, R_a	0.021	0.046	0.081	0.099
Root mean squared, R_q	0.026	0.060	0.110	0.135
Maximum valley depth, R_v	-0.076	-0.228	-0.577	-0.636
Maximum peak height, R_p	0.090	0.173	0.248	0.405
Maximum height of the profile, R_t	0.166	0.401	0.826	1.042

2.3 Results and discussion

The experimental results are presented in the current section, namely the relation between the applied load and the mid-span deflection, crack width, crack pattern and failure modes. All characteristic results for the cracking, yielding, and ultimate loading state are presented in **Table 2.5**. The results discussion complies the difference between anchorage systems, laminate geometries and surface treatment.

2.3.1 Deflection evolution

The relationship between the applied force and the deflection at mid-span was monitored and it is represented in **Figure 2.7**. As expected, the strengthening increased the stiffness of the RC slab and, as a consequence, reduced the deflection for a specific load level. **Table 2.5** summarizes the key results, for which the prestress level and the geometry of the CFRP strip were the influential factors.

Prestressing did not significantly change the stiffness of the elastic phase (K_I). However, substantial differences were observed in the stages after the crack initiation: firstly, cracking (δ_{cr}, F_{cr}) and steel yielding (δ_y, F_y) were delayed when compared with the non-prestressed specimens; and the stiffness after cracking (K_{II}) was higher in the strengthened slabs. Larger CFRP strips attract higher tensile forces and hence also induce higher system stiffness. Results show an average increase of 39%, 84% and 106% in the stiffness K_{II} of the GD series prestressed specimens with 50×1.2 [mm], 50×1.4 [mm] and 80×1.2 [mm] CFRP laminates, respectively. The same comparison shows an increase of 39% for the series GD prestressed specimens.

In general, both prestressing strengthening techniques presented similar performances in terms of serviceability load/deflection up to yielding initiation.

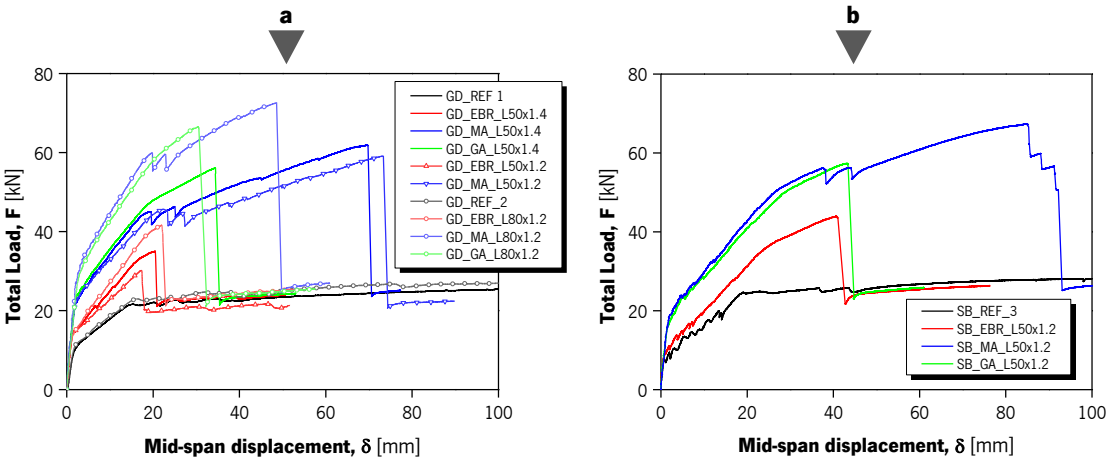

Figure 2.7: Total force *versus* mid-span deflection: (a) series GD; (b) series SB.

2.3.2 Crack width

The crack width was monitored by the referred handheld USB microscope (with a magnification factor of 20×). For that purpose three cracks were selected in the pure bending zone of each slab, two close to the point of loads and one at the mid-span. For every picture taken with the microscope, three measurements were performed in order to obtain the average crack width, as depicted in **Figure 2.8**. **Figure 2.8** also plots the evolution of the average crack width *versus* the applied force. Results show that, for a specific load level, strengthened specimens exhibited lower crack widths when compared to the reference specimens. The MA and the GA systems presented similar results that could be foreseen due to their identical response in terms of force-deflection (at serviceability level). Resembling results were obtained for the series GD and SB.

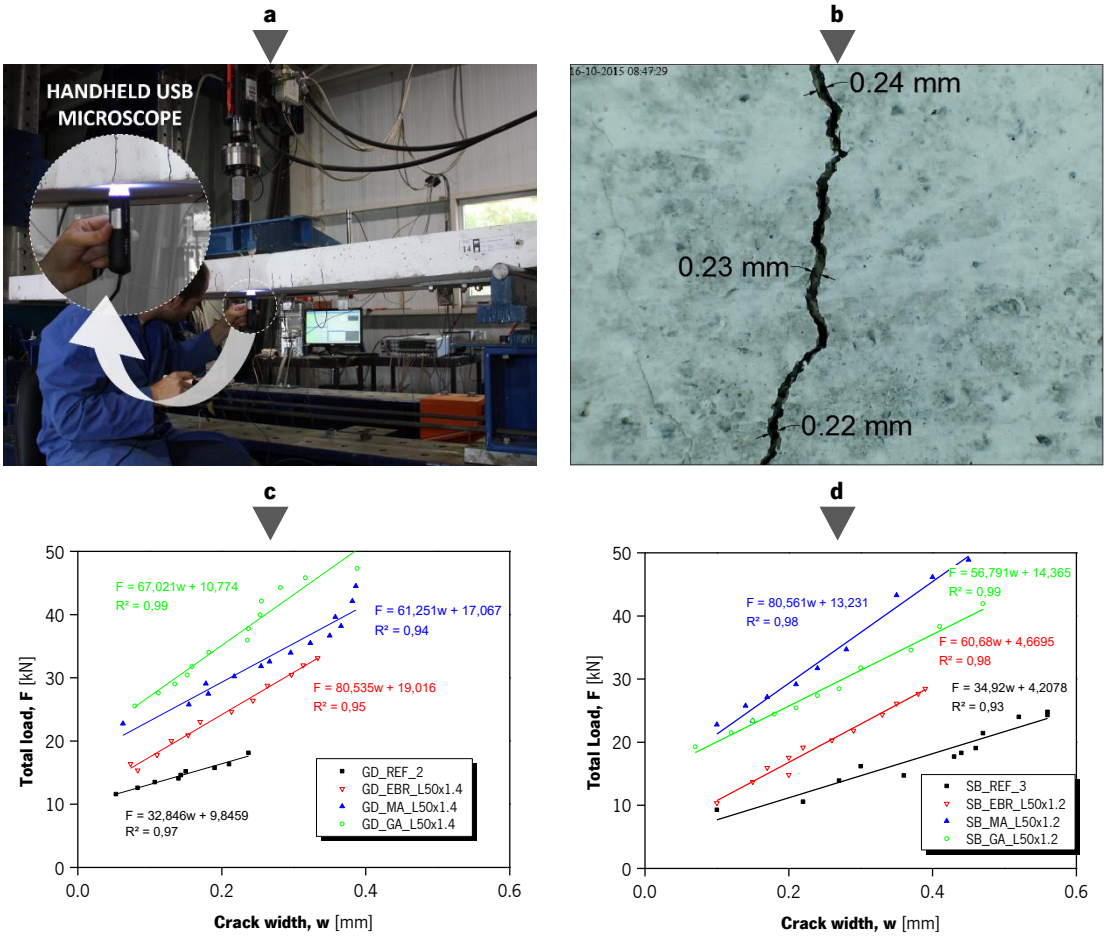

Figure 2.8: Crack width monitoring: (a) handheld USB microscope, (b) typical photo of a crack (SB_MA_L50x1.2), (c) evolution on series GD; and (d) evolution on series SB.

2.3.3 Crack pattern

The crack pattern was also evaluated at the end of each test. **Figure 2.9** shows the crack pattern on the lateral surface of each tested slab and **Figure 2.10** presents the values obtained in terms of average crack spacing. The results indicate that, in a general way, the crack spacing is reduced with the strengthening. This effect is more noticeable with the prestressed specimens: in series GD the average distance between cracks of the five prestressed slabs was reduced to 79% of the reference specimens (GD_REF_1 and GD_REF_2); whereas for the prestressed specimens on series SB, the crack spacing reduction was equal to 36% of the value obtained with SB_REF_3. Through the crack pattern drawn in **Figure 2.9** one can observe that the number of cracks in the pure bending zone is higher on the prestressed specimens.

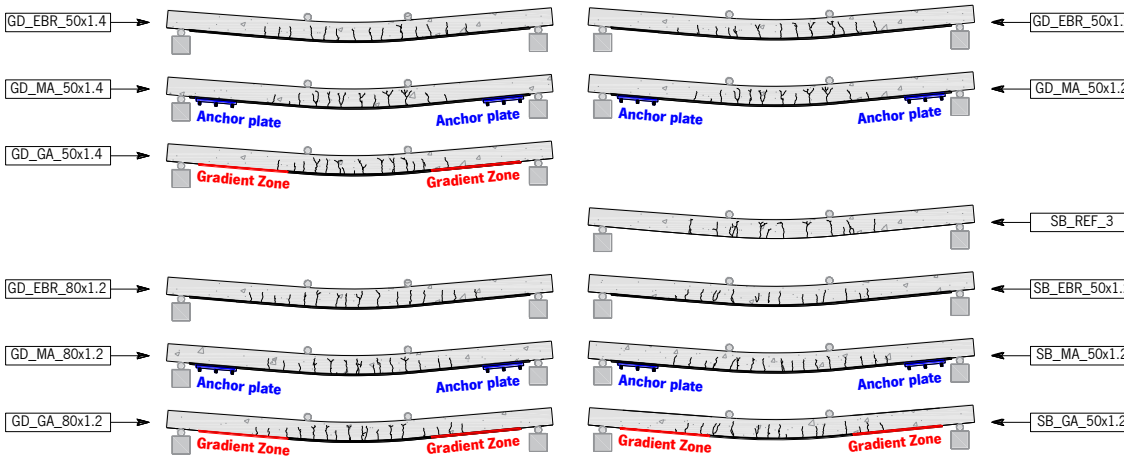

Figure 2.9: Crack pattern at the end of the test of each slab.

2.3.4 Influence of prestress

The overall behaviour of the prestressed specimens was considerably more satisfying than the un-prestressed ones in terms of ductility and load carrying capacities. Prestressing clearly improved the cracking and yielding initiation, stiffness and load carrying capacity. Even though the stiffness at the uncracked stage (K_I) was similar (prestressed *versus* un-prestressed) mainly due to the low level of strengthening ratio and level of prestrain that has been used, the cracking load was significantly higher: with series GD an increase close to 55%, 69% and 117% was observed on specimens with the CFRP strip of 50×1.2 [mm], 50×1.4 [mm], and 80×1.2 [mm], respectively;

whereas the cracking load duplicated in series SB prestressed slabs. Similar observations can be made for the cracked stage (before yielding initiation). The load carrying capacity of prestressed slabs increased when compared with the unprestressed specimen. Results show that the ultimate carrying capacity growth was higher on series GD (in between 60% and 95%) than on series SB (within 30% and 53%).

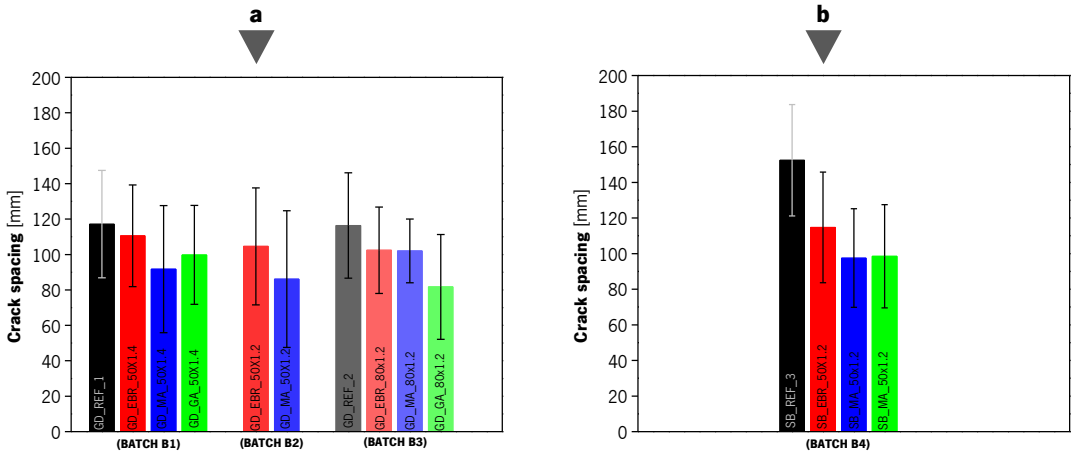

Figure 2.10: Crack spacing of each slab of: (a) series GD and (b) series SB.

Ultimately, **Figure 2.11** shows the evolution of the CFRP and concrete strains at mid-span with the total force. Results also show a higher ultimate strain in the concrete for the prestressed specimens. Consequently, it can be stated that prestressing the CFRP laminates not only improved the slabs overall performance but also assured a better use of the materials. It should be also referred that a greater portion of the CFRP tensile capacity was engaged with the prestress (see **Figure 2.11** and **Table 2.5**): on series GD the strain at the ultimate load (F_{max}) was at least 124% higher than the observed on the slabs with the same CFRP laminate geometry; and on series SB an increase of 95% and 53% was obtained for the SB_MA_50×1.2 and SB_GA_50×1.2, respectively.

2.3.5 Failure modes

During the monotonic tests, the reference slabs (GD_REF_1, GD_REF_2, and SB_REF_3) were stopped at a midspan deflection of 100 mm due to the corresponding LDVT measurement range limitation. Failure mode would in this case most likely be concrete crushing on the top fibre. All

strengthened slabs exhibited CFRP strip debonding and the SB_MA_50×1.2 specimen (see **Figure 2.13a**) failed by FRP rupture in unidirectional tension when the CFRP strain at the mid-span was close to 1.48 %, as it is showed on **Table 2.5**.

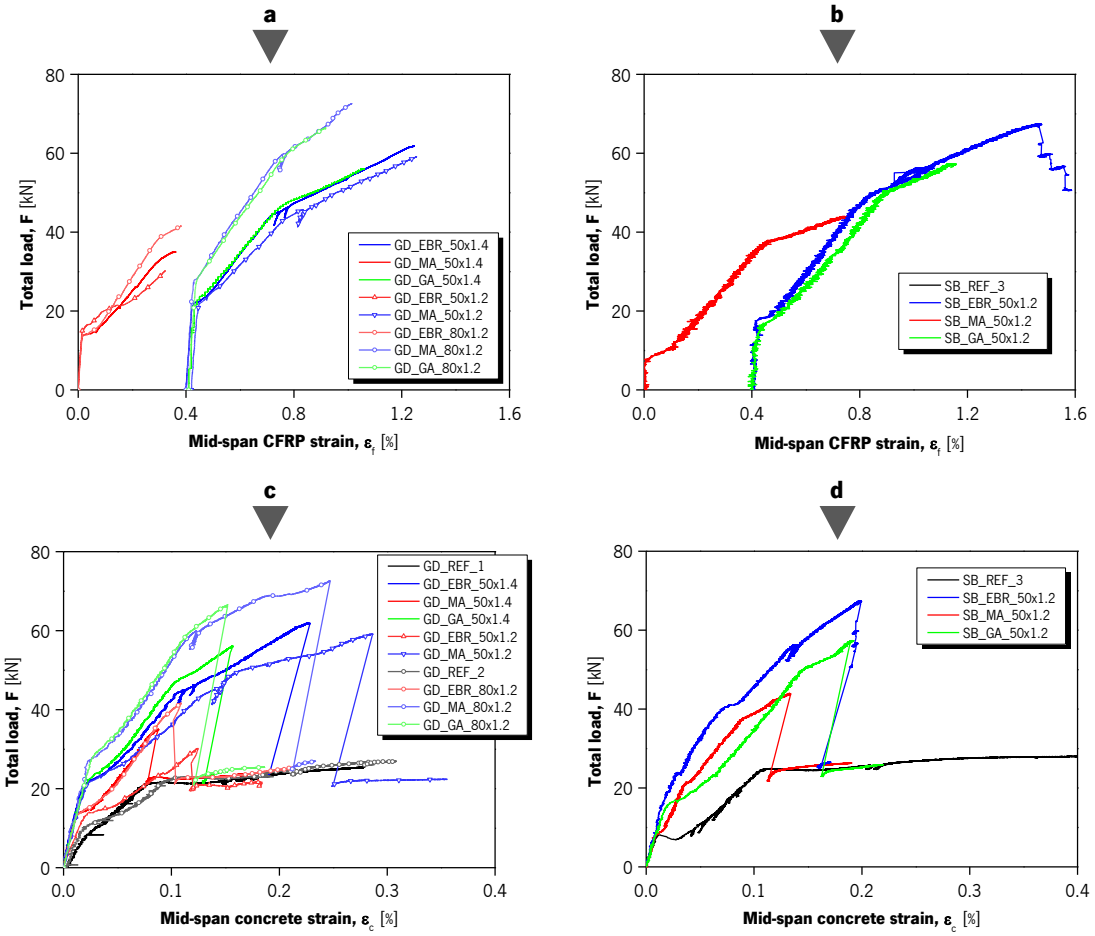

Figure 2.11: Total force *versus* CFRP/concrete strain: (a) Mid-span CFRP strain in series GD; (b) Mid-span CFRP strain in series SB; (c) Mid-span concrete strain in series GD; (d) Mid-span concrete strain in series SB.

Typically, four failure modes of FRP-strengthened EBR structure members due to debonding can be identified [19], [20]: (i) laminate strip end-debonding (Mode 1), (ii) debonding by flexural cracks (Mode 2), (iii) debonding by diagonal shear cracks (Mode 3), and (iv) debonding by irregularities and roughness of the concrete surface (Mode 4). Based on the thorough quality control kept during the preparation and strengthening of the specimens, Mode 4 is the less probable failure mode. Also, in the present experimental campaign, debonding by diagonal shear cracks (Mode 3) was

disregarded because no critical shear cracks were observed during the monotonic tests. Several approaches are available in the literature to predict the remaining failure modes [19]–[22]. In the present work, the debonding Mode 1 and Mode 2 included in the Italian design recommendations CNR [19] have been used :

- End anchorage failure (Mode 1)

The CNR [19] defines the ultimate design strength, f_{fdd}, in [MPa], as the maximum allowed strength before debonding of the laminate ends, and can be estimated using the following expression:

$$f_{fdd} = \frac{1}{\gamma_{f,d}} \cdot \sqrt{\frac{2 \cdot E_f \cdot \Gamma_{Fd}}{t_f}} \tag{2.3}$$

where $\gamma_{f,d}$ is the partial factor, assumed as 1.0 to obtain the expected ultimate design strength (dimensionless parameter); E_f is the laminate strip's elastic modulus, in [MPa]; t_f is the laminate strip's thickness, in [mm]; and Γ_{Fd} is the design fracture energy of the strip/concrete interface, in [N/mm], and is computed as follows [19]:

$$\Gamma_{Fd} = \frac{k_b \cdot k_G}{FC} \cdot \sqrt{f_{cm} \cdot f_{ctm}} \tag{2.4}$$

where k_G is an additional corrective factor, in [mm], that considers the bonding system (equal to 0.063 mm for pre-cured system); FC is a confidence factor (dimensionless parameter), also assumed as 1.0; f_{cm} and f_{ctm} are the concrete compressive and tensile strength, in [MPa]; and k_b is a geometrical corrective factor (dimensionless parameter). For values where the ratio between the laminate strip width (b_f) and concrete width (b) are smaller than 0.25 ($b_f/b < 0.25$), the geometrical factor is equal to 1.18. In the remaining cases ($b_f/b \geq 0.25$), k_b can be computed with the following equation:

$$k_b = \sqrt{\frac{2 - b_f/b}{1 - b_f/b}} \geq 1 \tag{2.5}$$

The CNR [19] also defines the optimal bond length, l_{ed}, in [mm], which is the minimum necessary length needed to reach the maximum anchorage resistance:

$$l_{ed} = \frac{1}{\gamma_{R,d} \cdot f_{bd}} \cdot \sqrt{\frac{\pi^2 \cdot E_f \cdot t_f \cdot \Gamma_{Fd}}{2}} \quad (2.6)$$

where $\gamma_{R,d}$ is a corrective factor equal to 1.25 and f_{bd} is the design bond strength between the FRP and concrete, in [MPa], equal to $2 \cdot \Gamma_{Fd}/s_u$, with $s_u = 0.25$ mm. Note that the Italian guideline [19] says that for optimal bond lengths shorter than 200 mm, the value of 200 mm should be used.

- Intermediate strip debonding (Mode 2)

  The failure from intermediate debonding mechanism occurs when the stress variation in the FRP system between two subsequent flexural cracks exceed the bond limit. Typically, the bond limit depends on the distance between transverse cracks, the level of stress in the FRP laminate strip, and on the bond characteristics between the concrete and FRP. The CNR [19] defines a simplified procedure to compute the maximum strength in the FRP system at the onset of Mode 2 debonding:

$$f_{fdd,2} = \frac{k_q}{\gamma_{f,d}} \cdot \sqrt{\frac{E_f}{t_f} \cdot \frac{2 \cdot k_b \cdot k_{G,2}}{FC} \cdot \sqrt{f_{cm} \cdot f_{ctm}}} \quad (2.7)$$

  being the k_q a coefficient that considers the load distributions (1.25 for distributed loads and 1.0 for all other load configurations); and $k_{G,2}$ is a corrective factor calibrated on experimental results and equal to 0.10 mm irrespective of the type of reinforcement.

Based on the abovementioned formulation, the expected level of stress in the CFRP at the onset of Mode 1 and Mode 2 debonding failure was computed and is presented in **Table 2.4** (note that these values were computed without safety factors). Regarding the Mode 1, an average ultimate anchorage strength, f_{fdd}, of 510.60 MPa and an average optimal bond length, l_{ed}, of 125.60 mm was estimated for specimens strengthened with the unstressed CFRP laminate (GD_EBR_50×1.2, GD_EBR_50×1.4, GD_EBR_80×1.2 and SB_EBR_50×1.2). Based on equation (2.7), the maximum strength in the FRP system, $f_{fdd,2}$, for these four EBR slabs was computed and, in average, is equal to 643.29 MPa.

Table 2.4
Failure mode study.

	GD_EBR_L50x1.4	**GD_EBR_L50x1.2**	**GD_EBR_L80x1.2**	**SB_EBR_L50x1.2**
f_{fdd} [MPa]	484.50	562.47	521.62	473.81
Γ_{Fd} [N/mm]	1.06	1.13	0.99	0.82
l_{ed} [mm]	125.47	117.08	123.92	135.93
$f_{fdd,2}$ [MPa]	610.41	708.64	657.18	596.94

Note: according to the CNR [19] an optimal bond length of 200 mm should be adopted.

Using a cross-section (CS) analysis, it is possible to predict the ultimate load/moment distribution for which the slabs would fail by laminate strip debonding (Mode 1 or Mode 2). **Figure 2.12** shows the results from the CS analysis, more precisely the bending moment diagram obtained: (i) experimentally at the maximum load (F_{max}); (ii) for the end-debonding (Mode 1) using a CS analysis; and (iii) for the intermediate debonding (Mode 2), also using a CS. The stress-strain relation for non-linear structural analysis of the concrete defined in the Eurocode 2 [23] was adopted:

$$\sigma_c = f_{cm} \cdot \frac{1.05 \cdot \frac{E_{cm} \cdot |\varepsilon_{c1}|}{f_{cm}} \cdot (\frac{\varepsilon_c}{\varepsilon_{c1}}) - (\frac{\varepsilon_c}{\varepsilon_{c1}})^2}{1 + (1.05 \cdot \frac{E_{cm} \cdot |\varepsilon_{c1}|}{f_{cm}} - 2) \cdot (\frac{\varepsilon_c}{\varepsilon_{c1}})} \tag{2.8}$$

where E_{cm} is the elastic modulus of the concrete, in [MPa]; f_{cm} is the mean compressive strength, in [MPa]; ε_c is the strain in the concrete (dimensionless parameter); and ε_{c1} is the strain at the peak stress, computed according to the following expression (dimensionless parameter):

$$\varepsilon_{c1} = 7 \cdot 10^{-4} \cdot {f_{cm}}^{0.31} \leq 2.8 \cdot 10^{-3} \tag{2.9}$$

Based on the maximum strength in the CFRP system, $f_{fdd,2}$, the expected strain in the CFRP at the onset of intermediate debonding, $\varepsilon_{fdd,2}$, was computed and, using the CS analysis, the expected bending moment in the mid-span section, $M_{fdd,2}$, was estimated. Then, the acting load, $F_{fdd,2}$, needed to produce the $M_{fdd,2}$ moment was obtained.

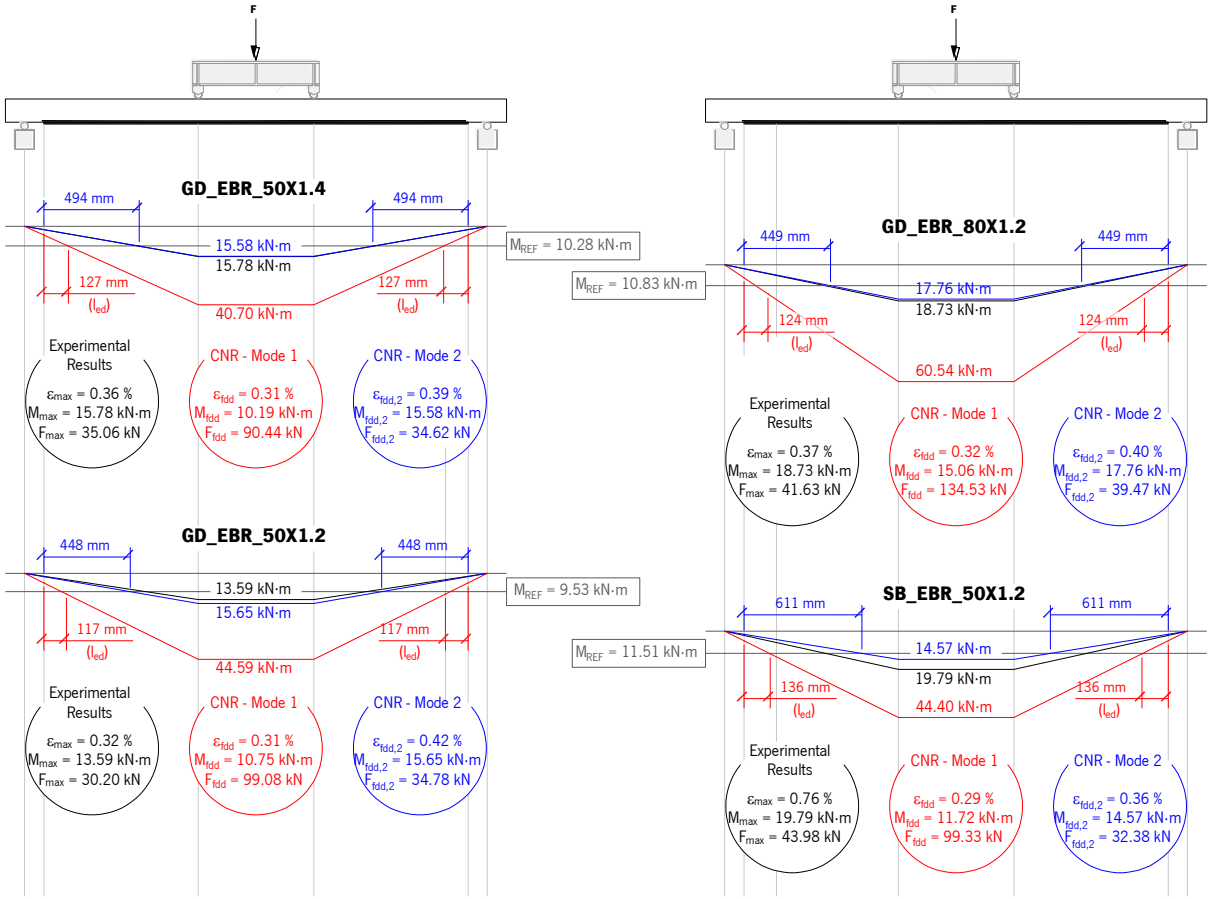

Figure 2.12: Results from the cross-section analysis.

For the end-debonding a similar procedure was carried out: firstly, the CFRP strain, ε_{fdd}, for the ultimate anchorage strength (f_{fdd}) was computed; with a CS analysis, the bending moment, M_{fdd}, was determined at end of the optimal bond length (l_{ed}); and, based on the latter value, the acting load, F_{fdd}, needed to produce the M_{fdd} moment was obtained. Thus, **Figure 2.12** presents the bending moment diagrams for maximum loads limited by Modes 1 and 2 and for the maximum load experimentally obtained. This figure also shows, for each case, the resisting bending moment of the slabs without the CFRP reinforcement (M_{REF}). Results clearly show that the intermediate debonding is the most probable type of failure. The load estimated with Mode 2 failure ($F_{fdd,2}$) is similar to the maximum load registered experimentally, whereas the Mode 1 failure load is always higher (in between 2.3 and 3.3 times). Slab SB_EBR_50×1.2 shows the highest gap between the experimentally and the predicted (Mode 2) values. This difference might be related to the surface

preparation and strengthening procedure: in contrast with all other specimens, the surface of this specimen had a rough finish which was rectified with the epoxy adhesive used for strengthening. If an optimal bond length of 200 mm (design value according to the CNR) is considered, the Mode 1 failure is expected for lower load levels (F_{fdd} equal to 71.70 kN, 67.97 kN, 100.41 kN and 78.12 kN for specimens GD_EBR_50×1.2, GD_EBR_50×1.4, GD_EBR_80×1.2 and SB_EBR_50×1.2). However, these values are still far from the failure loads observed experimentally.

An interfacial failure at the epoxy adhesive/CFRP laminate was observed at the anchorage zone of the MA and GA specimens (see **Figure 2.13b**, **Figure 2.13c** and **Figure 2.13d**). The remaining CFRP strip region seemed to simultaneously have an interfacial failure at epoxy adhesive/CFRP laminate and cohesive failure in the concrete. These interfacial failure modes observed may be justified by the higher compressive/tensile strength of the used concrete. In some of these specimens a layer of concrete was detached from the RC slab.

The slabs GD_EBR_50×1.4, GD_EBR_50×1.2 and GD_EBR_80×1.2 seemed to have an interfacial failure between adhesive and the concrete (see **Figure 2.13e**), whereas SB_EBR_50×1.2 slab's failure looked like an interfacial failure amongst the adhesive and the CFRP strip (see **Figure 2.13f**).

Based on the previous analysis, the failure on the prestressed specimens was, most-likely, a consequence of the intermediate debonding. In slabs with the GA anchorage the debonding initiation was rapidly transformed into the complete debonding, whereas slabs with the MA anchorage endured the CFRP strip debonding and failed when the CFRP ends were pulled out from the anchorage. Moreover, a video (available at https://tinyurl.com/y85jgy7b) of the anchorage zone of the SB_MA_50×1.2 shows that the debonding started from the mid-span and propagated towards the CFRP strip ends. This video was recorded using a GoPro HERO4 action camera at 120 fps with the resolution of 1280×720 pixels. **Figure 2.14** presents three video frames of the CFRP strip debonding. This figure shows the debonding crack evolves from the middle of the slab to the anchorage region (several details of the region where the crack is developed are presented in **Figure 2.14**. The limit of each detail is red when the crack is visible and blue when it is not).

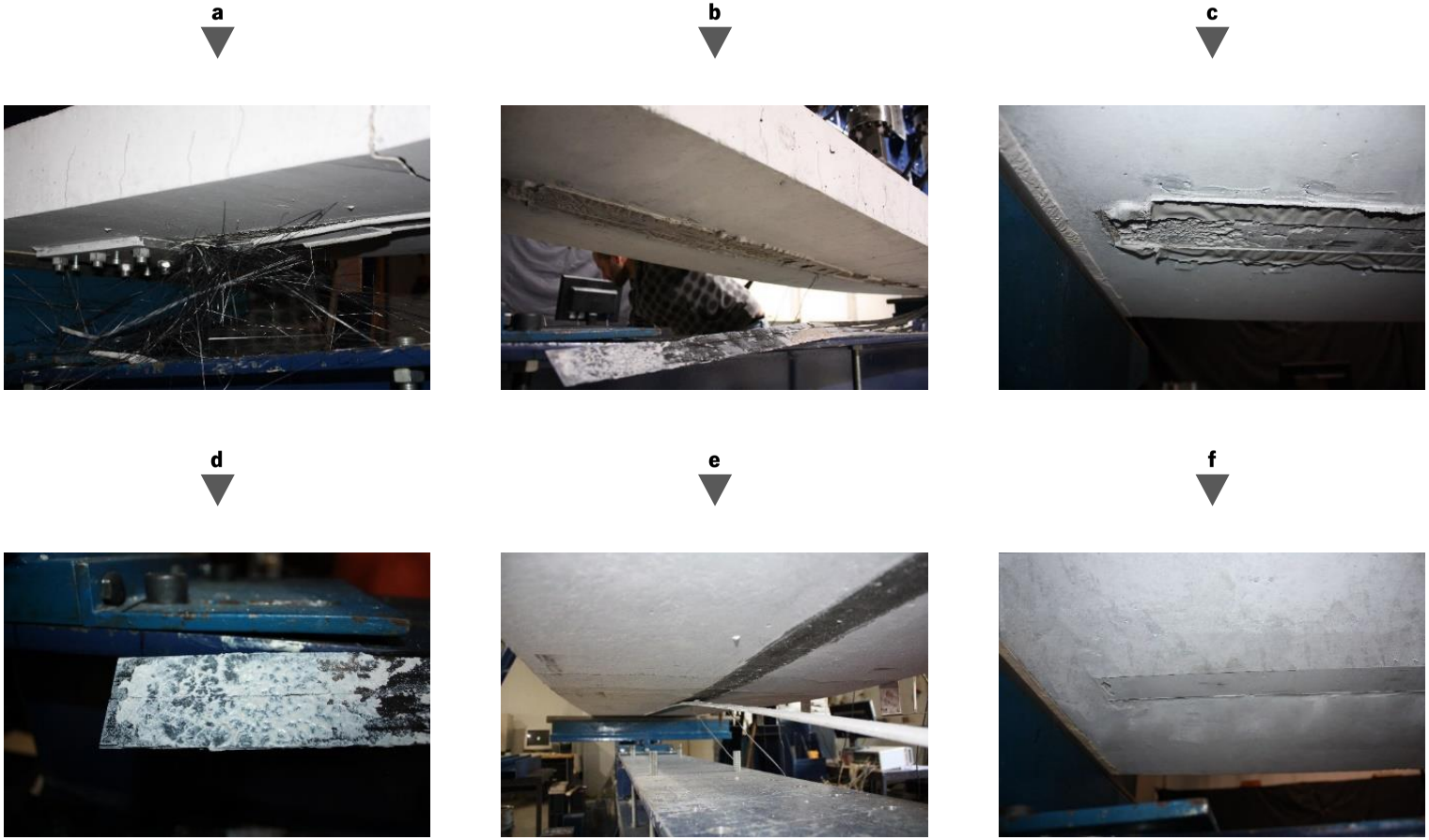

Figure 2.13: Typical failure modes: (a) FRP rupture in unidirectional tension (SB_MA_50×1.2); (b) interfacial failure at the epoxy adhesive/CFRP laminate (SB_GA_50×1.2); (c) detail at the anchorage zone (SB_GA_50×1.2); (d) detail of the CFRP strip's extremity (SB_GA_50×1.2); (e) interfacial failure between adhesive and the concrete (GD_EBR_50×1.4); (f) interfacial failure amongst the adhesive and the CFRP strip (SB_EBR_50×1.2).

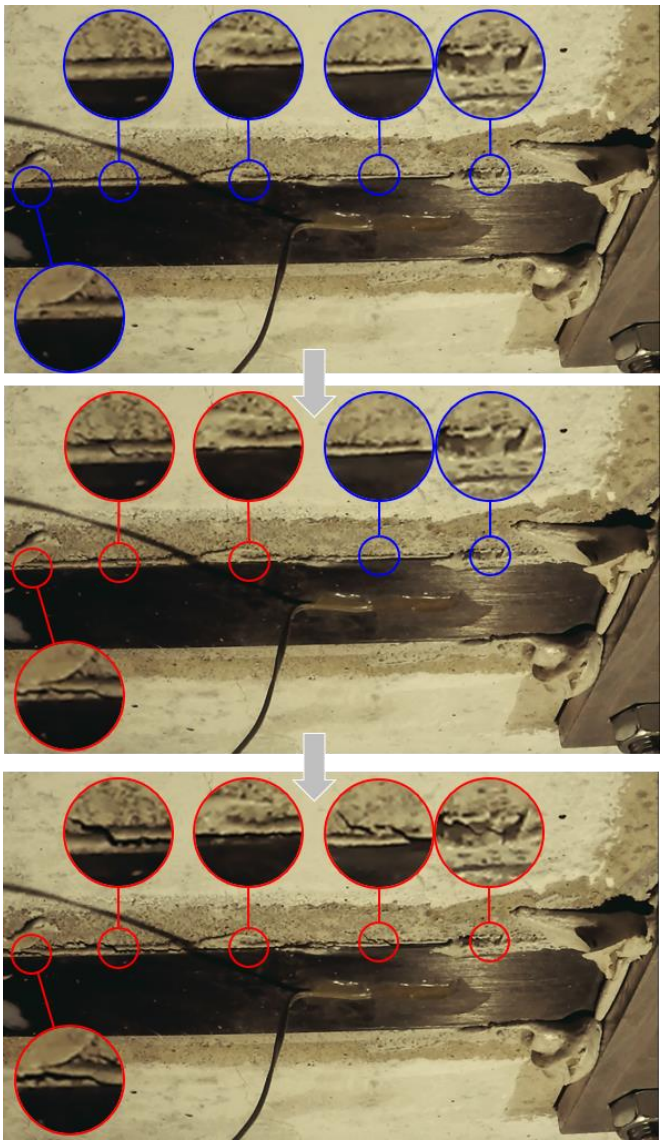

Figure 2.14: CFRP laminate strip debonding in slab SB_MA_50×1.2.

2.3.6 Anchorage systems

Both GA and MA systems present a similar behaviour until steel yielding (see **Figure 2.7**). After this point, the CFRP material is responsible to carry the additional loads as a result of the diminished contribution of the internal steel reinforcement (it must be pointed out that the steel reinforcement exhibits a quite small hardening modulus of elasticity after yielding). Consequently,

the force increment supported by the CFRP laminate strip increased significantly at the onset of the yielding initiation, as shown in **Figure 2.11a** and **Figure 2.11b**.

The mechanical anchorage system exhibits two drop points on the *F-δ* curves (see **Figure 2.7**) after the steel reinforcement yielding. This behaviour is related to the debonding initiation that occurred between the metallic plate anchors and the force application point. This statement is supported on the visual observation performed during and after the tests and by comparing e.g. the location of the drop points of the slab GD_MA_L50×1.4 with the failure slab GD_EBR_L50×1.4 (in **Figure 2.7a**). From these two drop points, the CFRP laminate works unbonded to the substrate and as a cable fixed at both extremities (the metallic anchors). Consequently, the metallic anchors composing the MA system prevented a premature failure by debonding and allowed the slab to continue carrying load after that point.

From the experimental observations, the MA system has a better performance when compared with the GA system: MA specimens presented higher ultimate load capacity (9% to 16% increase depending on the laminate geometry) and a greater use of CFRP tensile capacity (an increase on ultimate strain in between 13% and 28% was observed) when compared with the GA series. It might be important to refer that the debonding of the CFRP strip always occurred firstly on the MA series, but, as mentioned before, the metallic plate anchors allowed the composite system RC slab/CFRP to continue carrying load. Lastly, it is important to stress out the influence of the specimen dimensions: with a shorter span length, the total gradient zone occupies a larger relative portion of the complete laminate length. This leads to the situation where the end of the gradient anchorage is much closer to the loading point. The cracks that develop reach the anchorage zone much faster than for instance in case of a much slender beam with a higher span/depth ratio. Aram *et al.* [44] reported about static loading tests where EBR strengthened beams exhibited an even higher load carrying capacity than the corresponding ones with a prestressed system and gradient anchorage. It was concluded that the short span had a negative effect on the anchorage capacity due to too high shear stresses in the end zone of the laminate. Similar conclusions can be drawn for the present investigation: a more slender slab with a larger span length might implicate more similar results for an MA or a GA, as the free length between the anchorage zones increases

Table 2.5
Main Results.

Specimen	Stiffness		Crack initiation		Yielding			Ultimate				Efficiency and ductility			Failure Modes
	K_I	K_{II}	δ_{cr}	F_{cr}	δ_y	F_y	φ_y	δ_{max}	F_{max}	φ_{max}	ε_{max}	μ_F	μ_δ	μ_φ	
	[kN/mm]	[kN/mm]	[mm]	[kN]	[mm]	[kN]	[10^{-3}m^{-1}]	[mm]	[kN]	[10^{-3}m^{-1}]	[%]	$\left(\frac{F_{max}}{F_y}\right)$	$\left(\frac{\delta_{max}}{\delta_y}\right)$	$\left(\frac{\varphi_{max}}{\varphi_y}\right)$	
Series GD															
GD_REF_1	4.47	0.79	2.47	11.04	15.74	21.50	–	100.02[a]	25.42[b]	–	–	–	--	–	–
GD_EBR_L50×1.4	8.98	1.21	1.64	14.73	17.00	33.30	31.59	20.47	35.06	36.42	0.36	1.05	1.20	1.15	D
GD_MA_L50×1.4	9.81	1.43	2.25	22.07	17.80	44.32	36.66	69.84	61.76	86.81	1.20	1.39	3.92	2.37	D
GD_GA_L50×1.4	10.60	1.48	2.25	23.84	18.86	48.35	41.48	34.39	56.02	65.20	1.03	1.16	1.82	1.57	D
GD_EBR_L50×1.2	10.37	1.05	1.30	13.48	17.08	30.00	36.01	17.19	30.20	36.20	0.32	1.01	1.01	1.01	D
GD_MA_L50×1.2	9.02	1.22	2.53	22.81	20.57	44.89	45.64	73.23	59.09	91.15	1.25	1.32	3.56	2.00	D
GD_REF_2	4.47	0.87	2.49	11.12	15.96	22.90	–	100.00[a]	26.94[b]	–	–	–	--	–	–
GD_EBR_L80×1.2	10.65	1.50	1.24	13.20	18.35	38.92	33.01	21.88	41.63	39.92	0.37	1.07	1.19	1.21	D
GD_MA_L80×1.2	11.44	1.88	2.51	28.71	18.43	58.67	39.40	48.62	72.58	70.03	1.01	1.24	2.64	1.78	D
GD_GA_L80×1.2	9.92	1.71	2.88	28.56	20.31	58.31	37.31	30.61	66.21	53.02	0.90	1.14	1.51	1.42	D
Series SB															
SB _REF_3	11.10	0.92	0.71	7.88	18.90	24.54	–	100.00[a]	28.07[b]	–	–	–	--	–	–
SB_EBR_L50×1.2	12.49	1.13	0.68	8.49	25.87	37.05	43.88	40.69	43.98	71.34	0.76	1.19	1.57	1.63	D
SB_MA_L50×1.2	9.82	1.31	1.82	17.87	26.88	50.58	44.81	84.78	67.46	77.26	1.48	1.33	3.15	1.72	F
SB _GA_L50×1.2	10.43	1.24	1.55	16.16	29.04	50.20	52.60	43.31	57.38	76.49	1.16	1.14	1.49	1.45	D

Notes: D = Debonding; F = CFRP tensile failure; [a] these beams reached the maximum pre-defined deflection without failing; [b] values for the mid-span deflection of 100 mm; [c] The maximum CFRP strain did not necessarily occur at the mid-span.

2.3.7 CFRP geometry

Different CFRP geometries were considered in this preliminary study. The thickness influence was evaluated through a performance comparison between GD_MA_L50×1.4 and GD_MA_L50×1.2. As shown in **Figure 2.7a** both specimens presented an identical behaviour. The resemblance is due to the fact that both specimens failed by laminate end debonding at the metallic anchor. This type of failure is indeed governed by the maximum shear stress that this region can attain and, as a result, by the CFRP surface area in contact with the metallic anchor plate. For these two specimens the maximum shear stress resistance seemed to be influenced primarily by the width of the laminate. Remark that the laminate at the metallic anchor zone is transversely compressed due to the torque (150 N×m) applied in the six bolts (see **Figure 2.3**).This compression might actually diminish the strip thickness influence on the maximum carrying capacity of the composite system RC slab/CFRP strip.

A better performance was observed with the wider laminate. The specimens GD_MA_L50×1.2 and GD_MA_L80×1.2 were compared and it was clear that the behaviour of the second was better: higher cracking and steel yielding forces, greater stiffness, and an increase on the ultimate carrying capacity by 23%. Analysing the effect of the axial stiffness of the CFRP laminate on the stiffness of the slab at fully cracked state (K_{II}), it is clear that this relation matches well: the K_{II} of specimen GD_MA_L80×1.2 is 1.57 times higher than the one of the GD_MA_L50×1.2 and the axial stiffness of 80×1.2 is 1.54 higher than the 50×1.2 one. This inference is no longer found for the case of the ultimate load, since the failure is governed by laminate end debonding at the metallic anchor and, consequently the ultimate carrying capacity only increased by about 23% (GD_MA_L80×1.2 *versus* GD_MA_L50×1.2). In fact, the maximum average shear stress in the CFRP laminate strip at the metallic anchorage zone was higher on the GD_MA_L50×1.2 (9.14 MPa) than on the GD_MA_L80×1.2 (7.40 MPa). This outcome implies that the shear stress is inconstant in the metallic anchor region and that, in the present experimental campaign, the MA anchorage system appears to be more efficient with laminates of smaller widths (the maximum average shear stress on MA slabs strengthened with a 50 mm wide laminate – 50×1.2 or 50×1.4 – varied in between 9.14 MPa and 10.71 MPa). Note that equal metallic anchors were used (270 mm × 200 mm) with

the same torque per bolt (150 N×m) and, as a result of the laminate width, different pressure levels were imposed (GD_MA_L50×1.2 – 20.83 MPa and GD_MA_L80×1.2 – 13.02 MPa).

2.3.8 Surface treatment

In the present experimental program the surface treatment was evaluated by comparing the specimens overall performance in series GD (grinded) and series SB (sand blasted). These two different surface treatment methodologies influence the surface roughness (see **Table 2.3**) and, consequently, the adherence between the epoxy adhesive and the concrete surface.

When the specimens GD_MA_L50×1.2 and SB_MA_L50×1.2 are compared, a better performance of the series SB specimens can be observed: firstly, the SB_MA_L50×1.2 failed by FRP rupture at its maximum tensile capacity (ultimate strain near 1.48%); and the debonding initiation, showed in **Figure 2.7h** as two drop points in the third branch of each F-δ curves, started earlier on the specimen with a grinded surface at the load close to 46 kN, while a value of 56 kN was registered for the sand blasted slab. Both slabs performed similarly in terms of cracking and yielding initiation, as they also had resembling stiffnesses (K_I and K_{II}).

The concrete plays a key role in the behaviour of each specimen in terms of ultimate carrying capacity, as well as in cracking and deflection development. For that reason, this comparison between series GD and series SB was made considering the improvement of the strengthening (relative to the reference specimens). SB_EBR_L50×1.2 indices that through sand blasting it was possible to obtain a better surface adherence. The ultimate force on this slab was 57% higher relative to the values registered on SB_REF_3. When the GD_EBR_L50×1.2 is compared with the GD_REF_1, an improvement of 19% on the ultimate carrying capacity is observed. Regardless of the thicker laminate strip, the GD_EBR_L50×1.4 improved the F_{max} by 38% when compared with the GD_REF_1.

Figure 2.13 shows the failure mode reported on both slabs. It is clear that the surface's adherence was higher on series SB as the SB_EBR_L50×1.2 debonding was in the interface epoxy adhesive/CFRP laminate instead of in the interface epoxy adhesive/concrete (GD_EBR_L50×1.4).

2.4 Conclusion

The main objective of these preliminary studies was to assess the service and ultimate behaviour of two different types of anchorage systems in the context of the use of prestressed CFRP laminates strips applied according to the EBR technique: the mechanical anchorage (MA) and the gradient anchorage (GA). The obtained results allow to draw a certain number of conclusions, namely:

- In general it was observed that, at service level, the strengthening (prestressed and non-prestressed) improved the slabs performance with lower deflections, crack width delay and lower crack spacing;
- A similar response was observed in both anchorage techniques. Yet, the metallic anchors composing the MA system prevented a premature failure by debonding and allowed the slabs to support higher ultimate loads and deflections;
- Eight of the nine strengthened specimens failed by strip debonding. Only the SB_MA_L50×1.2 failed by FRP rupture at its maximum tensile capacity. An analysis based on the available literature clearly implies that the debonding failure started from middle of the slabs (intermediate debonding) and then shifted to the extremities of the slabs;
- A greater use of the CFRP laminate strip tensile capacity was attained when prestressing was applied to the CFRP laminates. The average ultimate strain on the CFRP laminate increased by 132% and 74% with prestressing in series GD and SB, respectively;
- The CFRP laminate width had a considerable influence on the general behaviour of the strengthened elements. The slab GD_MA_L80×1.2 showed an increase on the ultimate carrying capacity of 23%, greater stiffness (54%) and higher cracking (26%) and steel yielding forces (31%) when compared with the GD_MA_L50×1.2. However, similar performance was observed for the strip with different thickness;
- In all MA specimens the ends of the CFRP laminate were transversely compressed by the metallic anchors through the same torque applied in each bolt (150 N×m). As a result, wider laminates exhibit lower compression pressures (GD_MA_L50×1.2 – 20.83 MPa *versus* GD_MA_L80×1.2 – 13.02 MPa). Results showed that the shear stress in the CFRP at the metallic anchor region is inconstant, as it was possible to observe higher values on the GD_MA_L50×1.2 (9.14 MPa) than on the GD_MA_L80×1.2 (7.40 MPa).

- Concrete surfaces that have been sand blasted achieved a higher roughness and adherence than those grinded with a stone wheel. The performance improvement observed for each method of surface preparation fundaments this idea: series SB specimens (sand blasted) showed relative higher ultimate loads and they did fail with higher CFRP strains.

Based on the obtained results a final geometry was adopted in the comprehensive experimental program developed to achieve the main objective of this thesis (additional details available in Chapter 3). All strengthened slabs showed a substantial increase in the load carrying capacity, but the slabs from series SB presented the most convenient traits. The ultimate load carrying capacity of the prestressed slabs from series SB, was twice the value observed on the unstrengthened specimen from the same series. For the abovementioned reasons, sand-blasting the concrete surface was used. Therefore, the configuration used on series SB was assumed for the main experimental campaign: CFRP laminate strip of 50 × 1.2 [mm], prestressed up to the strain of 0.4% on a previously sand-blasted concrete surface.

2.5 References

[1] M. R. Mostakhdemin Hosseini, S. J. E. Dias, and J. A. O. Barros, "Effectiveness of prestressed NSM CFRP laminates for the flexural strengthening of RC slabs," *Compos. Struct.*, vol. 111, pp. 249–258, May 2014.

[2] M. R. Mostakhdemin Hosseini, S. J. E. Dias, and J. A. O. Barros, "Flexural strengthening of reinforced low strength concrete slabs using prestressed NSM CFRP laminates," *Compos. Part B Eng.*, vol. 90, pp. 14–29, Apr. 2016.

[3] L. Correia, T. Teixeira, J. Michels, J. A. P. P. Almeida, and J. Sena-Cruz, "Flexural behaviour of RC slabs strengthened with prestressed CFRP strips using different anchorage systems," *Compos. Part B Eng.*, vol. 81, pp. 158–170, 2015.

[4] J. Sena-Cruz, J. Michels, Y. E. Harmanci, and L. Correia, "Flexural Strengthening of RC Slabs with Prestressed CFRP Strips Using Different Anchorage Systems," *Polymers (Basel).*, vol. 7, no. 10, pp. 2100–2118, 2015.

[5] L. Correia, J. Sena-Cruz, J. Michels, and P. M. França, "Reforço à flexão de lajes de betão

armado com laminados de CFRP pré-esforçados usando distintos métodos de ancoragem," *Eng. Civ.*, vol. 51, no. ISSN 0873-1152, pp. 5–22, 2015.

[6] T. Teixeira, L. Correia, J. Sena-Cruz, and J. Michels, "Reforço à flexão de lajes de betão armado com laminados de CFRP pré-esforçados: comportamento em estado limite último e de utilização," in *JPEE - 5as Jornadas Portuguesas de Engenharia de Estruturas*, 2014.

[7] L. Correia, T. Teixeira, J. Sena-Cruz, and J. Michels, "Flexural strengthening of RC slabs with prestressed CFRP strips using different anchorage systems," in *CICE - The 7th International Conference on FRP Composites in Civil Engineering*, 2014.

[8] J. Sena-Cruz, L. Correia, T. Teixeira, and J. Michels, "Flexural strengthening of RC slabs with prestressed CFRP strips: serviceability and ultimate load state behavior," in *CBPAT - 1º Congresso Brasileiro de patologia das construçoes*, 2014.

[9] LNEC E397-1993:1993 and LNEC E397, *Concrete - Determination of the elasticity Young modulus under compression*. Portugal, 1993.

[10] IPQ - Instituto Portugues da Qualidade;, *NP EN 12390-3:2011*. Caparica, 2011.

[11] NP EN ISO 6892-1, "Metallic materials - Tensile testing – Part 1: Method of test at room temperature," *IPQ - Inst. Port. da Qual.*, 2012.

[12] NP EN 1992-1-1, "Design of concrete structures. Part 1-1: General rules and rules for buldings," *IPQ - Inst. Port. da Qual.*, 2010.

[13] Iso-527-5, "Plastics–determination of tensile properties – Part 5: Test conditions for unidirectional fibre-reinforced plastic composites," *London Br. Stand. Inst.*, 1997.

[14] J. Sena-Cruz, J. Michels, C. Czaderski, and M. Motavalli, "Mechanical behavior of epoxy adhesives cured at high temperatures," *Tech. Rep. no. 880163, EMPA, Switz.*, p. 30, 2012.

[15] P. Fernandes, J. L. Granja, A. Benedetti, J. Sena-Cruz, and M. Azenha, "Quality control and monitoring of NSM CFRP systems: E-modulus evolution of epoxy adhesive and its relation to the pull-out force," *Compos. Part B Eng.*, vol. 75, pp. 95–103, Jun. 2015.

[16] J. Michels, C. Czaderski, R. El-Hacha, R. Brönnimann, and M. Motavalli, "Temporary bond

strength of partly cured epoxy adhesive for anchoring prestressed CFRP strips on concrete," *Compos. Struct.*, vol. 94, no. 9, pp. 2667–2676, Sep. 2012.

[17] J. Michels, J. J. Sena-Cruz, C. Czaderski, and M. Motavalli, "Structural Strengthening with Prestressed CFRP Strips with Gradient Anchorage," *J. Compos. Constr.*, vol. 17, no. 5, pp. 651–661, 2013.

[18] CEB-FIP, *Model Code for Concrete Structures 2010*. 2013.

[19] CNR, "Guide for the design and construction of externally bonded FRP systems for strengthening existing structures," 2013.

[20] International Federation for Structural Concrete (fib), "Externally bonded FRP reinforcement for RC structures," Lausanne, Switzerland, 2001.

[21] C. Czaderski, "Flexural strengthening of reinforced concrete Swiss Code 166 and other codes/guidelines - ETH Lecture 101-0167-01L (lecture notes)," Zürich, Switzerland, 2017.

[22] Schweizer Ingenieur-und Architektenverein and (SIA), "Klebebewehrungen (Externally Bonded Reinforcements)," Zürich, Switzerland, 2004.

[23] Eurocode, "BS EN 1992-2:2005 - Eurocode 2: Design of concrete structures - Part 2: Concrete bridges - Design and detailing rules," *Eurocode 2*, 2005.

CHAPTER 3

DURABILITY AND LONG-TERM BEHAVIOR OF RC SLABS STRENGTHENED WITH PRESTRESSED CFRP STRIPS UNDER DIFFERENT ENVIRONMENTAL AND LOADING CONDITIONS

3.1 Introduction

Despite the recent research developments on the durability and long-term behaviour of prestressed RC elements with FRPs [1–4], the effects of environmental exposure conditions such as immersion in water, immersion in water with chlorides or wet/dry cycles with water, on RC elements strengthened with prestressed EBR CFRP laminates has not yet addressed by the scientific community.

With the insights obtained from the preliminary studies, an experimental program was carried out with the main objective of contributing to the knowledge on durability and long-term behaviour of RC slabs strengthened with prestressed CFRP laminate strips according to the EBR technique. For that purpose, twenty strengthened RC specimens were submitted to the following environmental conditions for approximately 8 months: (i) reference environment – specimens kept in a climatic chamber at 20 °C; (ii) water immersion in tank at 20 °C of temperature; (iii) water immersion in tank with 3.5% of dissolved chlorides (NaCl) at 20 °C of temperature; and (iv) wet/dry cycles in a tank with a water temperature of 20 °C. Additionally, half of the specimens were subjected to sustained loading at a load level of 1/3 of the ultimate load, with the occurrence of cracking.

This chapter details the work carried out. Firstly, the experimental program is introduced. Then, in Section 3.3, the results obtained from the monitoring program adopted since the strengthening phase (prestress application) are presented. The monitoring program included the register of the strains in the CFRP laminate, the temperature variation, and, for specimens subjected to the creep loading, the mid-span vertical deflection. Based on these results, an analysis on the prestress losses and on the creep behaviour is presented. After the exposure period the slabs were monotonically tested up to failure by using a four-point bending test configuration. The observed performance of the tested RC slabs allowed several conclusions regarding the durability and overall performance of both anchorage systems. Section 3.4 presents the results, discussion and main conclusion of the monotonic tests.

3.2 Experimental programme

The experimental programme included twenty reinforced concrete (RC) slabs as presented in **Table 3.1**: (i) four control specimens (series T0); (ii) eight slabs subjected to distinct environmental conditions (labelled with the suffix _U); and, (iii) eight slabs subjected to the combined effect of environmental and loading conditions (labelled with the suffix _C). Loading and the exposure to different environmental conditions lasted for approximately eight months. Four distinct environmental conditions were considered: (i) specimens subjected to laboratory premises with a controlled temperature of 20 °C and relative humidity of 55% (series REF and T0); (ii) specimens immersed in tap water at 20 °C (series TW); (iii) specimens immersed in water at 20 °C with 3.5% of chlorides (series CW); and, (iv) specimens subjected to wet/dry cycles in tap water at 20 °C (series WD). Each cycle used for series WD lasted one week, on which the slabs were fully immersed on tap water for 3 days and, during the remaining four days, they were subjected to laboratory premises (20 °C). As it is shown in **Table 3.1**, all specimens are labelled with a generic denomination: X_Y_Z, where X indicates the specimens series (T0, REF, TW, CW, and WD), Y indicates the type of anchorage (MA or GA) and Z indicates the cracking state when the specimens are first exposed to the environmental conditions (U for uncracked and C for cracked).

The four control specimens from series T0, are the same four slabs from series SB presented in Chapter 2: one unstrengthened RC slab (T0_REF, labelled as SB_REF_3 in Chapter 2); a second slab strengthened with a simple CFRP laminate strip according to the EBR technique without prestressing (T0_EBR, labelled as SB_EBR_L50×1.2 in Chapter 2); a third slab strengthened with one externally bonded prestressed CFRP laminate strip with the MA system (T0_MA, labelled as SB_MA_L50×1.2 in Chapter 2); and a forth slab strengthened with one externally bonded prestressed CFRP laminate strip with the GA system (T0_GA, labelled as SB_GA_L50×1.2 in Chapter 2).

Table 3.1
Experimental programme.

Specimen	Environmental Conditions/Observations	Anchorage System	Initial Strain [%]	Prestress Force [kN]	Sustained Load
Series T0					
T0_REF	Specimens tested at the beginning of the	–	–	–	–
T0_EBR	experimental program.	–	0.00	0.00	–
T0_MA		MA	0.42	41.6	–
T0_GA		GA	0.40	39.6	–
Series REF					
REF_MA_U	Specimens subjected to laboratory	MA	0.41	40.6	NO
REF_GA_U	premises: 20 °C and 55% of RH for a	GA	0.41	40.6	NO
REF_MA_C	period of 8 months.	MA	0.37	36.6	YES
REF_GA_C		GA	0.41	40.6	YES
Series TW					
TW_MA_U	Specimens immersed in tap water at	MA	0.40	39.6	NO
TW_GA_U	20 °C for a period of 8 months.	GA	0.41	40.6	NO
TW_MA_C		MA	0.41	40.6	YES
TW_GA_C		GA	0.41	40.6	YES
Series CW					
CW_MA_U	Specimens immersed in tap water at	MA	0.40	39.6	NO
CW_GA_U	20 °C with 3.5% of chlorides for a period	GA	0.41	40.6	NO
CW_MA_C	of 8 months.	MA	0.41	40.6	YES
CW_GA_C		GA	0.40	39.6	YES
Series WD					
WD_MA_U	Specimens subjected to wet/dry cycles	MA	0.40	39.6	NO
WD_GA_U	in tap water at 20 °C for a period of 8	GA	0.40	39.6	NO
WD_MA_C	months.	MA	0.42	41.6	YES
WD_GA_C		GA	0.42	41.6	YES

Notes: GA = Gradient Anchorage; MA = Mechanical Anchorage.

3.2.1 Specimens and test configuration

All specimens have the same geometry and longitudinal inner reinforcement as the specimens described in Chapter 2 (see **Figure 3.1**). Strengthening was performed by using 2200 mm long CFRP laminate strips with a rectangular cross-section of 1.2 mm by 50 mm. In all slabs, prior to

the strengthening the surface of the concrete substrate was sand-blasted to enhance the bond between materials. The strengthening procedures followed the procedure described in Section 2.3 of Chapter 2.

The prestress level was controlled by strain gauges previously placed at the mid-span of the CFRP laminate strip. The average prestrain imposed was approximately 0.4%. **Table 3.1** shows the values of the registered prestrain and prestress force at the middle of the CFRP laminate for all specimens at the end of the strengthening procedure. The strain in the CFRP laminate was continuously registered for the following weeks and a deeper analysis on the short-term prestress losses is given in Section 3.3.1.

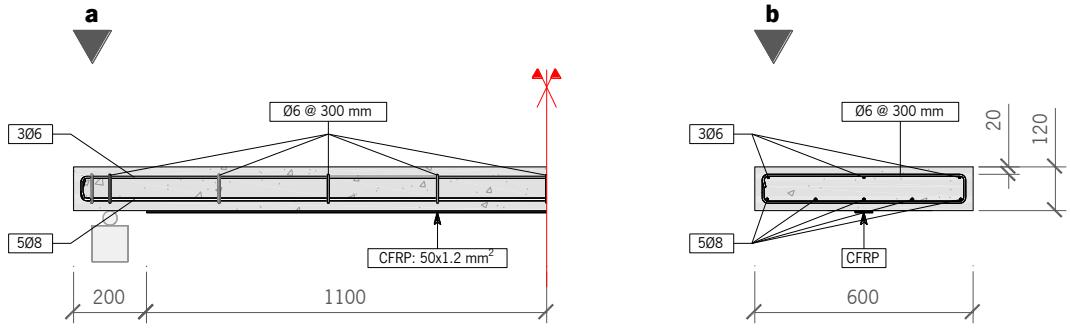

Figure 3.1: Specimens geometry: (a) longitudinal and (b) transverse view. Note: All units are in millimetres.

A schematic schedule representing the main tasks performed during this work is shown in **Figure 3.2**. Approximately six months after the strengthening, the slabs were exposed to the different studied environmental conditions. Initially, the prototypes were placed in the empty water tanks (see **Figure 3.3a**, **Figure 3.3b**, and **Figure 3.3c**), or inside a climatic chamber in the case of the slabs REF (see **Figure 3.3b** and **Figure 3.3h**). In each tank, or climatic chamber, four slabs were placed: two slabs (one MA and one GA) to be subjected to the corresponding environmental condition and two others (one MA and one GA) to be subjected to the combined effect of the environmental condition and the sustained loading. Several granite blocks (weight from 0.8 kN to 4.6 kN) were used to achieve the predefined load (20 kN, see **Figure 3.3e**). While the weights were being laid (see **Figure 3.3f**), a continuous observation of the slab's bottom surface was carried out. Crack initiation was observed in all "_C" specimens for an average mid-span vertical displacement of 1.7 mm and a load of approximately 17 kN. These values of cracking load and

corresponding mid-span displacement were in agreement with the results obtained in the monotonic tests of the slabs of series T0 (see Section 3.4).

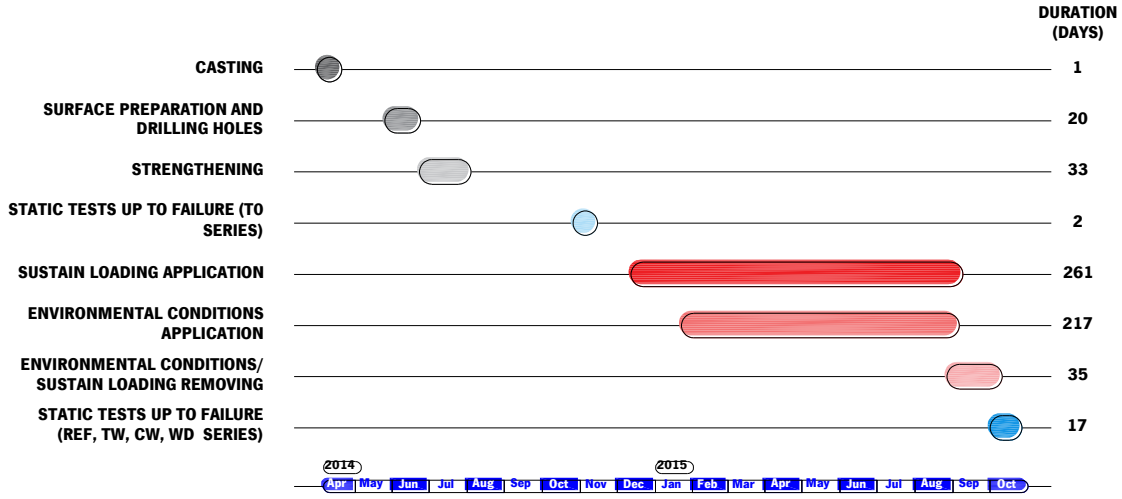

Figure 3.2: Timeframe of developed work.

As shown in **Figure 3.2**, the environmental conditions were imposed approximately one month after loading and lasted for 8 months. During this period, the slabs creep behaviour was monitored in terms of mid-span deformation and CFRP laminate strain variation. **Figure 3.4** illustrates the creep test configuration and the instrumentation. The creep loading was applied according to a four-point bending test, identical to monotonic test set-up (see Chapter 2, section 2.2.1). In order to measure the mid-span vertical deflection two distinct devices were used: (i) one LVDT with the range of ±75 mm and linearity of ±0.10%; and (ii) one mechanical dial with the measuring span of 40 mm and graduation value of 0.01 mm. The instrumentation also included two optical fibre strain sensors (OFSS1 and OFSS2) that continually measured the strain evolution in the CFRP laminate strip (see **Figure 3.4**). The optical fibre sensors (HBM FiberSensing® FS6200) are Fibre Bragg Grating (FBG) based sensors with a gauge length of 92 mm (measuring range of ±2500 $\mu\varepsilon$ and a resolution equal to 1 $\mu\varepsilon$).

The slabs subjected only to the environmental conditions (suffix "_U", bottom slab on **Figure 3.4**) were also monitored in terms of CFRP strains. For that purpose, two optical fibre strains sensors (OFSS1 and OFSS2) were fixed at the mid-span and at the load application point. All OFSS have identical technical characteristics.

Figure 3.3: Prototypes: (a) in Tank 1 (tap water); (b) in Tank 2 (water with chlorides) and REF slabs (before the pre-fabricated climatic chamber was installed); (c) in Tank 3 (wet/dry cycles); (d) data acquisition system; (e) creep load; (f) loading the specimens; (g) specimen loaded; (h) Installed pre-fabricated climatic chamber (REF slabs); (i) in Tank 2 (water with chlorides, during creep test).

Due to a technical problem that occurred on the air-conditioning system of the climatic chamber where the REF specimens were placed, the specimen REF_GA_C was disregarded. Finally, the specimens were removed from the exposure environments and the sustained loads were removed. After a resting period of one month, the slabs were tested up to failure, using the same four-point configuration. The test set-up and instrumentation used for the monotonic tests can be found in Section 2.2.1 of Chapter 2. Additional strain gauges (TML BFLA-5-3) were placed on the CFRP laminate, near the anchorage zone: on the MA slabs, one strain gage was fixed 30 mm away from the each anchorage plate (SG1 and SG4); whereas on the GA slab, one strain gauge was fixed 630 mm away from the extremities of the CFRP laminate (SG1 and SG4) and another strain gauge

was placed at the middle of the anchorage zones (SG1' and SG4'). All strengthened slabs uses two strain gauges to monitor the strain variation on the laminate at mid-span (SG2) and under the applied load point (SG3). The concrete strain was assessed with a strain gauge (SG5) placed at mid-span on the top surface, and the steel reinforcement strain by means of another strain gauge (SG6) fixed in the tensile rebar positioned in the middle of the cross-section, at mid-span.

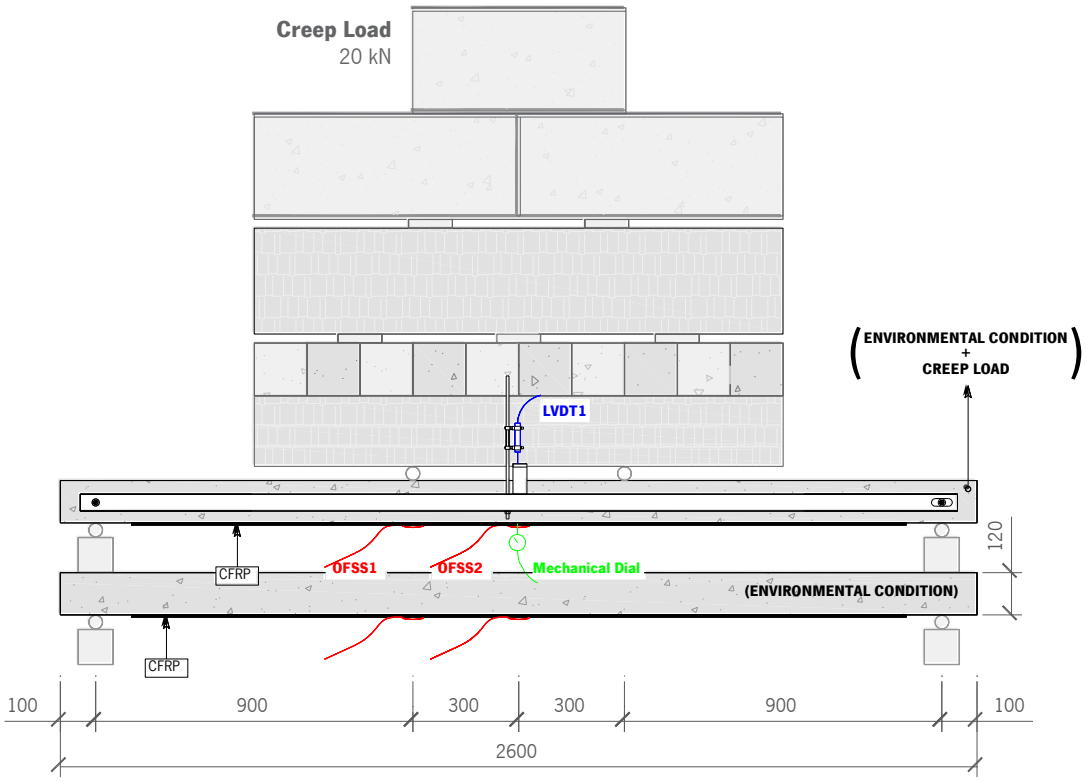

Figure 3.4: Specimens geometry. Note: All units are in millimetres.

To document the evolution of the processes that lead to the degradation of the strengthening effect provided by the CFRP laminate, the bottom surface of the specimens at which the laminates were inserted was analysed using a Digital Image Correlation procedure [5]. The lens used had an aperture of f11 and the focal length was 36 mm. Led lights were used to illuminate the surface of the specimen. The camera sensor was a full frame size, with 36 Mpix. Considering that the priority was to trace the initiation and propagation of the cracks at the tensioned face of the specimens during testing, the principal tensile strain fields were mapped using a fine facet mesh.

3.2.2 Materials

Material characterization included the evaluation of the mechanical properties of the materials involved in this experimental program, namely: concrete, steel, CFRP laminate strip and epoxy adhesive. The ready-mixed concrete (grade of C30/37) was produced based on the proportions of mixing components by weight of 1: 2.95: 2.93: 0.02: 0.56 (cement: fine aggregate: coarse aggregate: superplasticizer: water). Aggregates were composed of crushed granite with a maximum size of 12.5 mm and Portland cement type CEM II/A-L 42,5R was used. A single concrete batch of 7.0 m^3 was prepared to cast all slabs and testing samples. For characterizing the mechanical properties of the concrete, six cylindrical specimens with 300 mm of height and 150 mm of diameter were used for each series. The modulus of elasticity and the compressive strength were evaluated 28 days after casting following the LNEC E397 1993:1993 [6] and NP EN 12390-3:2011 [7] recommendations, respectively. Additionally, the modulus of elasticity and the compressive strength were also characterized at the time when the static tests of the slabs up to failure occurred (see **Table 3.2**). Results show the evolution of the modulus of elasticity (E_c) and the compressive strength (f_c) for specimens in contact with water (series TW, CW and WD), which is related to the process of hydration of the cement [8]. When comparing the concrete specimens fully immersed in water (series TW) with the reference series (T0), an additional increase of 20% and 35% of the E_c and f_c, respectively, were observed.

In order to determine the tensile properties of steel reinforcement, four samples of each bar type were used. Tensile tests were carried out according to NP EN ISO 6892-1:2012 [9] recommendations and the results in terms of mean values for the modulus of elasticity (E_s), as well as yield (f_y) and ultimate (f_u) tensile strengths are presented in **Table 3.2**.

The pultruded CFRP laminate strips (Type: S&P Laminates CFK) were used in the experimental work [10]. Tensile properties were assessed using six samples and the experimental procedure followed was the one described by ISO 527-5:1997 [11]. A Young's modulus (E_f) of 168 GPa and an ultimate strength (f_f) of 2944 MPa were obtained (see **Table 3.2**).

The two-component epoxy adhesive (Type: S&P Resin 220) used to bond the CFRP laminate to the concrete surface is solvent free, thixotropic and grey. Previous studies have shown that, after 7 days

of curing at 21 °C, a modulus elasticity of 8.7 GPa (CoV=6.0%) and a tensile strength of 20.7 MPa (CoV=11.0%) are obtained [12].

Table 3.2
Material characterization (average values).

Material	Series	Modulus of elasticity [GPa]	Compressive strength [MPa]	Tensile strength [MPa]	Yield strength [MPa]	Ultimate strength [MPa]
Concrete						
Age: 28 days(a)	T0	27.8 (2.9%)	37.3 (1.9%)	–	–	–
Age: 209 days(b)	T0	30.0 (-)	40.2 (0.7%)	–	–	–
Age: 570 days(b)	REF	27.0 (2.4%)	39.5 (5.3%)	–	–	–
Age: 570 days(b)	TW	33.4 (1.3%)	50.2 (1.3%)	–	–	–
Age: 570 days(b)	CW	33.9 (1.1%)	45.9 (8.0%)	–	–	–
Age: 570 days(b)	WD	32.2 (5.1%)	48.6 (2.1%)	–	–	–
Steel						
Bar type: Ø6	–	206.9 (0.4%)	–	–	519.4 (6.1%)	670.2 (5.1%)
Bar type: Ø8	–	235.1 (4.6%)	–	–	595.9 (4.1%)	699.0 (2.1%)
CFRP						
50×1.2 [mm]	–	167.7 (2.9%)	–	2943.5 (1.6%)	–	–

Notes: [a] Tests at 28 days; [b] Tests at the age of the monotonic tests of the slabs; the values between parentheses are the corresponding coefficients of variation (CoV).

3.3 Prestress losses and creep behaviour

This section presents the results obtained from the monitoring program adopted since the strengthening phase (prestress application) until the monotonic test up to failure. The strains in the CFRP laminate were measured immediately after the first hour of strengthening to evaluate the instantaneous prestress losses. Then, before the start of the environmental exposure or the creep loading, all slabs were monitored in terms of different parameters. The CFRP strain evolution, mid-span vertical displacement and temperature variation are presented below and discussed.

3.3.1 Short-term prestress losses

As mentioned earlier, the strains in the CFRP laminate were monitored by using strain gauges and optical fibre sensors, as depicted in **Figure 3.5**. During the prestress application, a single optical fibre sensor was placed at the mid-span of the strengthened slab; whereas four strain gauges were installed in three strategic positions of the CFRP strip: (i) one in each end anchorage side, more precisely, 80 mm apart the steel plate (for the MA slabs) or 40 mm after the end of each gradient anchorage; (ii) one fixed at the middle of the specimens; and (iii) one strain gauge placed 300 mm from the mid-span, where a load point would be applied during the creep and monotonic tests up to the failure. In some specimens the monitoring of the mid-span deflection was conducted using a Mechanical Dial (see **Figure 3.5b**). The Fibre Bragg Grating datalogger (see **Figure 3.5a**) used to measure the mid-span strain with OFSS was set with a record frequency of 0.1 Hz, whereas the frequency of acquisition for the remaining strain gauges was kept at 1 Hz (see **Figure 3.5d**).

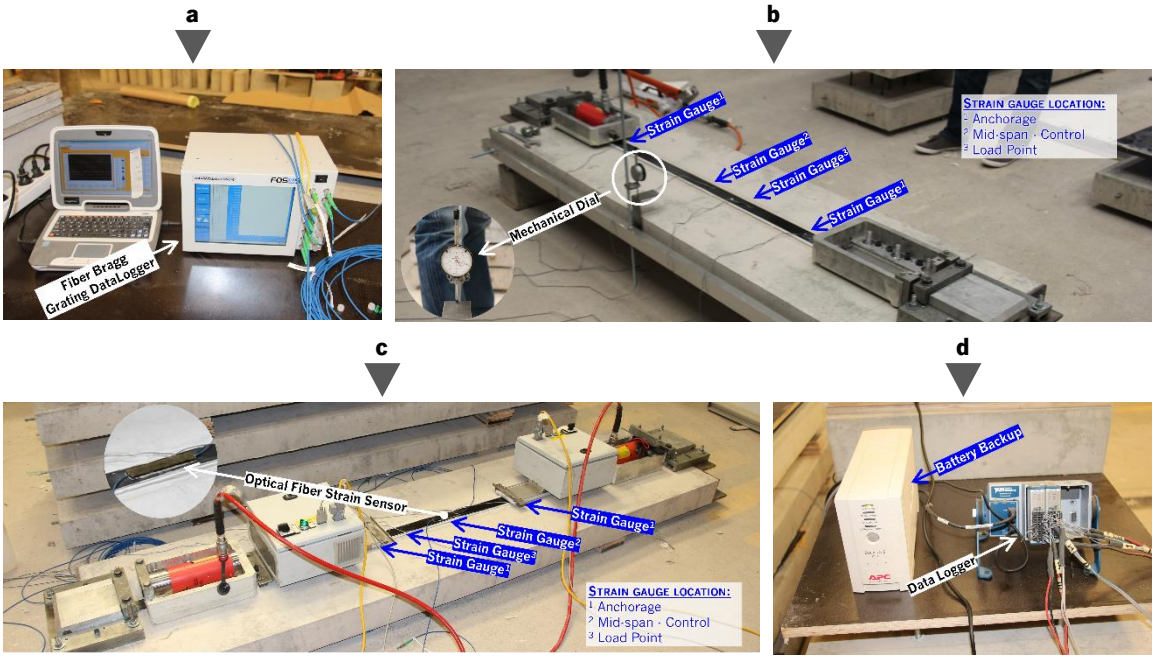

Figure 3.5: (a) Data acquisition system of optical fibre strain sensors (OFSS); (b) mid-span deflection and CFRP strain measurements during prestress application of the MA_T0; (c) typical sensors distribution on the CFRP laminate; (d) Data acquisition system of strain gauge (SG) sensors.

Figure 3.6 shows the typical CFRP strain evolution, at the mid-span and at near the anchorage, after the prestress application for the case of the MA and GA systems. In general, the prestress

losses, presented in **Table 3.3**, are very low (at about 0.01% of strain – absolute value – and maximum variation of 3.6% – relative value) for both anchorage systems.

In the case of the present test specimens, the instantaneous losses are solely dependent on the prestressing systems because the friction between the materials (CFRP laminate and concrete) does not exist and the instantaneous elastic deformation of the concrete are inevitably compensated with the prestress application system. In some cases, at prestressing application stage, a difference between the strain at the mid-span and the strain near the anchorages was observed. The maximum difference between both regions was equal to 0.013% and was observed on slabs TW_MA_C and REF_GA_U. As can be observed in **Figure 3.6**, in some specimens, the highest value was registered in the mid-span section, whereas in others the greatest value was observed near the anchorage. Due to its relatively small value, this difference (misalignment of the strain gauges might be the reason) can be overlooked.

For the case of slabs strengthened with the MA system, short-term prestress losses can be attributed to the process of applying the fixing screws between the aluminium frame and the clamp units (see **Figure 3.6a** and **Figure 3.6c**), typically at about 10 minutes after the application of the prestress. It should be pointed that these spacers are used to block the prestressing system and, consequently, avoid prestress losses during the curing of the epoxy. Once installed, these fixing screws perform as expected and no CFRP strain losses were identified. **Figure 3.6** presents the strain variation during the prestress application on slabs MA_REF_U (**Figure 3.6a**) and MA_REF_C (**Figure 3.6c**). As can be observed, shortly after reaching the predefined CFRP strain (0.4% - absolute value), a variation of 3.3% and 3.6% of the initial prestrain (relative value) is observed for specimens MA_REF_U and MA_REF_C, respectively (which, in average, represents a variation of 1.2 kN of the prestress load).

The gradient anchorage system uses the adhesive's ability to cure fast at high temperatures and hence to create a non-mechanical anchorage. In this experimental campaign the anchorages, as previously referred, were divided into three sectors and, as a consequence of its step-wise releasing of the prestress force, a strain loss was observed. This event occurred after the releasing of the first 1/3 of the prestress force in the first sector. In average the instantaneous prestress losses

variation on slabs with the gradient anchorage were equal to 2.1% of the initial prestrain (0.8 kN). As can be seen in **Figure 3.6**, with the gradient anchorage the prestress losses occur after 50 minutes, when 1/3 of the prestress force is released.

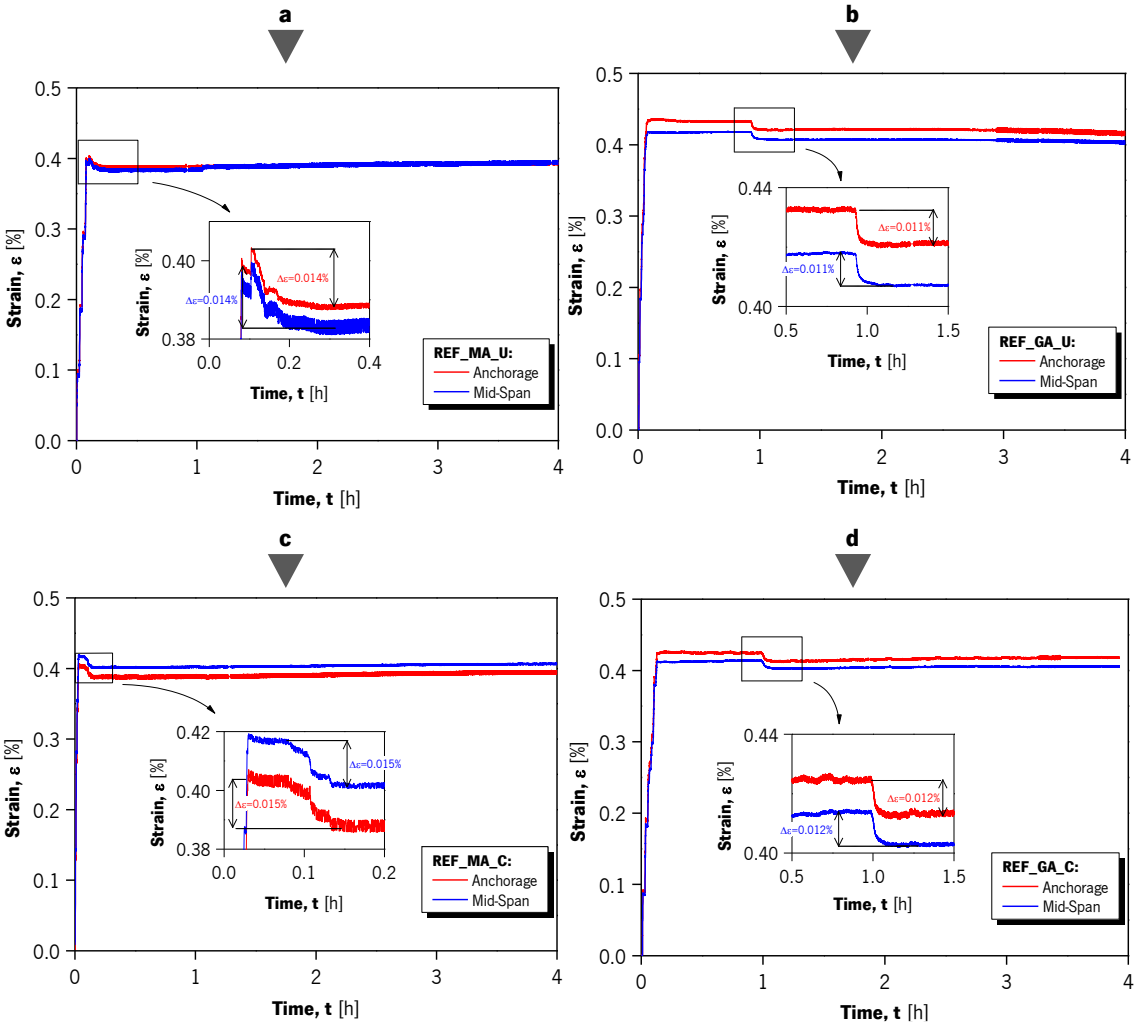

Figure 3.6: Typical evolution of CFRP strain after prestressing: (a) REF_MA_U; (b) REF_GA_U; (c) REF_MA_C; (d) REF_GA_C.

The refereed short-term prestress losses can be overlooked because they represent approximately 1 kN of prestress force loss. These results show that the gradient anchorage system has lower instantaneous losses than the mechanical anchorage system. However, with the mechanical anchorage it is possible to compensate the initial prestress loss: as the load is transferred from the hydraulic jack to the fixing screws (and prestrain losses start to occur), the hydraulic cylinder can be jacked to compensate the prestress losses because the epoxy adhesive is still fresh.

During the application of prestress, the mid-span displacement was recorded using a mechanical dial on two slabs with the MA anchorage system. For the applied CFRP prestrain level (0.40%), a mid-span displacement of 0.62 mm was registered. The camber mid-span displacement observed experimentally is in agreement with the numerical and analytical predictions (see Chapter 5). Additionally, it should be referred that this action did not cause any crack since materials remain in their linear elastic stage.

3.3.2 Long-term prestress losses

The CFRP strain at mid-span of each slab was monitored using an optical fibre strain sensor since the prestress application until the monotonic test up to failure. **Figure 3.7** shows the mid-span CFRP strain variation for all slabs subjected solely to the four environmental conditions (without creep loading). It should be noted that, in all prestressed slabs, the mid-span CFRP strain at the onset of the creep loading (t=0 h in **Figure 3.7**) is close to 0.4%; but, for the purpose of a clear analysis of the long-term CFRP strain evolution, the absolute value of the CFRP strain variation, $\Delta\varepsilon_f$, is presented ($\Delta\varepsilon_f$=0 when t=0, in **Figure 3.7**). The green line presented in **Figure 3.7a**, **Figure 3.7b**, **Figure 3.7c**, and **Figure 3.7d** show the difference of mid-span strain variation between both slabs ($\Delta\varepsilon_{MA\_U} - \Delta\varepsilon_{GA\_U}$) of series REF, TW, CW and WD, respectively. As can be seen, the strain was significantly influenced by the type of environmental condition and temperature.

Both specimens kept in a laboratory environment (series REF, see **Figure 3.7a**) show small CFRP strain variation during the eight months test period. As expected, when the temperature increases, the CFRP strain also increases (this effect can be explained with the thermal expansion of slabs, including the composing materials). By subtracting the mid-span strain variation of slab REF_GA_U from the mid-span strain variation of the slab REF_MA_U (green line in **Figure 3.7a**) it is clear that the temperature produced similar effect on both specimens. As referred before, a technical problem occurred on the air-conditioning system of the climatic chamber and the temperature reached over 40 °C (marked as **(TP)** in **Figure 3.7a**). As expected, the CFRP strain in both specimens increased, but returned back to the previous strain value once the problem was solved.

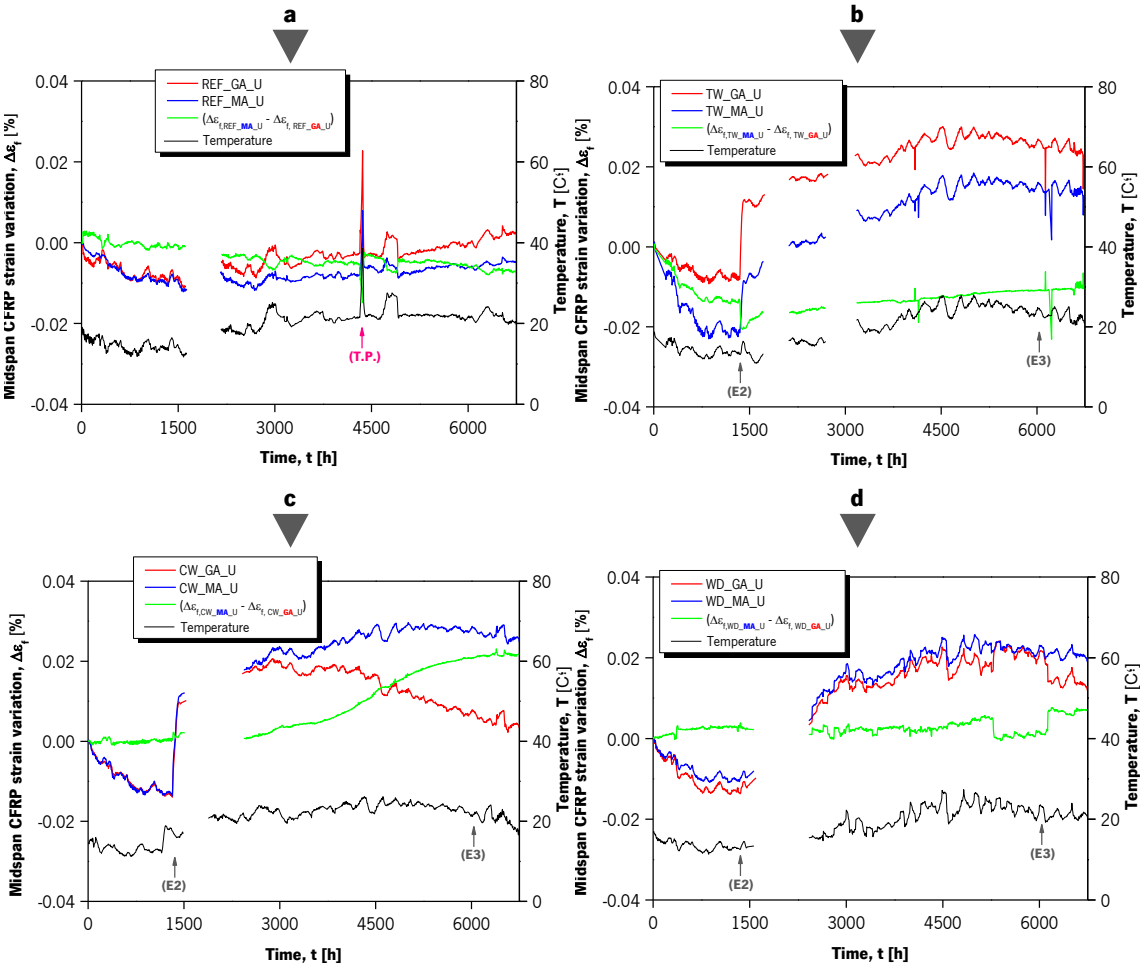

Figure 3.7: Evolution of the mid-span CFRP strain of the slabs (without creep loading) from: (a) series REF; (b) series TW; (c) series CW; and (d) series WD.

The immersion in tap water (series TW, see **Figure 3.7b**) and immersion in water with 3.5% of chlorides (series CW, see **Figure 3.7c**) produced an increase on the mid-span CFRP strain of approximately 0.02% (absolute value, marked as (E2) in **Figure 3.7**). A volumetric expansion mainly due to the concrete water absorption might be the reason for such behaviour. The behaviour was previously observed in other experimental research works [13]. The slabs from series WD (see **Figure 3.7d**) also show higher mid-span CFRP strain variation (same values as series TW and CW) than both REF slabs. Contrary to series TW and CW, where the CFRP strain increase can be considered as instantaneous (duration of two days), in series WD the mid-span CFRP strain increased gradually during the first two months of wet-dry cycles. It should be highlighted that when the slabs were submitted to their water-based environments (TW, CW and WD) the water and the slabs were at the same temperature.

The CW_GA_U shows a decrease in the mid-span CFRP strain variation since the 3000 hours (see **Figure 3.7c**). It should be mentioned that during the monitoring tests, this specimen presented the highest ultimate load and highest ultimate deflection from all GA slabs. Based on the aforesaid information, the most probable explanation for this CFRP strain decrease might be an acquisition system malfunction.

Note that the time when the slabs start to be submitted to the environmental conditions are marked in **Figure 3.7** with the label "**(E2)**", whereas the label "**(E3)**" is used to highlight the end of the environmental exposure. At last, it should be highlighted that, regardless of the anchorage systems, small CFRP strain variations were observed. As it is shown in **Figure 3.7** the differences between both anchorage systems can be neglected.

3.3.3 Creep behaviour

The evolution of the displacement at mid-span along time of the eight slabs subjected to the creep load of 20 kN is presented in **Figure 3.8**. The creep load was based on the results obtained from the monotonic test of the slabs from series T0, carried out at the onset of the experimental program. This value corresponds to 1/3 of the slabs ultimate capacity. This load also yields to a compressive stress in concrete at about 1/3 of its ultimate strength at the time of the loading. As referred before, the evolution of displacement at mid-span over the time was measured with a redundant system composed of a LVDT and a mechanical dial gage within a period of 7000 hours. A good agreement between the readings from the mechanical dial gauge and from the LVDT for each slab was observed, increasing the reliability of the obtained results since no torsional deformation would be expected. In two specimens, TW_MA_C and CW_GA_C, the mechanical dial was damaged after a few months of use due to corrosion caused by the water-based environments and, for that reason, these slabs do not present measurements with the mechanical dial gage until the end of the creep tests. **Figure 3.8** also presents the temperature variation in each environment and four events: **(E1)**, the initiation of the creep test (loading of the specimens with the gravity load of 20 kN); **(E2)**, the moment when the slabs were submitted to the environmental conditions; **(E3)** , the time when the environmental exposure was ended, and the slabs were kept at in laboratory premises; and, **(E4)**, the time when the slabs were unloaded.

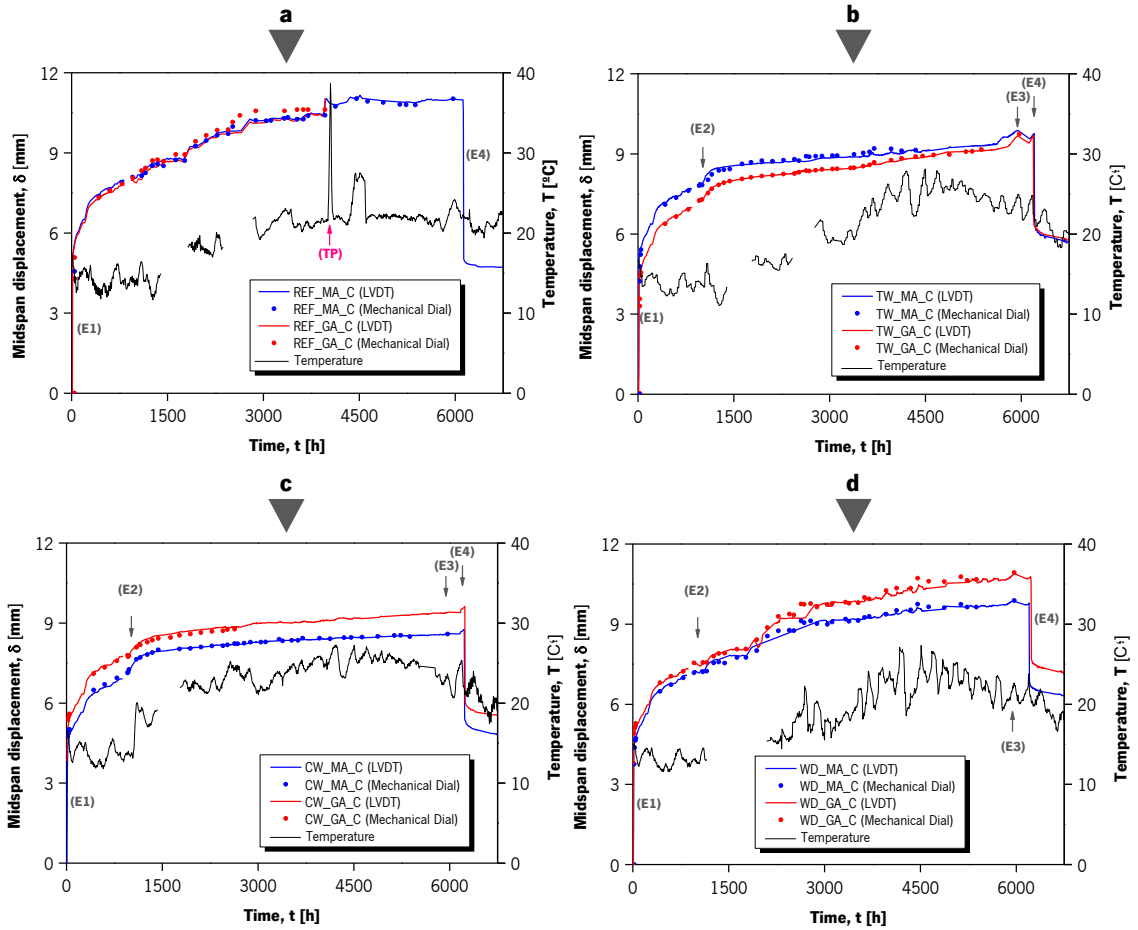

Figure 3.8: Evolution of the mid-span displacement by a LVDT and mechanical dial gage of the slabs from: (a) series REF; (b) series TW; (c) series CW; and (d) series WD.

The instantaneous vertical displacements measured after the application of the gravity loading ($\delta_{c,ela}$), the displacements measured before unloading ($\delta_{c,ult}$) and after unloading ($\delta_{c,rec}$) are presented in **Table 3.3**. The specimens composing series REF presented identical mid-span displacement variation overtime (see **Figure 3.8a**). An initial elastic deformation ($\delta_{c,ela}$) of 4.8 mm and 4.7 mm was observed for the MA and GA specimens, respectively. It should be noted that this level of elastic deformation is expected and is in agreement with the monotonic tests up to failure (see Section 3.4). In both slabs the typical primary and secondary creep stages were observed. As stated above, the GA strengthening failed after five months due to a technical problem that occurred in the air-conditioning system of the climatic chamber. Yet, the results obtained during these first five months indicate the behaviour of the GA slab could be identical to the one observed on the MA.

Table 3.3
Prestress losses and creep results.

Specimen	Initial	Prestress Losses		Creep parameters					
	Strain	$\Delta\bar{\varepsilon}_{f,i}$	$\Delta F_{p,i}$	$\delta_{c,ela}$	$\Delta\delta_{c,env}$	$\delta_{c,ult}$	$\delta_{c,rec}$	φ_{ult}	$\varphi_{t\infty}$
	[%]	[-]	[kN]	[mm]	[mm]	[mm]	[mm]	[-]	[-]
Series T0									
T0_REF	–	–	–	–	–	–	–	–	–
T0_EBR	0.00	–	–	–	–	–	–	–	–
T0_MA	0.42	2.2%	0.9	–	–	–	–	–	–
T0_GA	0.40	1.9%	0.8	–	–	–	–	–	–
Series REF									
REF_MA_U	0.40	3.3%	1.3	–	–	–	–	–	–
REF_GA_U	0.41	2.6%	1.1	–	–	–	–	–	–
REF_MA_C	0.42	3.6%	1.5	4.8	–	11.2	5.1	1.3	1.5
REF_GA_C	0.41	2.7%	1.1	4.7	–	10.9[a]	–[a]	1.3[a]	1.5[a]
Series TW									
TW_MA_U	0.40	1.8%	0.7	–	–	–	–	–	–
TW_GA_U	0.41	2.4%	1.0	–	–	–	–	–	–
TW_MA_C	0.41	3.1%	1.3	4.8	0.6	9.4	6.4	1.0	1.1
TW_GA_C	0.41	1.3%	0.5	3.9	0.7	9.2	6.4	1.4	1.5
Series CW									
CW_MA_U	0.40	1.7%	0.7	–	–	–	–	–	–
CW_GA_U	0.41	2.0%	0.8	–	–	–	–	–	–
CW_MA_C	0.41	3.1%	1.3	4.0	1.0	8.6	5.5	1.1	1.2
CW_GA_C	0.40	2.4%	1.0	4.3	0.8	9.3	6.1	1.2	1.3
Series WD									
WD_MA_U	0.40	3.7%	1.5	–	–	–	–	–	–
WD_GA_U	0.40	1.2%	0.5	–	–	–	–	–	–
WD_MA_C	0.42	3.2%	1.3	4.1	–	9.8	6.9	1.4	1.5
WD_GA_C	0.42	2.1%	0.9	4.3	–	10.7	7.7	1.5	1.7

Notes: [a] This specimen was disregarded due to a malfunction in the air-conditioning system; $\Delta\bar{\varepsilon}_{f,i}$ represents the relative strain variation due to short-term prestress loss; $\Delta F_{p,i}$ corresponds to absolute value of the short-term prestress loss; $\delta_{c,ela}$ is the instantaneous mid-span vertical displacement due to the gravity load ; $\Delta\delta_{c,env}$ is the instantaneous mid-span vertical displacement due to the environmental action; $\delta_{c,ult}$ is the mid-span vertical displacement before unloading; $\delta_{c,rec}$ is the final mid-span vertical displacement (after unloading); φ_{ult} is the creep coefficient based on the period of loading; and $\varphi_{t\infty}$ is the long-term creep coefficient.

Specimens immersed in tap water (TW) and immersed in water with 3.5% of chlorides (CW) presented an initial (elastic) average deformation of 4.30 mm as a structural response to the gravity loading. Likewise, this level of elastic deformation is expected and is in agreement with the monotonic tests up to failure (see Section 3.4). An abrupt displacement growth was registered when the specimens were immersed (see **Figure 3.8b** and **Figure 3.8c**). The existence of cracks in the bottom face of the slabs causes differential water absorption, and consequently differential volumetric variation, yielding to this steepest displacement growth. This behaviour had been also registered in other experimental programs with similar environmental and loading conditions, e.g. [13]. The self-weight of each slab (4.68 kN) was partially opposed by the water uplift, which is equal to 1.84 kN. The water uplift effect was not noticed in any specimen. The mid-span vertical displacement growth in the following 10 days after the environmental exposure ($\Delta\delta_{c,env}$) was, in average, equal to 0.8 mm (approximately 20% of the elastic deformation, $\delta_{c,ela}$). In general, the mid-span vertical displacement observed on these four slabs had an identical decreasing growth overtime. The slabs subjected to wet-dry cycles do not have a noticeable increase due to the lower contact with water as did the specimens from series TW and CW. When compared with the full immersion on water, the wet-dry cycles produced higher mid-span vertical displacements during the creep loading. These two specimens (series WD) were subjected to a higher temperature oscillation during the creep test period, and that factor might be the reason for the greater vertical mid-span displacements. Additionally, the water absorption by the concrete (porous material) in between 4.6% and 5.7% (0.21 kN to 0.26 kN) of its own weight was expected [14,15].

Figure 3.9 and **Figure 3.10** shows the mid-span vertical displacement evolution after the creep loading, $\delta_{c,CREEP}$. For an easier analysis, slabs with the same anchorage system were grouped into a single plot (**Figure 3.9a** for MA system and **Figure 3.9b** for GA system). Regardless of the anchorage system, the vertical displacement evolution after the elastic deformation is consistent with the environmental condition: the highest mid-span vertical displacement values are observed for the environments REF and WD, whereas the smallest mid-span vertical displacement values are observed in specimens immersed in water with 3.5% of chlorides (CW).

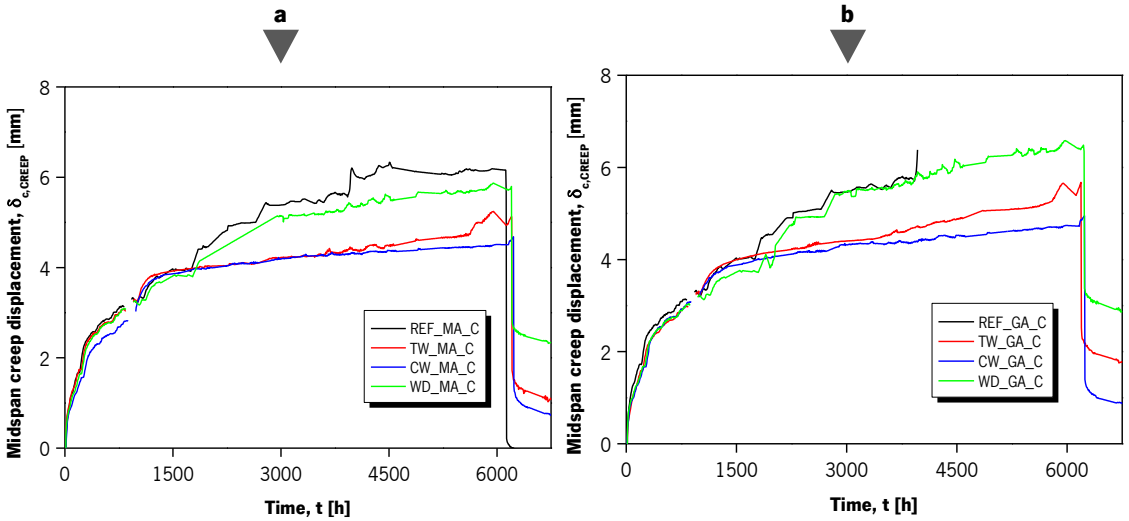

Figure 3.9: Evolution of the mid-span displacement due to creep on slabs with: (a) mechanical anchorage; and (b) gradient anchorage

As referred before, the mechanical properties of the concrete had a different evolution with every environmental condition. In the environmental condition TW and CW the strength and elastic modulus of the concrete was 22% and 25% higher than the concrete kept in the REF environment, at the end of the creep tests. In contrast, the immersion on water had a negative effect on mechanical properties of the epoxy adhesive [16]. As the adhesive absorbs water, it plasticizes and, therefore, there is an expansion of its volume and a reduction on its stiffness, tensile strength and glass transition temperature [17–19]. As explained by Jones [19], in aqueous environments the crosslinked resins (such as the used epoxy adhesive) are effective semi-permeable membranes. The large polar ions and molecules in the epoxy adhesive might act as osmotic centres and, in consequence, provide a thermodynamic driving force for transport of moisture into the adhesive [19]. In theory, this osmatic effect would be higher in the TW environment than in the CW environment because in the later environment there is a higher concentration of ions in the water. This last factor might be the reason why the CW slabs had a lower mid-span vertical displacement than the TW slabs. The concrete properties appear to be responsible for the creep evolution difference between the fully immersed environments (TW and CW) and the remaining environments (REF and WD). Also the creep effect on the concrete decreases with the humidity [20]. Lastly, the REF slabs and the WD slabs exhibit similar creep evolutions. Although the final concrete properties were better in the WD slabs, these specimens (WD) were exposed to a higher temperature

oscillation than any other slab. In fact, creep on the concrete trends to increase when the temperature is high, being 25% higher at the temperature of 40 °C than at 20 °C [21]. And, since the environmental conditionals were applied to the slabs mainly during spring and summer, this may cause the increase of creep deflection.

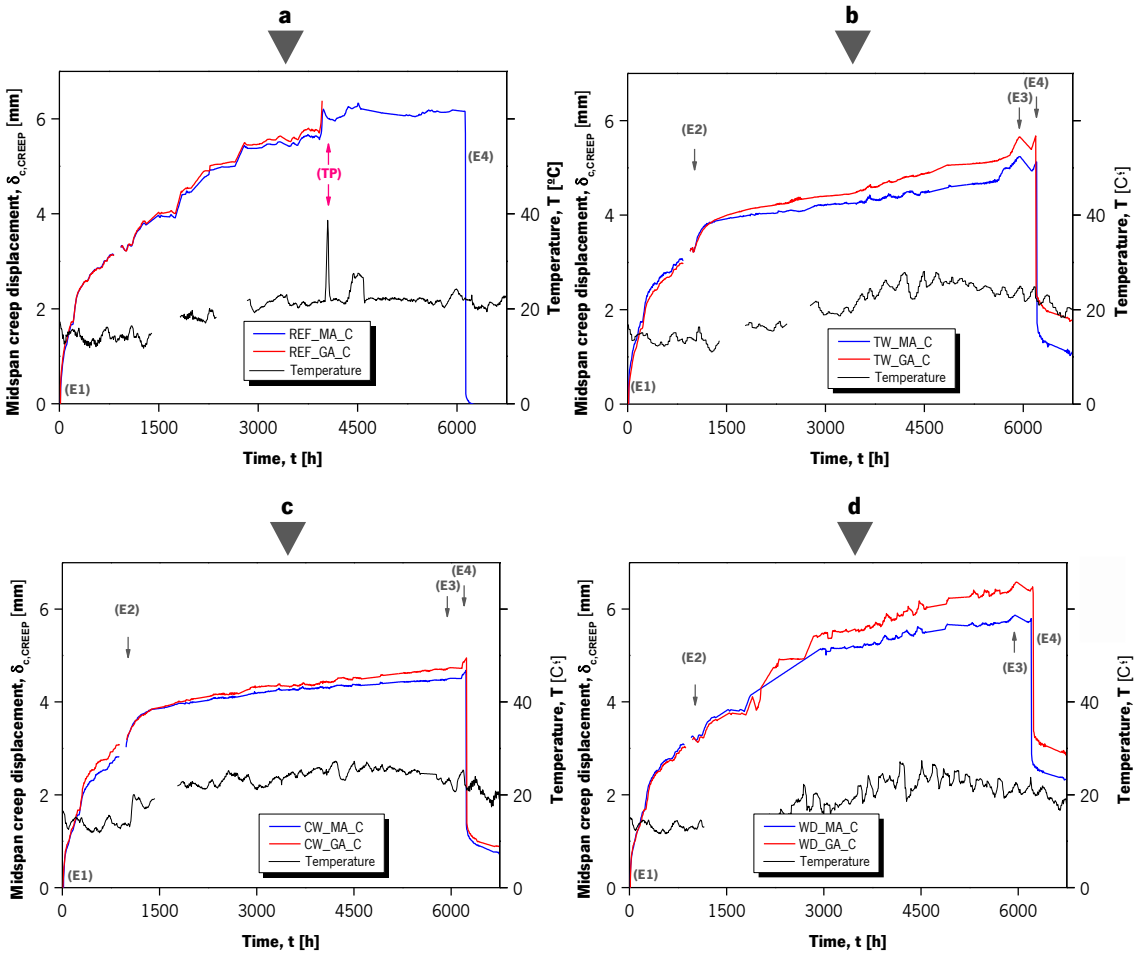

Figure 3.10: Evolution of the mid-span displacement due to creep effect on slabs from: (a) series REF; (b) series TW; (c) series CW; and (d) series WD.

Figure 3.10 shows the mid-span vertical creep displacement evolution after the creep loading application grouped by environmental condition. The slabs subjected to laboratory premises (REF_MA_C and REF_GA_C) exhibit the same creep mid-span vertical displacement variation. However, in the remaining three environmental conditions, series GA have shown larger deformations. This behaviour can be related to the lower mechanical properties of the epoxy adhesive at the anchorage zone of such strengthening system and degraded by the environmental

conditions. In fact Michels *et al.* [12] have concluded that the tensile strength of the epoxy adhesive fast cured using the heating devices is lower (at about 25%) than the same material cured at room temperature. Consequently, GA adhesively bonded joints are softer by comparison with the ones that use epoxy adhesive cured and room temperature [12,22,23].

The creep coefficient, φ_{ult}, based on the period of loading and a prediction of the long-term creep coefficient (φ_{t_∞}) based on the studied period are also presented in **Table 3.3**. The creep coefficient based on the period of loading, φ_{ult}, was computed based on the following expression:

$$\varphi_{ult} = \frac{\delta_{c,CREEP}}{\delta_{c,ela}} = \frac{(\delta_{c,ult} - \delta_{c,ela})}{\delta_{c,ela}} \tag{3.1}$$

Through these results an average creep coefficient (φ_{ult}) of 1.3 and 1.4 was obtained for the MA and GA slabs, respectively. According to the ACI 318 code [24], the long-term deflection of a RC concrete element can be calculated as follows:

$$\delta_{c,CREEP} = \frac{S}{1+50\cdot\rho'} \cdot \delta_{c,ela} \tag{3.2}$$

where, S is a time-dependent factor, (see **Table 3.4**); and ρ' is the compression reinforcement ratio obtained from:

$$\rho' = \frac{A'_s}{b\cdot d} \tag{3.3}$$

where, A'_s is area the top reinforcement; b is the width of the slab's cross section; and d is the distance from the extreme compressive fibre to centroid of longitudinal tension reinforcement. Based on the study period of 8 months, ACI 318 [24] predicts a creep coefficient of 1.30. This value is in agreement with the experimental results (see **Table 3.3**), which means that the observed creep deflection is mainly due to the creep of concrete.

Considering the inverse of time, it was possible to estimate the long-term creep coefficient, φ_{t_∞} (see **Table 3.3**). Results showed a long-term creep coefficient that varied in between 1.1 and 1.7. For a period superior to five years or more, the ACI 318 code [24] predicts an long-term creep coefficient equal to 1.9. However other authors [13,25,26] have already studied the long-term deflection of RC elements strengthened with CFRP (without prestress) and obtained smaller creep coefficients than

the ACI 318 [24]. Several authors [25,26] have proposed a different time-dependent factor (S) for the equation (3.2), which are presented **Table 3.4** together with the expected long-term creep coefficient (φ_{t_∞}).

Table 3.4
Suggested time-dependent factor S and long-term creep coefficient φ_{t_∞}

Loading Period	**ACI 318 code** [24]		**Arockiasamy *et al.*** [26]		**G. Al Chami *et al.*** [25]	
	S [-]	φ_{t_∞} [-]	S [-]	φ_{t_∞} [-]	S [-]	φ_{t_∞} [-]
1 month	0.50	0.5	–	–	0.40	0.4
3 months	1.00	0.9	0.70	0.6	0.60	0.6
6 months	1.20	1.1	0.85	0.8	0.80	0.7
12 months	1.40	1.3	1.15	1.1	1.00	0.9
18 months	1.60	1.5	–	–	1.10	1.0
60 months or more	2.00	1.9	1.40	1.3	1.30	1.2

Note: The long-term creep coefficient was computed based on equations (3.1) and (3.2), on the proposed time-dependent factor by the above-mentioned literature, and on the geometrical properties of the tested specimens.

Arockiasamy *et al.* [26] studied the time-dependent deformations of four 2.4 m long concrete beams reinforced exclusively with CFRP bars. Every specimen was subjected to a different load level (77%, 110% and 123% of its cracking load). Al Chami *et al.* [25] studied the creep behaviour in twenty (1.8 m long) RC beams strengthened with EBR CFRP laminates. The applied sustained loads varied from 59% to 78% of the ultimate static capacities of the un-strengthened beams. One of the conclusions of the later study affirm that the major factor that affect the creep rate and the long-term deflection are the level of sustained load and the compressive strength of the concrete. In fact, the FRP strengthening produces no improvement in performance with regard to the long-term deflection [25].

As a concluding remark, it should be mentioned that despite these environmental actions being severe, the obtained long-term creep coefficient, φ_{t_∞}, did not exceed 1.9 (expected in RC structures [24]). Additionally, the test results also show that compressive strength of the concrete is one of the factor that affected the creep rate and long-term deflection.

When the creep load was removed, an average recovery mid-span vertical displacement of 3.7 mm was observed. This value represents 83% of the elastic deformation registered when loading. As it

is shown in Section 3.2.2 (see **Table 3.2**), the concrete properties have evolved with the environments. At the end of the creep test, the concrete strength and elastic modulus of the slabs exposed to environments TW, CW and WD was higher, and a result of this, the stiffness of the slabs increased. Thus, considering the final slabs stiffness, the observed recovery in the mid-span vertical displacement (of 3.7 mm) represents 91% of the elastic deformation.

The CFRP strain evolution of the slabs subjected to the sustained loading was also monitored and it is presented in **Figure 3.11**. As expected, strain values change over time with the applied load, temperature and environmental condition. An initial variation (almost elastic variation), that ranged from 0.06 % to 0.13 %, can be observed in all eight prototypes. It is clear that this variation is related to the applied load and to the stiffness of each composite system RC slab/CFRP strip. When comparing the initial strain variation (see **Figure 3.11**) with the mid-span deflection at the same time (see **Figure 3.8**), it can be observed that there is a relationship between both measurements: greater CFRP variation means higher mid-span deflection. The strain variation after the application of the gravity loads are related to the stress redistribution from concrete to the CFRP reinforcement due to concrete creep effect. It is clear that the strain evolution during this period had a similar evolution to the one observed on the mid-span deflection (see **Figure 3.8**). In addition, the temperature also plays a considerable effect on the strain in the CFRP: results show that the short-time peaks of high temperatures produce a simultaneous raise in the mid-span CFRP strain.

Through the analysis of **Figure 3.11** it is possible to draw conclusion on the CFRP strain evolution over time for the specimen strengthened with the MA and GA system. The slabs with the MA anchorage system, showed an initial strain variation that rounded the 0.10 % after the application of the gravity load (event **(E1)** in **Figure 3.11**). This CFRP strain variation is in agreement with the values observed during the monotonic tests (see Section 3.4). Like in the MA series, the GA slabs also experienced an almost elastic increase of their CFRP strain with the loading. However, in two GA slabs (TW_GA_C and CW_GA_C) the initial strain increment was smaller than expected (0.07%). At this stage of the creep test both slabs showed the expected mid-span displacement, which was in agreement with the remaining specimens (REF_GA_C and WD_GA_C). For that reason, this low value of initial strain variation might be an acquisition system malfunction. Then,

after the loading, different behaviours are observed for the slabs subjected to different environments.

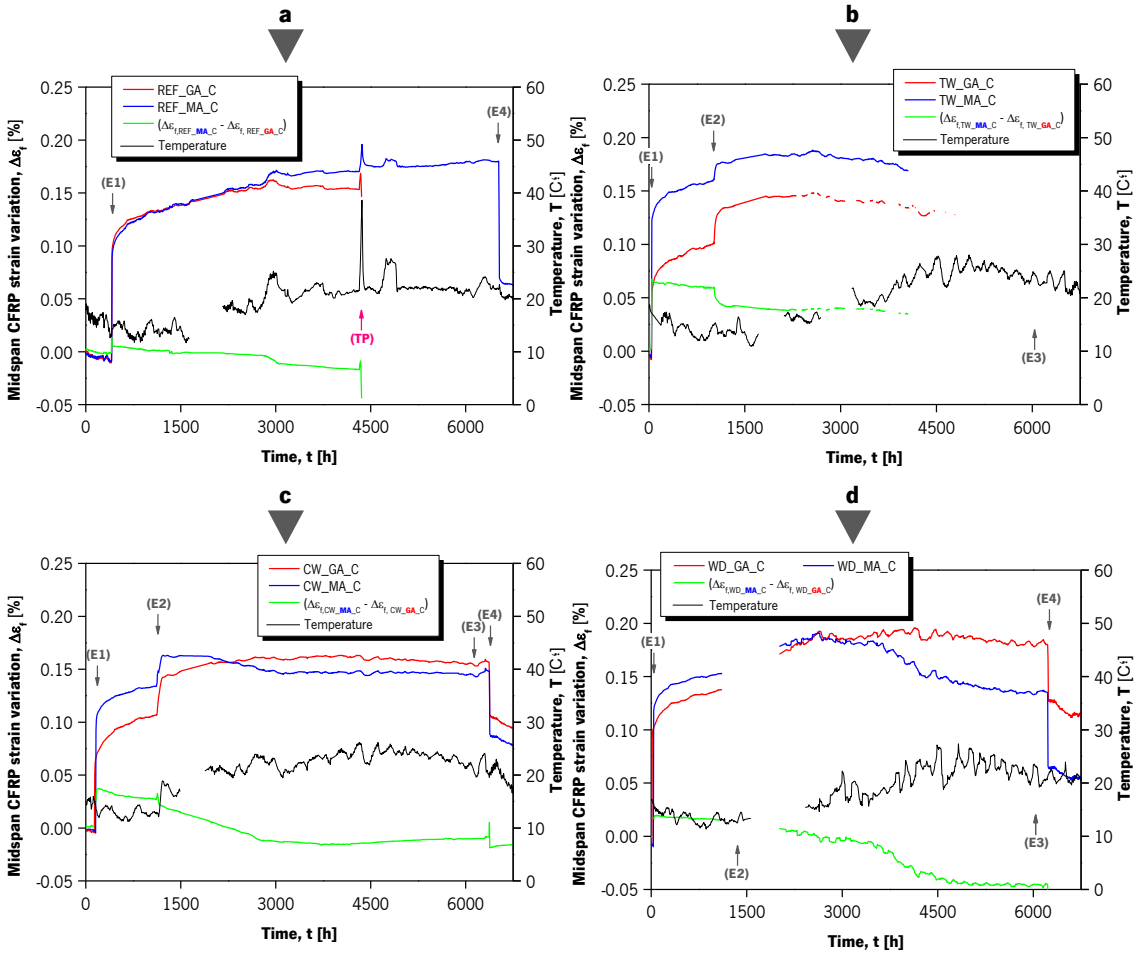

Figure 3.11: Evolution of the mid-span CFRP strain of the slabs from: (a) series REF; (b) series TW; (c) series CW; and (d) series WD.

The Reference MA specimen seemed to have a strain increase over time, with a decreasing slope. This behaviour is, as explain before, related to the migration of the stresses from concrete to the CFRP reinforcement due to concrete creep effect. **Figure 3.12** presents the mid-span CFRP strain and vertical displacement evolution of the REF_MA_C slab. The figure shows a perfect correlation between both the CFRP strain and the vertical displacement. Also, **Figure 3.12** clearly shows the influence of the temperature variation on both parameters.

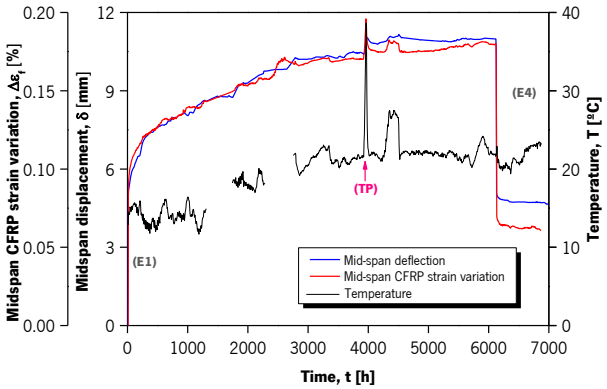

Figure 3.12: Comparison between the Mid-span deflection and the CFRP strain variation of REF_MA_C

For that reason the MA mid-span deflection curve over time presented on **Figure 3.8a** is similar to the mid-span CFRP strain curve presented on the **Figure 3.11a**. Three peaks can be observed (at 2600 h, at 3900 h and at 4500 h) on the temperature that directly influenced the CFRP strain. These temperature peaks resulted from an equipment malfunction. When these malfunctions were fixed, the strain in the CFRP returned to its expected value. Just like on the REF_MA_C, the REF_GA_C slab presented a gradual strain increase due to the concrete creep effect and consequent migration of the stresses from concrete to the CFRP reinforcement. As referred before, around 3980 h of testing (event **(TP)** in **Figure 3.11a**), the REF_GA_C had to be disregarded. There are several similarities between both REF slabs during the first months of the creep loading, as it is shown in **Figure 3.8a** and **Figure 3.11a**. These results clearly indicate the temperature variations produced a higher impact on the GA slab. At 2600 h, a first temperature peak was registered and, with it, a deviation from the CFRP strain variation registered in both slabs (see green line in **Figure 3.11a**). Nonetheless, a similar performance would be expected for both anchorage systems, if the temperature is kept, continually and consistently, in between 18 °C and 22 °C.

The slabs subjected to the immersion on tap water (series TW) and on chloride water (series CW) presented a different behaviour. It should be highlighted that before the start of the environmental actions, the water was poured into temporary tanks inside the laboratory. This way, when the water was discharged inside the tanks its temperature was ranging the lab's air temperature (and specimens). Nevertheless, the two MA specimens presented a rapid strain growth (around 0.02 %) when they were immersed in water (event **(E2)** in **Figure 3.11**). This strain growth is, similarly to the rapid deflection increase (see **Figure 3.8**), a result of the water absorption. The two GA slabs

exposed to the same to environments also presented a rapid strain growth. It should be noticed that the mid-span strain variation due to this event was slightly higher in the GA slabs. It should be pointed that the slabs subjected to wet/dry cycles (series WD) has a higher temperature variation overtime and that temperature can be one of the highest degradation factors.

All specimens presented a decreasing growth and posterior stabilization for strain values that did not exceed 0.2 %. This behaviour was expected, considering that primary creep deformation occurred in the first 3000 h, and secondary creep stage occurs afterwards. The unloading of the slabs (event **(E4)** in **Figure 3.11**), is responsible for a modest reduction on the mid-span CFRP strain. An average reduction in CFRP strain of 0.08% and 0.05% was observed for the MA slabs and GA slabs, respectively. Yet, a residual fraction of the CFRP strain (in between 0.05% and 0.10%) was observed at the end of the test. For the MA specimens, this could represent a CFRP strip slip from the anchorage plates. However, a visual inspection after the conclusion of these tests highly indicate that there was no slip.

3.4 Monotonic tests up to failure

At the end of the environmental exposure all specimens were tested up to failure using a four-point test configuration. The present section reports the obtained results, taking in consideration the influence of the environmental conditions, the influence of the sustained loading and the influence of the anchorage system. The deflection, CFRP strain, crack width, crack pattern are some of the parameters that were measured, compared and briefly discussed.

3.4.1 Stiffness

During the monotonic tests the deflections along the longitudinal axis of the slabs were monitored. **Figure 3.13** presents the evolution of the mid-span deflection with the applied force for all tested slabs. The strengthening of the slabs with CFRP laminate significantly increased their stiffness and reduced the corresponding mid-span deflection for a specific load level. All prestressed specimens presented a delay in the crack initiation (δ_{cr}, F_{cr}) and steel yielding (δ_y, F_y) when compared to the non-prestressed specimens (see **Table 3.5**). However, no significant changes due to the use of strengthening and/or prestressing were observed regarding the stiffness of the elastic phase (K_I).

This behaviour was expected considering the low amount of strengthening reinforcement used. The longitudinal steel reinforcement ratio of T0_REF and equivalent longitudinal steel reinforcement ratio of all the strengthened slabs were equal to 0.46% and 0.53%, respectively. In average, slightly higher K_I was observed for specimens immersed in water (series TW, CW and WD) whereas the lower values were registered for the REF series. The previously mentioned results obtained for concrete's elastic modulus (see **Table 3.2**) support these observations. Results show that the uncracked concrete's contribution to the overall slabs stiffness is, by far, the largest. Also, specimens subjected to sustained loading (with the suffix "_C") appear to have a similar behaviour to the uncracked slabs (with the suffix "_U") during the initial stages of testing: **Figure 3.13d** and **Figure 3.13e** show that the cracking stabilization only occurred for a load level of around 27 kN; before that, the contribution of the concrete for the initial slab's stiffness seems to be more relevant, since all environmental conditions that include water exposure (series TW, CW and WD) led to higher stiffness's. In contrast, REF_MA_C presents the lowest initial stiffness, which can be explained by the lower stiffness and most likely the lower tensile strength of concrete that was not immersed in water.

The overall stiffness at cracked stage (K_{II}) of the strengthened slabs is substantially less influenced by the mechanical properties of the concrete. For that reason, higher K_{II} values were obtained for all strengthened slabs, in contrast to the observed for the T0_REF (unstrengthened slab). For the same reason values of KII are relatively similar for all strengthened specimens.

In general, all prestressed slabs presented similar behaviour, which clearly means that the anchorage system type and the environmental exposure did not have a noticeable influence in the development of the deformations with the applied force. As expected, the sustained loading altered the initial deformation state of the slabs prior to static testing. As shown in **Figure 3.13**, cracked specimens (with the suffix "_C") exhibited yielding and failure at lower deformation values, when the residual deformation obtained prior to static testing is disregarded.

Table 3.5
Main Results (Part I).

Specimen	Stiffness		Crack initiation		Yielding			Ultimate				Efficiency and ductility			Failure Modes
	K_I	K_{II}	δ_{cr}	F_{cr}	δ_v	F_v	φ_v	δ_{max}	F_{max}	φ_{max}	ε_{max}	μ_F	μ_δ	μ_φ	
	[kN/mm]	[kN/mm]	[mm]	[kN]	[mm]	[kN]	[10^{-3}m^{-1}]	[mm]	[kN]	[10^{-3}m^{-1}]	[%]	$\left(\frac{F_{max}}{F_v}\right)$	$\left(\frac{\delta_{max}}{\delta_v}\right)$	$\left(\frac{\varphi_{max}}{\varphi_v}\right)$	
Series T0															
T0_REF	11.1	0.9	0.71	7.88	18.90	24.54	–	100.00[a]	28.07[b]	–	–	–	--	–	–
T0_EBR	12.5	1.1	0.68	8.49	25.87	37.05	43.88	40.69	43.98	71.34	0.76	–	--	–	D
T0_MA	9.8	1.3	1.82	17.87	26.88	50.58	44.81	84.78	67.46	77.26	1.48	1.33	3.15	1.72	F
T0_GA	10.4	1.2	1.55	16.16	29.04	50.20	52.60	43.31	57.38	76.49	1.16	1.14	1.49	1.45	D
Series REF															
REF_MA_U	8.3	1.3	2.04	16.1	26.26	46.1	50.36	67.34	59.9	97.87	1.40	1.3	2.56	1.94	D
REF_GA_U	8.0	1.2	1.85	15.9	28.45	48.6	51.14	38.21	53.5	68.33	1.10	1.1	1.34	1.34	D
REF_MA_C	--	1.3	--	–	26.22	48.1	71.75	65.85	61.6	108.63	1.26	1.3	2.51	1.51	D
Series TW															
TW_MA_U	8.6	1.3	1.68	15.6	24.54	47.1	46.06	39.56	54.4	68.17	1.13	1.2	1.61	1.48	D
TW_GA_U	10.9	1.3	1.05	12.8	25.60	47.1	47.98	41.65	55.8	78.32	1.19	1.2	1.63	1.63	D
TW_MA_C	--	1.5	--	–	22.02	50.5	55.74	41.33	57.7	83.76	1.15	1.1	1.88	1.50	D
TW_GA_C	--	1.2	--	–	23.58	49.3	42.20	37.05	56.2	63.23	1.06	1.1	1.57	1.50	D

Notes: D = Debonding; F = CFRP tensile failure; [a] these beams reached the maximum pre-defined deflection without failing; [b] values for the mid-span deflection of 100 mm; [c] The maximum CFRP strain did not necessarily occur at the mid-span.

Table 3.5
Main Results (Part II).

Specimen	Stiffness		Crack initiation		Yielding			Ultimate				Efficiency and ductility			Failure Modes
	K_I	K_{II}	δ_{cr}	F_{cr}	δ_v	F_v	φ_v	δ_{max}	F_{max}	φ_{max}	ε_{max}	μ_F	μ_δ	μ_φ	
	[kN/mm]	[kN/mm]	[mm]	[kN]	[mm]	[kN]	[10^{-3}m^{-1}]	[mm]	[kN]	[10^{-3}m^{-1}]	[%]	$\left(\frac{F_{max}}{F}\right)$	$\left(\frac{\delta_{max}}{\delta}\right)$	$\left(\frac{\varphi_{max}}{\varphi}\right)$	
Series CW															
CW_MA_U	11.5	1.3	1.92	18.5	24.57	47.35	43.7	65.45	60.9	81.86	1.23	1.3	2.66	1.87	D
CW_GA_U	8.4	1.3	2.11	17.0	24.71	46.94	45.8	41.70	56.4	77.44	1.19	1.2	1.69	1.69	D
CW_MA_C	--	1.4	--	–	19.65	47.42	47.0	38.38	58.7	79.43	1.12	1.2	1.95	1.69	D
CW_GA_C	--	1.3	--	–	21.92	47.04	49.4	39.01	57.0	80.83	1.05	1.2	1.78	1.64	D
Series TW															
WD_MA_U	10.7	1.3	1.30	14.2	25.53	47.64	46.3	61.33	58.8	86.20	1.27	1.2	2.40	1.86	D
WD_GA_U	10.3	1.2	1.49	16.5	26.98	48.62	47.7	40.21	55.3	69.09	1.08	1.1	1.49	1.54	D
WD_MA_C	--	1.3	--	–	20.10	48.61	38.0	32.89	55.6	63.57	1.04	1.1	1.64	1.67	D
WD_GA_C	--	1.2	--	–	23.67	49.15	49.0	37.55	56.3	73.24	1.17	1.2	1.59	1.50	D

Notes: D = Debonding; F = CFRP tensile failure; [c] The maximum CFRP strain did not necessarily occur at the mid-span.

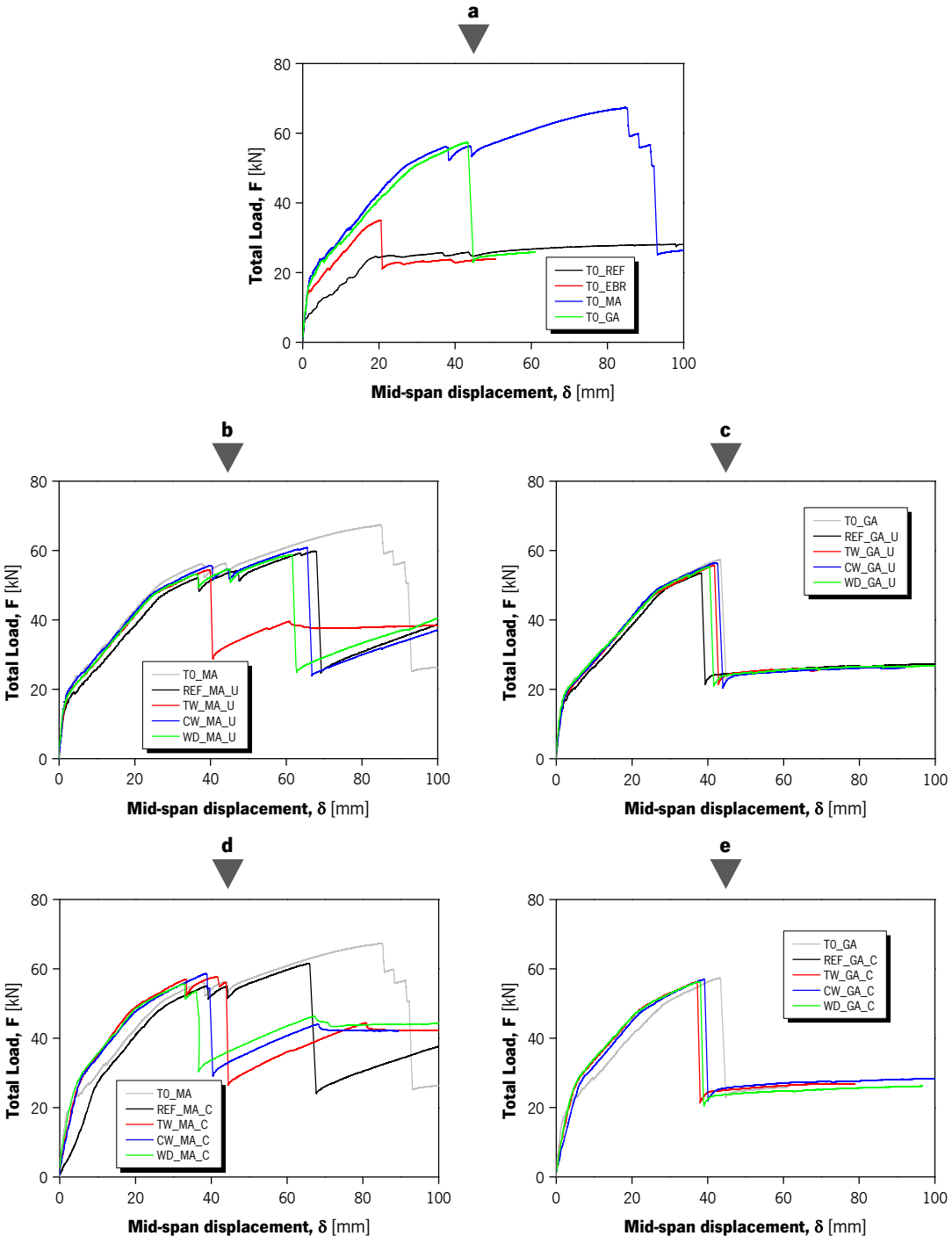

Figure 3.13: Total force *versus* mid-span deflection: (a) Control specimens; (b) uncracked MA specimens; (c) uncracked GA specimens; (d) cracked MA specimens; and (e) cracked GA specimens.

3.4.2 Crack evolution and failure modes

As previously referred, the crack width was assessed through the use of a handheld USB microscope during the execution of the static tests. The evolution of the average crack width *versus* the applied force is plotted in **Figure 3.14**. It should be noted that in the case of "_C" specimens, the crack width was measured since the onset of the static tests because several cracks were already visible.

Results show that the strengthening influenced the crack width increase with the applied force: for a specific load level, strengthened slabs exhibited lower crack widths when compared to the T0_REF specimen. Prestress changed the onset of cracking by increasing the first-cracking load, at an average growth of 89% when compared with the T0_EBR. Crack measurements support the previous statement. In fact, **Figure 3.14** shows that for the same load level, the prestressed specimens exhibit lower average crack widths. Both anchorage systems presented similar performance. The trend of crack width measurements observed for the control specimens (T0_MA and T0_GA) was similar to the one observed for the uncracked specimens.

The different exposure environment conditions seemed to have no significant influence on the crack width evolution. In spite of that, specimens subjected to environments TW, CW and WD appeared to have an even lower crack width growth with the load increments. Conversely, specimens subjected to sustained loading showed a different crack width evolution: the linear regression shows a higher slope when compared to the ones relative to the remaining strengthened slabs.

A study on the crack pattern and crack spacing was carried out for all specimens. **Figure 3.15** shows the average crack spacing, whereas **Figure 3.16** and **Figure 3.17** show the final crack pattern on the lateral surface and bottom surface, respectively. The average crack spacing was measured on the bottom surface of the slabs along two lines parallel to the longitudinal axis, each of these 150 mm away from the lateral face of the slab. As expected, the results clearly showed a crack spacing reduction due to strengthening and an even greater reduction when the strengthening was prestressed. For both prestressing systems the average crack spacing decreased and, consequently, the number of cracks increased.

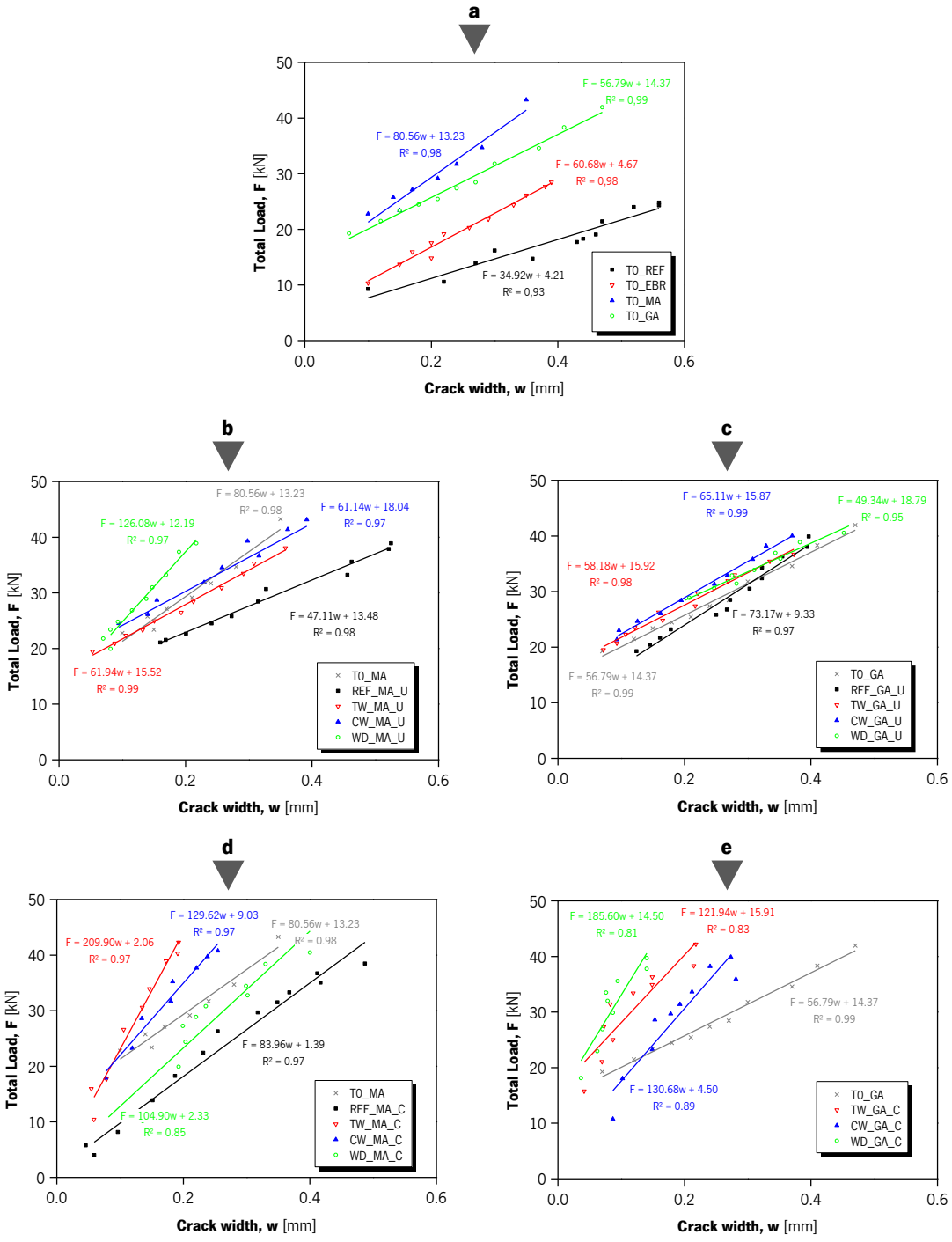

Figure 3.14: Crack width evolution of: (a) Control specimens; (b) uncracked MA specimens; (c) uncracked GA specimens; (d) cracked MA specimens; and (e) cracked GA specimens.

However, the MA and GA systems produced different effects on the final crack pattern. The gradient anchorage allowed the formation of cracks along the gradient zones (occupying approximately 2/3 of these zones) and between these regions. The cracks over the gradient zone indicate that the

CFRP laminate is mobilized throughout its entire length. The MA slabs presented a crack pattern that developed between the anchorage plates. The absence of cracks over the anchorage zones is related to the confinement produced in this region by the anchoring devices. As mentioned before, a torque of 150 N×m was applied in each of the six bolts that fix the CFRP laminate to the concrete with the metallic anchor plate, confining the laminate and the surrounding concrete substrate, in addition to the complementary reinforcement provided by the bolts themselves.

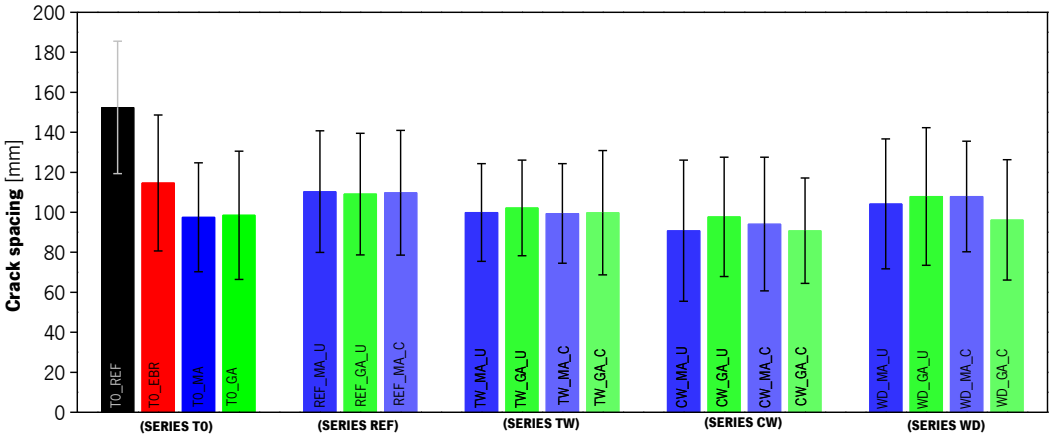

Figure 3.15: Crack spacing: (a) Control specimens; (b) uncracked MA specimens; (c) uncracked GA specimens; (d) cracked MA specimens; and (e) cracked GA specimens.

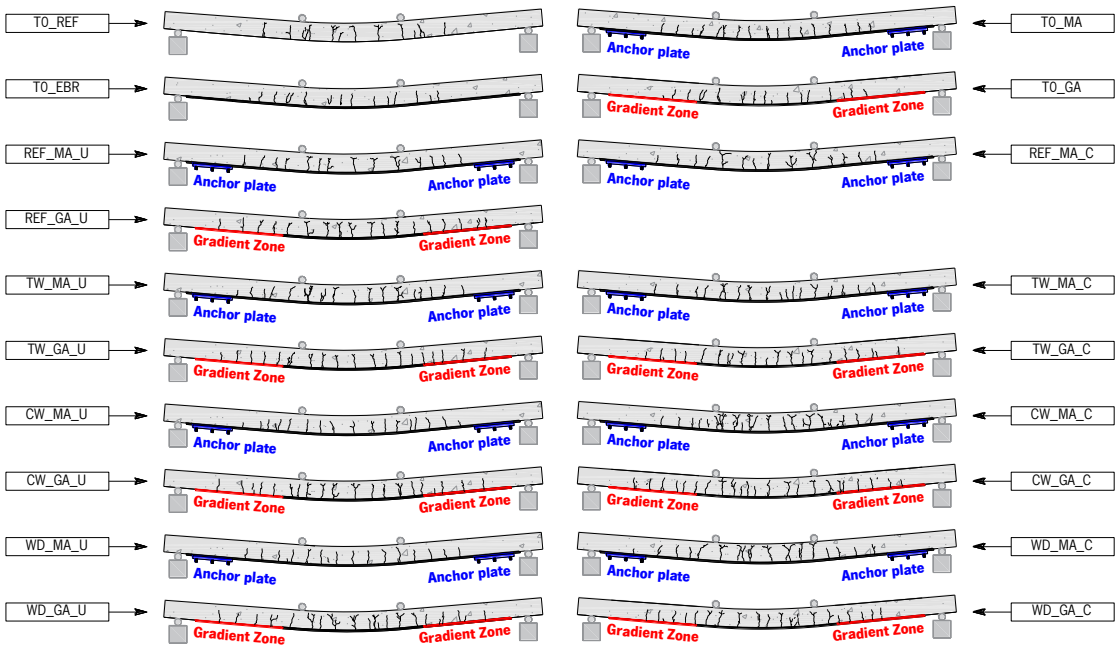

Figure 3.16: Crack pattern (lateral surface) at the end of the test of each slab.

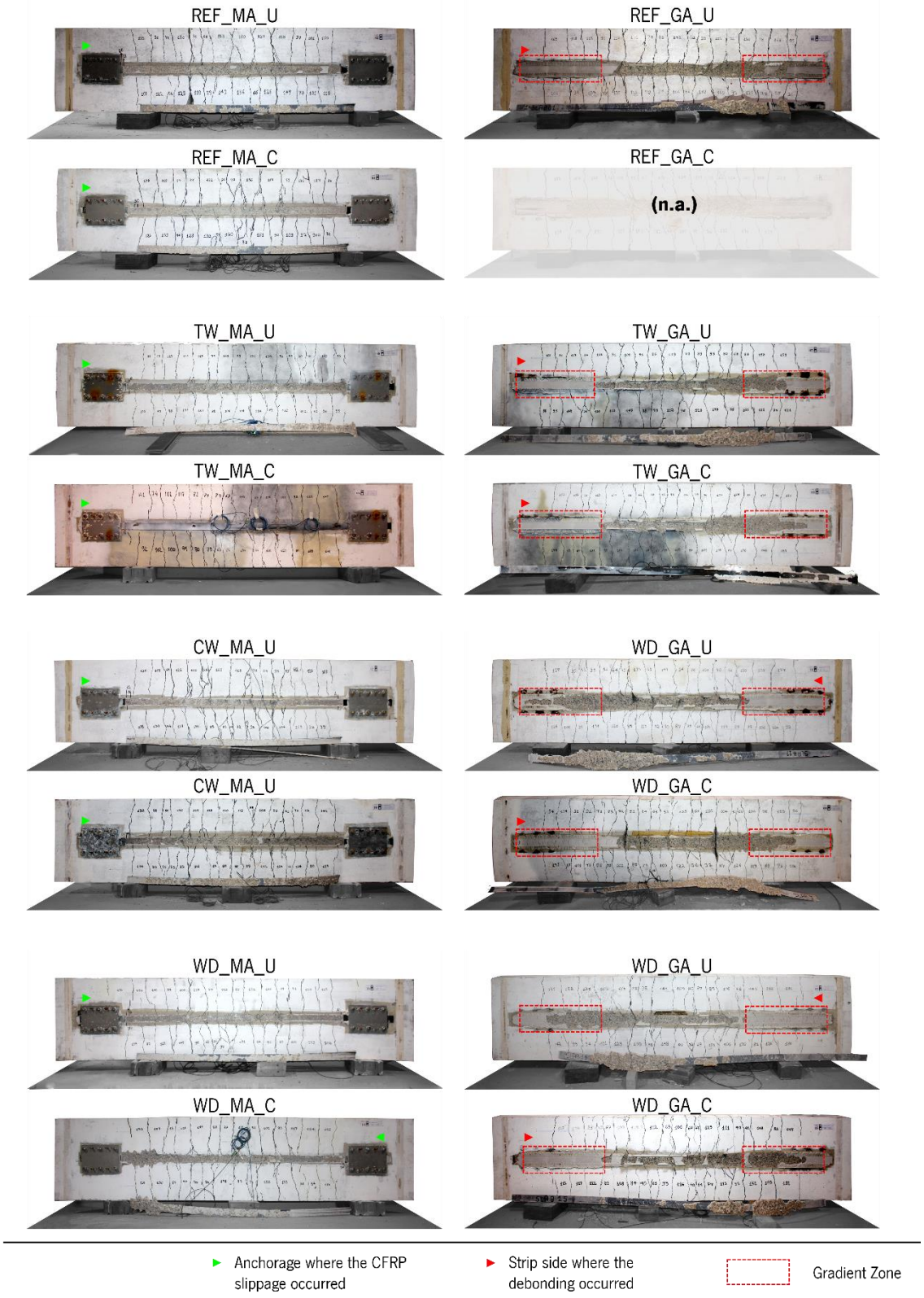

Figure 3.17: Crack pattern (bottom surface) at the end of the test of each slab.

As previously stated, T0_REF is an unstrengthened specimen that was tested at the onset of the environmental condition exposure. The test was stopped once the mid-span deflection reached 100 mm, the maximum deflection that can be registered by the LVDT. Concrete crushing at the top fibre would most likely be the expected failure mode (according to a cross section analysis, concrete crushing was expected for a load level close to 28 kN, when the strain of the steel in tension reaches 3.3%. The analysis assumed of a rectangular stress distribution in the compressed concrete region, as suggested by fib [27]). The strengthened slabs exhibited two distinct failure modes: (i) strip debonding and (ii) CFRP tensile rupture in unidirectional tension. The T0_MA failed by CFRP rupture in unidirectional tension when the strain in the laminate strip was 1.48% (see **Table 3.5** and **Figure 3.18a**). As in most slabs strengthened using mechanical anchorage, failure in the REF_MA_T0 did not occur immediately after the strip debonding, since the CFRP strip was held at both ends by the mechanical anchorages. As shown in **Figure 3.19a**, the observed debonding of the CFRP strips in MA slabs occurred in two phases: in a first stage deboding occurred near one of the two anchorages, and after a while the same happens in the anchorage placed at the opposite side of the slab. Due to this behaviour, the strains at the CFRP strip near the anchorages suddenly increased and almost reached the mid-span strain. From this point onwards the CFRP laminate strip behaved as an unbounded reinforcement, with minor strain variations along the strip length caused by the friction and interlock developed at the debonded region. Eventually, the strip was pulled out from the mechanical anchorage as shown in **Figure 3.18c**. A cross section analysis based on the CNR [28] debonding failure modes presented in Chapter 2 (Section 2.3.5) shows that intermediate debonding is the expected primary type of failure. Digital image correlation (see **Figure 3.20**) clarifies that the debonding process of the MA slabs is caused due to flexural cracks. The observed intermediate debonding was cohesive at the concrete and started with the formation of flexural cracks at mid-span of the slab that propagated towards the ends. In **Figure 3.20**, it is possible to see primary flexural cracks and, when higher load levels are achieved, secondary shear cracks due to the CFRP reinforcement. All specimens with gradient anchorages exhibited a brittle failure, as in this case no mechanical end-fixing existed to provide additional anchorage. Because the strip detachment developed rapidly and very sudden, it is difficult to clearly identify the exact failure mode: although it seems that intermediate debonding caused by flexural cracks promoted the detachment of the CFRP in the GA specimens (see **Figure 3.21**), failure could also have started

from the anchorage at the CFRP/epoxy interface and then propagate towards the middle of the concrete substrate. **Figure 3.17** shows flexural cracks across the gradient anchorage and they might have been the trigger that caused the failure. Nevertheless, considering the GA slabs, the strip end where the detachment occurred failed at the CFRP/epoxy interface, whereas cohesive failure in the concrete was observed for the remaining CFRP strip (see **Figure 3.17**). Details regarding the influence of the anchorage systems on the structural behaviour will be discussed further in the subsequent section.

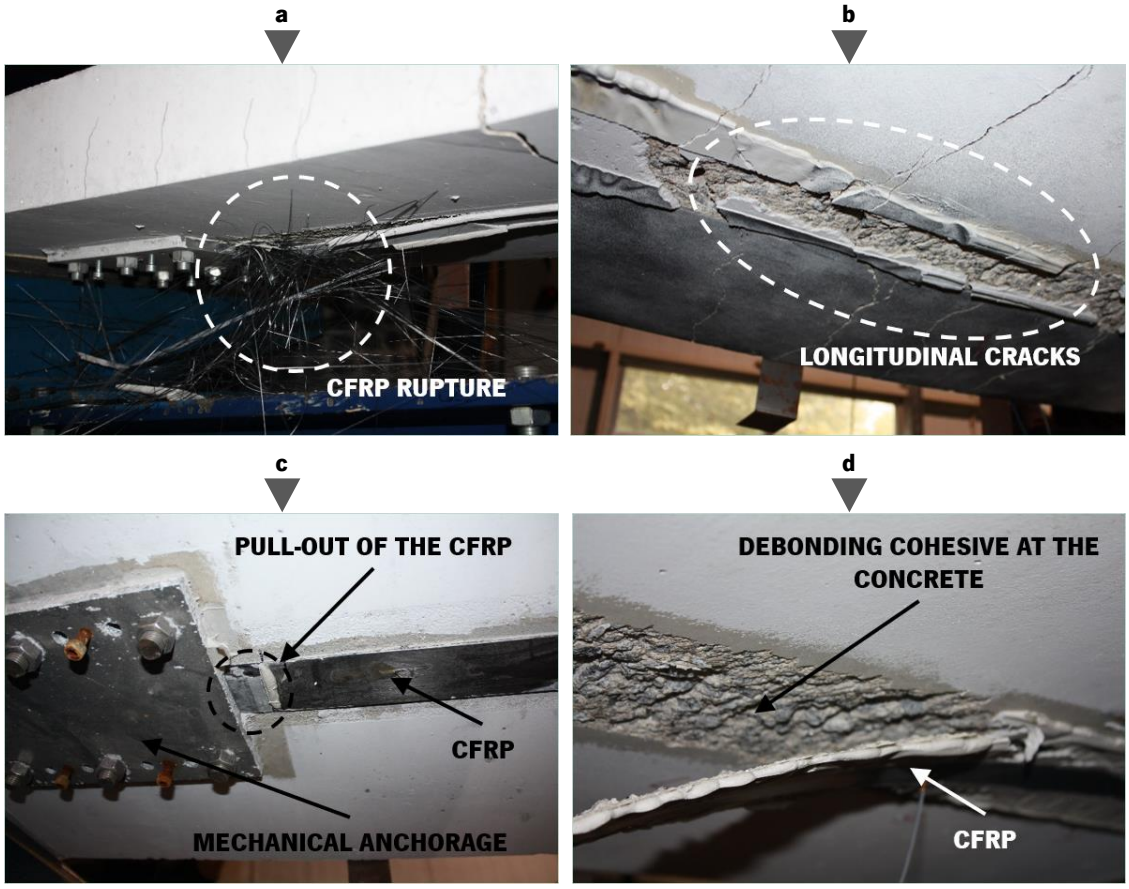

Figure 3.18: Failure modes: (a) CFRP rupture in unidirectional tension (T0_MA); (b) observed longitudinal cracks at the epoxy region (TW_GA_C); (c) CFRP strip pull-out from the mechanical end/anchorage (WD_MA_C); and (d) detail of a cohesive at the concrete debonding (WD_GA_U).

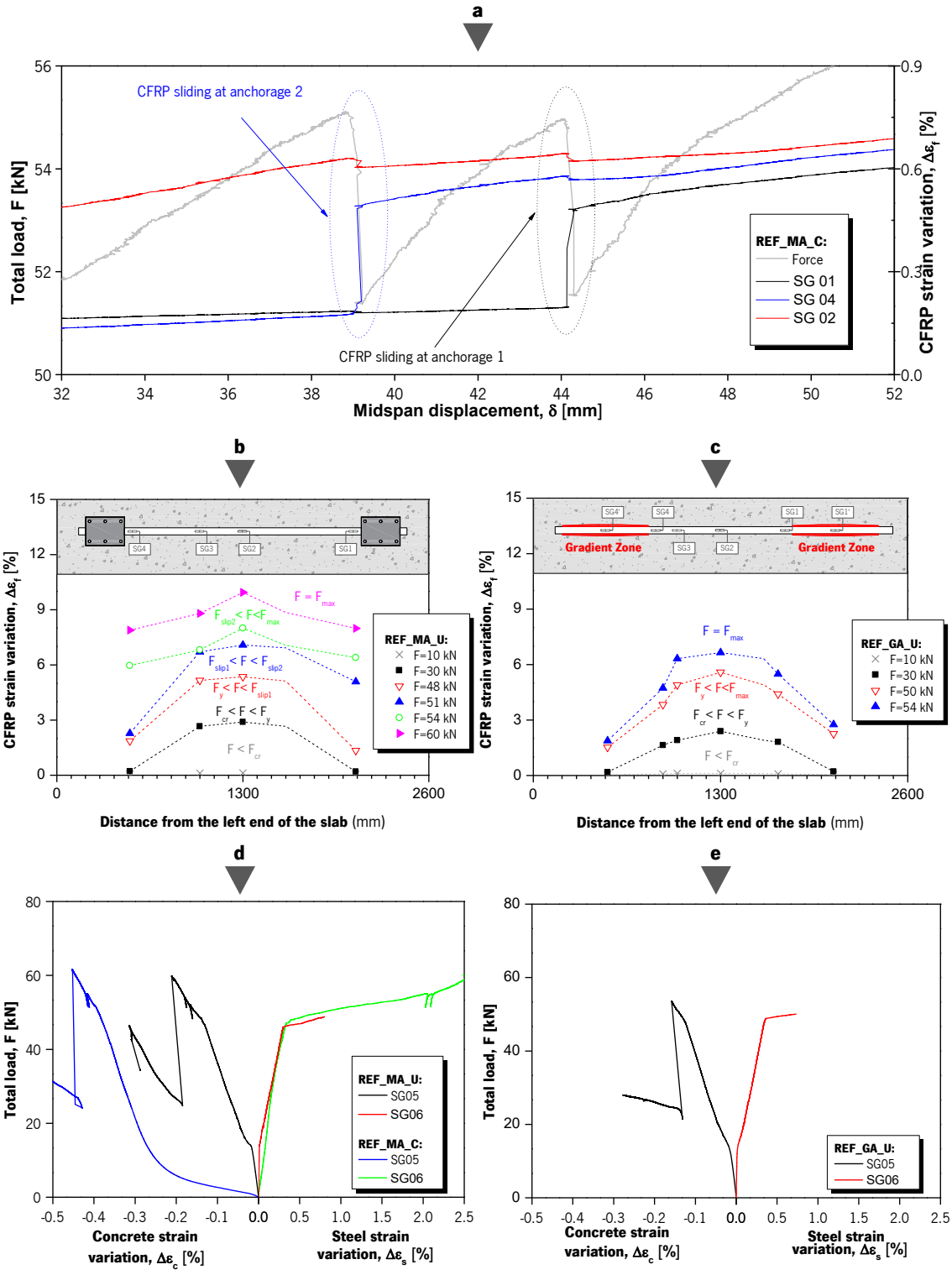

Figure 3.19: Materials strain variation: (a) CFRP sliding at anchorages for REF_MA_C; (b) CFRP strain variation for REF_MA_U; (c) CFRP strain variation for REF_GA_U; (d) concrete and steel strain variation for REF_MA_U and REF_MA_C; and (e) concrete and steel strain variation for REF_GA_U.

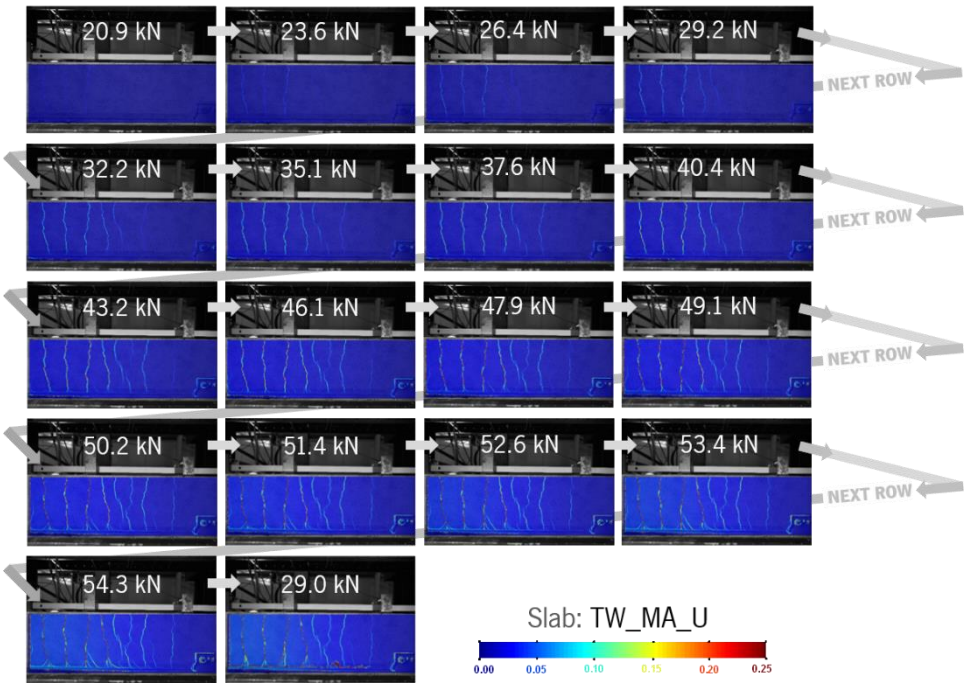

Figure 3.20: Digital image correlation on TW_MA_U slab (maximum principal strains). Note: Video available at < https://tinyurl.com/y9m3q7dj >

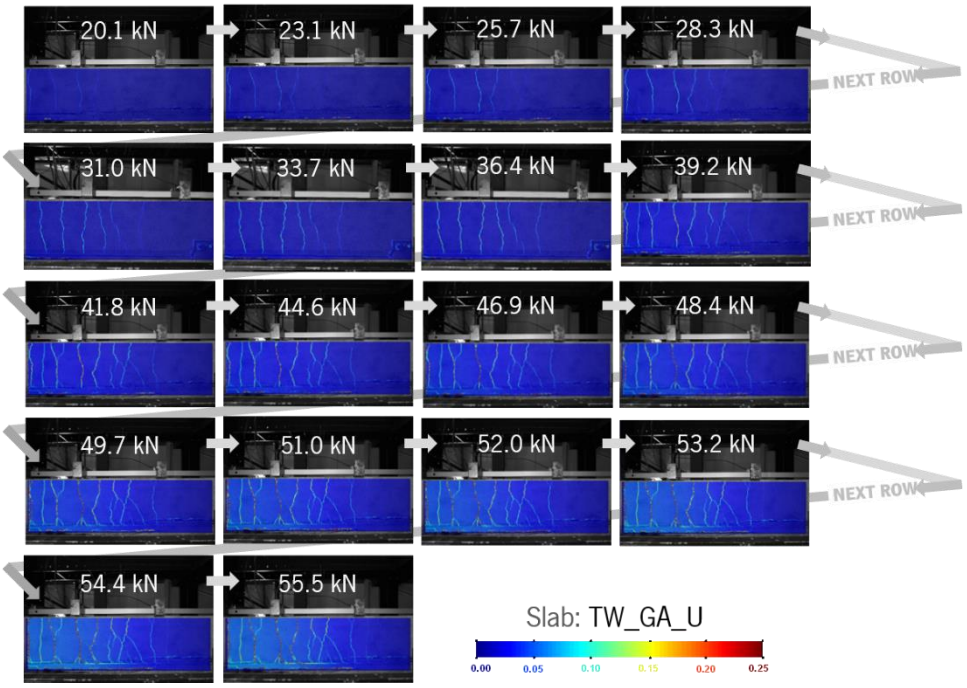

Figure 3.21: Digital image correlation on TW_GA_U slab (maximum principal strains). Note: Video available at < https://tinyurl.com/ydgzgafb >

3.4.3 Influence of prestressing

As previously stated, literature points out several advantages deriving from the prestressing of FRP materials. In this research the average level of prestress load reached was about 40 kN, resulting in a tensile stress of about 680 MPa in the CFRP laminate strip. When prestressed slabs are compared with the un-prestressed specimen (T0_EBR), a relatively small increase on the stiffness K_I and K_{II} (about 19% and 11%, respectively) is observed. Nevertheless, the first-cracking, yielding and failure loads increased substantially (approximately 90%, 30% and 31%, respectively) and, as a result, for the same load level, these specimens exhibited smaller deflections (see **Table 3.5**).

One of the main advantages of using prestressed externally bonded FRP materials for strengthening existing structures is the reduction of the existing deflections and crack widths. In the experimental programme, when the sustained loading was removed, the majority of the cracks have closed and became invisible to the naked eye. Strengthening using prestressed FRP materials may be regarded as a way to partially or totally cancel the effect of sustained loads and, consequently, as a way to improve both crack width and deflection reduction.

Prestressed slabs exhibit a more efficient use of the mechanical properties of both the concrete and the CFRP: the average concrete strain in the top surface at failure of the slab was approximately 0.20%, and the average CFRP strain at failure was approximately 1.18%. In contrast, immediately before failure, the concrete and CFRP strains registered in the T0_EBR specimen were 0.13% and 0.76%, respectively (see **Table 3.5**).

3.4.4 Anchorage systems

The anchorage system plays an important role on the effectiveness of the prestressing technique, allowing a proper transfer of high shear stresses from the strip ends to the concrete [29]. In the case of the mechanical anchorage (MA) system, hard aluminium plates avoid the premature peeling-off of the CFRP strip by holding the laminates extremities and, in the particular case of this experimental program, by increasing the concrete's shear strength at the substrate surface due to the confinement provided by the torque applied on each anchor bolt fixing the plates. Alternatively, the gradient anchorage (GA) gradually reduces the prestressing force over several gradient segments towards the ends of the strip, eliminating the risk of premature debonding failure.

However, during the monotonic tests the major difference between the behaviour of slabs with the two different anchorage systems was observed after steel yielding, on the onset of the CFRP strip debonding. After yielding, the steel reinforcement contribution to the increase of the slabs load carrying capacity is limited, thus making the CFRP material the greatest responsible for carrying the additional load increments. Promoted by the flexural cracks at the intermediate zone of the slab, strip debonding initiated when the load level was close to 55 kN and 56 kN for the MA and GA slabs, respectively. It should be highlighted that with the GA system the initial debonding process quickly progressed into the complete strip detachment. For the majority of the MA specimens, strip debonding produced two sudden load drops in the $F - \delta$ responses (see **Figure 3.13a**, **Figure 3.13b** and **Figure 3.13d**), each drop relative to the strip detachment at each of the two extremities. Once completely detached, the CFRP strip continues to carry additional loading as an unbounded external reinforcement fixed by the metallic plates. In average the MA system allowed reaching an ultimate load of 59 kN (6.2% higher than the one observed with the GA system) and an ultimate mid-span deflection of 86 mm (GA slabs presented an average ultimate mid-span deflection of 73 mm). In essence, both anchorage systems presented similar behaviours until the yielding of the steel reinforcement. Then, for similar load/deflection levels the initiation of strip debonding led to the failure of the GA system and to the CFRP strip detachment in the MA system. Although the majority of the MA slabs presented a ductile behaviour by allowing larger deflections and greater load levels, in some cases (specimens TW_MA_U, CW_MA_C and WD_MA_C) failure was observed shortly after the strip debonding initiation.

3.4.5 Influence of environmental condition

Four environmental conditions were considered to evaluate the durability of the studied strengthening systems: (i) reference environment (REF); (ii) water immersion in tank at 20 °C of temperature (TW); (iii) water immersion in tank with 3.5% of dissolved chlorides at 20 °C of temperature (CW); and (iv) wet/dry cycles in a tank with water at 20 °C (WD). As mentioned before, the concrete mechanical properties changed differently with each environmental condition. Likewise, results indicate that the properties of the epoxy adhesive might have changed throughout the 8 months' exposition to these environments. In fact, a recent study [16] with the same epoxy adhesive under the same environment conditions (REF, TW and CW) has shown a decrease on the

elastic modulus (about 14%, 43% and 34% for the REF, TW and CW respectively) and a decrease on the strength (about 6%, 38% and 30% for the REF, TW and CW respectively) after eight months of exposure. In contrast, Fernandes [30] have shown that the CFRP tensile properties suffer negligible losses when subjected to full immersion in water (about 3% and 2% for the tensile strength and E-modulus, respectively) or to full immersion in water with 3.5% of chlorides (about 7% and 1% for the tensile strength and E-modulus, respectively) for a period of time that lasted up to 720 days. Because all materials properties changed differently with each environmental condition, the overall behaviour of each composite system (RC slab/epoxy adhesive/CFRP laminate strip) also changed. For all four environmental conditions a decrease on the first-cracking, yielding and ultimate loads for both MA and GA specimens was observed. When compared to the reference specimens (T0_MA and T0_GA), all aged specimens presented a reduction on the ultimate parameters (in average the ultimate load, mid-span displacement and CFRP strains decreased 8.4%, 28.4% and 11.9%, respectively). In both anchorage systems the epoxy adhesive can be one of the crucial factors for its success. The deterioration of the adhesive's adherence and tensile properties seems to be the major reason for the earlier debonding initiation on the aged specimens. Regarding the GA specimens, the strip detachment always occurred at lower load levels, even in the less aggressive environmental conditions for the adhesive (CW). The lowest ultimate loads and deflections (F_u=53.52 kN and δ_u=38.21 mm) were observed for the environment REF (REF_GA_U). The T0_MA and the remaining MA slabs presented similar load levels at the onset of the strip's detachment. The MA slab subjected to the full immersion in water presented the most significant degradation. These results are in agreement with the evolution of the mechanical properties of the epoxy adhesive in time: the environmental actions TW and CW resulted in the most significant decrease in terms of the mechanical properties of the adhesive [16].

For each strengthened slab, three ductility parameters were calculated to evaluate the influence of each environmental condition on the ductility of the slab (see **Table 3.5**). In general, the increase of force (F_{max}/F_y), deflection (δ_{max}/δ_y) and curvature (φ_{max}/φ_y) ratios between the yielding and the failure stages was higher for MA specimens. The T0_MA presented the highest ductility parameters ($F_{max}/F_y = 1.33$, $\delta_{max}/\delta_y = 3.15$ and $\varphi_{max}/\varphi_y = 2.13$) and similar results were observed for MA slabs exposed to REF, CW and WD environments. Again, the immersion in

water (series TW) resulted in the highest ductility reduction for MA specimens, being the ratio δ_{max}/δ_y of specimen TW_MA_U 49% lower than the one obtained for T0_MA. This observation may be justified by the degradation experienced by the epoxy adhesive when exposed to certain environments [16]. Specimens prestressed with the GA system presented the highest ductility parameter on series TW and CW.

3.4.6 Influence of sustained loading

In real-life situations, a RC structure can be subjected to combined effects of physical and environmental factors, which in some cases may be synergetic. In order to evaluate their influence, as previously referred (see section 3.2.1), a sustained load of 20 kN was applied simultaneously to the four studied environments. The sustained load led to the pre-cracking of all specimens allowing a greater exposure of the reinforcement and strengthening elements to the environmental conditions and, consequently, a greater degradation of the composite system. During the sustained loading, the maximum deformation of the slab almost reached 12 mm and cracks were visible by naked eye. When loading was removed, more than 50% of the previously reached deformation was recovered.

During the static tests, a sudden stiffness loss was observed when the applied load was close to 25 kN indicating that the cracking process was not stabilized during the application of the sustained load. Up to this point, the stiffness of the slab assumed an intermediate value between the stiffness K_I and K_{II} of the "_U" specimens. As shown in **Table 3.5**, the sustained load and consequent cracking did not have a significant influence on the ultimate behaviour. In the static tests, the failure occurred for the same load level as for the "_U" slabs but, as expected, for lower deflection values (23.6% and 6.4% lower for the MA and GA systems, respectively). For the specimens subjected to the sustained loading the separation between the debonding initiation stage and the anchorage slippage stage has decreased, reducing the ductility. Ductility parameters presented in **Table 3.5** can quantify the reduction of the slabs ductility due to the effect of the synergies between sustained loading environmental conditions exposure. The GA specimens (TW_GA_C; CW_GA_C and WD_GA_C) presented similar ductility parameters to those obtained to the T0_GA. However, all "_C" specimens strengthened with the mechanical anchorage showed significant ductility

reductions. The lowest F_{max}/F_y, δ_{max}/δ_y and φ_{max}/φ_y ratios for the MA slabs were observed for series TW ($F_{max}/F_y = 1.14$), WD ($\delta_{max}/\delta_y = 1.64$) and TW ($\varphi_{max}/\varphi_y = 1.67$), respectively. In this matter, the less damaging synergy comprehended the sustained loading and the REF environment. Yet, the REF_MA_C showed a decrease higher than 20% in each of its ductility parameters when compared to the T0_MA.

In summary, the ductility of each slab was evaluated through three parameters (F_{max}/F_y, δ_{max}/δ_y and φ_{max}/φ_y) and three major factors have been observed: (i) specimens strengthened with the GA system showed minor variations in their ductility parameters after being exposed to the different environmental conditions solely (series "_U") or combined with the sustained loading (series "_C"); (ii) the ductility of MA specimens on series "_U" and "_C" was considerably lower than the ductility observed on slab T0_MA; and (iii) the combined effects (sustained loading + environmental action) produced a more severe effect on the ductility reduction of MA specimens than the exposure to each environment separately.

3.5 Conclusion

The main objective of this experimental campaign was to assess the durability of RC slabs strengthened with prestressed CFRP laminate strips using two different anchorage systems: the mechanical anchorage (MA) and gradient anchorage (GA). For eight months, sixteen slabs were subjected to the effect of four environmental conditions (reference environment - REF; immersion in tap water at 20 °C - TW; immersion in water with 3.5% of chlorides - CW; and wet/dry cycles in tap water at 20 °C - WD). Additionally, half of these specimens were subjected to a sustained load of 20 kN. Out of the presented results, several conclusions can be drawn:

- An average prestress loss of about 1 kN (in 40 kN) were observed in both anchorage systems. In the MA system short-term prestress losses were observed when the system is blocked with the fixing screws; whereas in the GA system these prestress losses were observed at the release of the first $1/3$ of force;
- The CFRP strain was continually monitored in all tested slabs and two main remarks should be highlighted: the strain increased when the specimens were immersed in water

(environment TW and CW) due to, mainly the volumetric expansion; the strain readings were highly influenced with the temperature oscillations;

- When the creep load was applied, the observed elastic deformation and CFRP strain variation were in agreement with the monotonic tests up to failure;
- In general, both systems (MA and GA) presented similar response during the creep loading. However, the GA slabs presented higher deformations than the MA slabs in the environmental conditions TW, CW and WD;
- The REF and WD environments are responsible for the highest mid-span vertical deflection due to creep. Despite of that, an average creep coefficient for the test period (φ_{ult}) of 1.3 was computed and are in agreement with the expected values for reinforced concrete elements. Based on the test period, a long-term creep coefficient (φ_{t_∞}) was estimated and it did not excess 1.9;
- During the monotonic tests, prestress allowed higher CFRP strains at failure, thus a better use of the involved materials;
- A similar response was observed for both anchorage techniques, but the mechanical anchors of the MA system prevented a premature failure and allowed the slabs to support greater ultimate loads and deflections;
- For the GA specimens, the initial debonding process was rapidly transformed into the complete strip detachment, resulting in a brittle failure, similar to conventional externally bonded reinforcement without any end-anchorages;
- The T0_MA slab was the only that failed by CFRP rupture at its maximum tensile capacity, whereas the remaining strengthened slabs seemed to have failed by strip intermediate debonding from the concrete;
- The exposure to water (series TW, CW and WD) improved the concrete strength and the corresponding modulus of elasticity, which increased the initial slabs' stiffness and delayed the crack initiation;
- All tested environmental conditions led to a reduction of the yielding and the failure loads for both anchorage systems, but the influence of each environment was different on each anchorage system: TW and REF environment conditions seemed to have the highest degradation influence over the MA and GA slabs, respectively;

- Debonding initiation on both systems was observed at earlier test stages for specimens exposed to all environments. The main reason resides in the fact that the epoxy adhesive's properties are susceptible to degradation when exposed to humidity or water;
- The ductility of all strengthened specimens was evaluated through three ductility parameters. In general, all tested exposure environments led to a reduction of the MA slabs ductility, especially in the case of cracked specimens. The MA specimens presented the lowest ductility after the immersion in water (series TW);
- The sustained loading amplified the effect of each environmental action. This effect was more pronounced on MA specimens, which presented lower structural ductility when comparing the deflection between failure and yielding;
- The performance and ductility losses of the strengthening systems when subjected to environmental conditions and sustained loading, separately or combined, were subtle. However, considering that the tests were carried out in only 8 months, the results give clear indications towards the importance of conducting similar tests over longer periods;
- During the static tests, the control specimens (series T0) exhibit a far superior performance and ductility compared to the remaining specimens. It is clear that the study of the effects of environmental actions and sustained loading is an essential topic to truly understand the long-term properties of prestressed CFRP strengthening systems;
- Based on the obtained results it is important to, in future works, evaluate the influence of the same environmental actions for a longer period, under the influence of temperature cycles and higher concentration of salts. However, the processes used in this work has revealed great potential for the establishment of standardized procedures for durability assessment of prestressed CFRP strengthening systems.

3.6 References

[1] Kim JHJ, Shi C, Bizindavyi L, Green MF. Applying Prestressed CFRP Sheets to Restore Prestress Losses in Prestressed Concrete Beams. ACI Spec Publ 2007;245:105–22.

[2] Omran HY, El-Hacha R. Effects of Sustained Load and Freeze-Thaw Exposure on RC Beams Strengthened with Prestressed NSM-CFRP Strips. Adv Struct Eng 2014. doi:10.1260/1369-

4332.17.12.1801.

[3] Huang J, Huang P, Zheng X. Experimental study of prestress losses of RC beams strengthened with prestress FRP. J Build Struct 2015;36:85–91.

[4] El-Hacha R, Wight RG, Green MF. Flexural behaviour of concrete beams strengthened with prestressed carbon fibre reinforced polymer sheets subjected to sustained loading and low temperature. Can J Civ Eng 2004;31:239–52. doi:10.1139/l03-091.

[5] Blaber J, Adair B, Antoniou A. Ncorr: Open-Source 2D Digital Image Correlation Matlab Software. Exp Mech 2015. doi:10.1007/s11340-015-0009-1.

[6] LNEC. LNEC E397-1993:1993. 1993.

[7] IPQ - Instituto Portugues da Qualidade; NP EN 12390-3:2011. Caparica: 2011.

[8] Termkhajornkit P, Nawa T, Kurumisawa K. Effect of water curing conditions on the hydration degree and compressive strengths of fly ash-cement paste. Cem Concr Compos 2006. doi:10.1016/j.cemconcomp.2006.05.018.

[9] NP EN ISO 6892-1. Metallic materials - Tensile testing – Part 1: Method of test at room temperature. IPQ - Inst Port Da Qual 2012.

[10] S&P. CFRP laminates, technical datasheet. Seewen, Switzerland: 2014.

[11] ISO NPEN. ISO 527-5 Plastics - Determination of tensile properties Part 5. Switzerland: 1997.

[12] Michels J, Sena-Cruz J, Christen R, Czaderski C, Motavalli M. Mechanical performance of cold-curing epoxy adhesives after different mixing and curing procedures. Compos Part B Eng 2016;98:434–43. doi:10.1016/j.compositesb.2016.05.054.

[13] Silva PM da. Time-dependent behaviour and durability of RC slabs strengthened with NSM CFRP strips. University of Minho, 2017.

[14] De Schutter G, Audenaert K. Evaluation of water absorption of concrete as a measure for resistance against carbonation and chloride migration. Mater Struct 2004;37:591. doi:10.1007/BF02483288.

[15] Zhang H. The Basic Properties of Building Materials. Elsevier; 2011. doi:10.1533/9781845699567.7.

[16] Silva PP, Fernandes P, Sena-Cruz JJ, Xavier JJJ, Castro F, Soares D, et al. Effects of different environmental conditions on the mechanical characteristics of a structural epoxy. Compos Part B Eng 2016;88:55–63. doi:10.1016/J.COMPOSITESB.2015.10.036.

[17] Cabral-Fonseca S, Correia JR, Rodrigues MP, A. Branco F. Artificial Accelerated Ageing of GFRP Pultruded Profiles Made of Polyester and Vinylester Resins: Characterisation of Physical–Chemical and Mechanical Damage. Strain n.d.;48:162–73. doi:10.1111/j.1475-1305.2011.00810.x.

[18] El Yagoubi J, Lubineau G, Saghir S, Verdu J, Askari A. Thermomechanical and hygroelastic properties of an epoxy system under humid and cold-warm cycling conditions. Polym Degrad Stab 2014;99:146–55. doi:10.1016/J.POLYMDEGRADSTAB.2013.11.011.

[19] Jones F. Durability of Reinforced plastics in liquid environments. In: Pritchard G, editor. Reinf. Plast. Durab., Boston: CRC Press; 1999, p. 70–110.

[20] CEB-FIP C. Model Code 1990. Com Euro-International Du Beton, Paris 1991. doi:10.1680/ceb-fipmc1990.35430.

[21] Gilbert RI, Ranzi G. Time-Dependent Behaviour of Concrete Structures. London: CRC Press; 2010.

[22] Czaderski C. Strengthening of reinforced concrete members by prestressed, externally bonded reinforcement with gradient anchorage. ETH ZURICH, 2012.

[23] Czaderski C, Martinelli E, Michels J, Motavalli M. Effect of curing conditions on strength development in an epoxy resin for structural strengthening. Compos Part B Eng 2012;43:398–410. doi:10.1016/J.COMPOSITESB.2011.07.006.

[24] ACI. Building Code Requirements for Structural Concrete (ACI 318-05) and Commentary (ACI 318R-05). 2005.

[25] Al Chami G, Thériault M, Neale KWW. Creep behaviour of CFRP-strengthened reinforced

concrete beams. Constr Build Mater 2009;23:1640–52.

[26] Arockiasamy M, Chidambaram S, Amer A, Shahawy M. Time-dependent deformations of concrete beams reinforced with CFRP bars. Compos Part B Eng 2000;31:577–92. doi:10.1016/S1359-8368(99)00045-1.

[27] CEB-FIP. Model Code for Concrete Structures 2010. 2013. doi:10.1002/9783433604090.

[28] CNR. Guide for the design and construction of externally bonded FRP systems for strengthening existing structures. 2013.

[29] Kotynia R, Walendziak R, Stoecklin I, Meier U. RC Slabs Strengthened with Prestressed and Gradually Anchored CFRP Strips under Monotonic and Cyclic Loading. J Compos Constr 2011. doi:10.1061/(ASCE)CC.1943-5614.0000081.

[30] Fernandes P. Bond behaviour of NSM CFRP-concrete systems: durability and quality control. University of Minho, 2016.

CHAPTER 4

BOND BEHAVIOUR OF TRANSVERSELY COMPRESSED MECHANICAL ANCHORAGE SYSTEM

4.1 Introduction

From the results obtained in the preliminary studies detailed in Chapter 2 and in the comprehensive experimental campaign detailed in Chapter 3 two types of failure modes were observed for slabs strengthened with the mechanical anchorage: (i) CFRP rupture at its maximum tensile capacity and (ii) CFRP slippage from the anchorage. In the abovementioned experimental studies, each mechanical anchorage was transversely compressed through six prestressed M16 anchor bolts with a torque of 150 N·m. From these tests, it was clear that the mechanical anchorage played a critical role on the response of the strengthened slabs. However, the absence of information from the existing literature and from the datasheet of the mechanical anchorage did not allow to get further conclusions about such system.

Thus, to better understand the mechanical anchorage behaviour an extensive experimental campaign was carried out. Composed by 22 large scale specimens, the experimental programme aimed at studying the effect of (i) compressive stress (controlled by the torque applied in each M16 anchor bolts of the MA system), (ii) laminate geometry and (iii) test temperature. Part of the work herein described has been already published in one journal [1] and several conference [2–4] papers.

4.2 Experimental programme

The experimental programme involved twenty-four prismatic concrete specimens of 200 mm × 500 mm × 800 mm. In these blocks, CFRP laminates were installed according to the EBR technique and were mechanically anchored to the concrete substrate through an aluminium alloy plate. Three main parameters were studied: (i) the laminate width, w_f, (50, 80 and 100 mm); (ii) the level of compressive stress, σ_L, through the torque (T_L) that was applied in the anchorage plate bolts (30, 100, 150 and 200 N·m); and (iii) the effect of the temperature, T, (20 °C, 60 °C and 80 °C). Regarding to the first parameter, the selected values are in agreement with the typical geometries of laminates used with this anchorage system. Concerning the level of torque, T_L, applied in the anchorage plate bolts, the value of 200 N·m was defined based on limitations of usual chemical bolt-concrete systems (used to fix the anchorage plate), which yielded to a

compressive stress level up to approximately 30 MPa. It should be highlighted that preliminary compression tests (in the transverse direction) on CFRP samples were performed up to 80 MPa, based on the mechanical properties of the CFRP laminates used. These tests revealed no signs of damage on the composite material. A torque of 150 N·m was used during the strengthening of the MA slabs (see Chapter 2 and Chapter 3). A negligible value of torque (30 N·m) was also considered in the present study, as well as an intermediate value between these last two mentioned torques. For the case of the later parameter, three temperature levels were adopted based on the glass transition temperature, T_g, of the epoxy adhesive used: a temperature lower than its T_g (20 °C), near its T_g (60 °C) and clearly above its T_g (80 °C). The temperature effect on the mechanical anchorage was evaluated through steady-state tests (with the temperature levels aforementioned) and through transient tests (with a constant pull-out force of 80 kN, 100 kN and 120 kN). Additional information regarding the later parameter is given in Section 4.2.1. As it is shown in **Table 4.1** all specimens are labelled with a generic denomination: LX_TY_Z, where X is the laminate width in [mm] (50, 80 or 100), Y is the torque level in [N·m] (30, 100, 150 or 200), and Z is related to the type of test configuration (steady-state tests carried out at 20 °C, 60 °C and 80 °C have the suffix SS20, SS60 and SS80, respectively; whereas the transient test that failed at 100 kN and 120 kN have the suffix CL100 and CL120, respectively). As two of the transient tests were repeated, four specimens were labelled with an additional suffix (a or b). For an easier analysis of the test results, all specimens were grouped in two series: Series 1, with all specimens tested with the steady-state configuration at room temperature (20 °C); and Series 2, with the slabs tested under a steady-state configuration at elevated temperatures (60 °C and 80 °C) and under the transient test configuration.

4.2.1 Specimens and test configuration

Figure 4.1 shows the test set-up used for the large scale pull-out tests. In order to study the transition from the debonding of the EBR CFRP laminate to the mechanical anchorage action, a total length of 522 mm of CFRP laminate was glued to the concrete surface: 272 mm corresponded to the length of the metallic anchorage plate, and 250 mm were assumed to be a bonded length. According to the CNR [5], the unconfined bonded length (henceforth referred simply as "EBR component") surpassed the theoretical effective length, l_e, needed to achieve the maximum

debonding load (equal to 200 mm for the present case). Consequently, with this specimen configuration, it was possible to study the behaviour of the EBR component, of the mechanical anchorage and the transfer of load from one region to the other.

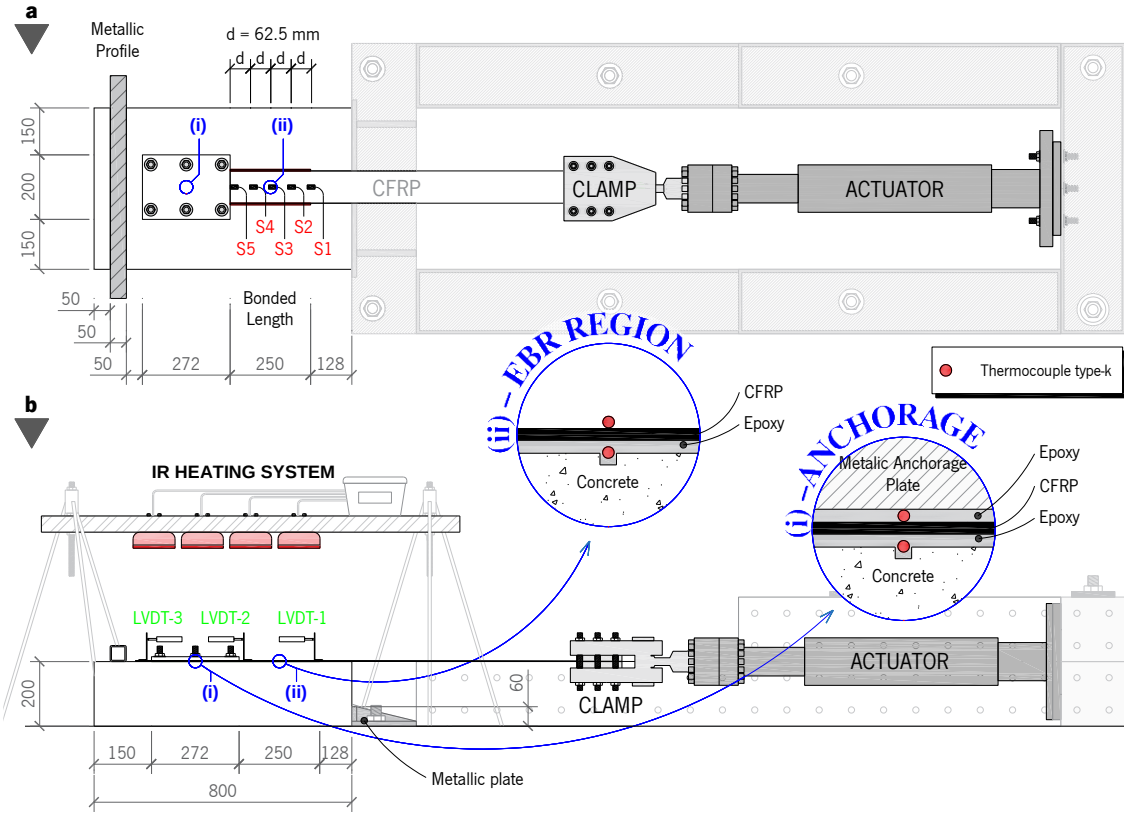

Figure 4.1: Specimen's geometry and test configuration. Note: All units are in millimetres.

The specimens were tested under the following two types of test configurations: (i) steady-state configuration, in which the temperature was kept constant at 20 °C, 60 °C and 80 °C while the specimens were loaded up to failure; and (ii) transient configuration, in which a pull-out force was kept constant at 80 kN, 100 kN and 120 kN (0.36%, 0.45% and 0.54% of CFRP strain) while the specimens were heated up to failure.

The concrete specimens were firstly placed onto the floor against a metallic plate with the height of 60 mm, which was assumed to be a rough measure of a hypothetical neutral axis depth for the case of a flexural member of 200 mm height. Next, the specimens were fixed to the strong floor through a metallic profile located at the top rear part of the specimen, 50 mm apart from the

bottom face of the block (see **Figure 4.1**). Once the concrete blocks had been correctly placed and fixed, the CFRP laminate was connected to the hydraulic actuator through a metallic clamp specially designed for these tests (see **Figure 4.2**). As shown in **Figure 4.2a**, these grips were 200 mm wide and 285 mm long and were closed with six M20 bolts. This clamping system was designed to withstand the failure by CFRP rupture at its maximum tensile capacity (close to 300 kN for the laminate of 100×1.2 [mm]). Depending on the type of test, different procedures were adopted: (i) in the steady-state tests the laminate was pulled using a servo-controlled machine at a constant rate of 0.30 mm/min until the total debonding of the laminate's bonded length. Then the speed was increased up to 2 mm/min until the end of the test. The moment when the displacement rate was also changed is presented in **Figure 4.6** and in **Figure 4.14** as a grey dot (with the label "A"). These figures clearly indicate that the change in the test velocity did not yield to critical changes on the load-slip relationships.

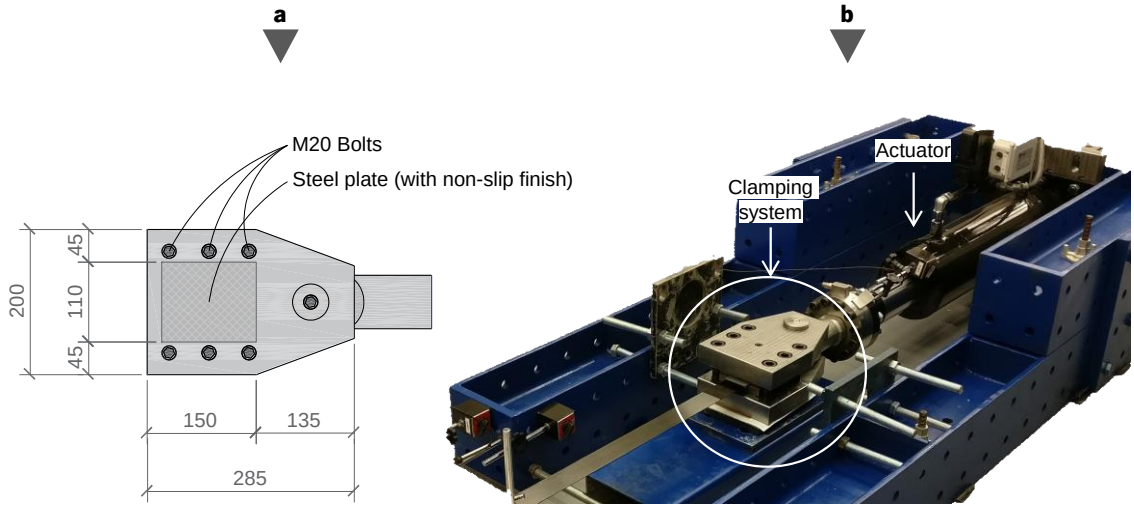

Figure 4.2: Clamping system: (a) detail of the clamping system; and (b) photo of the clamping system and hydraulic actuator

During the steady-state tests the temperature was kept constant in the anchorage zone and EBR component. The temperature was achieved using an infra-red (IR) heating system, and the temperature levels were meant to keep the epoxy adhesive inside the mechanical anchorage (in-between the concrete and the CFRP laminate) at a temperature lower than its T_g (20 °C), near its T_g (60 °C) and above its T_g (80 °C). **Figure 4.3** presents the temperature evolution in the mechanical anchorage and in the EBR component.

Table 4.1
Experimental programme.

Specimen	w_f [mm]	T_L [mm]	T [°C]	σ_L [MPa]	E_f [GPa]	f_{fu} [MPa]	CB
Series 1: Tests performed at room temperature							
L50_T30_SS20	50[i]	30	20°C	4.6	176.4 (2.0%)	2222.4 (4.7%)	B1
L50_T100_SS20	50[i]	100	20°C	15.3	176.4 (2.0%)	2222.4 (4.7%)	B1
L50_T150_SS20	50[i]	150	20°C	23.0	176.4 (2.0%)	2222.4 (4.7%)	B1
L50_T200_SS20	50[i]	200	20°C	30.6	176.4 (2.0%)	2222.4 (4.7%)	B1
L80_T30_SS20	80[iii]	30	20°C	2.9	170.5 (0.3%)	2428.0 (4.6%)	B1
L80_T100_SS20	80[iii]	100	20°C	9.6	170.5 (0.3%)	2428.0 (4.6%)	B1
L80_T150_SS20	80[iii]	150	20°C	14.4	170.5 (0.3%)	2428.0 (4.6%)	B1
L80_T200_SS20	80[iii]	200	20°C	19.2	170.5 (0.3%)	2428.0 (4.6%)	B1
L100_T30_SS20	100[iv]	30	20°C	2.3	169.4 (1.4%)	2480.2 (4.0%)	B1
L100_T100_SS20	100[iv]	100	20°C	7.7	169.4 (1.4%)	2480.2 (4.0%)	B1
L100_T150_SS20	100[iv]	150	20°C	11.5	169.4 (1.4%)	2480.2 (4.0%)	B1
Series 2: Tests performed at high temperature							
L80_T150_SS60	80[iii]	150	60°C	14.4	174.6 (1.1%)	2867.9 (1.6%)	B2
L80_T150_SS80	80[iii]	150	80°C	14.4	174.6 (1.1%)	2867.9 (1.6%)	B2
L100_T100_SS60	100[v]	100	60°C	7.7	187.2 (0.9%)	2895.2 (0.2%)	B2
L100_T100_SS80	100[v]	100	80°C	7.7	187.2 (0.9%)	2895.2 (0.2%)	B2
L100_T150_SS60	100[v]	150	60°C	11.5	187.2 (0.9%)	2895.2 (0.2%)	B2
L100_T150_SS80	100[v]	150	80°C	11.5	187.2 (0.9%)	2895.2 (0.2%)	B2
L100_T200_SS60	100[iv]	200	60°C	15.3	169.4 (1.4%)	2480.2 (4.0%)	B1
L100_T100_CL100	100[v]	100	–	7.7	187.2 (0.9%)	2895.2 (0.2%)	B2
L100_T100_CL120	100[v]	100	–	7.7	187.2 (0.9%)	2895.2 (0.2%)	B2
L100_T150_CL100a	100[v]	150	–	11.5	187.2 (0.9%)	2895.2 (0.2%)	B2
L100_T150_CL100b	100[v]	150	–	11.5	187.2 (0.9%)	2895.2 (0.2%)	B2
L100_T150_CL120a	100[v]	150	–	11.5	187.2 (0.9%)	2895.2 (0.2%)	B2
L100_T150_CL120b	100[v]	150	–	11.5	187.2 (0.9%)	2895.2 (0.2%)	B2

Notes: The laminates of 50 mm belong to a single batch [i]; The laminates of 80 mm belong to two different batches, batch [ii] and batch [iii]; the laminate of 100 mm belongs to two different batches, batch [iv] and batch [v]; the values between parentheses are the corresponding coefficients of variation (CoV).
w_f – CFRP laminate width; T_L– Torque level; T – Test temperature; σ_L – Confinement level; E_f – CFRP modulus of elasticity; f_{fu}– CFRP tensile strength; **CB** – Concrete batch.

In the transient tests the IR heating system was used to gradually increase the temperature in the anchorage zone and EBR component. In a first stage of the transient tests, the temperature was kept constant at 30 °C and the stress level on the laminate was increased up to a predefined pull-out load of 80 kN, 100 kN and 120 kN. Then the temperature was raised up (average rate of about 0.4 °C/min) until failure keeping the stress level constant. If the temperature in the mechanical anchorage reached 80 °C and failure was not observed, the conditions of temperature (80 °C) and pull-out load (80 kN, 100 kN or 120 kN) were kept for a period of one additional hour before ending the test (see **Figure 4.3c**).

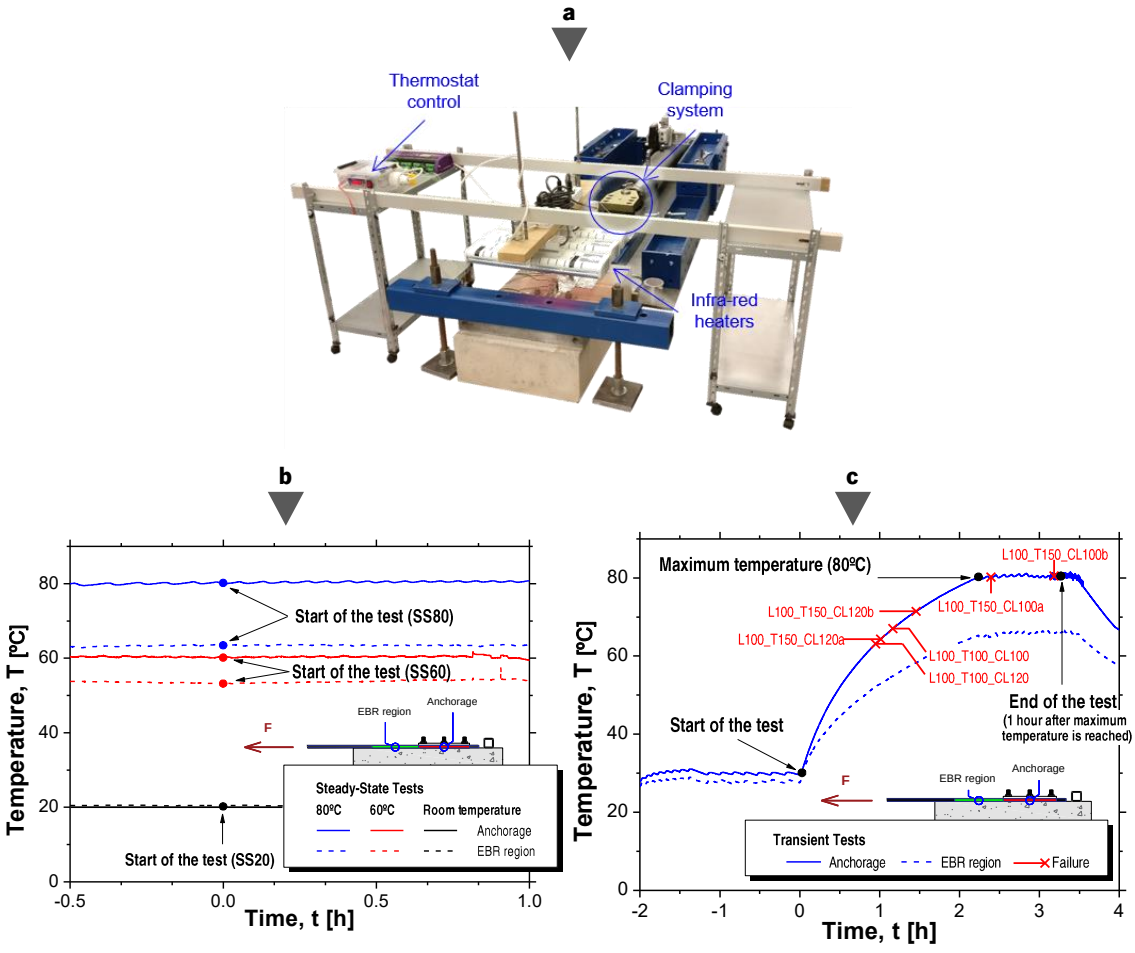

Figure 4.3: Heating system: (a) photo of the set-up; (b) typical temperature evolution for steady-state tests; and (c) typical temperature evolution for transient tests.

The IR heating system is composed by four IR heaters of 1200 W, controlled by a thermostat. This system was developed to reach the maximum temperature of 80 °C in a relative short period of time (2 hours) and to produce an even distribution of temperature across the anchorage plate and on the EBR component. The photograph in **Figure 4.3a** shows the test set-up including the IR heating system.

The relative displacement of the CFRP laminate with respect to the concrete block was acquired by means of linear variable differential transformers (LVDT) placed at different locations (see **Figure 4.1b**): (i) at the location where the CFRP laminate starts to be bonded to the concrete (loaded end, LVDT-1), (ii) at the side of the anchorage plate that the laminate is pulled (mid end, LVDT-2) and (iii) at the other side of the anchorage plate (free end, LVDT-3). The LVDT-1 has a range of ±5.0 mm and a linearity error of ±0.24%, whereas the LVDT-2 and LVDT-3 range of ±2.5 mm and a linearity error of ±0.24%. The load cell used has a maximum measuring capacity of 300 kN and a linear error of ±0.05%. The evolution of the strain profile in the laminate was registered by strain gauges (S1 to S5, TML PFL-30-11-3L) placed every 62.5 mm that were glued along the CFRP bonded length (see **Figure 4.1a**). Five thermocouples were used to measure the temperature in tests performed with elevated temperatures (see **Figure 4.1b**). The thermocouples (type K) had a range from -50 °C to 250 °C and were placed at the centre of the anchorage and at the EBR component, each location with several thermocouples. It is noteworthy to mention that during the design of the IR heating system preliminary tests were carried out with several thermocouples, placed in the anchorage region (5 thermocouples, equally distributed in between the epoxy adhesive and the concrete; particularly, one near each corner of the anchor plate – approximately 30 mm - and one at the geometrical its centre), and in the EBR region (3 thermocouples, equally distributed in between the epoxy adhesive and the concrete; each one spaced by 83 mm, at the middle line of the CFRP strip – transversal section). During these preliminary tests, the temperature variation between the thermocouples of the same region was negligible.

4.2.2 Materials

The behaviour of the strengthening system and performance of the test specimens is related to the mechanical properties of the materials used. Concrete, CFRP laminate, and epoxy adhesive are the

main materials used in the present experimental study. The ready-mixed concrete (exposure class of XC4(P) according to Eurocode 2 [6]) was composed of crushed granite aggregates with a maximum aggregate size of 12.5 mm and Portland cement type CEM II/A-L 42,5R. It was used two batches (B1 and B2) to cast the concrete prisms (see **Table 4.1**). The concrete compressive strength and modulus of elasticity were assessed using compression tests following NP EN 12390-3:2011 [7] and LNEC E397 1993:1993 [8] recommendations, respectively. For each concrete batch six cylindrical specimens (300 mm of height and 150 mm of diameter) were used. These tests were performed at the same age of the pull-out tests. An average compressive strength (f_c) of about 33.4 MPa (CoV=4.33%) and 45.0 MPa (CoV=1.24%) was obtained for batches B1 and B2, respectively. The modulus of elasticity was also assessed for batch B1 (30.8 GPa, CoV=2.84%) and for batch B2 (32.8 GPa, CoV=0.72%). Although the concrete compressive strength was higher in batch B2 than in B1, the governing failure mode of all specimens was adhesive type at the concrete/adhesive interface. Thus, the difference in f_c presents marginal influence in the results of the research.

Similarly to the slab specimens (see Chapter 2 and Chapter 3), the CFRP laminate strips used in the experimental work consisted of unidirectional carbon fibres (volume content is higher than 68%) held together by an epoxy vinyl ester resin matrix. The tensile properties of the CFRP laminate were assessed thought the ISO 527-5:1997 [9] recommendations. The CFRP laminate came from five different batches as described in **Table 4.1**. For each batch, six samples were used to assess the modulus of elasticity (E_f) and the tensile strength (f_{fu}), with the results presented in **Table 4.1**). An average E_f of 176.4 GPa, 172.6 GPa and 178.0 GPa was obtained for the laminates with the width of 50 mm, 80 mm and 100 mm, respectively. The maximum tensile strength varied between 2222.4 MPa and 2895.2 MPa. All specimens presented an explosive failure type, by rupture of the fibres located mainly at the middle height of the test sample.

The S&P Resin 220 used was the same two-component epoxy adhesive utilized in the strengthening of the slabs for the short and long-term behaviour. The expected modulus of elasticity and tensile strength was presented in section 2.2.2 (Chapter 2) and section 3.2.2 (Chapter 3). It should be referred that Silva *et al.* [10] performed a Dynamic Mechanical Analysis (DMA) to assess the glass

transition temperature (T_g) of the same type of epoxy adhesive. Based on the onset of the glass transition of the storage modulus, a value of 47.2 °C was obtained.

The anchorage plates are a commercially available solution for the end-anchorage of a CFRP laminate prestressing system, from the same company that supplied the CFRP laminate strip and epoxy resin. A 2D drawing of the anchorage plate is presented in **Figure 4.4**. With the dimensions of 200 mm (height) by 272 mm (width) and a thickness of 12 mm, the metallic plate is made of hard aluminium and has 6 major holes (diameter of 18 mm) meant to accommodate M16 anchorage bolts. This aluminium plate also presents 12 additional threaded holes (4 M8 and 8 M12) that are used for the prestressing system. Two different types of anchor bolts were used in this experimental programme: M16 grade 8.8 for a predefined torque level of 30 N·m, 100 N·m and 150 N·m, and M16 10.9 for the torque level of 200 N·m.

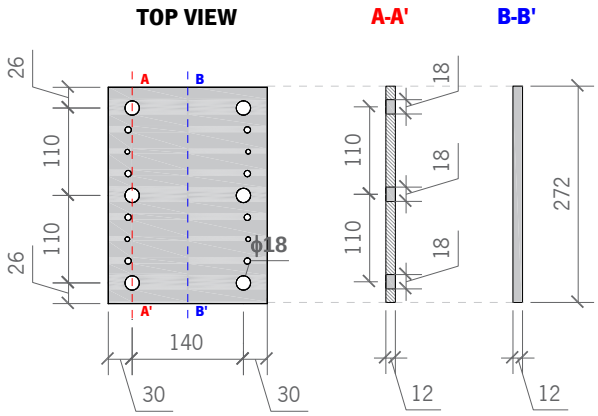

Figure 4.4: Drawing of the anchorage plate. Note: All units are in millimetres.

4.2.3 Preparation of specimens

As stated before, the specimen configuration was conceived in order to accommodate the anchorage and EBR components. This option assures better representativeness of the real applications and allows better understanding of the bond behaviour in the transition between the EBR and anchorage components. Thus, the following procedure was implemented in the preparation of all specimens:

1. The surface roughness of the concrete was enhanced with a sandblasting technique. Six holes with a diameter of 18 mm and a total depth of 150 mm were drilled on the concrete surface to allocate the metallic anchor bolts (see **Figure 4.5a**);
2. After sandblasting and drilling, the holes and the concrete surface were carefully cleaned by using pressurized air (see **Figure 4.5b**);
3. The metallic anchor bolts were glued with HIT-HY 200-A® which is a chemical bond agent to fix each aluminium anchorage plate (see **Figure 4.5c**);
4. The bi-component epoxy resin was prepared according to the requirements provided by the supplier (see **Figure 4.5c**). The CFRP laminate strip was properly cleaned with a solvent and the adhesive was applied on the surface of the CFRP laminate (see **Figure 4.5d**), with a target minimum regular thickness of 1.5 mm along a total length of 272 mm (corresponding to the length of the plate) plus 250 mm (which was considered an adequate upperbound value for the bonded length of the laminate according to formulations suggested by technical literature, [5], in order to exceed the effective bond length);
5. A similar epoxy layer was applied on the cleaned concrete surface and the laminate was carefully placed centred on the surface of the concrete block (see **Figure 4.5f**);
6. The surface of the anchorage plate was slightly grinded with sandpaper and cleaned with a solvent before applying the same batch of epoxy resin that was applied on the CFRP laminate and the concrete (see **Figure 4.5e**);
7. Then, the metallic plate, which had 6 holes of 18 mm diameter to accommodate 6 bolt anchors of 16 mm, was placed on its predefined location (see **Figure 4.5g**);
8. Just after the mechanical anchorage was placed in its correct place, it was torqued to the concrete element with the aid of a dynamometric key that ensured the target level of compressive stress (torque level of 30, 100, 150 and 200 N·m, see **Figure 4.5h**);

According to the adhesive's supplier [11], the epoxy is fully cured after 3 days at 20 °C. Specimens were kept in laboratory premises (average temperature of 20 °C and 55% of relative humidity) for a period of 7 days before testing. Aluminium tabs were glued at the end of the laminate for not damaging the CFRP when hold by the clamping system.

It is commonly accepted that the bond stress of the concrete-FRP interface highly depends on the concrete roughness [12–14]. For that purpose, the concrete roughness characteristics after sandblasting procedure were measured in all blocks at three different locations (one at the middle of the bonded length, and two on the metallic anchorage zone) with a laser sensor - each sample with a total length of 150 mm. The properties of the measuring device are further detailed in Section 2.2.4 of Chapter 2.

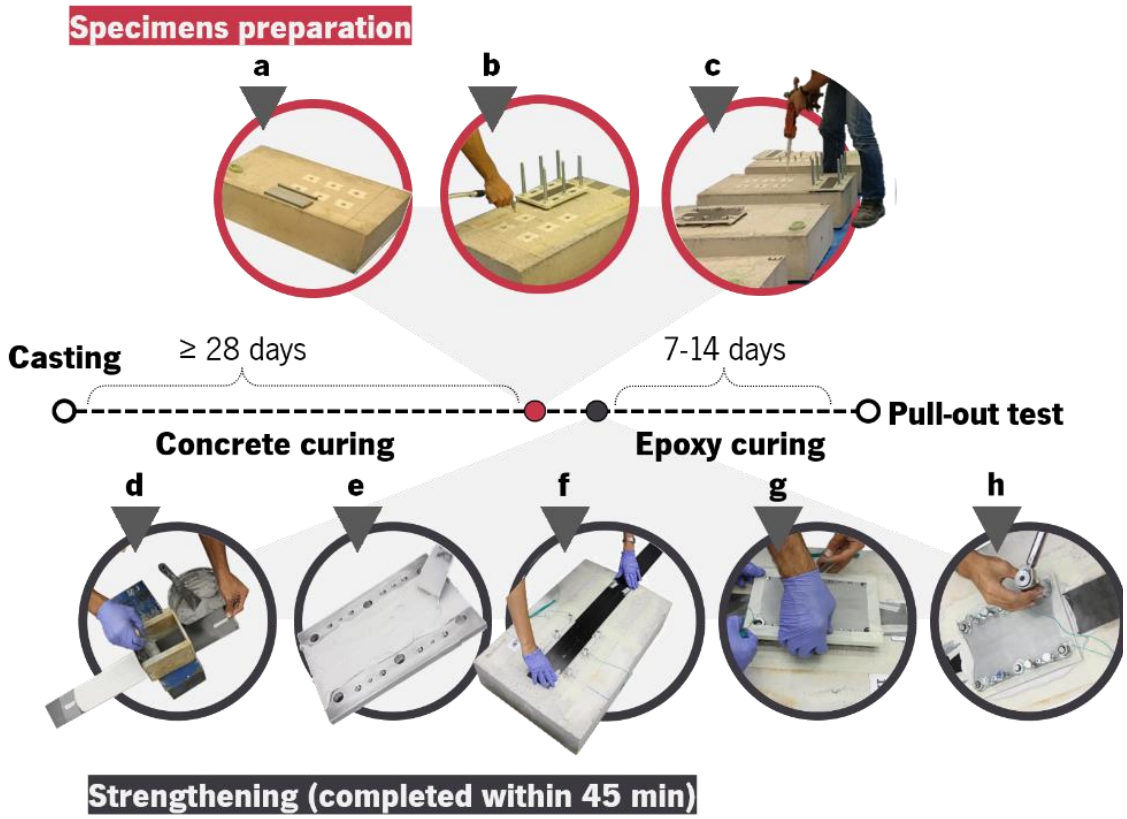

Figure 4.5: Specimens calendar and strengthening procedures.

Up to now, there is not a standard parameter to evaluate the concrete roughness in EBR applications, reason why in the current work the concrete roughness was evaluated following the Model Code 2010 [13]. Three parameters are generally used to evaluate the surface roughness on concrete-to-concrete interfaces [13]: the average roughness R_a, the root mean square R_q and the peak to valley height R_t. **Table 4.2** presents these roughness parameters, the maximum valley depth (R_v) and the maximum peak height (R_p). The procedure used herein to obtain these

parameters is described in Section 2.2.4 of Chapter 2. According to Model Code 2010 [13], the results included in **Table 4.2** correspond to a smooth surface roughness. Only in 3% of the assessed lengths, a peak-to-valley-deviation higher than 3 mm (rough surface roughness) was observed. It is worth emphasising that this concrete-to-concrete interfaces categorisation (very smooth, smooth, rough and very rough) presented in the Model Code 2010 [13] is useful for design purposes (shear resistance). However, in EBR applications a different categorisation should be considered, taking into consideration recent studies on this subject [14–16].

Table 4.2
Concrete surface roughness.

	R_a [mm]	R_q [mm]	R_v [mm]	R_p [mm]	R_t [mm]
Minimum	0.116	0.147	-1.573	0.534	1.098
Maximum	0.244	0.296	-0.374	2.678	3.525
Average	0.167	0.217	-0.888	0.955	1.843
CoV	19.03%	17.94%	-26.24%	41.17%	25.35%

Note: R_a – Arithmetic average of absolute values; R_q– Root mean squared; R_v – Maximum valley depth; R_p – maximum peak height; R_t – Maximum height of the profile.

4.3 Tests performed at room temperature

As previously described, in the pull-out tests one extremity of the laminate was pulled while the other was fixed against the concrete with a bonded region of 250 mm (EBR component) followed by the transversely compressed metallic anchorage with 272 mm of length (anchorage component). Firstly, the bonded region supports the increasing loads but when its maximum capacity is attained the new load increments are supported by the compressed metallic anchorage. In the current section the experimental results from Series 1 (tests performed at room temperature) are presented and discussed. Additionally, an analytical prediction is carried out to understand better the debonding process of the EBR component.

4.3.1 Load-Slip behaviour

All concrete specimens experienced a similar pattern in terms of load-slip behaviour, which is represented in **Figure 4.6**. A first almost linear branch, governed by the EBR component, with a

steep slope being observed in the loaded end until EBR debonding (**Figure 4.6**: 0-1). During this phase, the slip registered in the mid end is negligible, meaning that all the force is carried by the bonded length outside the mechanical anchorage. Next, the debonding starts to occur (**Figure 4.6**: 1). During the debonding process (**Figure 4.6**: 1-2), the load does not increase whilst the slip increases considerably due to the elastic energy accumulated in the bonded length. At the end of the debonding phase, the mid end immediately starts to register some slip; at that point, the mechanical anchorage activates. The pull-out test was controlled by the displacement of the laminate loaded end and, due to the configuration of the test, the transition from the EBR to the anchorage, although swift, occurred without damaging the CFRP laminate and without any loss in the total pull-out force. Once all the bonded length of the laminate is detached from the concrete surface, the CFRP laminate is firmly held between the clamping system and the mechanical anchorage plate, facing a continuous increase in its strain and sustained load. Due to the elastic behaviour of the CFRP laminate, a fairly linear load-slip response is registered in all cases. Finally, in the last stages of the test (**Figure 4.6**: 3-4), the laminate strain continues increasing but its linearity is lost due to some minor slip taking place in the mechanical anchorage and the aggregate interlock that exists at the CFRP/concrete interface (debonded zone). The test typically fails by CFRP rupture; consequently, LVDT-3 (free end) generally registers negligible results. The data from LVDT-3 can be, however, interpreted as an indication of the level of damage inside the metallic anchorage. The data registered in all three LVDTs is analysed in the following sub-chapters 4.3.2 and 4.3.3.

By subtracting the displacement obtained in LVDT 2 (mid end) from displacement obtained in LVDT 1 (loaded end), the effect of this minor slip derived from the mechanical anchorage can be removed from the loaded end slip. As a result, a linear load-slip curve is obtained after the debonding phase (black dashed line in **Figure 4.6**). The average slope of each curve allows the computation of the elastic modulus of each CFRP laminate and the values are similar to those obtained in the material characterization (169 GPa, 173 GPa and 162 GPa for the laminates of 50 mm, 80 mm and 100 mm, respectively). Also, these curves showed that the influence of the aggregate interlock that exists at the deboned zone is relatively small (less than 4.7%). Finally, a line representing the axial stiffness of the CFRP laminate is also shown in **Figure 4.6** for comparison purposes (dashed

green line). The load-slip curve without considering the mid end slip compares relatively well with the axial stiffness of the CFRP.

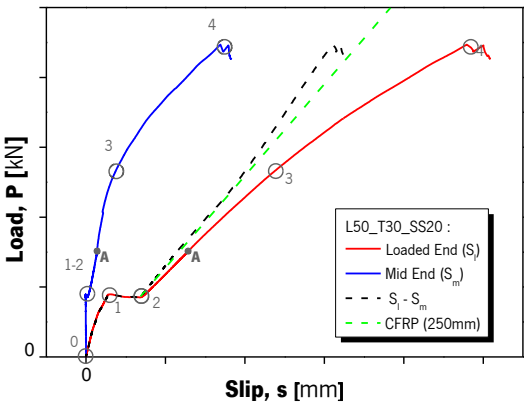

Figure 4.6: Typical load-slip at the loaded end and mid end (L50_T30_SS20). Note: The point "A" shows the stage when the velocity of the test was increased from 0.3 mm/min to 2.0 mm/min.

In **Figure 4.7**, the load-slip behaviour of all specimens is represented at the loaded end, mid end and free end for comparison purposes. The dependence of laminate width is clearly observed in terms of stiffness and load carrying capacity of the overall system: the wider the laminate, the higher the stiffness and capacity. The influence of the level of torque can be also appreciated in the bond shear stress-slip curves after debonding of the EBR component: lower values of torque provide, in general, a less stiff response in terms of pullout-slip, meaning that more damage is generated inside the mechanical anchorage. On the contrary, higher levels of torque cause slightly stiffer responses. Therefore, specimens with the smallest level of toque (30 N·m) exhibit the highest ultimate slip and, as shown in **Figure 4.7**, as the torque level is increased, smaller values of the ultimate slip are observed at the loaded-end and at the mid-end. The values of slip at the free end are only illustrative of the potential movement of the laminate with respect to the metallic plate and the concrete; however, it is observed that lower values of torque (i.e. 30 N·m) provide more movement at the free end of the laminate, proving that the level of damage inside the metallic anchorage is higher in these cases than for higher torque values.

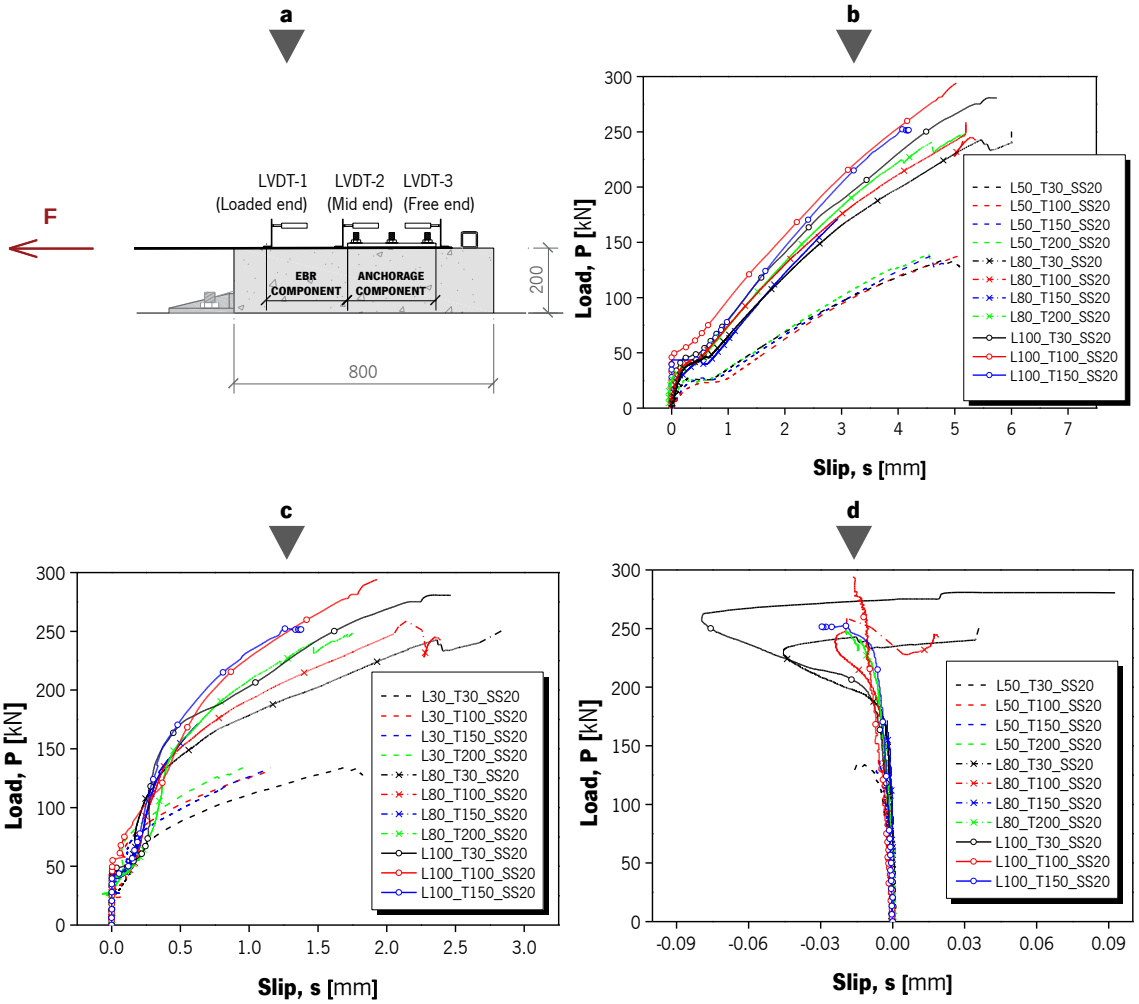

Figure 4.7: (a) Location of the LVDTs and load-slip curves: (b) at loaded end, (c) at mid end, and (d) at free end. All units in [mm].

4.3.2 EBR component

4.3.2.1 Debonding load and fracture energy

The debonding load ($P_{deb,exp}$, **Table 4.3**) is defined in this experimental programme as the load at which the laminate (at the EBR component) is debonded from the concrete substrate and, consequently, the mechanical anchorage starts to carry the entire load. Because the anchorage component had a length higher than the effective bond length, it was possible to obtain a very stable value of the debonding load (**Figure 4.6**: 1-2), which represents the asymptotic value of the transmissible force by an anchorage of infinite length (without compressive stresses). In this

experimental programme, the debonding process is observed to occur suddenly and abruptly in all cases. Moreover, the failure mode obtained is cohesive in the concrete, a few millimetres beneath the concrete/epoxy interface, as it is well reported in the literature [17].

Table 4.3
Experimental debonding loads and comparison with analytical predictions.

Specimen	$P_{deb,exp}$ [kN]	$P_{deb,ave}$ [kN]	$G_{f,exp}$ [N/mm]	$G_{f,th1}$ [N/mm]	$G_{f,th2}$ [N/mm]	$P_{deb,th}$ [kN]	η
Series 1: Tests performed at room temperature							
L50_T30_SS20	26.85	26.25 (6.0%)	0.65	0.69	0.64	26.02	1.01
L50_T100_SS20	23.54						
L50_T150_SS20	27.30						
L50_T200_SS20	27.30						
L80_T30_SS20	46.48	43.17 (5.0%)	0.71	0.69	0.64	40.94	1.05
L80_T100_SS20	42.70						
L80_T150_SS20	43.00						
L80_T200_SS20	40.50						
L100_T30_SS20	48.10	48.73 (10.8%)	0.58	0.69	0.64	51.00	0.96
L100_T100_SS20	55.50						
L100_T150_SS20	42.60						

Notes: The values between parentheses are the corresponding CoV.
$P_{deb,exp}$ – Debonding load; $P_{deb,ave}$– Average debonding load; $G_{f,exp}$ – Fracture energy computed with equation (4.3); $G_{f,th1}$ – (Predicted) Fracture energy computed with equation (4.4); $G_{f,th2}$ – (Predicted) Fracture energy computed with equation (4.5); $P_{deb,th}$ – (Predicted) Debonding load computed with equation (4.7); and η – ratio between the $P_{deb,ave}$ and $P_{deb,th}$.

In the case where the CFRP laminate and adhesive properties were identical, equal values of ultimate debonding strength would be assumed for all specimens, and hence a linear dependence of $P_{deb,exp}$ on the laminate width would be expected. As stated before, according to the literature [5,17,18] the used bonded length (250 mm) surpasses the theoretical effective length, l_e, in this case of 200 mm [5], needed to achieve the maximum debonding load. Although different CFRP modulus of elasticity were observed, the relation between the mean value of $P_{deb,exp}$ and the laminate width can be assumed to be linear (a constant value of 0.520 kN (CoV= 8.2%) per unit length of CFRP width was obtained for all specimens).

In general terms, the fracture energy associated to the bond shear stress-slip law $\tau(s)$ in the bonded length, G_f, can be expressed as:

$$G_f = \int_0^\infty \tau(s)ds \tag{4.1}$$

Assuming a stiffness in concrete much higher than the stiffness of the EBR reinforcement, the equilibrium of energies can be assumed in the section where the maximum stress σ_f in the CFRP strip is applied and the following relationship can be deduced for a unit length [19]:

$$\int_{A_f} \frac{1}{2}\sigma_f \varepsilon_f dA = w\int_0^\infty \tau(s)ds \tag{4.2}$$

Hence, the value of the fracture energy G_f corresponding to debonding load, P_{deb}, can be calculated as:

$$G_f = \frac{P_{deb}^2}{2E_f w A_f} \tag{4.3}$$

where A_f, E_f and w are the cross-section area, the modulus of elasticity and the width of the CFRP laminate, respectively. The values of G_f calculated according to Eq.(4.3) , taking into account the experimental values of $P_{deb,exp}$ are also shown in **Table 4.3**. As expected, G_f keeps almost constant for all the specimens, ranging between 0.58 and 0.71 N/mm.

The experimental values of G_f can be compared with the ones predicted by different analytical approaches. For this particular case, CNR [5] predictions are assumed. CNR proposes a value for the design fracture energy (Eq. (4.4) – in [N/mm]) depending on the concrete compressive and tensile strengths (f_{cm} and f_{ctm}, respectively – in [N/mm^2]), a confidence factor (FC), adopted equal to 1, a geometrical corrective factor k_b (dimensionless parameter) and an additional corrective factor taking into account the bonding system k_c (pre-cured or wet lay-up systems are considered), in [mm] :

$$G_f = \frac{k_b k_G}{FC}\sqrt{f_{cm} f_{ctm}} \tag{4.4}$$

The theoretical results obtained with Eq. (4.4) assuming k_c equal to 0.063 mm (mean value for a pre-cured system, [5]) are presented in **Table 4.3**. It is observed a reasonable good fit between theoretical and experimental values, with a slight trend to theoretically overestimate G_f. In fact, on average, G_f obtained experimentally is equal to 0.65 N/mm, whereas according to the CNR is equal to 0.69 N/mm.

The influence of the concrete roughness on the bond shear stress-slip behaviour has been previously reported in the literature [20], and some studies have provided a roughness coefficient to take into account its influence on G_f [14,21]. Iovinella *et al.* [14], for instance, adjusted the CNR formulation (Eq. (4.4)) thought a roughness factor I_R that considers the average of individual measures peak-to-valley heights and the inclination angle of the profile. A more recent study [21] has proposed an improvement of Eq. (4.4) to consider the effect of the roughness of the concrete surface on the calculation of the fracture energy, by only considering a roughness coefficient k_R (dimensionless parameter based on the average roughness, R_a):

$$G_f = \frac{k_b k_G k_R}{FC}\sqrt{f_{cm} f_{ctm}} \tag{4.5}$$

were,

$$k_R = 1.1R_a + 0.8 \tag{4.6}$$

In **Figure 4.6,** the value of G_f taking into account the roughness coefficient ($G_{f,th2}$) is shown together with the experimental value and the one obtained by Eq. (4.5). It can be easily observed that for this experimental programme, the approach proposed by [21] provides a better fit to the experimental values.

The ultimate strength, f_{fdd} [5], defined as the maximum allowed strength before debonding assuming that the provided bonded length is equal or larger to the optimal bonded length, is assumed to be:

$$f_{fdd} = \frac{1}{\gamma_{f,d}} \sqrt{\frac{2E_f G_f}{t_f}} \tag{4.7}$$

where $\gamma_{f,d}$ is a partial safety factor. In **Table 4.3**, the ultimate strength has been calculated considering a safety factor $\gamma_{f,d}$ of 1.0 in order to obtain the theoretical value of P_{deb} and considering the theoretical value of G_f obtained by Eq. (4.5). The η value shows the ratio between the experimental ($P_{deb,exp}$) and the predicted ($P_{deb,th}$) value for P_{deb}. In general terms, the experimental value of P_{deb} is in accordance (with a confidence interval of ±5%) with the predicted by CNR taking into account the roughness coefficient k_R. **Figure 4.8** shows the values of the debonding and the ultimate load for all the specimens, together with theoretical predictions. The theoretical prediction of the debonding load was obtained from equations (4.3) and (4.7). A good relation between the experimental debonding load, $P_{deb,exp}$ (grey bars) and the predicted debonding load, $P_{deb,th}$, (black bars) can be observed.

4.3.2.2 Strain profile in the CFRP laminate

The strain profile along the CFRP laminate in its bonded length, which in this study was assumed to be 250 mm, can provide information about the active transfer length at different levels of load. The strain profile obtained from the L50_T30_SS20 and L80_T30_SS20 is presented in **Figure 4.9a** and **Figure 4.9b**, respectively. Both graphs show that the activated length increases with the applied load, and complete debonding takes place when there is no more undeformed bonded length. It can be seen that the strain at the loaded end (S1, x = 0 mm) increases with the load from the beginning of the test at an almost constant rate, as expected. At the beginning of the debonding process, the load is transferred to the next strain gauge, and, in most cases, it is transferred to the next strain gauge in a relatively sudden pattern with almost no increase in load (**Figure 4.9a**). In other cases, the debonding process is somehow less abrupt, and the load is transmitted through the bonded length with a slight increase of its value (**Figure 4.9b**). Once debonding has taken place, the strain in the laminate increases in a similar strain rate in all positions.

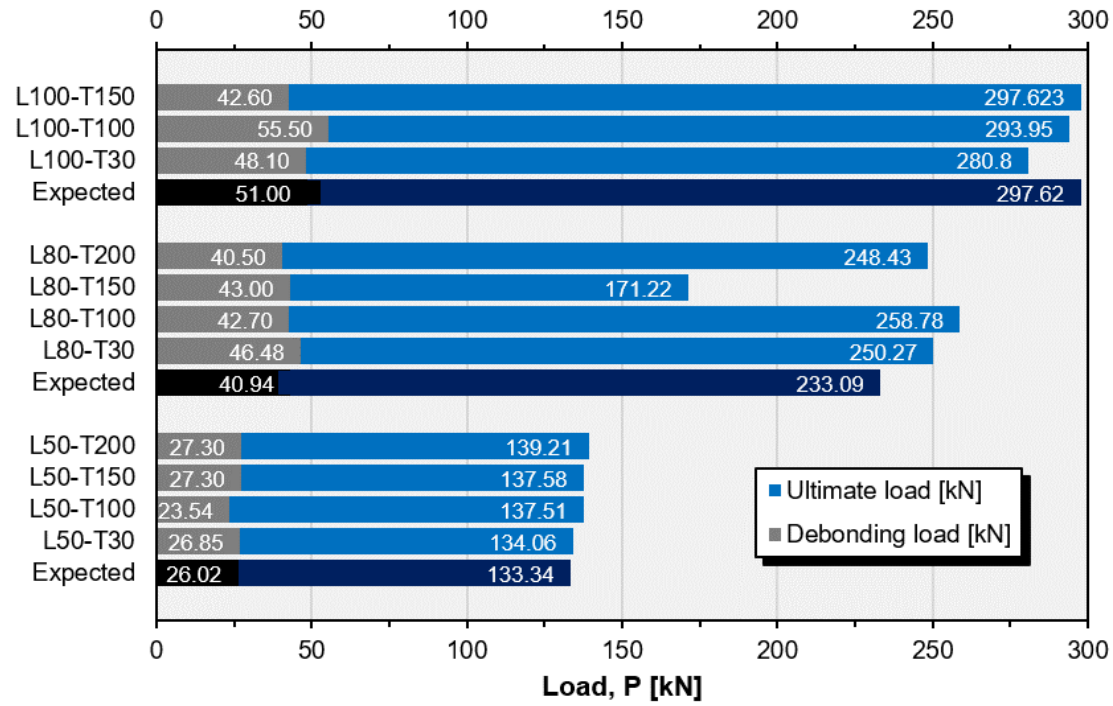

Figure 4.8: Debonding load and ultimate load. Notes: [a] The ultimate load was not registered due to a technical problem (data acquisition system). This value is the expected value, considering the failure mode (CFRP rupture); [b] Premature CFRP slippage from the clamping system.

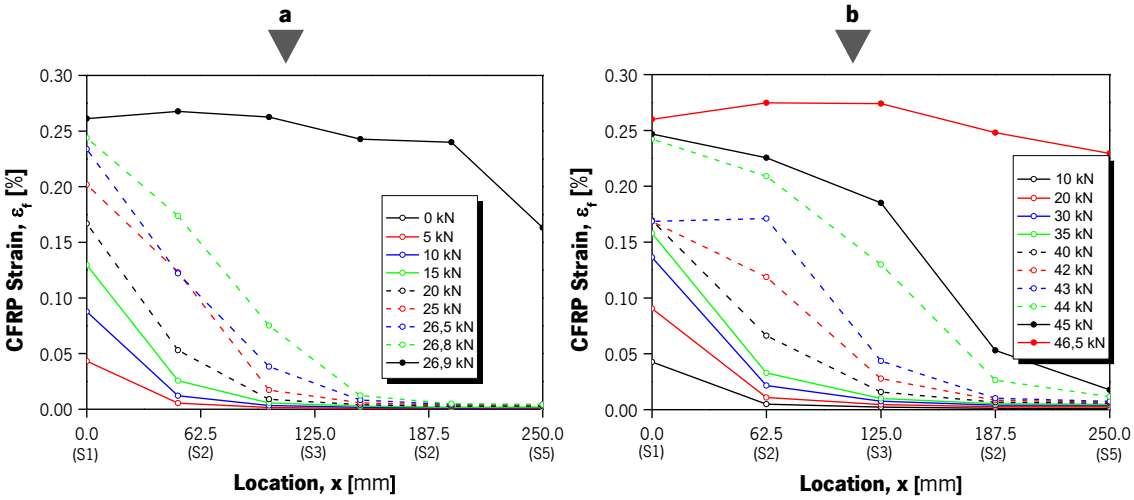

Figure 4.9: Strain profile in the CFRP laminate for (a) L50_T30_SS20, (b) L80_T30_SS20. Note: exceptionally, in L50_T30_SS20 six strain gauges spaced by 50 mm were used.

4.3.2.3 Bond stress-slip curves

The local bond stress-slip curve along the bonded length can be easily derived from the strain values. The mean bond shear stress between two consecutive strain gauges ($\tau_{i+1/2}$) was calculated by equilibrium between the tensile pull-out force carried by the CFRP laminate and the shear force supported at the interface between concrete and laminate:

$$\tau_{i+1/2} = E_f t_f \frac{\varepsilon_{i+1} - \varepsilon_i}{x_{i+1} - x_i} \tag{4.8}$$

where t_f is the thickness of the CFRP laminate, ε_i and ε_{i+1} are the strain values at "i" and "$i+1$" locations, respectively, and x_i and x_{i+1} are the locations of the strain gauges. Similarly, the slip of the CFRP laminate at the mean location "$i+1/2$" ($s_{i+1/2}$) was calculated by integrating the experimental values of strain:

$$s_{i+1/2} = s_{i-1/2} + \frac{\varepsilon_i + \varepsilon_{i+1}}{2}(x_{i+1} - x_i) \tag{4.9}$$

A typical bond shear stress *versus* slip relationship is depicted in **Figure 4.10**. This figure presents the experimental bond shear stress-slip curves and the average experimental bond shear-slip curve. A first fairly linear ascending branch is observed in all cases up to 50% of the peak value of the bond stress τ_{max}. The ascending branch is observed to be similar amongst the different pairs of strain gauges. After the peak bond stress is attained, the typical softening descending curve is registered, albeit the scatter of results is higher in this case. An upperbound value of 0.30 mm is considered for the maximum slip for not interfering with the results derived from the mechanical anchorage.

There are several approaches in the literature to model the local bond shear stress-slip law of FRP/concrete interfaces [22–24]. In this work, the law described in [25], adapted from [26], is adopted and calibrated to the experimental results:

$$\tau(s_p) = \bar{\tau}\frac{s_p}{\bar{s}}\frac{n}{(n-1)+(s_p/\bar{s})^n} \tag{4.10}$$

where τ and s are the interface shear stress and slip, $\bar{\tau}$ and $\bar{s}$ represent the maximum shear stress and its corresponding slip, and n (> 2) is the parameter governing the descending branch (higher values of n diminish the fracture energy of the system, whereas values lower than 2 provide negative and/or finite quantity values of the fracture energy, [25]).

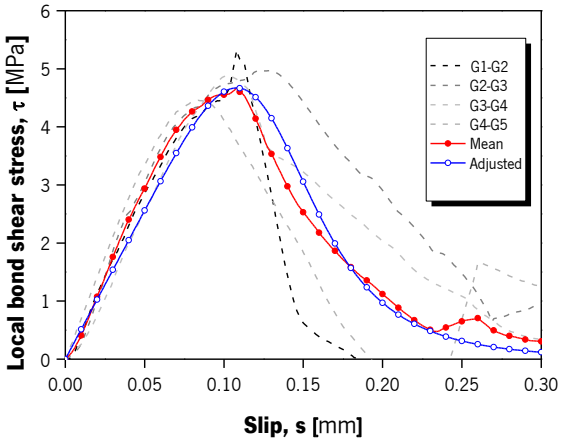

Figure 4.10: Typical adjustment curve of local bond shear stress – slip law (L80_T30_SS20).

The resultant parameters $\bar{\tau}$, $\bar{s}$ and n have been calibrated to the bond stress-slip law by a least-squares methodology and are summarised in **Table 4.4** for the tested specimens. In general terms, the resultant parameters are relatively similar to the ones obtained in [20]. The maximum bond stress ($\bar{\tau}$) tends to reduce with the laminate width, being its value between 3.23 and 4.97 MPa. The influence of the width of FRP plate on the debonding process was recently investigated in [27]. In their study, the authors conclude that the maximum stress is higher near the FRP plate edge than in its centre due to the non-homogeneity of material at the mesoscale level and due to the difference between the elastic modulus between FRP and concrete. Based on the width effect reported by [27], variations in the maximum shear stress $\bar{\tau}$ can be expected for each laminate width because the experimental values were measured in the centre of the CFRP laminate. The corresponding slip and the n parameter, however, do not present a clear trend depending on the

laminate width. In **Figure 4.11**, the mean experimental bond shear stress-slip curve is depicted for each case, together with its adjusted analytical expression.

Table 4.4
Experimental parameters for adjustment of the bond stress-slip law in Eq. (4.10)..

Specimen	$\bar{\tau}$ [MPa]	$\bar{s}$ [mm]	n	$\bar{\tau}_{ave}$ [MPa]	$\bar{s}_{ave}$ [mm]	n_{ave}
Series 1: Tests performed at room temperature						
L50_T30_SS20	4.62	0.077	2.8			
L50_T100_SS20	4.72	0.070	3.4	4.79 (2.74%)	0.081 (12.91%)	3.33 (18.46%)
L50_T150_SS20	4.86	0.098	4.3			
L50_T200_SS20	4.97	0.078	2.8			
L80_T30_SS20	4.67	0.108	6.4			
L80_T100_SS20	4.48	0.087	3.7	4.15 (10.49%)	0.089 (12.69%)	4.30 (28.53%)
L80_T150_SS20	3.85	0.080	3.3			
L80_T200_SS20	3.61	0.081	3.8			
L100_T30_SS20	3.23	0.070	2.9			
L100_T100_SS20	3.98	0.091	3.3	3.53 (9.18%)	0.077 (12.51%)	3.43 (14.53%)
L100_T150_SS20	3.38	0.071	4.1			

Notes: The values between parentheses are the corresponding CoV.

4.3.3 Anchorage component

4.3.3.1 Debonding load and fracture energy

The results, in terms of ultimate load and failure mode are shown in **Figure 4.5**. Contrary to what was obtained in the experimental campaign with RC slabs (see Chapter 2 and Chapter 3), the rupture of the laminate was attained in most of the cases, proving the good performance of the mechanical anchorage in the actual test setup.

The ultimate load P_u was defined as the load at which the whole specimen faced failure. As expected, in those cases where the rupture of the CFRP laminate was attained, a clear dependence between P_u and the laminate width was observed. In these cases, P_u was adequately predicted by the tensile strength obtained from characterization of the CFRP laminates, and a maximum difference between the predicted (from tensile tests) and experimental (from pull-out tests) P_u of 6.9% was obtained. In the particular case of L80_T150_SS20 specimen, the value of ultimate load

was not possible to acquire, due to slippage of the laminate from the clamping system, and in the case of L100_T150_SS20, the ultimate load was not registered due to an acquisition problem during the last stages of the test. The only specimen that faced slippage of the CFRP laminate from the mechanical anchorage system was L100_T30_SS20, at a load of 280.80 kN, which was approximately 94% of the capacity of the laminate. The ultimate load is presented in **Figure 4.8** which allows for a visible comparison between the experimental results (light blue bars) and the expected ultimate load (dark blue bars) considering the maximum CFRP strength.

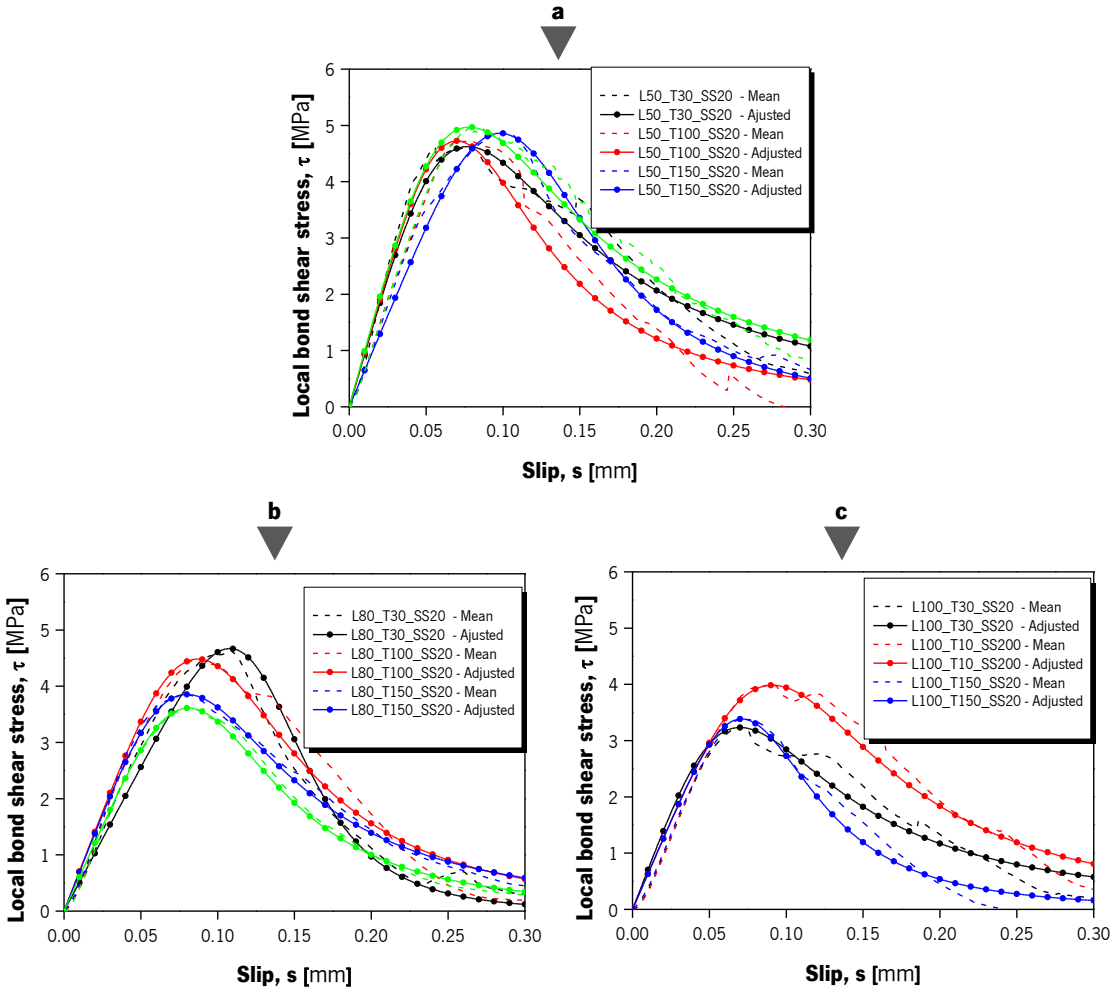

Figure 4.11: Experimental mean and adjusted local bond shear stress–slip law for (a) L50, (b) L80 and (c) L100 specimens.

The ultimate strain shown in **Table 4.5** is the maximum strain registered by the strain gauges all along the bonded length at the ultimate load. In the cases where the rupture of the laminate is

attained, its value is very close to the ultimate strain obtained by the characterization of the CFRP laminate, being the ratio theoretical/experimental ultimate strain between 0.92 and 1.18.

Based on the observed failure modes and values of normal stress attained in the CFRP laminate at the ultimate load, it can be concluded that the studied anchorage system did not cause premature failure of the CFRP laminate, mainly due to gripping effects.

Table 4.5
Experimental values at ultimate and mode of failure.

Specimen	P_u [kN]	$P_{u,ave}$ [kN]	ε_u [%]	$\varepsilon_{u,ave}$ [%]	$s_{u,1}$ [GPa]	VD [%]	Failure Mode
Series 1: Tests performed at room temperature							
L50_T30_SS20	134.06	137.09	1.30	1.33	5.09	72.22	R-CFRP
L50_T100_SS20	137.51		1.34		5.06	55.19	R-CFRP
L50_T150_SS20	137.58		1.35		4.91	0.00	R-CFRP
L50_T200_SS20	139.21		1.34		4.57	0.00	R-CFRP
L80_T30_SS20	250.27	252.49 [d]	1.41	1.47 [d]	6.00	92.22	R-CFRP
L80_T100_SS20	258.78		1.51		5.36	79.63	R-CFRP
L80_T150_SS20	171.22		0.97		2.93	22.96 [a]	– [a]
L80_T200_SS20	248.43		1.49		5.18	58.51	R-CFRP
L100_T30_SS20	280.80	295.79 [e]	1.34	1.38 [e]	5.74	100.00	Slippage [b]
L100_T100_SS20	293.95		1.51		5.03	-	R-CFRP
L100_T150_SS20	297.62 [c]		1.24		4.19	62.59	R-CFRP

Notes: [a]Premature slippage from the clamping system; [b]Slippage from the anchorage system; [c]The ultimate load was not registered due to a technical problem. This value corresponds to the theoretically expected result; [d],[e]The specimens L80_T150_SS20 and L100_T30_SS20 were not included in the assessment of the corresponding parameters.
P_u – Ultimate load; $P_{u,ave}$– Average ultimate load; ε_u – Ultimate strain; $\varepsilon_{u,ave}$ – Average ultimate strain; $s_{u,1}$ – Ultimate slip at the loaded end; VD– Percentage of visible damage.

4.3.3.2 Influence of the torque level

Although rupture of the CFRP laminate was the dominant failure mode, there is an intrinsic relation between the compressive stress level and anchorage performance, which could be observed in the present experimental programme. The ultimate slip registered at the loaded end (LVDT-1, **Figure 4.7b**) was always higher than the expected elastic deformation of the CFRP laminate in the bonded length (250 mm) – between LVDT's 1 and 2 – indicated that slip at mid-end always occurred.

Furthermore, the ultimate slip increased with the decrease of the torque level, showing that increasing the compressive stress provided by torqueing the anchorage allowed less slip inside the mechanical anchorage. The same relation can be observed in the mid end (LVDT-2, **Figure 4.7c**). For each laminate width, the specimens with the smallest torque level (30 N·m, black line in **Figure 4.7c**) presented the highest ultimate slip. In fact, the relation between the torque level and the slip in the metallic anchorage can be easily observed in the mid end because, contrary to the slip registered at the loaded end, the elastic deformation of the CFRP laminate can be neglected. As referred before, the slip registered in the free end (LVDT-3, **Figure 4.7d**) shows negligible results. Contrary to L100_T30_SS20, where the failure mode was slippage, the remaining specimens failed by CFRP rupture, thus making very difficult the correlation between the slip registered in the free end at the maximum load and the torque level. However, **Figure 4.7d** shows that during the pull-out test some specimens exhibit higher movement on the free-end. The registered movement on LVDT-3 is related to the (increasing) degradation of the bond conditions provided by the anchorage system that occur during the increase of pull-out force. Here, a similar remark related to the level of torque can be made: for the lowest torque level and, consequently, the smallest compressive stress level on the anchorage component, the highest the damage on the inside of the metallic anchorage is observed.

Finally, a measure of the level of visible damage inside the mechanical anchorage at the ultimate load was analysed by separating the metallic plate from the concrete specimen at the end of the pull-out test. As can be seen in **Figure 4.12**, there is a visible damage that can be observed over the laminate and in the metallic plate. The visible damage over the laminate is composed mainly by missing fragments of epoxy, which stayed glued to the metallic plate. This kind of damage was not observed on specimens L50_T150_SS20 and L50_T200_SS20. In these two specimens, a peculiar dark stain could be observed on the metallic anchor but no visible damage was observed over the laminate (in the adhesive). The dark stain can be also observed in other plates, however in these two cases no fragments of epoxy were detected. This area of visible damage has a rectangular shape with the same width of its respective laminate and variable length. Then, the length of the visible damage was recorded and, based on the measurements, the percentage of damage was assessed. The percentage of visible damage (VD) is the ratio between the damaged length and the total length of the plate (**Table 4.5**).

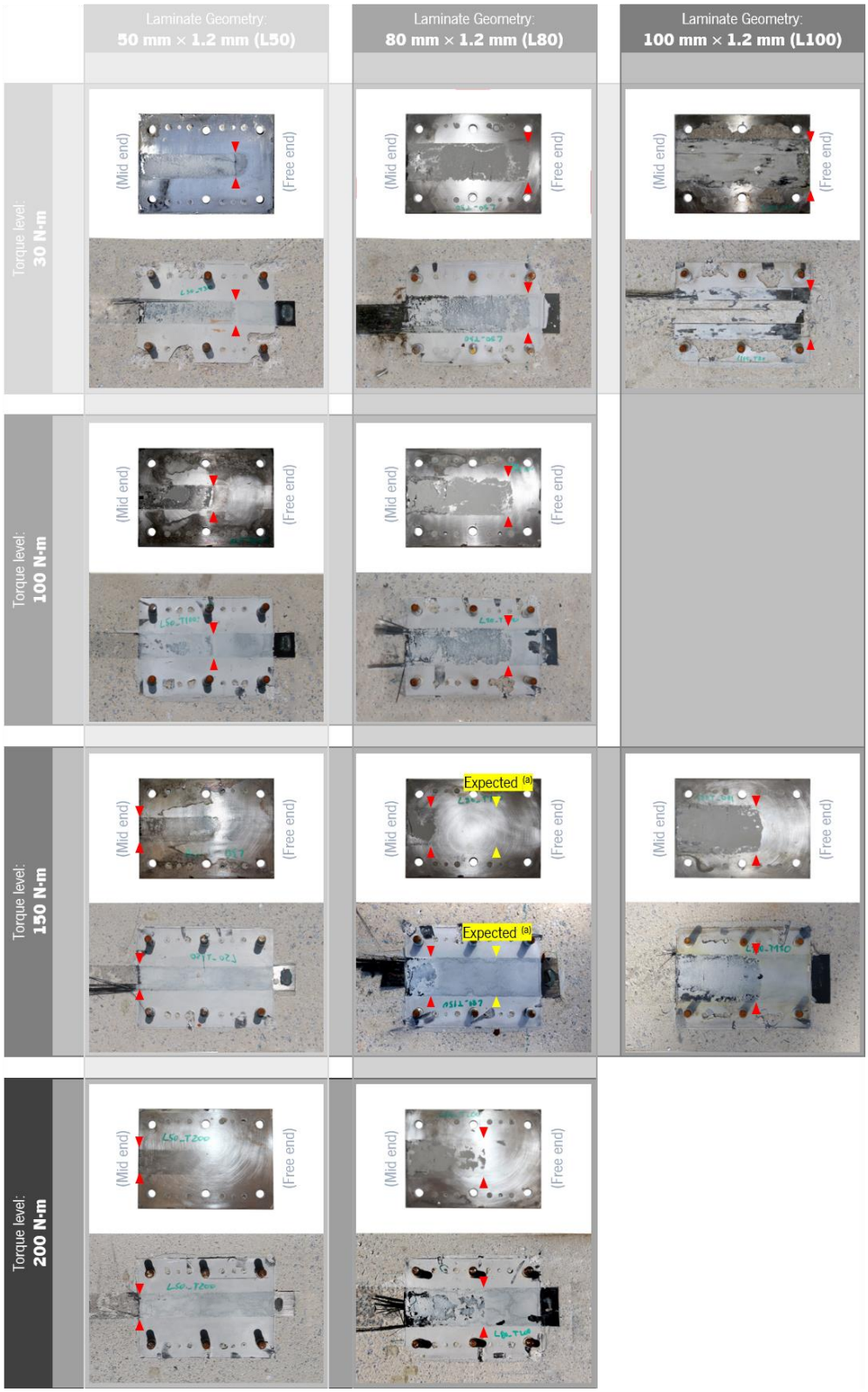

Figure 4.12: Damage level observed in each anchorage plate. Note: (a) Estimation based on the observation of the damage zones of specimens L80_T100_SS20 and L80_T200_SS20; the edge of the observed visible damage is highlighted with two red triangles.

In general terms, the level of visible damage inside the metallic plate increased with the decrease of torque, which proved the effectiveness of a transversely compressed anchorage. In the case of L80_T150_SS20, the observed degree of visible damage was lower than expected due to the premature failure obtained in this test. On the other hand, the level of visible damage increased with the laminate width. Assuming a constant distribution of compressive stress (in transverse direction) along the laminate width, it is foreseen that for the same level of torque (and hence the same transverse force), a wider laminate receives less compressive stress and consequently the system suffers higher degree of damage. Finally, in most of the cases, it could be observed that the increase in visible damage along the laminate width was not evenly distributed, being more pronounced in the centre of the CFRP (see **Figure 4.12**). This observation indicates that there are, inside the anchorage, higher axial stresses in the centre of the laminate. In fact, the prestress of the anchor bolts slightly bended the anchorage plate (deformation not measured, just observed by naked eye) and, consequently, produced higher compressive stress in the extremities of the laminate. This bent deformation was not prevented in order to be representative of the real applications of this commercial anchorage system.

Figure 4.13 plots the influence of the compressive stress level over the average tangential stress inside the anchorage for the load of failure. It should be pointed out that the area and shape of tangential stress distribution inside the anchorage region could not be precisely identified. Therefore the average tangential stress is based on the area of visible damage. Here, the area of visible damage is considered to be the area for which the tangential stresses are developed at the joint between laminate and concrete. The compressive stress level was computed based on the prestress applied in the six M16 anchor bolts and the area of the CFRP laminate in contact with the metallic plate. The prestress level was measured with a dynamometric key and, simultaneously, in two of the six bolts of each anchorage system, using strain gauges. Because the strain in the monitored anchor bolts was constantly measured it was possible to observe that the compressive stress level was the same in the test day.

Because the average tangential stress and compressive stress level exhibit a good relation, it can be foreseen that the anchorage ultimate load capacity can be increased with the torque level applied in the M16 anchor bolts. In **Figure 4.13** specimens L50_T150_SS20 and L50_T200_SS20 were

not represented because the visible damage (mobilized anchorage zone) was close to zero, being the level of tangential stresses in this zone very high.

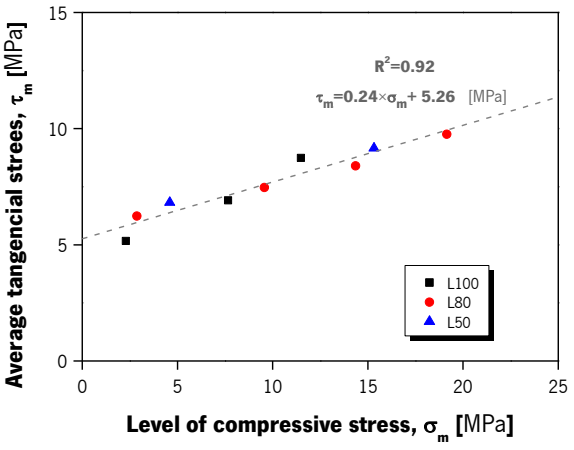

Figure 4.13: Effect of transverse compressive stress in the tangential stress.

As referred before, the maximum load attained at failure corresponds to the maximum tensile capacity of the FRP. In consequence, applying a compressive stress in the anchorage region seems to be a practical solution for increasing the anchorage resistance. However, the ultimate load capacity of the anchorage could be reduced due to environmental exposure, thermal or loading cycling, as is the case of the observations in Chapter 3.

4.4 Tests performed at elevated temperature

The present section shows the results of the tests performed at elevated temperatures, namely, from steady state tests carried out at 60 °C and 80 °C and from all transient tests (Series 2). The following discussion is divided into two sections: one for to the steady-state test results, and the other for the transient test results. In both cases, the analysis foresees on the overall behaviour, debonding process and failure modes. **Table 4.6** summarizes the obtained results. For sake of better understanding, this table also incorporates some results from Series 1 (tests performed at room temperature, see Section 4.3) which are compared with the outputs of the test Series 2.

4.4.1 Steady state tests

4.4.1.1 Load-slip behaviour

Typical load-slip response at the loaded-end, the mid-end and free-end are illustrated in **Figure 4.14a** for the specimens tested at room temperature (20 °C) and in **Figure 4.14b** for the specimens tested at 60°C. As referred before, the tests at room temperature starts with an almost linear branch at the loaded-end. At the mid-end and at the free-end the registered slips are negligible and, consequently, the pull-out load is supported exclusively by the bonded length outside the mechanical anchorage. Then the debonding of the EBR component starts to occur and, during this phase the load remains almost constant whilst the slip increases considerably due to the elastic energy accumulated in the bonded length and due to the deformation of the new portion of CFRP strip that slips. The end of the debonding process in the EBR component is reached when the LVDT-2 starts to register displacements in the mid-end. After this stage, as the load increases so does the relative displacement at the loaded-end and the mid-end sections, until rupture of the CFRP is attained. In this last stage (after debonding), a fairly linear load-slip response is registered in all cases. Failure was obtained when the CFRP laminate reached its maximum tensile capacity. The LVDT-3, placed at the free-end, generally does not register any movement during the test. From these results it was clear that the mechanical anchorage used in this experimental programme provided adequate transverse confinement of the laminate to the concrete substrate regardless of the applied confinement level.

When the test temperature was 60 °C, the load-slip behaviour significantly changed. In the early stages of the test, as the pull-out load increased, also did the slip registered with the LVDT-1. However, the relative displacement in the mid-end does not remain null. While the debonding process of the EBR component is in course, the LVDT-2 shows a small but consistent displacement increase with the load. These results demonstrate that since early stages of the test the anchorage zone supports part of the load. As the pull-out load increases and the debonding process evolves, the fraction of load supported at the EBR component decreases. Further details of the debonding process are given in the following section. From this stage onwards, the slip increases in both locations (loaded-end and mid-end). Then, the maximum force is reached and displacements in the free-end are also observed, marking the anchorage failure (slippage). Then, the displacements

at the three locations (loaded-end, mid-end and free-end) increase while the pull-out load decreases. However, the load does not decrease to zero, but stabilizes at a load level that represents a residual bond stress. This last behaviour was also observed in other works, e.g. Biscaia [28].

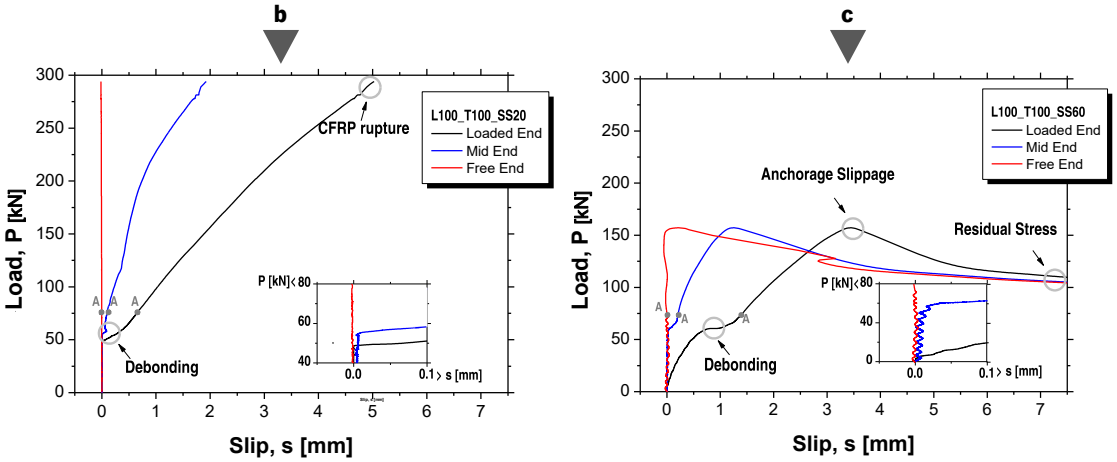

Figure 4.14: Typical load-slip behaviour for specimens tested (a) at room temperature (L100_T100_SS20) and (b) at elevated temperatures (L100_T100_SS60). Note: The point "A" shows the stage when the velocity of the test was increased from 0.3 mm/min to 2.0 mm/min.

4.4.1.2 Debonding process

Like the load-slip behaviour, the debonding process of the EBR component in specimens tested at room temperature was different from those tested at elevated temperatures. **Figure 4.15** shows the strain evolution in the EBR component of specimens with the laminate of 100 mm and torque of 100 N·m, tested at different temperatures. The debonding load, P_{deb}, and temperature in the EBR component during the debonding process, T_{deb}, are presented in **Table 4.6**. During the first stages of loading at room temperature (20 °C), the strain has a peak value at the loaded-end (location x=0mm, see **Figure 4.15a**) and null values near the anchorage plate (location x=250mm, see **Figure 4.15a**). As the test continues, more bonded area of EBR component is needed to support the additional loads and a change can be observed in the strain profile. When the length of the EBR component needed to support the load equals the effective bond length, l_e, the maximum debonding load is reached. As stated in Section 4.2.1, according to the CNR [5] the l_e of the tested specimens is around 200 mm. However, in the current test, the load does not remain constant until failure because the mechanical anchorage holds the CFRP extremity and

avoids premature failure. At room temperature, the debonding load was set when the LVDT-2 starts to register movement. At this exact time, the strain near the anchorage plate increases significantly as does the slip at the mid-end (see **Figure 4.14a** and **Figure 4.15a**). Immediately after this point, the strain and slip continue to increase but at a lower rate and the CFRP laminate is completely detached from the concrete surface in the EBR component.

Table 4.6
Main results from tests performed at high temperature.

Specimen	T_{deb} [°C]	P_{deb} [kN]	T_u [°C]	P_u [kN]	ε_u [%]	$s_{u,1}$ [mm]	$s_{u,2}$ [mm]	P_{res} [kN]	Failure Mode
Series 1: Tests performed at room temperature									
L80_T100_SS20	20.0[a]	42.7	20.0[a]	258.8	1.51	5.4	2.1	0.0	R-CFRP
L80_T150_SS20	20.0[a]	43.0	20.0[a]	171.2[b]	0.97[b]	2.3[b]	0.8[b]	0.0	-[b]
L100_T100_SS20	20.0[a]	55.5	20.0[a]	294.0	1.51	5.0	1.6	0.0	R-CFRP
L100_T150_SS20	20.0[a]	42.6	20.0[a]	297.6[c,d]	1.53[c,d]	4.2[c,e]	1.2[c,e]	0.0	R-CFRP
Series 2: Tests performed at high temperature									
L80_T150_SS60	49.3	82.6[f]	60.8	132.8	0.78	2.9	1.4	87.0	Slippage
L80_T150_SS80	69.0	46.0[f]	80.5	123.3	0.72	2.5	1.0	86.4	Slippage
L100_T100_SS60	50.2	60.6[f]	60.5	157.1	0.76	3.5	1.3	103.3	Slippage
L100_T100_SS80	66.8	51.5[f]	80.3	104.6	0.49	2.1	0.7	75.7	Slippage
L100_T150_SS60	53.8	59.9[f]	60.5	189.0	0.91	3.4	1.2	125.1	Slippage
L100_T150_SS80	64.5	64.9[f]	80.4	122.6	0.59	2.3	1.0	84.9	Slippage
L100_T200_SS60	67.3	40.2[f]	60.3	166.5	0.83	3.3	1.5	117.8	Slippage
L100_T100_CL100	30.0	68.0	67.7	120.0	-	-	-	-	Slippage
L100_T100_CL120	28.0	54.5	63.4	120.0	-	-	-	-	Slippage
L100_T150_CL100a	29.5	60.1	80.0	100.0	-	-	-	-	Slippage
L100_T150_CL100b	30.0	58.3	80.0	100.0	-	-	-	-	Slippage
L100_T150_CL120a	29.7	60.1	64.2	120.0	-	-	-	-	Slippage
L100_T150_CL120b	29.4	69.9	71.2	120.0	-	-	-	-	Slippage

Notes: [a] Estimated temperature based on the room temperature; [b] Premature failure from the clamping system; [c] The ultimate load, strain and relative displacement were not registered due to a technical problem; [d] This value corresponds to the theoretical expected result; [e] This value corresponds to the last registered value, at a load of 252 kN; [f] a fraction of the load was supported by the anchorage.
T_{deb} – Temperature in the bonded length during the debonding process; P_{deb} – Debonding load; T_u – Temperature in the anchorage region at failure; P_u – Load at failure; ε_u – CFRP strain at failure; $s_{u,1}$ – Slip at failure registered at the loaded-end; $s_{u,2}$ – Slip at failure registered at the mid-end; P_{res} – Residual load.

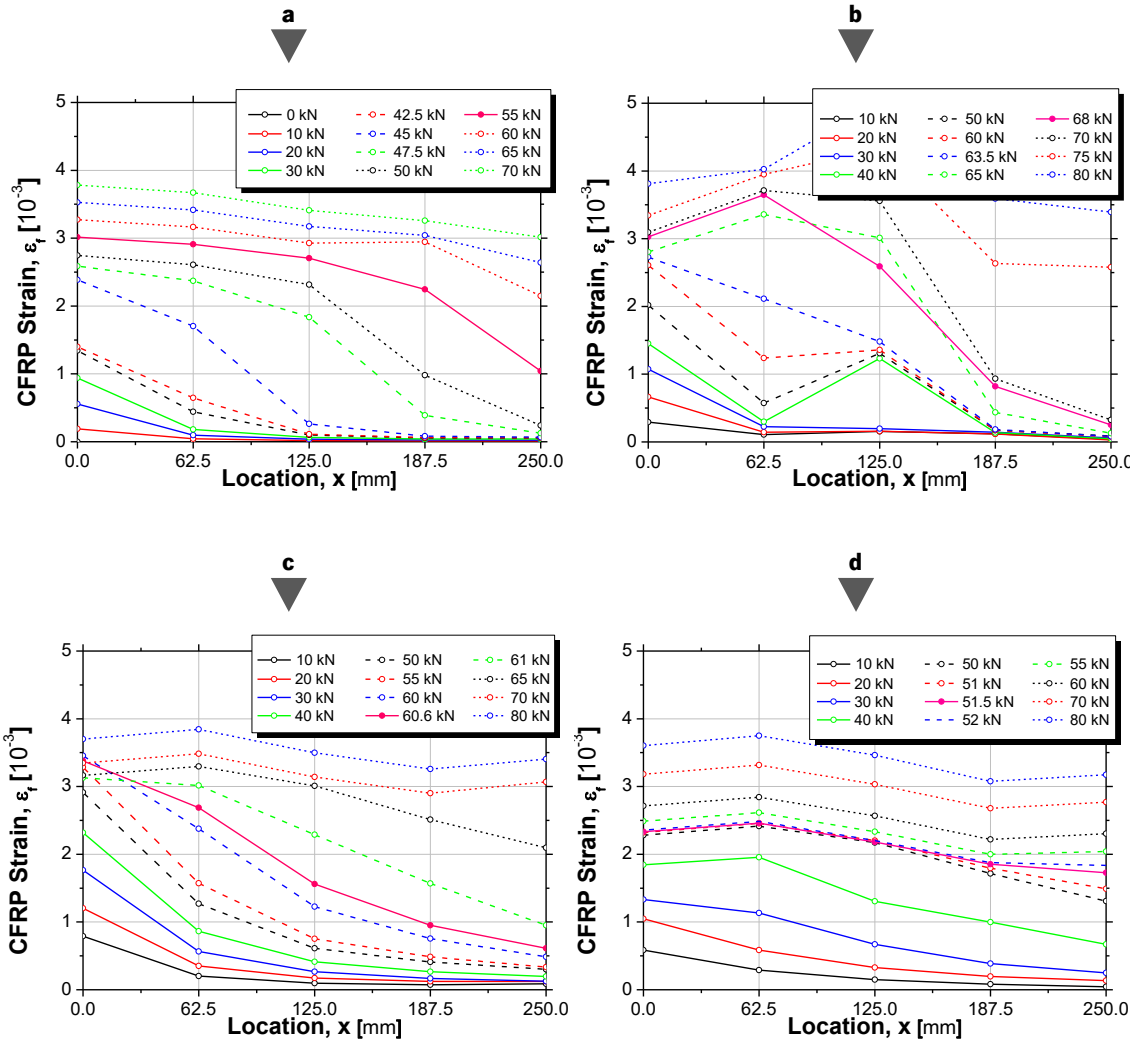

Figure 4.15: Strain profiles at: (a) 20 °C (L100_T100_SS20); (b) 30 °C (L100_T100_CL100); (c) 60 °C (L100_T100_SS60); and (c) 80 °C (L100_T100_SS80).

The debonding process observed in the specimens tested at elevated temperatures was different since their early stages. Results show an almost linear strain evolution (see **Figure 4.15c** and see **Figure 4.15d**), with a peak strain value on the loaded-end (location x=0mm) and a gradual decrease towards the anchorage plate (location x=250mm). All strain gauges show a continuous increase in strain since the test onset and, during the debonding process, the shape of the strain profile remains almost unaffected. Also, the LVDT-2 starts to register relative displacement since the initial stages of the test. Contrary to tests carried out at room temperature, where the complete

debonding of the EBR component was observed with the swift and simultaneous increase of values at the LVDT-2 and at the strain gauge near the anchorage plate, in tests carried out at elevated temperatures, the strain gauge near the anchorage plate and the LVDT2 started to register movement before the CFRP laminate was completely detached. As can be seen in **Table 4.6**, for the case of the tests at elevated temperatures the temperature in the EBR component during the debonding process, T_{deb}, surpassed the epoxy's T_g. The transition from a solid to a rubber-like state is a continuous process over a temperature range of 10-20 °C [29] and, during the steady-state tests, the epoxy adhesive at the EBR component either was at the beginning (T_{deb}≈51.1 °C for L80_T150_SS60, L100_T100_SS60 and L100_T150_SS60) or at the end (T_{deb}≈66.9 °C for L80_T150_S80, L100_T100_SS80, L100_T150_SS80 and L100_T200_SS60) of this range. The reduction in the adhesive stiffness might be responsible for smoothing the shear stresses distribution at the interface CFRP/concrete and for the early strain and displacements increase near the mid-end. For that reason, it was impossible to clearly identify the debonding load. However, due to the elastic energy accumulated in the EBR component, there is a stage in the load-slip curves where a plateau can be observed at the mid-end region (see **Figure 4.14b**). This stage shows the load, P_{deb}, for which the complete debonding of the EBR component occurs. At this point, the load supported by the EBR component does not represent the totality of the pull-out force because, as referred before, the anchorage is also responsible for supporting a fraction of the load since the early stages of the test. Tests carried out with the highest temperatures showed less strain variation from the loaded-end (x=0mm, see **Figure 4.15d**) to the mid-end (x=250mm, see **Figure 4.15d**).

As referred before, the experimental results from tests carried out at room temperature are in accordance with the expected values (computed according to the CNR [5], see Section 4.3). As could be seen, the temperature changed the debonding process and the CNR [5] formulation does not consider the effect of high temperatures on the debonding process. In all tests carried out at room temperature, a typical cohesive failure in the concrete and interface failure between the concrete and epoxy was observed in the EBR component (see **Figure 4.17a**). However, in the tests carried out at elevated temperature, remains of epoxy adhesive stayed adhered to the concrete surface. This observation points to the fact that, at elevated temperatures, the failure of the EBR component was, in part, cohesive in the adhesive (see **Figure 4.17**).

Finally, it should be referred that the influence of the EBR component/mechanical anchorage could be separately identified based on the strain measurements obtained during the pull-out tests. **Figure 4.16** presents the typical evolution of the total load (F), the load supported by the EBR component (EBR) and the load supported by the Anchorage (F - EBR) versus the slip at the loaded end (s_1). **Figure 4.16a** clearly shows the debonding of the EBR region (specimen L100_T100_SS20). At the early stages of the test, the EBR component is responsible for carrying the load. When the debonding starts occurring, there is a transference of load from the EBR region to the anchorage. After this stage the load is mostly supported by the anchorage. In **Figure 4.16b**, the typical debonding observed on tests carried out at elevated temperatures is presented: since early stages of the pull-out test, the total load (F) is partially supported by the anchorage. **Figure 4.16b** clearly shows that the load transfer from the EBR component (EBR) to the anchorage (F-EBR) starts in the beginning of the test and increases as the test is carried on. This analysis presents a peak value on the load supported by the EBR component, and the moment when the load supported by the EBR component can be neglected. This figure also indicates that the length of the EBR component (250 mm) is shorter than the effective bond length for tests carried out at high temperatures.

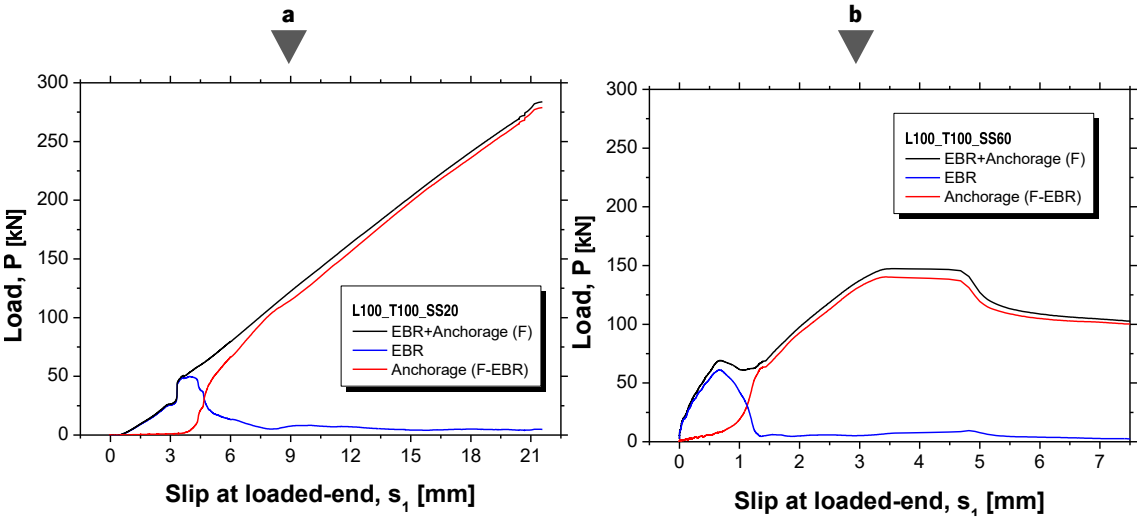

Figure 4.16: Typical evolution of the total load, the load supported by the EBR region and the load supported by the Anchorage *versus* the slip at the loaded end: (a) L100_T100_SS20; and (b) L100_T100_SS60.

4.4.1.3 Failure Modes

As referred before, at room temperature, the mechanical anchorage system provided adequate transverse confinement of the CFRP laminate to the concrete substrate and enabled the full use of the reinforcement material (see **Figure 4.17c**). Additional information is presented in Section 4.3.3. In contrast, all tests carried out at elevated temperature presented anchorage slippage as the failure mode (see **Figure 4.17d**).

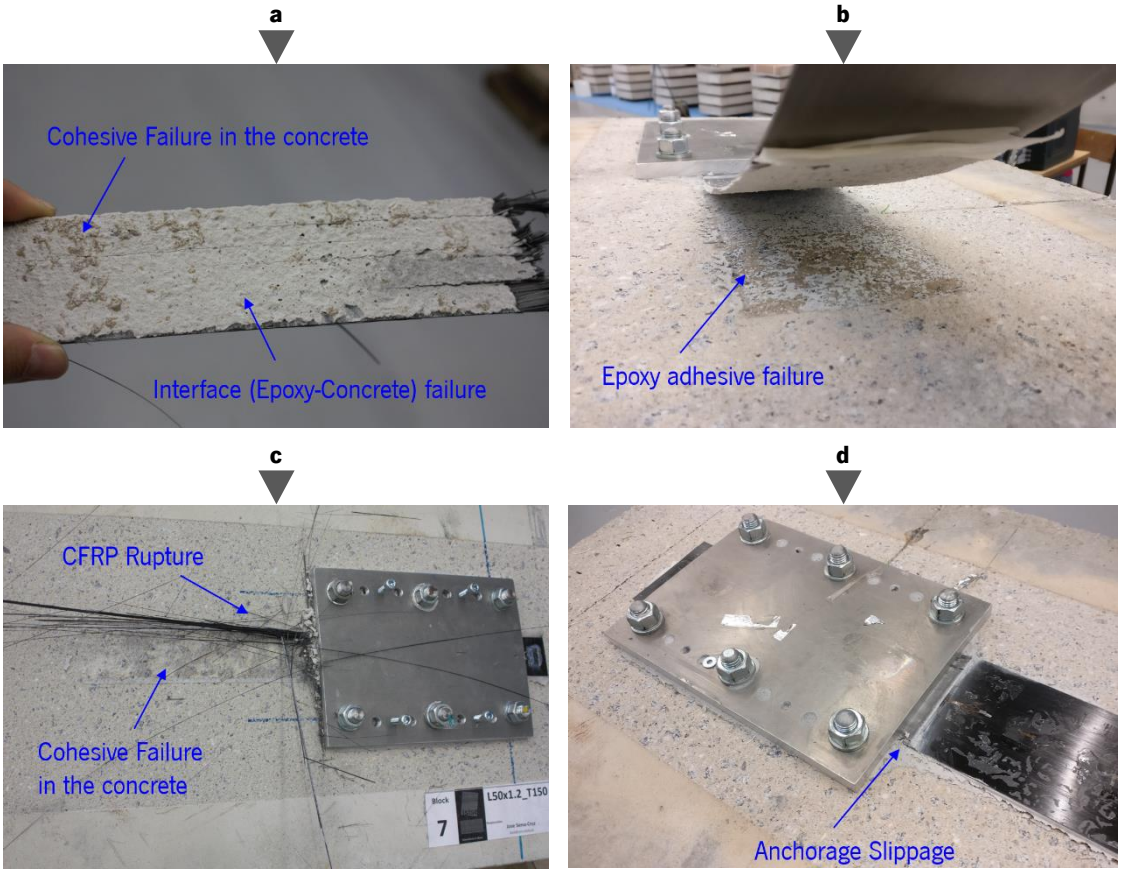

Figure 4.17: Failure modes: (a) interface (Epoxy-Concrete) failure in EBR component at room temperature (L50_T100_SS20); (b) epoxy adhesive failure in EBR component at elevated temperature (L100_T150_SS80); (c) FRP rupture (L50_T150_SS20); and (d) slippage from the anchorage (L100_T150_SS80).

Results show (see **Table 4.6**) that failure is highly influenced by the test temperature and by the confinement level. In comparison to specimens tested at room temperature, the average reduction in the ultimate load, P_u, for specimens tested at 60 °C and 80 °C equals to 43.9% and 58.5%, respectively. Also, the ultimate slip registered at the mid-end, $s_{u,2}$, was higher in specimens tested

at 60 °C (1.3±0.2 mm) than in specimens tested at 80 °C (0.9±0.2 mm). **Figure 4.18** shows the load-slip behaviour of specimens with the confinement level, σ_L, of 7.7 MPa (**Figure 4.18b**, w_f = 100 and T_L = 100 N·m), 11.5 MPa (**Figure 4.18c**, w_f =100 and T_L = 150 N·m), and 14.4 MPa (**Figure 4.18a**, w_f = 80 and T_L = 150 N·m). As can be seen, the load-slip behaviour of each test is dependent on the test temperature (by comparing series 20 °C, 60 °C and 80 °C) and confinement level (by comparing series "L100_T100", σ_L=7.7 MPa, and L100_T150, σ_L=11.5 MPa) and follows the same stages that were described previously. Contrarily to CFRP rupture, the failure by anchorage slippage did not result in a swift decrease of load down to zero, but to a softened reduction of the supported load down to a residual value of 65.5-70.8% of its maximum capacity. The bond stress responsible for the residual supported load is a consequence of the transverse confinement stresses applied on the anchorage zone [28]. As expected, there is a relation between the residual capacity of the anchorage and the applied confinement level: the residual load, P_{res}, corresponds to a level of CFRP stress of 745.8 MPa, 875.0 MPa, 903.1 MPa and 981 MPa in specimens with the confinement level, σ_L, of 7.7 MPa, 11.5 MPa, 14.4 MPa and 15.3 MPa, respectively (only one specimen, L100_T200_SS60, was tested with the σ_L of 15.3 MPa; whereas, for the other cases, two specimens tested at different temperatures were considered). The level of confinement also influenced the value of P_u and ε_u. In fact, results show that the load and CFRP strain at failure were higher in specimens with the greatest confinement level (see **Table 4.6**). Despite the positive influence of the confinement level, the temperature was the major influential factor in all ultimate parameters. As can be seen in **Table 4.6**, the reduction in the ultimate parameters P_u and ε_u, is close to 44% when specimens tested at 60 °C are compared with the ones tested at 20 °C; and is around 25% when specimens tested at 80 °C are compared with the ones tested at 60 °C.

4.4.2 Transient tests

4.4.2.1 Temperature-slip behaviour

In the transient tests, six specimens were loaded up to a fraction of the CFRP strength (0.36%, 0.45% and 0.53% of CFRP strain) at room temperature and then heated up until 80 °C. For each pull-out load level (80 kN, 100 kN and 120 kN) the maximum temperature supported was

registered. The ultimate temperature (T_u) registered in the anchorage is presented in **Table 4.6** and the slip evolution in the loaded-end and mid-end with the temperature is shown in **Figure 4.19** for specimens tested at a constant pull-out load of 100 kN and 120 kN. The **Figure 4.19** also shows the instant when the temperature started to increase (t_i), the time when failure was observed (t_u), the time when the predefined maximum temperature was reached ($t_{80\,℃}$) and the duration until failure was observed ($\Delta t_{80\,℃}$). During the test of specimen L100_T150_CL120b the heating was stopped when temperature reached 60 °C ($t_{60\,℃}$) for a period of one hour ($\Delta t_{60\,℃}$). This stage is presented in **Figure 4.19b**.

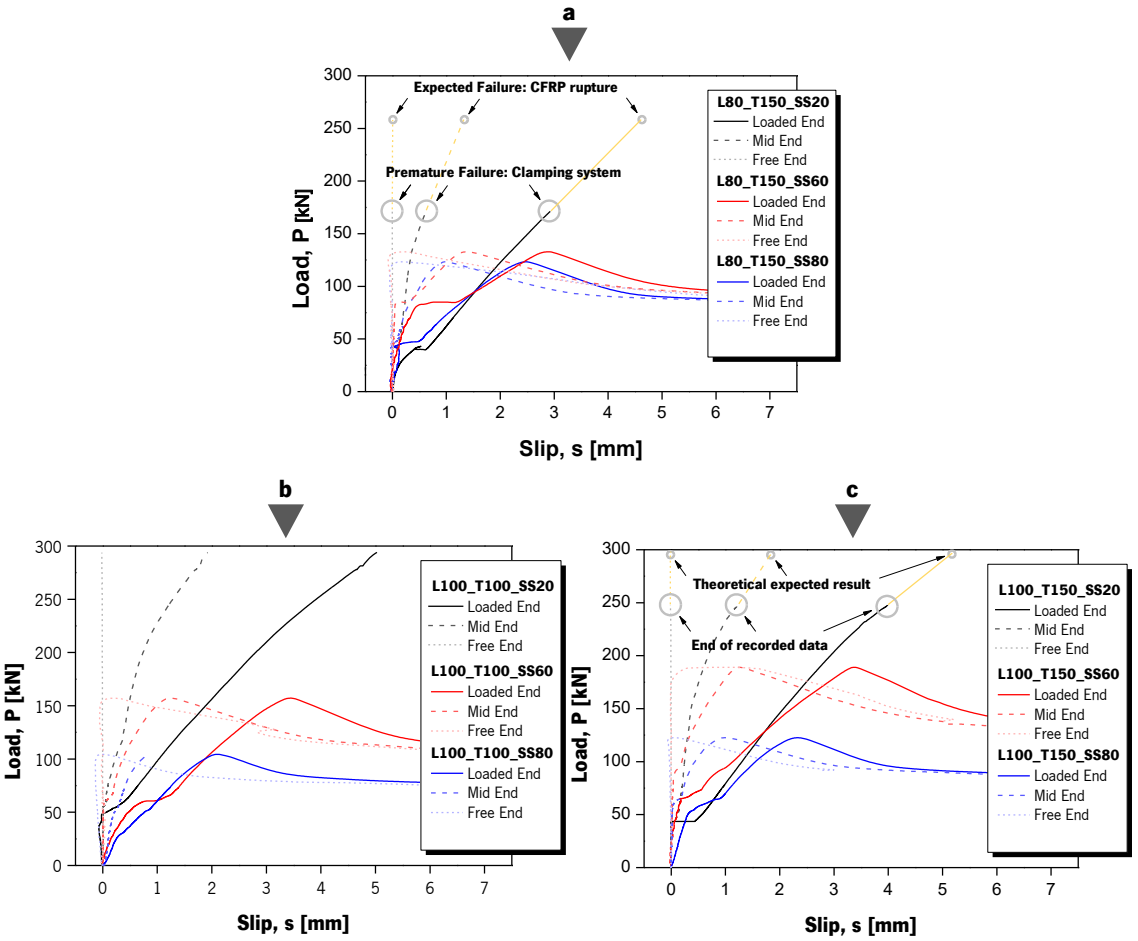

Figure 4.18: Load-slip behaviour for specimens (a) with a laminate of 80 mm and torque level of 150 N·m; (b) with a laminate of 100 mm and torque level of 100 N·m; and (c) with a laminate of 100 mm and torque level of 150 N·m.

It should be pointed out that specimens L100_T100_CL100, L100_T150_CL100a and L100_T150_CL100b, were previously tested under a transient configuration with a load of 80 kN and subsequently with a load of 100 kN. These three specimens endured the initial tests (temperature variation from 30 °C to 80 °C and the subsequent steady-state of 80 °C over one hour) without showing any traces of damage. At the end of the initial test, the strain registered at the EBR region and the relative displacement between the CFRP and the concrete surface (LVDT-1, LVDT-2 and LVDT-3) resumed their initial values. The tests in specimens L100_T100_CL100 and L100_T150_CL100a were repeated once again after 24 hours and the same result was observed. These three specimens were then tested with the final pull-out load of 100 kN and the behaviour is presented in the **Figure 4.19a**.

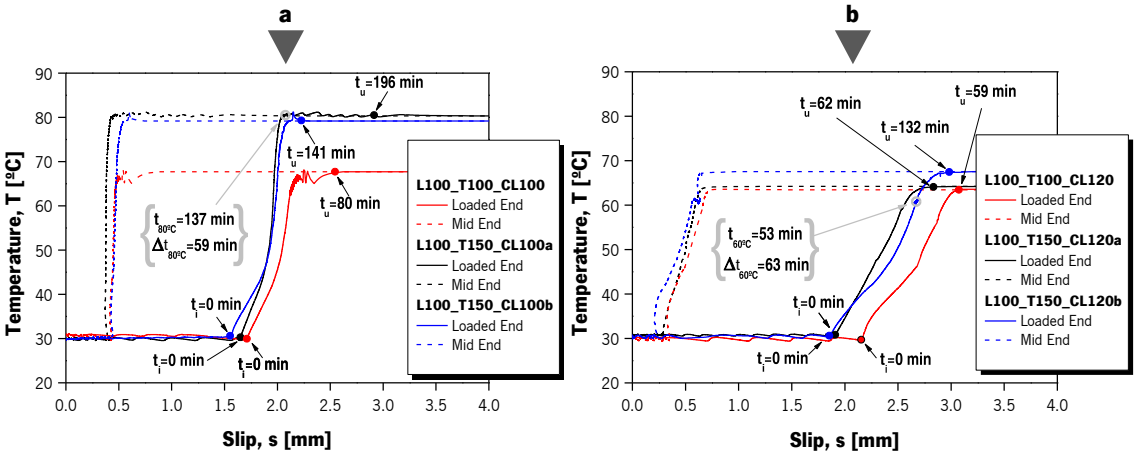

Figure 4.19: Slip evolution with the temperature variation in specimens with the constant load of (a) 100 kN and (b) 120 kN

The first stage of the transient test was the application of the pull-out load (80 kN, 100 kN, or 120 kN). The relative displacement at the loaded-end and mid-end when the predefined pull-out load was achieved are in agreement with the values obtained in the steady-state tests. As expected, higher pull-out loads matched with higher slip values at the loaded-end (1.0 mm, 1.6 mm and 2.0 mm for pull-out load of 80 kN, 100 kN and 120 kN, respectively) and mid-end (0.2 mm, 0.3 mm and 0.4 mm for pull-out load of 80 kN, 100 kN and 120 kN, respectively). Then, the second stage of the test started (at time t_i, see **Figure 4.19**), and the IR system heated up the specimens up to 80 °C. Most of the specimens failed during this stage (at time t_u, see **Figure 4.19**) and the maximum temperature supported (T_u) was achieved, which was lower than the

maximum predefined temperature. Specimen L100_T150_CL100a did not fail during this heating up phase. The following test step was to keep the temperature (80 °C) and pull-out load (100 kN) constant for one hour and, within this period of time, failure of L100_T150_CL100a was observed. Also, in specimen L100_T150_CL120b, the heating was paused at the temperature of 60 °C (at time $t_{60ºC}$, see **Figure 4.19b**) and, for a period, $\Delta t_{60ºC}$, of 63 min, the load and temperature conditions were kept constant. Specimens L100_T150_CL120b kept the same values of relative displacement in all three locations and no signs of failure were noticed. The test was resumed, with the aim of reaching 80 °C, and failure was observed shortly afterwards.

4.4.2.2 Debonding process

The debonding process of the EBR region was also analysed during the transient tests. In the first stage of the test, the pull-out load was increased up to the predefined values using the same procedure used in the steady-state tests: the laminate was pulled at a constant rate of 0.30 mm/min until the total debonding of the EBR region; then, the speed was increased up to 2 mm/min until the predefined load was achieved. During this stage, all specimens were kept at a constant temperature of 30 °C. **Table 4.6** shows the debonding load, P_{deb}, and the temperature in the EBR region T_{deb}. The typical strain evolution in the EBR region of specimens tested using the transient configuration can be observed in **Figure 4.15b**.

Few differences were observed between the debonding process at 20 °C and 30 °C. At both temperatures levels, the strain profile started with a peak strain value at the loaded-end (location x=0mm, see **Figure 4.15b**) and a null strain at the mid-end (location x=250mm, see **Figure 4.15b**). As the load increased, the strain profile changed, enabling higher strain values in middle of the EBR region. Eventually, the maximum capacity was achieved and, with the complete debonding of laminate, not only the strain in the mid-end started to increase but also did the relative displacement registered by the LVDT-2. In general, at the same load levels, similar strain levels were observed for both temperatures. However, the debonding load, P_{deb}, for specimens tested at 30 °C was around 61.8 kN. This value corresponds to a relative increase of 26%, when compared with the specimens tested at room temperature, and can be justified by the post-curing of the epoxy adhesive [10].

4.4.2.3 Failure modes

All specimens tested under the transient configuration exhibit the same failure mode than those tested under the steady-state configuration at elevated temperatures, which was laminate slippage from the anchorage (see **Figure 4.17**).

As referred before, no signs of failure were noticeable when the transient tests were carried out with the lowest pull-out load of 80 kN. However, for the case of a pull-out load of 100 kN, failure was observed when the temperature at the anchorage was of 67.7 °C (L100_T100_CL100) and 80 °C (L100_T150_CL100a and L100_CL150_T100b), depending on the torque level. For this pull-out load (100 kN), the confinement level induced by the level of torque proved to be a major factor in the anchorage capacity: the specimen with the lowest torque level failed when the temperature reached 67.7 °C (above the adhesive T_g), whereas the specimens L100_T150_CL100a and L100_T150_CL100b reached the predefined maximum test temperature (80 °C, well above the adhesive T_g). The L100_T150_CL100a specimen not only supported the highest predefined temperature but also endured almost one hour at those conditions before slippage failure. As can be seen in **Figure 4.19a**, specimen L100_T150_CL100a showed a displacement increase in both locations after reaching the maximum predefined temperature ($t_{80ºC}$ = 137min). However, the registered slip, which was almost negligible in the first 30 minutes, gradually increased up to 1 mm in all LVDT's just before failure was observed (t_u = 193min). The L100_T150_CL100b is a specimen with the same properties of the specimen L100_T150_CL100a and, for that reason, was able to reach the predefined maximum temperature.

The remaining three specimens, tested with the highest pull-out load of 120 kN, failed shortly after the temperature in the anchorage surpassed the adhesive's T_g: the specimen L100_T100_CL120 failed at 63.4 °C, the specimen L100_T150_CL120a failed at 64.2 °C and the specimen L100_T150_CL120b failed at 71.2 °C. These results show that there was a small increase of anchorage resistance with the confinement level. However, for this pull-out load, the confinement level has a considerable lower influence in the anchorage resistance when compared with the specimens with the load level of 100 kN. Results show that the increase in the confinement level, from 7.7 MPa to 11.5 MPa corresponded to an increase on the ultimate temperature, T_u, of 18.2% and 6.8% in tests carried out with the pull-out load of 100 kN and 120 kN, respectively.

In short, the transient tests results showed the three possible scenarios when the pull-out load is the studied variable: (i) the first scenario is characterized by the low load level (80 kN) and the anchorage capacity of enduring the high temperatures without failure; (ii) the second scenario corresponds to a load level (100 kN) where failure is observed but it is highly influenced by other factors like the confinement level; and (iii) the third and last scenario is related to the highest load level (120 kN), for which failure is attained shortly after the specimens temperature surpasses the adhesive's T_g, regardless of the confinement level.

4.5 Large-scale pull-out tests *versus* MA slabs

In the present section the results obtained in the pull-out tests are compared with the results obtained in the monotonic tests of slabs strengthened with the mechanical anchorage, previously described in Chapters 2 and 3. **Table 4.7** presents the main results obtained from the monotonic tests of slabs strengthened with the mechanical anchorage system. In Chapter 2, four MA slabs were monotonically tested up to failure shortly after the strengthening, to evaluate the short-term behaviour. As referred before, in this experimental campaign FRP rupture was obtained in one specimen (SB_MA_50×1.2). In the remaining three tests, slippage from the anchorage was observed when the stress in the laminate was close to 72% of its ultimate tensile strength. The slippage from the anchorage was immediately followed by the rupture of the FRP. It is noteworthy to state that the concrete surface of these three MA slabs was prepared with a stone wheel, whereas the sand blasting technique was used in the SB_MA_50×1.2 slab. As mentioned before surface roughness is an important factor on the anchorage resistance and it might be a crucial factor on these results. Nonetheless, on the preliminary tests a good performance of the mechanical anchorage system was observed.

Table 4.7
Review of the results from MA slabs.

Specimen	$\varepsilon_{f,max}$ [%]	$\sigma_{f,max}$ [MPa]	$\sigma_{f,u}$ [°C]	$\sigma_{f,max}/\sigma_{f,u}$ [%]	Surface Preparation	Failure Mode
Chapter 2: Short-term behaviour of MA Slabs						
GD_MA_50×1.4	1.20	1857.6	2457.1 (1.2%)	75.6	Grinding	Slippage
GD_MA_50×1.2	1.25	2096.3	2943.5 (1.6%)	71.2	Grinding	Slippage
GD_MA_80×1.2	1.01	1662.5	2455.3 (5.0%)	67.7	Grinding	Slippage
SB_MA_50×1.2	1.48	2427.2	2374.9 (2.5%)	102.2	Sand Blasting	FRP Rupture
Chapter 3: Long-term behaviour of MA Slabs						
REF_MA_U	1.40	2296.0	2374.9 (2.5%)	96.7	Sand Blasting	Slippage
REF_MA_C	1.26	2066.4	2374.9 (2.5%)	87.0	Sand Blasting	Slippage
TW_MA_U	1.13	1853.2	2374.9 (2.5%)	78.0	Sand Blasting	Slippage
TW_MA_C	1.15	1886.0	2374.9 (2.5%)	79.4	Sand Blasting	Slippage
CW_MA_U	1.23	2017.2	2374.9 (2.5%)	84.9	Sand Blasting	Slippage
CW_MA_C	1.12	1836.8	2374.9 (2.5%)	77.3	Sand Blasting	Slippage
WD_MA_U	1.27	2082.8	2374.9 (2.5%)	87.7	Sand Blasting	Slippage
WD_MA_C	1.04	1705.6	2374.9 (2.5%)	71.8	Sand Blasting	Slippage

Notes: the values between parentheses are the corresponding coefficients of variation (CoV).
$\varepsilon_{f,max}$ – Maximum strain in the CFRP laminate during the monotonic test; $\sigma_{f,max}$ – Maximum stress in the CFRP laminate during the monotonic test; $\sigma_{f,u}$ – Tensile strength of the CFRP laminate.

The results obtained with the pull-out tests carried out at room temperature are in agreement with the results obtained in the preliminary studies. These pull-out tests showed FRP rupture as the dominant failure mode and clearly demonstrated that the mechanical anchorage provides adequate compressive stress of the CFRP laminate to the concrete substrate. The concrete surface of all pull-out specimens was sand blasted, therefore it can only be compared with specimen SB_MA_50×1.2. However, from the preliminary results, it can also be observed a relation between the compressive stress level and the anchorage resistance. As mentioned in Chapter 2, a torque level of 150 N·m was used in all specimens. As shown in **Table 4.7**, the failure on specimen GD_MA_80×1.2 (compressive stress level, σ_L, close to 14.4 MPa) was observed when the CFRP strain was 1.0% (67.7% of the laminate tensile strength), whereas the failure on specimens GD_ MA_50×1.2 and GD_ MA_50×1.4 (compressive stress level, σ_L, close to 23.0 MPa) was observed when the CFRP strain was close to 1.2% (73% of the laminate tensile strength). This 60% increase

on the confinement level (from 14.4 MPa to 23.0 MPa) produced an increase on the ultimate strain ($\varepsilon_{f,max}$) of 20% and a growth on the ultimate tangential shear stress of 24%. In section 4.3.3 a relation between the compressive stress level and the average tangential stress inside the anchorage for the large-scale pull-out tests is presented. According to the pull-out test results (see **Figure 4.13**), specimens with the compressive stress level 23.0 MPa presented an increase on the average tangential stress of 24% when compared with specimen with σ_L equal to 14.4 MPa.

After the long-term exposure to different environmental conditions, all slabs strengthened with the mechanical anchorage experienced slippage from the anchorage. **Table 4.7** shows that the stress on the CFRP laminate at the onset of the failure ($\sigma_{f,max}$) varied between 72% and 97% of its tensile strength. As stated in Chapter 3, all environments were able to change the mode of failure, being the full immersion on water (TW_MA_U and TW_MA_C) responsible for the higher reduction. The specimens kept in a laboratory premises (REF_MA_U and REF_MA_C) showed the highest CFRP strain and stress at failure. The pull-out programs did not include a study on the long-term performance of the mechanical anchorage system. The abovementioned results point to the fact that the resistance of this anchorage system might be highly influence by environmental factors, such as, immersion on water (with and without chlorides) or wet-dry cycles. Thus, a study focused on the durability of these anchorages should be carried out.

4.6 Conclusion

This Chapter has presented the results of the experimental programme aimed at studying the effectiveness of a mechanical anchorage of EBR CFRP laminates bonded to concrete structures. For this purpose, the results of 22 large-scale pull-out tests comprising prismatic concrete blocks externally bonded with CFRP laminates (of three different widths) and mechanically anchored (with four torque levels), have been presented and discussed. From the experimental results, the following observations and conclusions can be drawn:

- At room temperature the mechanical anchorage provides adequate compressive stress of the CFRP laminate to the concrete substrate, regardless of the torque level (30, 100, 150 or 200 N·m). However, for a laminate width of 100 mm, the lowest torque level (30 N·m) led to slippage of the CFRP laminate;

- At room temperature, a typical cohesive failure in the concrete and interface failure between the concrete and epoxy was observed in the bonded length (EBR component). The debonding load increased with the laminate width. However, some deviations are observed due to the different modulus of elasticity of the laminates;
- The load-slip behaviour at the loaded end showed all the typical stages during the debonding process of tests carried out at room temperature: (i) a first almost linear and steep branch, (ii) debonding of the laminate and (iii) a phase where the laminate was firmly held by the mechanical anchorage plate, until rupture of the laminate, or, in case of L100_T30_SS20 specimen, slippage of the laminate from the plate;
- At room temperature the debonding process along the EBR bonded length was registered by the strain gauges placed along the laminate, showing similar behaviour to the one reported by the literature, mainly [5,19–21];
- A local bond shear stress-slip curve was experimentally obtained from the data registered by the strain gauges for each specimen (at room temperature), and was adjusted to the model presented in [30], indicating an average bond shear strength, corresponding slip and the parameter governing the descending branch of 4.2 MPa, 0.082 mm and 3.7;
- By removing the anchorage plate from the specimens tested at room temperature, an assessment of the visible damage was carried out and a Mohr-Coulomb relation between the compressive stress level and average shear stress at the maximum load was observed with a cohesion and friction angle of 5.26 MPa and 13.7°, respectively;
- Anchorage slippage was the failure mode observed in all specimens tested at elevated temperatures, including the steady state tests carried out at 60 °C, at 80 °C and all the transient tests;
- In the steady-state tests, by comparing specimens tested at 60 °C and 80 °C to the ones tested at room temperature, a reduction on the ultimate load of 44% and 59%, respectively, was observed;
- When the temperature in the EBR component was 30 °C (initial stage of transient tests), a relative increase (when compared with the room temperature) in the debonding load of 23% was observed. Results also show that a fraction of the pull-out load was supported by the

mechanical anchorage since the early stages of the debonding process for the specimens tested at 60 °C and 80 °C;

- In the transient tests, three different outcomes were observed: (i) the low load level of 80 kN (0.36% of CFRP strain) was not enough to result in failure for the defined temperature variation; (ii) the medium load level of 100 kN (0.45% of CFRP strain) resulted in failure, but the confinement level worked as a relevant factor in the anchorage capacity; and (iii) the high load level of 120 kN (0.54% of CFRP strain) led to the anchorage failure shortly after the temperature reached the adhesive's T_g;
- The torque level was the tool used to control the confinement level of the anchorage and, based on the results from both test configurations it is a relevant factor to increase the anchorage capacity.
- The results obtained in the preliminary studies (Chapter 2) are in agreement with the results obtained with the pull-out tests carried out at room temperature, since the CFRP rupture was observed in similar conditions. In the monotonic tests performed on MA slabs subjected to the long-term environmental exposures, a reduction on the anchorage resistance was observed, since the failure mode shifted from CFRP rupture to CFRP slippage at the mechanical anchorages. These observations indicate that durability of mechanical anchorages may be an important issue to be analysed. Thus, a study focused on the durability of these anchorages should be carried out.

4.7 References

[1] Barris C, Correia L, Sena-Cruz J. Experimental study on the bond behaviour of a transversely compressed mechanical anchorage system for externally bonded reinforcement. Compos Struct 2018;200:217–28. doi:10.1016/J.COMPSTRUCT.2018.05.084.

[2] Barris C, Correia L, Sena-Cruz JM. Experimental study on the bond behaviour of a transversely compressed mechanical anchorage system for externally bonded reinforcement. 6th Asia-Pacific Conf. FRP Struct. (APFIS 2017), Singapore: 2017.

[3] Correia L, Barris C, Sena-Cruz JM. Temperature effect on the bond behaviour of a transversely compressed mechanical anchorage system. 9th Int. Conf. Fibre-Reinforced

Polym. Compos. Civ. Eng. (CICE 2018), Paris: 2018.

[4] Sena-Cruz JM, Correia L, Barris C. Behaviour of metallic anchorage plates for prestressing CFRP laminates under room and elevated temperatures. IABSE Conf. – Eng. Dev. World, Kuala Lumpur, Malaysia: 2018.

[5] CNR. Guide for the design and construction of externally bonded FRP systems for strengthening existing structures. 2013.

[6] Eurocode. BS EN 1992-2:2005 - Eurocode 2: Design of concrete structures - Part 2: Concrete bridges - Design and detailing rules. Eurocode 2 2005.

[7] NP EN 12390-3. Testing hardened concrete. Part 3: Compressive strength of test specimens. Caparica; IPQ-Instituto Português de Qualidade: 2011.

[8] LNEC E397-1993:1993, LNEC E397. Concrete - Determination of the elasticity Young modulus under compression. Portugal: 1993.

[9] ISO-527-5. Plastics–determination of tensile properties – Part 5: Test conditions for unidirectional fibre-reinforced plastic composites. London Br Stand Inst 1997.

[10] Silva PP, Fernandes P, Sena-Cruz JJ, Xavier JJJ, Castro F, Soares D, et al. Effects of different environmental conditions on the mechanical characteristics of a structural epoxy. Compos Part B Eng 2016;88:55–63. doi:10.1016/J.COMPOSITESB.2015.10.036.

[11] S&P. Resin 220 epoxy adhesive, technical datasheet. Seewen, Switzerland: 2013.

[12] Myers J, Shen X, Maerz N. Effect of varied surface roughness, putty thickness and concrete strength on the interfacial bond strength of FRP to concrete. Transp. Res. board, 2007.

[13] CEB-FIP. Model Code for Concrete Structures 2010. 2013. doi:10.1002/9783433604090.

[14] Iovinella I, Prota A, Mazzotti C. Influence of surface roughness on the bond of FRP laminates to concrete. Constr Build Mater 2013. doi:10.1016/j.conbuildmat.2012.09.112.

[15] Mazzotti C, Bilotta A, Carloni C, Ceroni F, D'Antino T, Nigro E, et al. Bond between EBR FRP and concrete. In: Pellegrino C, Sena-Cruz J, editors. Des. Proced. Use Compos. Strength. Reinf. Concr. Struct. State-of-the-Art Rep. RILEM Tech. Comm. 234-DUC, Dordrecht:

Springer Netherlands; 2016, p. 39–96. doi:10.1007/978-94-017-7336-2_3.

[16] Correia L, Teixeira T, Michels J, Almeida JAPP, Sena-Cruz J. Flexural behaviour of RC slabs strengthened with prestressed CFRP strips using different anchorage systems. Compos Part B Eng 2015;81:158–70. doi:10.1016/j.compositesb.2015.07.011.

[17] Chen J, Teng J. Anchorage Strength Models for FRP and Steel Plates. J Struct Eng 2001;127:784–91.

[18] Seracino R, Raizal Saifulnaz MR, Oehlers DJ. Generic Debonding Resistance of EB and NSM Plate-to-Concrete Joints. J Compos Constr 2007;11:62–70. doi:10.1061/(ASCE)1090-0268(2007)11:1(62).

[19] Ceroni F, Pecce M, Bilotta A, Nigro E. Bond behavior of FRP NSM systems in concrete elements. Compos Part B Eng 2012;43:99–109. doi:10.1016/j.compositesb.2011.10.017.

[20] Mazzotti C, Savoia M, Ferracuti B. A new single-shear set-up for stable debonding of FRP-concrete joints. Constr Build Mater 2009;23:1529–37. doi:10.1016/j.conbuildmat.2008.04.003.

[21] Soares S, Cruz JR, Fernandes P, Sena-Cruz J. Bond behavior of EBR CFRP systems in concrete : influence of surface preparation. Proc. 6th Asia-Pacific Conf. FRP Struct., Singapore: 2017.

[22] Lu XZ, Teng JG, Ye LP, Jiang JJ. Bond-slip models for FRP sheets/plates bonded to concrete. Eng Struct 2005;27:920–37.

[23] Neubauer U, Rostasy FS. Bond Failure of Concrete Fiber Reinforced Polymer Plates at Inclined Cracks—Experiments and Fracture Mechanics Model. ACI Spec Publ 1999;188:369–82.

[24] Monti G, Renzelli M, Luciani P. FRP ADHESION IN UNCRACKED AND CRACKED CONCRETE ZONES. Sixth Int. Symp. FRP Reinf. Concr. Struct. - FRPRSC-6., 2003, p. 183–92. doi:10.1142/9789812704863_0015.

[25] Ferracuti B, Savoia M, Mazzotti C. Interface law for FRP-concrete delamination. Compos

Struct 2007;80:523–31. doi:10.1016/j.compstruct.2006.07.001.

[26] Popovics S. A numerical approach to the complete stress strain curve for concrete. Cem Concr Res 1973;3:583–99.

[27] Xu T, He ZJ, Tang CA, Zhu WC, Ranjith PG. Finite element analysis of width effect in interface debonding of FRP plate bonded to concrete. Finite Elem Anal Des 2015;93:30–41. doi:10.1016/j.finel.2014.08.009.

[28] Biscaia HC, Chastre C, Silva MAG. Bond-slip model for FRP-to-concrete bonded joints under external compression. Compos Part B Eng 2015;80:246–59. doi:https://doi.org/10.1016/j.compositesb.2015.06.004.

[29] Michels J, Widmann R, Czaderski C, Allahvirdizadeh R, Motavalli M. Glass transition evaluation of commercially available epoxy resins used for civil engineering applications. Compos Part B Eng 2015;77:484–93. doi:10.1016/J.COMPOSITESB.2015.03.053.

[30] Micelli F, Rizzo A, Galati D. Anchorage of composite laminates in RC flexural beams. Struct Concr 2010;11:117–26. doi:10.1680/stco.2010.11.3.117.

CHAPTER 5

NUMERICAL SIMULATION OF RC SLABS STRENGTHENED WITH PRESTRESSED CFRP LAMINATES

5.1 Introduction

This chapter presents the tools used to numerically simulate the behaviour of the slabs strengthened with prestressed CFRP laminates according to the EBR technique. The experimental results presented in Chapter 3 were used in the development of the finite element analyses. The selection of the constitutive material models for each composing material and interface (concrete, steel reinforcement, interface between concrete and CFRP reinforcement, and CFRP reinforcement) were properly done. The simulations account for the strengthening particularities and test configuration. The performance of these simulations was compared with the results of the slabs submitted to monotonic tests up to failure. Subsequently, these models were used on a parametric study that intended to investigate the influence of different parameters affecting the behaviour of the slabs.

5.2 Geometry, type of elements and type of analysis

From the experimental campaign described in Chapter 3, four slabs were chosen to be modelled: one unstrengthened RC slab (T0_REF); a second slab strengthened with a CFRP laminate strip according to the EBR technique (T0_EBR); a third slab strengthened with one externally bonded prestressed CFRP laminate strip with the MA system (T0_MA); and a fourth slab strengthened with one externally bonded prestressed CFRP laminate strip with the GA system (T0_GA). The label given to each slab in Chapter 3 is kept the same in the present chapter. Additional information regarding the geometry of each slab or the properties of the materials used is given in Chapter 3.

5.2.1 Model geometry and mesh

As previously referred, the specimens were tested up to the failure, under a four-point bending test configuration. The test configuration exhibits a symmetry that was considered in the numerical simulations to reduce computational time. The model geometry, finite element (FE) mesh, loading configuration and boundary conditions used in the analysis of the four experimentally tested specimens are presented in **Figure 5.1**.

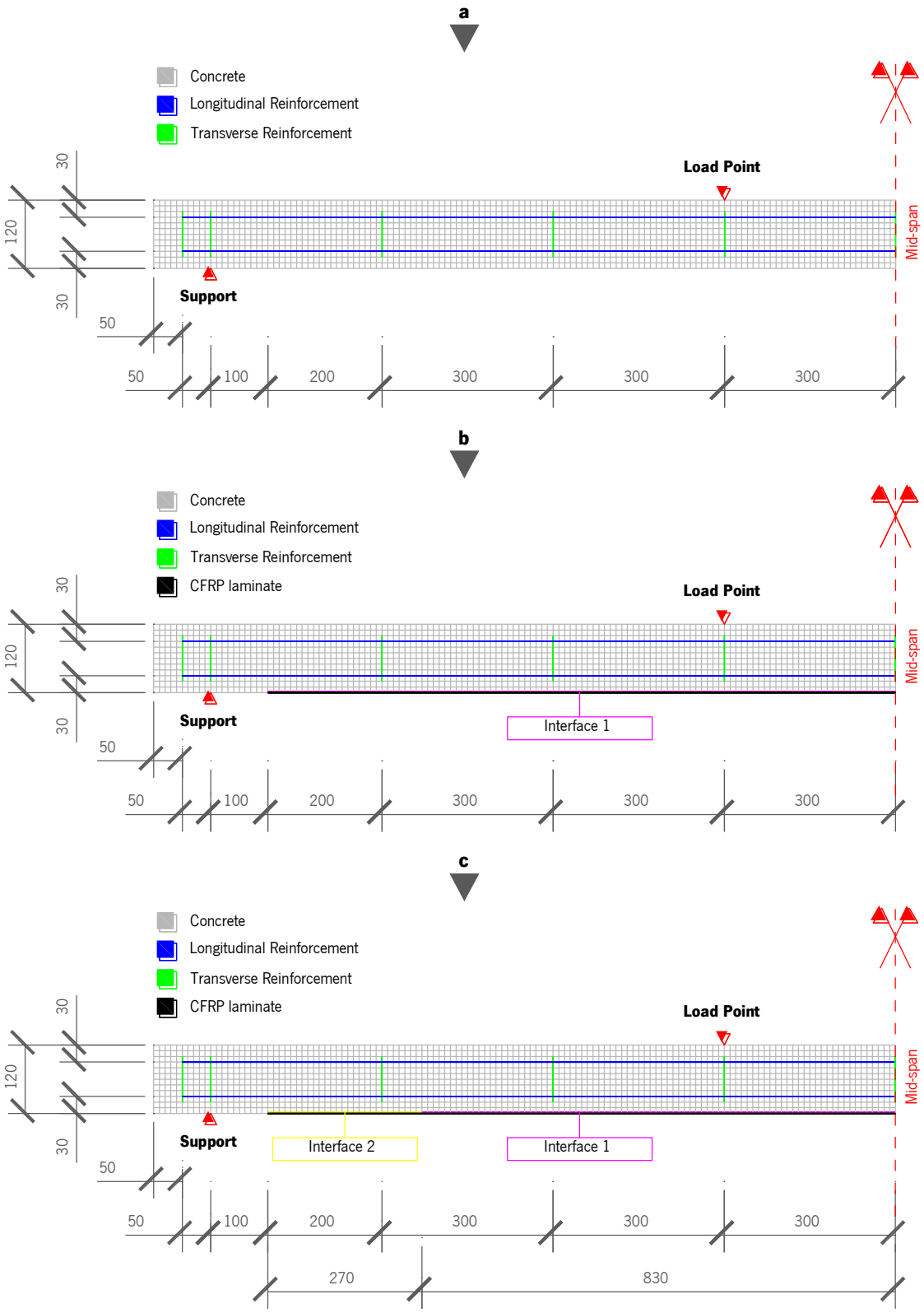

Figure 5.1: Characteristics of the used models in the case of: (a) slab T0_REF, (b) slabs T0_EBR and T0_GA; and (c) slab T0_MA. Note: units in [mm].

A regular mesh composed of square finite elements with 10 mm of edge were used for modelling the concrete component of the slabs. Line and interface elements were also used to simulate the reinforcements (steel and CFRP) and interfaces between concrete and CFRP, respectively. The type and number of elements used to model each material is presented in **Table 5.1**.

Table 5.1
Summary of the types of elements and number of elements used in the models.

Material	**Element Type**	**Number of elements**			
	Diana® Syntax (version 10.2)	T0_REF	T0_EBR	T0_GA	T0_MA
Concrete	CQ16M	1560	1560	1560	1560
Steel Reinforcement	EMBEDDED REINFORCEMENT	8	8	8	8
CFRP Reinforcement	CL6TR	–	110	110	110
Interface 1	CL12I	–	110	110	83
Interface 2	CL12I	–	–	–	27

5.2.2 Type of elements

The slabs were simulated as a plane state problem. In the present finite element models, a total of four type of elements were used: (i) CQ16M (Diana® syntax, version 10.2) to model the concrete; (ii) CL6TR (Diana® syntax, version 10.2) to model the CFRP reinforcement; (iii) CL12I (Diana® syntax, version 10.2) to model the interface between the CFRP material and the concrete; and (iv) 'EMBEDDED REINFORCEMENT' to model the longitudinal and transverse steel reinforcement. The mesh typology, boundary conditions and property assignments were relevant factors for the selected type of elements.

The FE CQ16M used to simulate the concrete (see **Table 5.2**) is an eight-node quadrilateral isoparametric element. A quadratic interpolation and Gauss-Legendre integration scheme was adopted [1]. The longitudinal and transverse steel reinforcement was modelled as embedded reinforcement. This element type does not allow relative slip between steel and concrete. This implies that a perfect bond between the reinforcement and the concrete was assumed. They are represented as lines in a two-dimensional finite element model. The input information for the embedded reinforcement are the mechanical properties, the area of the cross-section and the integration scheme. To embed bar reinforcement in plane stress elements, DIANA® needs for each

plane stress element the location points of the particle that is embedded in that element (the points "⊗" in **Table 5.2**). Regarding the integration scheme, two integration points for each particle along the ξ axis of the bar was assumed (see **Table 5.2**, where a bar particle in plane stress element is represented).

Table 5.2
Type of elements used (adapted from [1]).

Material	**Element Type** Diana® Syntax	**Representation**	**Additional input geometry**
Concrete	CQ16M	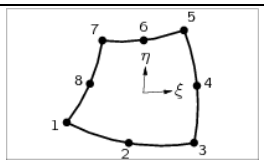	THICKNESS (120 mm)
Steel Reinforcement	EMBEDDED REINFORCEMENT	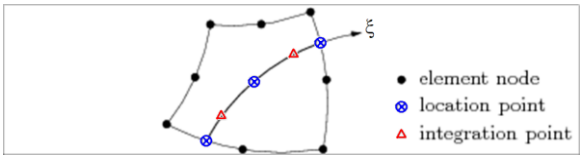	CROSS-SECTION AREA (5Φ8: 251.3 mm²) (3Φ6: 84.8 mm²) (2Φ6: 56.6 mm²)
CFRP Reinforcement	CL6TR		CROSS-SECTION AREA (60 mm²)
Interface 1 and Interface 2	CL12I	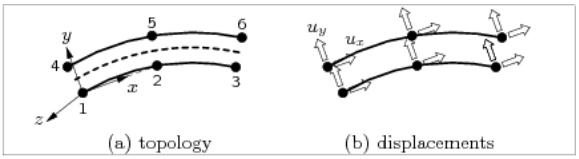	THICKNESS (Interface 1: 50 mm) (Interface 2: 100 mm)

The CFRP laminate strip was discretized using the truss element CL6TR. As it is shown in **Table 5.2**, the CL6TR is a three-node numerically integrated truss element.

The interface elements describe the interface behaviour in terms of normal and shear stresses linked with tractions/compressions and relative displacements across the interface, respectively. The interface between the CFRP and the concrete subtract, was modelled based on the CL12I element. This element is also based in a quadratic interpolation and is an interface element between two lines in a two-dimensional configuration (see **Table 5.2**). The CL12I has three nodes in each line which match of nodes per line of the CL6TR (used for the CFRP laminate strip) and CQ16M (used for the concrete) elements.

5.2.3 Boundary and loading conditions

A four-point bending test configuration was used on the experimental campaign and the finite element modelling tried to replicate it. As stated before, due to the symmetry of the test configuration and slab geometry, only half of the actual slab was modelled (see **Figure 5.1**). The symmetry at the mid-span section was assessed by restricting the displacements in the X direction. The support, as it is shown in **Figure 5.1**, is located at 100 mm from the edge of the slab and provides a constrain only in the Y direction.

Three load cases were considered: (i) the self-weight; (ii) the prestress; and (iii) the monotonic loading of the slab. In Chapter 3, the results from the monotonic tests performed on slabs T0_REF, T0_EBR, T0_MA and T0_GA were presented. However, at the onset of these static tests, all slabs were already submitted to a stress state and deformation caused by its own self-weight and, for the case of slabs MA and GA, additionally the existing prestress in the CFRP laminate strip.

The self-weight was applied using a distributed force of -1.8 N/mm in the Y direction, over the complete length of the slabs. Typically the prestress is simulated with a temperature variation applied in the prestress element; however, the "equivalent loads" method was adopted in the present case since the current used version of Diana® (version 10.2) does not include this feature. Thus, a distributed load, applied over the anchorage region was the method used to simulate the application of prestress. For the MA slab a load of 154.15 N/mm in the X direction was applied over a length of 270 mm (size of metallic anchorage), which gives a total load of 41.62 kN in the bottom surface of the concrete surface; whereas, for the GA slab a load of 65.27 N/mm in the X direction was applied for a length of 600 mm (size of gradient anchorage), which gives a total of 39.16 kN in the bottom surface of the concrete surface. A prescribed displacement on the loading point (300 mm from the mid-span at the superior edge of the slab) was applied to simulate the monotonic loading.

The self-weight and prestress of the CFRP laminate was applied over twenty steps (10 steps for each load case). The monotonic loading used a minimum of 700 steps, each one with a total displacement increase of 0.1 mm. The imposed displacements were sufficient to record the slab's behaviour during all test stages (before, during and after peak load).

To compare the FE analysis with the experimental results, a new origin of the relationship between force and displacement was considered, being the origin point coincident with the last step of the self-weight load case (for REF and EBR slabs) or last step of the prestress load case (for the MA and GA slabs). In **Figure 5.2** is presented the relation between the mid-span displacement and the total load, using the aforementioned axis. The self-weight (identified with the blue dots in **Figure 5.2**) produces a mid-span displacement close to 0.3 mm that was analytically validated. As can be seen in **Figure 5.2b**, the prestress load case caused a camber mid-span displacement close to 0.7 mm. The prestress influence was slightly higher in the MA specimens than in the GA specimen, because the applied load was also greater. The origin of the original vertical axis (see **Figure 5.2**) considers all the load cases (gravity, self-weight and monotonic loading), whereas the origin of the new vertical axis only considers the monotonic loading. The later axis was used in order to properly compare the FEA results with the experimental results.

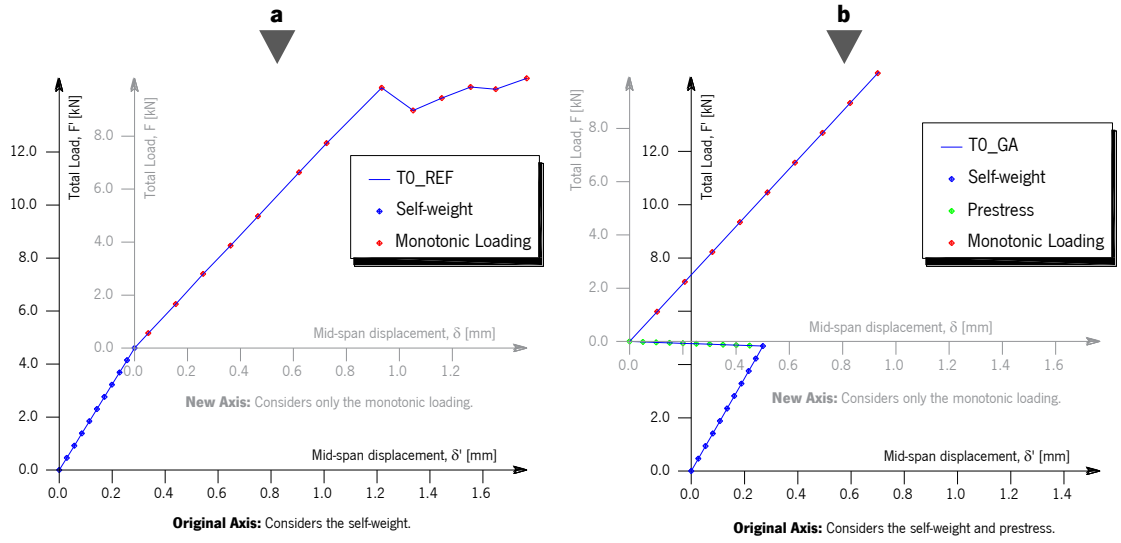

Figure 5.2: Axis considered in the FEA of the slabs: (a) T0_REF and (b) T0_GA.

Regular Newton-Raphson interactive method was used to obtain convergence between internal and external forces in the models for the self-weight and prestress load cases. For the monotonic loading, the Secant (Quasi Newton) method was adopted. The Secant method does not set up a completely new stiffness matrix every iteration, thus being a more stable over the development of the analysis [1].

5.3 Constitutive material models

5.3.1 Concrete

The concrete exhibits non-linear behaviour under uni-and-multi-axial stress states. A smeared crack approach was used to model the crack propagation in concrete. DIANA® includes over seven smeared crack models, like the total strain-based crack model (TSCM) and the multidirectional fixed crack model (MFCM). The constitutive model used to predict the concrete behaviour was the total strain based fixed crack model. The model is suited for serviceability and ultimate analyses which are predominantly governed by cracking or crushing of the material [1]. The input data adopted for the TSCM constitutive model is the presented in **Table 5.3**. The input data describe the tensile and compressive behaviour of the concrete with one stress-strain relationship. The value of the concrete elastic modulus measured experimentally (see Chapter 3) was used. The TSCM complies several predefined relationships for the concrete tension softening. Among them, the non-linear tension softening model defined by Hordijk *et al.* [2] was selected. The tensile strength and fracture energy, required by this model, were computed based on the CEB-FIP Model Code 1990 [3]. The concrete fracture energy, G_f, the energy required to propagate a tensile crack of unit area, was estimated according to:

$$G_f = G_{f0} \cdot \left(\frac{f_{cm}}{f_{cm0}}\right)^{0.7} \tag{5.1}$$

where f_{cm0} is equal to 10 MPa, f_{cm} was obtained experimentally (equal to 40 MPa, see Chapter 3) and G_{f0} is the base value of fracture energy related to the maximum aggregate size. The maximum aggregate size was equal to 12.5 mm, which means that the G_{f0}=0.0275 N/mm. The tensile strength, f_{ctm}, was obtained according to the following equation, obtained from the CEB-FIP Model Code 1990 [3]:

$$f_{ctm} = f_{ctk0} \cdot \left(\frac{f_{cm} - \Delta f}{f_{cm0}}\right)^{2/3} \tag{5.2}$$

where f_{ctk0} is equal to 1.4 MPa, f_{cm} was obtained experimentally (equal to 40 MPa, see Chapter 3), Δf is equal to 8 MPa, and f_{cm0} is equal to 10 MPa.

The crack band-width, h, is the width of the finite element for which the fracture zone is distributed. In order to ensure mesh objectivity, the used crack band-width was mesh dependent. Based on Sena-Cruz [4], the crack band-width was computed as:

$$h = \sqrt{2 \cdot A} \tag{5.3}$$

where A is area of the corresponding element mesh.

Table 5.3
Input data used for the concrete model.

Property	Values	Diagram
Linear material properties		
Elastic modulus[a]	30030 N/mm²	
Poison's ratio	0.2	
Density[a]	2500 kg/m³	
Tensile behaviour		
Tensile curve	Hordijk *et al.* (1987)	
Tensile strength	3.04 N/mm²	
Mode-I tensile fracture energy	0.07 N/mm	
Crack bandwidth	15 mm	
Residual tensile strength	0 N/mm²	
Poison's ratio reduction	No reduction	
Compressive behaviour		
Compression Curve	Elastic	
Shear behaviour		
Shear retention function	Constant	
Shear retention factor	1	

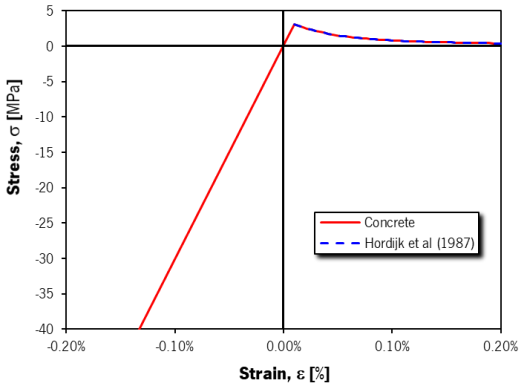

Notes: [a] Value obtained experimentally.

5.3.2 Steel Reinforcement

The embedded steel reinforcement was modelled using the Von Mises plasticity and hardening model. The main properties used for the modelling of the steel reinforcement and the bilinear stress-strain relationship diagram are presented in **Table 5.4**. The properties measured experimentally were used to define the corresponding relationships (see Chapter 3). However, the elastic modulus of the Φ8 steel reinforcement was assumed to be 200 GPa, and the ultimate strain for both types of steel reinforcements were assumed to be 0.1.

Still regarding the modelling of the steel reinforcement, the cross-sectional area used for the upper longitudinal reinforcement (3Φ6) was 84.8 mm², for the bottom longitudinal reinforcement (5Φ8)

was 251.3 mm², and for the transverse reinforcement (2Φ6) was 56.6 mm². Due to the symmetry effect, the cross-sectional area of the mid-span stirrup was equal to the area of a single Φ6 steel bar (28.3 mm²).

Table 5.4
Input data used for the steel reinforcement model.

Property	Values	Diagram
Steel (Φ6)		
Linear material properties		
Elastic modulus[a]	206900 N/mm²	
Von Mises plasticity		
Yield stress[a]	519.3 N/mm²	
Ultimate stress[a]	670.2 N/mm²	
Ultimate strain	0.1	
Steel (Φ8)		
Linear material properties		
Elastic modulus	200000 N/mm²	
Von Mises plasticity		
Yield stress[a]	595.9 N/mm²	
Ultimate stress[a]	699.0 N/mm²	
Ultimate strain	0.1	

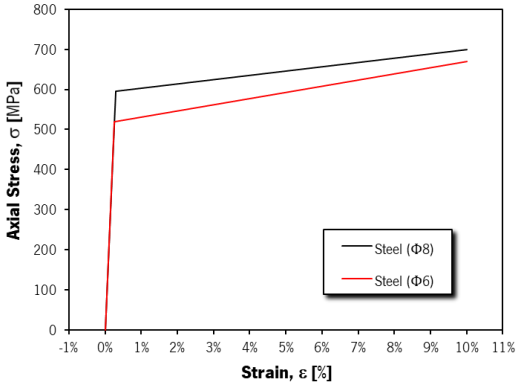

Notes: [a] Value obtained experimentally.

5.3.3 CFRP laminate strip

The CFRP was modelled as linear-elastic up to tensile failure, as observed in the uniaxial tensile tests carried out. Based on the results from the material characterization, an elastic modulus of CFRP of 164 GPa and ultimate strength of 2374 MPa were used. To simulate the CFRP failure, the Von Mises and Tresca plasticity material model was used. When the ultimate strength is reached, the strength falls to 0 MPa, as it is depicted in **Table 5.5**. In the prestress specimens, the ultimate strength was reduced to 1718 MPa. As referred before, the prestress was simulated with the "equivalent loads" method. Consequently, the distributed load applied over the anchorage region (see Section 5.2.3) does not induce 0.4% of strain on the CFRP laminate. Thus, to properly model the CFRP laminate, when prestressed, the ultimate strength was reduced in 656 MPa (0.4% of strain), as presented in **Table 5.5**.

Table 5.5
Input data used for the CFRP reinforcement model.

Property	Values	Diagram
Linear material properties		
Elastic modulus [a]	164000 N/mm²	
Poison's ratio [b]	0.3	
Density [b]	1600 kg/m³	
Von Mises and Tresca plasticity		
Plasticity model	Von Mises plasticity	
Ultimate stress [a]	2374.9 N/mm²	
Ultimate strain [a]	0.0145	

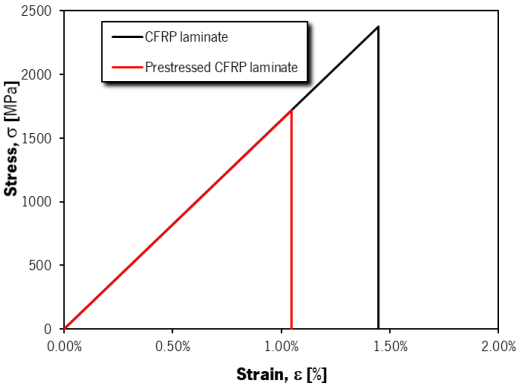

Notes: [a] Value obtained experimentally; [b] Value according to manufacturer [5].

5.3.4 Interface

The interface material model chosen to represent the interface between the concrete and the CFRP laminate has the named "BOND-SLIP". This model set a nonlinear relation between shear traction and shear slip, whereas the relation between normal traction and normal relative displacement is kept linear. The bilinear bond-slip law proposed by Lu *et al.* [6] has been used and the parameters governing (τ_{max}, s_0, G_f and s_f) the bond-slip model were estimated as follows:

$$\tau_{max} = 1.5 \cdot \beta_w \cdot f_{ctm} \tag{5.4}$$

$$s_0 = 0.0195 \cdot \beta_w \cdot f_{ctm} \tag{5.5}$$

$$G_f = 0.308 \cdot {\beta_w}^2 \cdot \sqrt{f_{ctm}} \tag{5.6}$$

$$s_f = \frac{2 \cdot G_f}{\tau_{max}} = \frac{2 \cdot 0.308 \cdot {\beta_w}^2 \cdot \sqrt{f_{ctm}}}{1.5 \cdot \beta_w \cdot f_{ctm}} = \frac{0.41 \cdot \beta_w}{\sqrt{f_{ctm}}} \tag{5.7}$$

where f_{ctm} is the tensile strength of the concrete, the G_f is the value of fracture energy of interface law and β_w is a geometrical factor (that considers the width of the FRP, b_f, and the width of the concrete member, b_c, which the FRP is applied) given by:

$$\beta_w = \sqrt{\frac{2.25 - {b_f}/{b_c}}{1.25 + {b_f}/{b_c}}} \tag{5.8}$$

As a result, this simplified bond-slip relation can be defined by three points on a shear-slip plot: the first point with values (0;0) is the origin; the second point with values (s_0; τ_{max}) shows the peak stress and corresponding slip; and the last point, with the values (s_f;0). This law was used to define the interface constitutive model (Interface 1, see **Figure 5.1** and **Table 5.1**) and the input values and shear-slip diagram is presented in **Table 5.6**.

Table 5.6
Input data used for the Interface 1.

Property	Values	Diagram
Linear material properties		
Normal stiffness modulus-y	1x10⁶ N/mm³	
Shear stiffness modulus-x	72 N/mm³	
Bondslip		
Bondslip model	Von Mises plasticity	
Maximum shear traction	5.73 N/mm²	
Slip at maximum shear traction	0.08 mm	
Ultimate slip	0.25 mm	

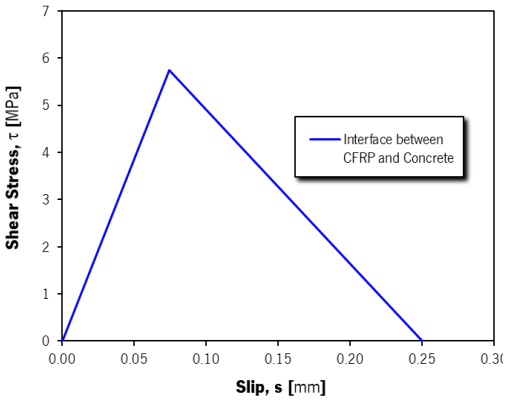

As it was mentioned before, another interface (Interface 2) was considered for the specimen MA (see **Figure 5.1** and **Table 5.1**). Thought the experimental test of the slab T0_MA, failure by CFRP rupture was observed. During the test the mechanical anchorage exhibit a flawless performed and no relative displacements between the CFRP laminate and the anchorage plate was detected. With the mindset on the experimental observations, the Interface 2, which represents the bond

between the CFRP laminate and the concrete in the anchorage region (270 mm) was modelled as linear elastic with the normal and shear stiffness modulus equal to $1x10^6$ N/mm^3.

5.4 Results and discussion

This section presents the results and discussion of FEA carried out. The relationship between the applied load and the mid-span displacement, the load applied load *versus* CFRP/concrete strain and the crack patterns were analysed. Each specimen has a generic label X_(Y), where X is the label of the experimental slab given in Chapter 3, Y identifies if is an experimental (EXP) or an numerical (FEM) result.

5.4.1 Total load *versus* mid-span displacement

Figure 5.3 shows the comparison between the experimental and numerical results regarding the relationship between the total load and mid-span displacement. All the numerical curves present a well-defined elastic phase, cracked phase and yielding phase. The elastic phase is observed at the beginning of the test, has the highest stiffness, and ends with the crack initiation of the concrete. In the flowing stage, the stiffness is significantly diminished due to the cracking of the concrete. This cracked phase ends when the steel reinforcement reaches the yielding stage. The steel yielding marks the beginning of the final test stage, the yielding phase. During the last phase, the contribution provided by the steel reinforcement on the supported load is limited and the slab presents the lowest stiffness observed.

In general, the relationship between the total load and the mid-span displacement obtained with the numerical simulation presented a good agreement with the experimental results. These results give an accurate prediction of the deformation response of all slabs during the elastic phase and cracked phase. In the FE models, the cracking initiation occurred for the same load and mid-span displacement values of the experimental tests. The stiffness of the slabs during the first two stages is identical for the numerical and experimental curves. The steel yielding and ultimate failure are also well captured. However, the numerical prediction on the steel yielding seems to be slightly below the one obtained experimentally. In contrast, in the REF slab (see **Figure 5.3a**), the yielding point appears to occur for a slightly superior load value. It is known that the average stress-strain

relationship for the reinforcement steel embedded in concrete is different from the average stress-strain relationship of a bare steel bar. To consider this fact, Stevens [7] proposes a methodology to reduce on the steel yielding and ultimate stresses. This methodology wasn't taken into account because the average steel properties obtained experimentally, were the best match for all four slabs. Another simplification of the numerical model was the perfect bond between the steel reinforcement and the concrete. There was no perfect bond between these two materials during the experimental tests and slip at their interface might have occur. Finally, it should be mentioned that the case of the strengthened slabs, since the CFRP significantly contributes for the overall resistance of the slabs, the yielding initiation is more masked compared to the case of the reference slab.

The ultimate load was well captured in all strengthened slabs. Although failure was not reached in the modelled REF slab, result show that the yielding phase started around step 290, when the total load, F, was 30.84 kN and the mid-span displacement, δ, was 29.02 mm. In the experimentally tested REF specimen, failure by concrete crushing would be expected. However, due to the concrete model adopted, this kind of failure would not be observed in the FE model. The stiffness of the last test stages, for the REF, exhibits similar results on the numerical and experimental curves. The maximum load for the specimens EBR, MA and GA was observed on step 374 (F=39.90 kN; δ=28.97 mm), 795 (F=70.00 kN; δ=89.84 mm), and 410 (F=57.70 kN; δ=42.45 mm), respectively. The failure on the T0_EBR and T0_GA (see **Figure 5.3b** and **Figure 5.3d**) specimens was attained when the interface between the CFRP laminate and the concrete reached its maximum capacity. The load and mid-span displacement registered on the numerical curves is similar to the experimental ones. For the case of the T0_MA slab (**Figure 5.3c**), the numerical simulation predicts failure by FRP rupture also at the similar load and mid-span displacement of the experimental test. The intermediate debonding registered at about 56 kN, was also captured in the numerical simulation of the T0_MA slab. The experimental results show two drops on the plot curve because the strip debonding occurred in two stages, first one side of the specimen and then on the other side (for more details see also Chapter 3). The numerical model comprehends only half the slab and, for that reason, there's only one drop. The intermediate debonding observed on the MA slab, divides the yielding phase into two stages: (i) a first, when the CFRP strip is bonded to the concrete and (ii) a second, where the CFRP is detached from the concrete substrate and

works as an external cable. These two stages are clearly observed in both experimental and numerical curves, and a good correlation between the experimental and the numerical results were obtained.

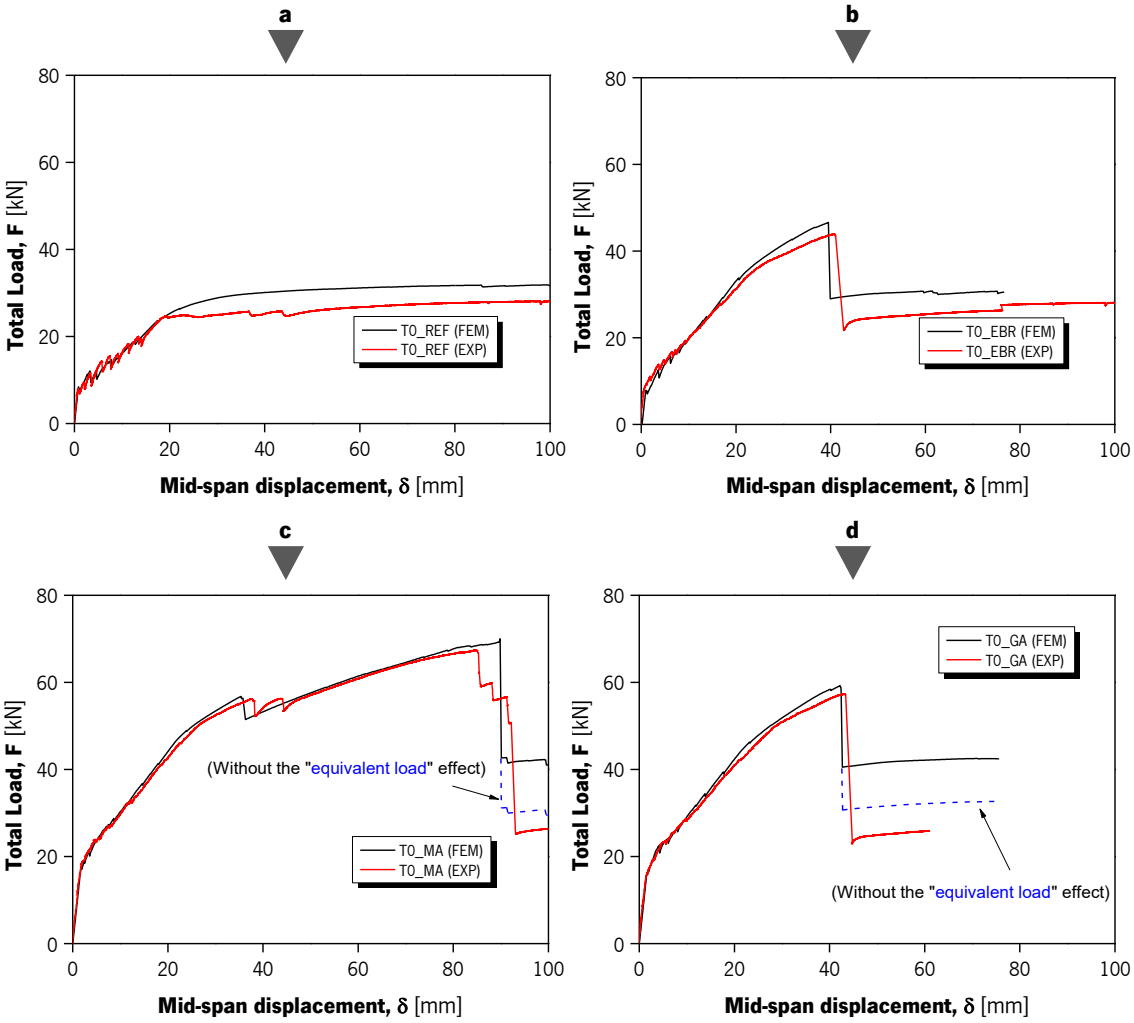

Figure 5.3: Comparison between the experimental results and numerical predictions in terms of total load *versus* mid-span displacement for: (a) T0_REF slab; (b) T0_EBR slab; (c) T0_MA slab; and (d) T0_GA slab.

It should be noted that after the failure of the strengthening system of the prestressed slabs, the load did not decrease to the value of reference slabs (see **Figure 5.3c** and **Figure 5.3d**). The prestress load was applied using an "equivalent load" on the FE model and, consequently, when failure occurs the equivalent prestress load must be discounted from the total load. In order to remove this "equivalent load" effect, a distributed load equal to the one used to simulate the

prestress, was applied on the anchorage region (in the opposite direction), after the step where peak load is reached. Results from this iteration are presented as a blue dashed line in **Figure 5.3c** and **Figure 5.3d**. As can be seen in these figures, the response without the "equivalent load" effect, after failure, is much closer to the experimental values.

Figure 5.4 shows the evolution of the CFRP strain variation across the CFRP length, measured experimentally and estimated numerically for the slab T0_MA. Since only half of the specimen was modeled, the symmetry at the mid-span was consider to represent the CFRP strain variation across the total length of the laminate strip. In short, for the same load levels, similar CFRP distribution were observed. The debonding of the CFRP is equally observed for the load of 56 kN; however, in the experimental curves the debonding process occurred in two stages (first the left side, followed by the right side); whereas in the numerical analysis the debonding only occurred in one stage. After this point, both numerical and experimental results, show that the CFRP strip behaves as a unbonded external cable with almost constant strain.

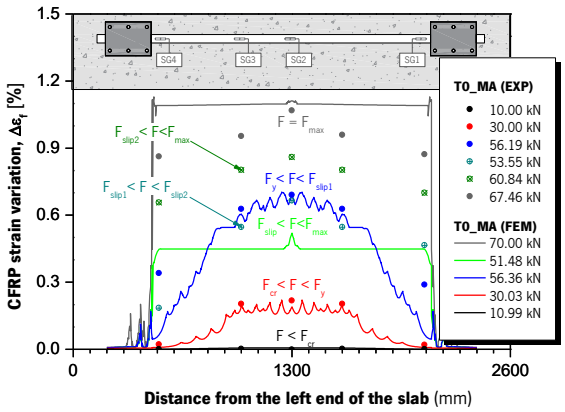

Figure 5.4: CFRP strain variation in T0_MA slab (experimentally tested and numerically predicted).

5.4.2 Total load *versus* concrete, steel and CFRP strains

The concrete strain variation was also evaluated in this FE analysis. The evolution of the concrete strain at the mid-span (top surface) with the total load is presented in **Figure 5.5a**. The numerical (FEM) and experimental (EXP) curves are similar for the T0_EBR and the T0_GA slabs. However, significant differences are observed, after the cracking of the concrete for the T0_REF and the T0_MA slabs. The difference between the experimental and the numerical results is related with the fact that a linear behaviour was adopted for the concrete behaviour under compressive stress

state. However, it should be also mentioned that the concrete strain measured on the experimental campaign is highly dependent of the location where the strain gauge was fixed.

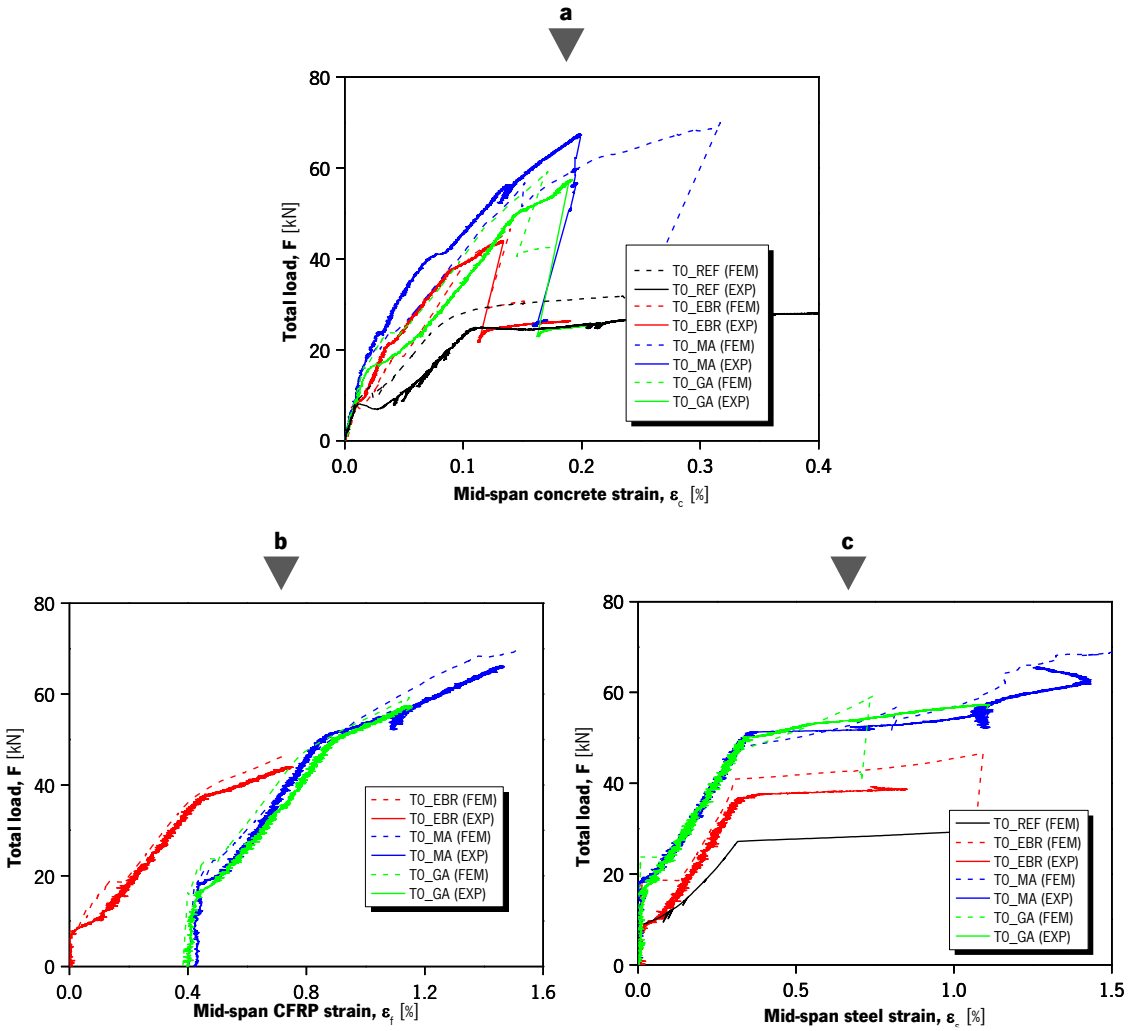

Figure 5.5: Total load *versus* CFRP/steel/concrete strain of the slabs experimentally tested and numerically predicted.: (a) mid-span concrete strain; (b) Mid-span CFRP strain; (c) Mid-span steel reinforcement strain.

The variation of the CFRP strain at the mid-span with the total load is presented in **Figure 5.5b**, for both experimentally tested and numerically predicted. As can be seen, the numerical predictions of the CFRP strains are in agreement with the experimental measurements. All three slabs clearly show the three test phases (elastic phase, cracked phase and yielding phase). The initial slope (elastic phase) is very stiff, mainly because the uncracked concrete is the biggest responsible for

supporting the increasing load. The crack initiation of the concrete is observed for similar load levels. During the test stage that follows the crack initiation, the influence of the steel and CFRP reinforcement is higher and the slop of the curves presented in **Figure 5.5b**, decreases. During yielding phase, the CFRP is greatest responsible for carrying the additional loads, because the steel reinforcement contribution to the load carrying capacity of the slabs is limited. As a result, the slop in the curves depicted in **Figure 5.5b** is the lowest in this last stage. With the numerical simulations, the maximum mid-span CFRP strain was equal to 0.7%, 1.5% and 1.1% in slabs T0_EBR, T0_MA and T0_GA, respectively. These values correspond to a variation in between -3.3% and 3.4% from the experimental results.

The steel reinforcement plays an important role in the overall behaviour of the RC slabs. After crack initiation of the concrete, the stiffness of all slabs is dependent on the steel reinforcement. The steel yielding of the numerically predicted slabs occurs for a strain value of 0.3%. **Figure 5.5c** shows the mid-span steel strain with the total load. This strain was experimentally registered for specimens T0_EBR, T0_MA and T0_GA. The experimental mid-span steel strain values were measured using a strain gauge fixed on the middle Ø8 rebar. Although representative of the tensile strain develops during the experimental tests, the strain gauge measures are highly dependent on the localization of the concrete tensile cracks and, consequently, the numerical and experimental onset might be different. Nonetheless, results show that there is a good agreement between the numerical and experimental results. Additionally, the FEM curves show the steel yielding for the similar load values of those measured experimentally.

5.4.3 Crack pattern

The crack patterns obtained on the numerical simulations of all four specimens is presented in **Figure 5.6**, for step 500, when the mid-span displacement was close to 54.26 mm. For this displacement value, failure of the strengthening system had already occurred for specimens T0_EBR, and T0_GA; the CFRP strip of the MA slab was already debonded (debonding occurred at step 347, when the F=56.35 kN, and the δ=35.78 mm); and, on the REF slab, the total load had already reached a plateau (an increase of 0.4% was observed since the steel yielding). With the mid-span displacement of 54.26 mm, the maximum crack width was observed near the mid-span and was equal to 6.7 mm, 4.7 mm, 4.4 mm and 4.4 mm for the numerically simulated

T0_REF, T0_EBR, T0_MA and T0_GA slabs, respectively. In the analysis of the crack width presented in Section 3.4.2 (Chapter 3) it was also observed that, for the same load level, highest crack widths were observed on the T0_REF specimen, followed by the T0_EBR.

In general, the numerical simulations predicted the overall crack pattern of the slabs. The average experimental space between consecutive cracks was, respectively, equal to 152.4 mm, 114.7 mm, 97.5 mm e 98.5 mm on specimens T0_REF, T0_EBR, T0_MA and T0_GA. The numerical results presented an average crack spacing of 80 mm, 72 mm, 68 mm e 67 mm for specimens T0_REF, T0_EBR, T0_MA and T0_GA, respectively. It should be referred that in the numerical simulation, the crack spacing was measured at the loading step 500 (mid-span displacement 56.26 mm), whereas the experimental crack spacing was measured at the end of each test. Finally, in both analyses (experimental and numerical) the greatest crack spacing was observed in the T0_REF, followed by the T0_EBR slab and then by the prestressed slabs. Additionally, in the present numerical simulations, perfect bond between steel reinforcement and concrete was assumed. With the incorporation of the bond-slip laws at the interface between the steel reinforcement, the crack spacing necessarily would increase.

5.5 Parametric Studies

Based on the results presented in Section 5.4, it was clear that the numerical models developed can predict the experimental results with high accuracy. Thus, parametric studies were carried out to assess the influence of the prestress level and of the CFRP laminate geometry on the slabs' structural performance. It should be mentioned that, in this parametric study, the geometry, boundary conditions and constitutive material models described in the previous chapters were used in the present parametric studies

5.5.1 Influence of the level of prestress

The influence of prestress was one of the main parameters studied in this work. The results obtained from the experimental campaign clearly shown that the prestress improved the slabs performance with lower displacement, crack width delay and lower crack spacing. However, the level of prestress applied on the CFRP laminate might affect the structural ductility.

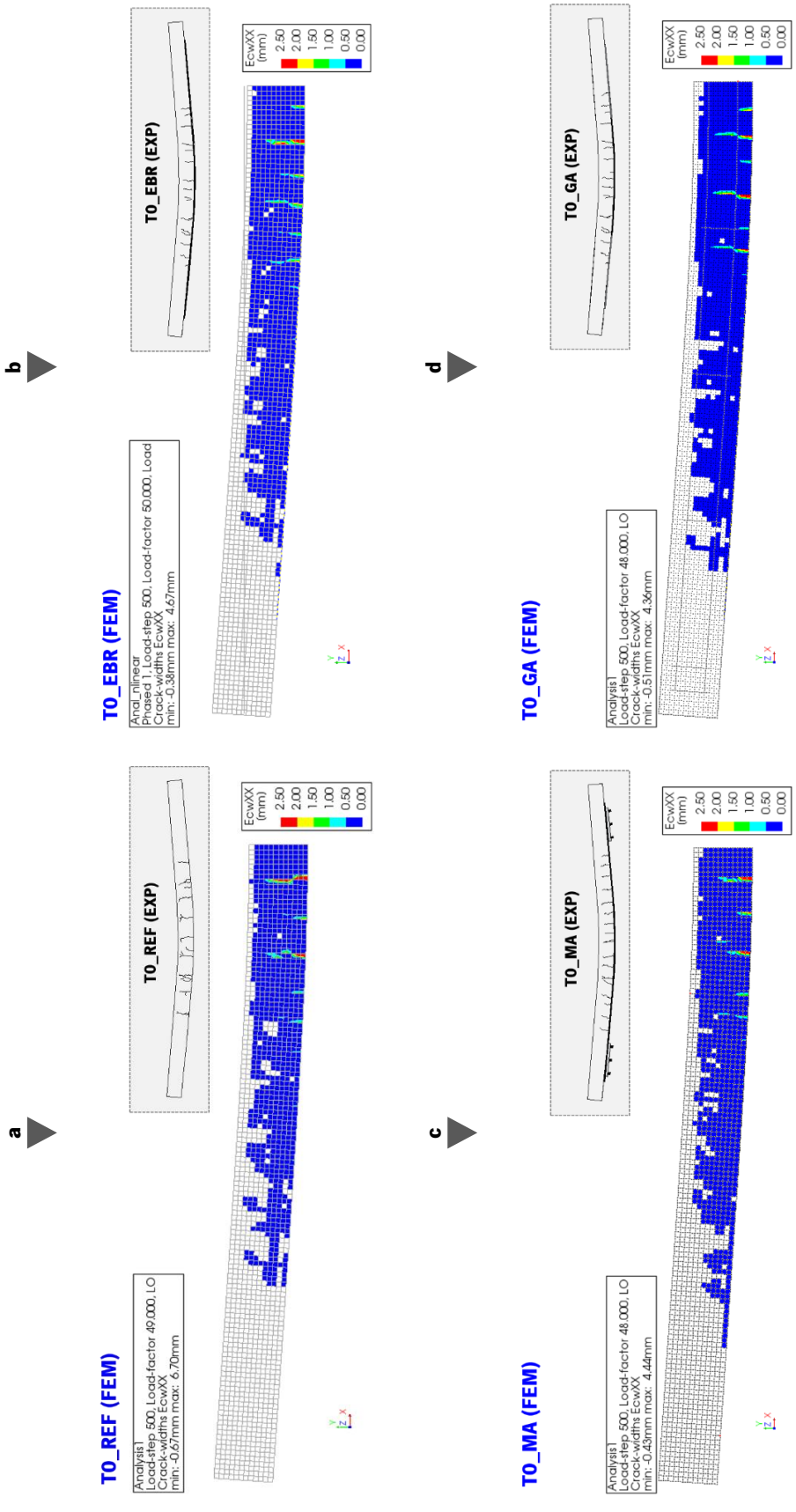

Figure 5.6: Crack patterns obtained in the numerical simulations of: (a) T0_REF slab; (b) T0_EBR slab; (c) T0_MA slab; (d) T0_GA slab.

Kim *et al*. [8] studied the ductility and cracking behaviour of concrete beams strengthened with prestressed CFRP sheets. These authors observed that the level of prestress significantly affected the structural ductility and, for the studied beam, the level of prestress should be in between 10% and 20% of the ultimate strain to meet the ductility recommendations of the Canadian standards [9]. Rezazadeh [10] also studied the influence of level of prestress on the structural ductility of RC beams strengthened with NSM CFRP elements. A normalized ductility index was computed based on the ratio between the mid-span displacement at failure and the mid-span displacement at the steel yielding, showing a direct relation between the prestress level and the RC element's ductility.

The present parametric study is composed of eight prestressed slabs, four strengthened with the MA anchorage system and the remaining with the GA anchorage system. The levels of prestress ranged between 0.2% and 0.8% of CFRP strain. Each specimen has a generic label "X (Y) – Z", where X is the label of the experimental slab given in Chapter 3, Y identifies if is an experimental (EXP) or an numerical (FEM) result, and Z corresponds to the equivalent level of CFRP strip prestrain (0.2%, 0.4%, 0.6% and 0.8%). As referred before, the main parameters adopted in numerical model were used in the present study and therefore, the model continues to admit that there is no slippage in the anchorage (Interface 2 is kept with a normal and shear stiffness modulus equal to $1x10^6$ N/mm^3). **Figure 5.7** shows the evolution of the mid-span displacement with the total load for the prestressed slabs. **Table 5.7** presents the main results of each slab, and the ductility and efficiency parameters already described in Chapters 2 and 3.

As expected, the increase on the prestress level manages to reduce the mid-span displacement and to delay the concrete cracking and steel yielding. All slabs strengthened with the mechanical anchorage system failed by CFRP rupture, for a load value close to 68.5 kN. However, with the increase of the prestress level there is a clear decrease in the structural ductility of the MA slabs (see **Figure 5.7a**). The CFRP strip debonding on the MA slabs occurred when mid-span displacement was close to 34 mm (load values that varied between 53.8 kN and 66.3 kN). In general, after the debonding of the CFRP laminate strip, the slab supports additional loads due to the anchorage system. The CFRP strip debonding is observed in as a drop point in the F-δ curves (two drop points in the experimental curves). The MA slab with the highest level of prestress (T0_MA (FEM) – 0.8%) does not present the same behaviour because the maximum tensile strain is reached

before the intermediate debonding. The reduction on the structural ductility can be easily observed through the μ_δ parameter, presented in **Table 5.7**, which is reduced with the increase of the prestress load. In fact, this parameter varies between 3.93 (T0_MA (FEM) - 0.2%) and 1.40 (T0_MA (FEM) - 0.8%) on the MA slabs, which means that the μ_δ parameter was reduced by 64% when the value of prestrain was increase from 0.2% to 0.8% (an increment of 300%).

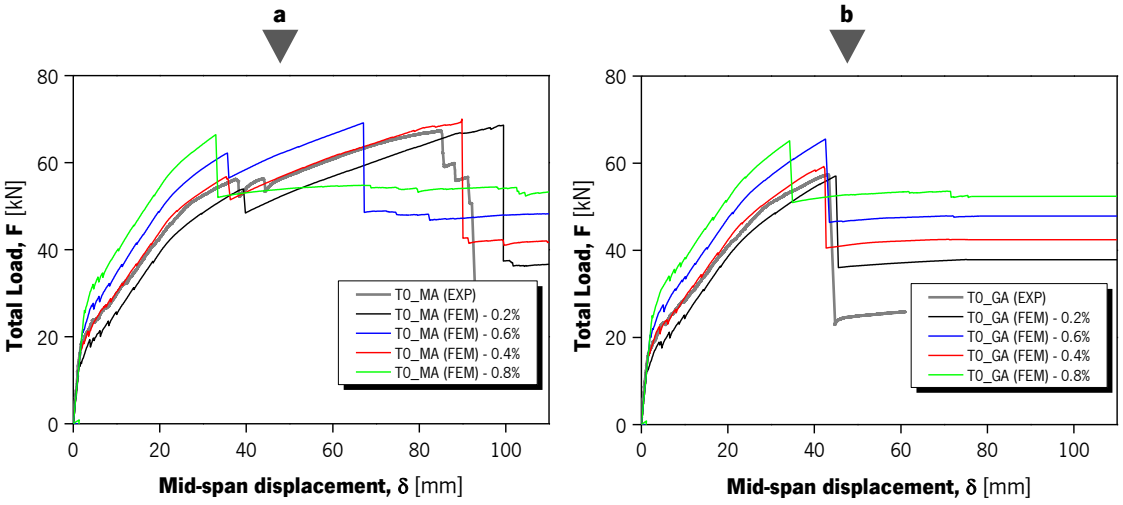

Figure 5.7: Effect of prestress level on the relationship between the total load and mid-span displacement on slabs (a) MA and (b) GA.

The GA slabs also present a loss on their structural ductility when the prestress load increased. It is clear, however, that this ductility reduction is higher in the MA slabs. Slabs with the gradient anchorage system present laminate debonding as its dominant failure mode. However, the failure mode on slab T0_GA (FEM) – 0.8% is CFRP rupture and the specimen slab T0_GA (FEM) – 0.6% reached its ultimate load when the CFRP strain was close to the CFRP's maximum tensile capacity. Higher prestrain levels are responsible for a better use of the materials and, consequently, the CFRP strain value at failure increased from 1.04% on slab T0_GA (FEM) – 0.2% to 1.45% on slab T0_GA (FEM) – 0.8%. The increase of prestrain level from 0.2% to 0.8% corresponded to a reduction on the μ_δ parameter of 23%.

Table 5.7
Main Results obtained from the parametric study analysing the influence of the prestress level.

Specimen	Stiffness		Crack initiation		Yielding		Ultimate			Efficiency and ductility parameters				Failure Modes
	K_I	K_{II}	δ_{cr}	F_{cr}	δ_y	F_y	δ_{max}	F_{max}	ε_{max}	μ_F $\left(\frac{F_{max}}{F_y}\right)$	μ_δ $\left(\frac{\delta_{max}}{\delta_y}\right)$	$\overline{\mu_F}$ $\left(\frac{\mu_F^{pre}}{\mu_F^{pas}}\right)$	$\overline{\mu_\delta}$ $\left(\frac{\mu_\delta^{pre}}{\mu_\delta^{pas}}\right)$	
	[kN/mm]	[kN/mm]	[mm]	[kN]	[mm]	[kN]	[mm]	[kN]	[%]					
T0_EBR (EXP)	**12.5**	**1.2**	**0.68**	**8.49**	**25.87**	**37.05**	**40.69**	**43.98**	**0.76**	**1.19**	**1.57**	**1.00**	**1.00**	**D**
T0_MA (EXP)	**9.8**	**1.3**	**1.87**	**17.87**	**26.88**	**50.58**	**84.78**	**67.46**	**1.48**	**1.33**	**3.15**	**1.12**	**2.01**	**F**
T0_MA (FEM) – 0.2%	9.9	1.3	1.41	13.97	25.29	45.02	99.49	68.60	1.45	1.52	3.93	1.28	2.50	F
T0_MA (FEM) – 0.4%	10.0	1.5	1.73	17.28	22.83	47.82	89.84	70.01	1.45	1.46	3.94	1.23	2.51	F
T0_MA (FEM) – 0.6%	10.1	1.5	2.17	21.61	23.54	53.29	67.08	69.13	1.45	1.30	2.85	1.09	1.82	F
T0_MA (FEM) – 0.8%	10.0	1.6	2.60	26.06	23.55	58.83	32.96	66.42	1.45	1.13	1.40	0.95	0.89	F
T0_GA (EXP)	**10.4**	**1.2**	**1.55**	**16.16**	**29.04**	**50.20**	**43.31**	**57.38**	**1.16**	**1.14**	**1.49**	**0.96**	**0.95**	**D**
T0_GA (FEM) – 0.2%	10.0	1.3	1.30	12.98	24.46	43.45	44.96	57.05	1.04	1.31	1.84	1.10	1.17	D
T0_GA (FEM) – 0.4%	10.1	1.4	1.62	16.31	24.71	47.57	42.21	59.24	1.16	1.25	1.71	1.05	1.09	D
T0_GA (FEM) – 0.6%	10.0	1.4	2.06	20.59	25.23	53.29	42.56	65.54	1.43	1.23	1.69	1.03	1.08	D
T0_GA (FEM) – 0.8%	10.0	1.5	2.49	24.99	24.19	56.76	34.28	65.14	1.45	1.15	1.42	0.97	0.90	F

Notes: D = Debonding; F = CFRP tensile failure.

In general, slabs with the MA anchorage system continue to have a better performance in terms of structural ductility and efficiency. However, for the prestrain of 0.8% both slabs presented identical behaviour in all stages of the test. Based on the ductility analysis performed by Rezazadeh [10], the normalized ductility parameter μ_δ and the normalized efficiency parameter $\overline{\mu_F}$ were computed (see **Table 5.7**). As defined by Rezazadeh [10], the normalized ductility parameter is equal to the ratio between the μ_δ parameter of the prestressed slab and the μ_δ parameter of a reference slab (strengthened but without prestress). In the present analysis the T0_EBR (EXP) was used as the reference slab. The relation between the normalized ductility index and the prestress level (ratio between the prestress and ultimate tensile capacity of the CFRP element) is presented in **Figure 5.8**.

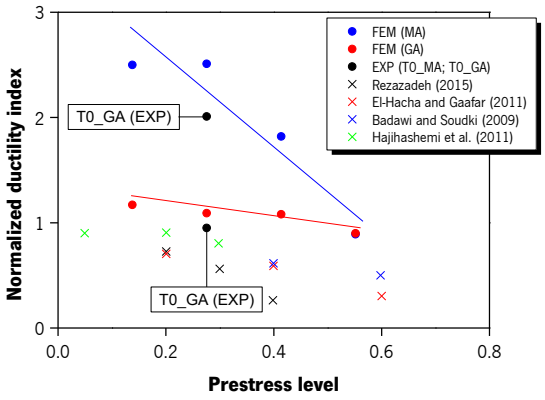

Figure 5.8: Normalized ductility index of the prestressed slabs (adapted from Rezazadeh [10]). Note: The plot includes the experimental results (prestressed NSM beams) of Rezazadeh [10], El-Hacha and Gaafar [11], Badawi and Soudki [12] and Hajihashemi *et al.* [13].

As referred by Rezazadeh [10], the normalized ductility index decreases with the increase of the prestress level. However, the results obtained in this parametric study show normalized ductility indexes higher than 1.0. This outcome reflects an increase of ductility from the T0_EBR (EXP) to the prestressed specimens. As referred before, the MA anchorage system prevented premature failure and, consequently, improved the structural ductility. With the GA system the normalized ductility parameter varied between 1.17 and 0.90. The mid-span CFRP strain evolution with the total load is presented in **Figure 5.9**. These curves show the effect of the different prestress levels, with the delay on the crack initiation and steel yielding. Greater level of prestress yields to higher use of the CFRP material.

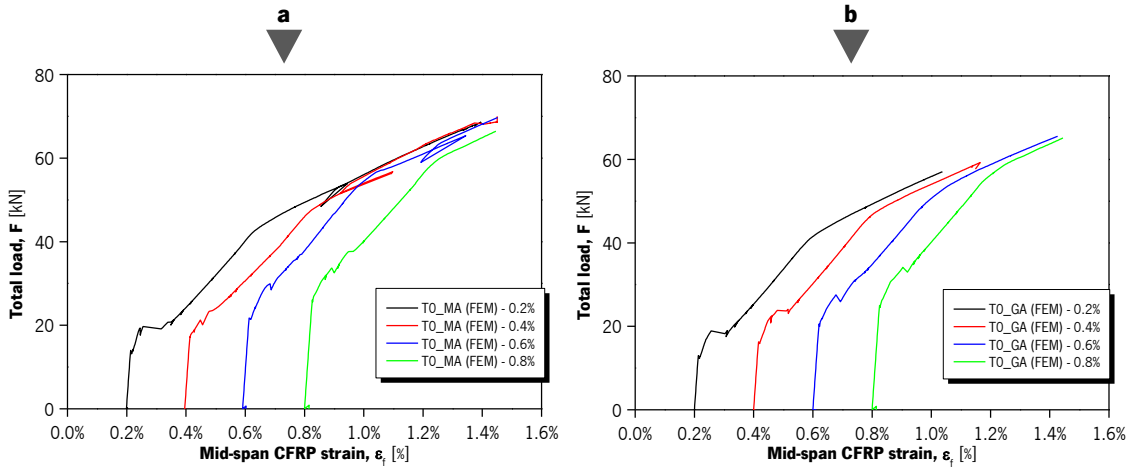

Figure 5.9: Effect of prestress load on the relationship between the total load and mid-span displacement on slabs (a) MA and (b) GA.

In short: (i) higher levels of prestress yielded to a delay on the crack initiation, steel yielding and a general increase on the stiffness; (ii) slabs with the mechanical anchorage always exhibit failure by CFRP rupture for a load level close to 68.5 kN, whereas the failure mode observed in slabs with the gradient anchorage shifted from laminate debonding to CFRP rupture with the increase on the prestress; (iii) higher levels of prestress yielded to a decrease on the structural ductility, which is considerable higher on slabs with the MA anchorage system; (iv) several ductility parameters were computed, through which is measured the variation on structural ductility with the prestress level; and (v) the mechanical anchorage prevented premature failure and, consequently, presented higher ductility than the non-prestressed slab T0_EBR (EXP).

5.5.2 Influence of the laminate geometry

The influence of the CFRP geometry was also assessed in the present study. From the available CFRP laminate geometries of [5], three were selected, with following cross section dimensions: 50×1.2 [mm], 80×1.2 [mm] and 100×1.2 [mm]. Then, nine numerical simulations were carried out to evaluate the influence of the CFRP geometry on the non-prestressed EBR slab, on the prestressed MA slab, and on the prestressed GA slab. The material model defined in Section 5.3 were kept through this parametric study. Each specimen has a generic label "X (Y) – Z", where X is the label of the experimental slab given in Chapter 3, Y identifies if it is an experimental (EXP) or

an numerical (FEM) result, and Z corresponds to laminate width (50 mm, 80 mm and 100 mm). The evolution of the mid-span displacement with the total load of the simulated slabs is presented in **Figure 5.10** and the main results are displayed in **Table 5.8**.

As expected, all EBR slabs exhibit the same stiffness during the elastic phase (K_I) and crack initiation, since the amount of reinforcement is not significant compared to the flexural stiffness of the concrete component. After this stage, the concrete contribution on the overall stiffness is significantly reduced and the influence of the CFRP laminate geometry can be noticed in the stiffness of the curves during the cracked phase and yielding phase. The increase on the CFRP laminate cross-section lead to the delay of the steel yielding and to the increase of the ultimate load. In fact, the 60% increase in the CFRP cross-section (50 × 1.2 [mm] → 80 × 1.2 [mm]) yielded to an increase on the ultimate load (F_{max}) of 20% and the 100% increase in the CFRP cross-section (50 × 1.2 [mm] → 100 × 1.2 [mm]) lead to an increase on the F_{max} of 47%. Debonding of the CFRP laminate was the dominant failure mode observed in all EBR slabs. All non-prestressed EBR slabs presented similar structural ductility and efficiency, which could be mathematically translated into the parameters μ_δ (varied between 1.5 and 1.7) and μ_F (varied between 1.2 and 1.3), presented in **Table 5.8**.

The prestressed slabs also present similar stiffness during the elastic phase (K_I) regardless of the laminate geometry or anchorage system. However, the crack initiation, steel yielding and ultimate load are highly influenced by the CFRP geometry. It should be noted that all MA and GA slabs were prestressed with a prestrain level of 0.4%. The increase on the prestress load is proportional to the laminate geometry. Therefore, the prestress load on slabs with the laminate of 50×1.2 [mm] is equal to 39.4 kN, on slabs with the laminate of 80×1.2 [mm] is equal to 63.0 kN, and on slabs with the laminate of 100×1.2 [mm] is equal to 78.7 kN. The change in the cross section of the laminate from 50×1.2 [mm] to 80×1.2 [mm] lead to the increase on the ultimate load of 24% and 39%, respectively, on slabs MA and GA. The prestressed slabs with the largest laminate cross-section (T0_MA (FEM) – 100 mm and T0_GA (FEM) – 100 mm) presented an increase of 27 - 48% on the ultimate load. The increase on the CFRP cross-section lead to the increase of the prestress load and, consequently, to the reduction on the structural ductility. Once again, the MA slabs present the highest reduction on the parameter μ_δ.

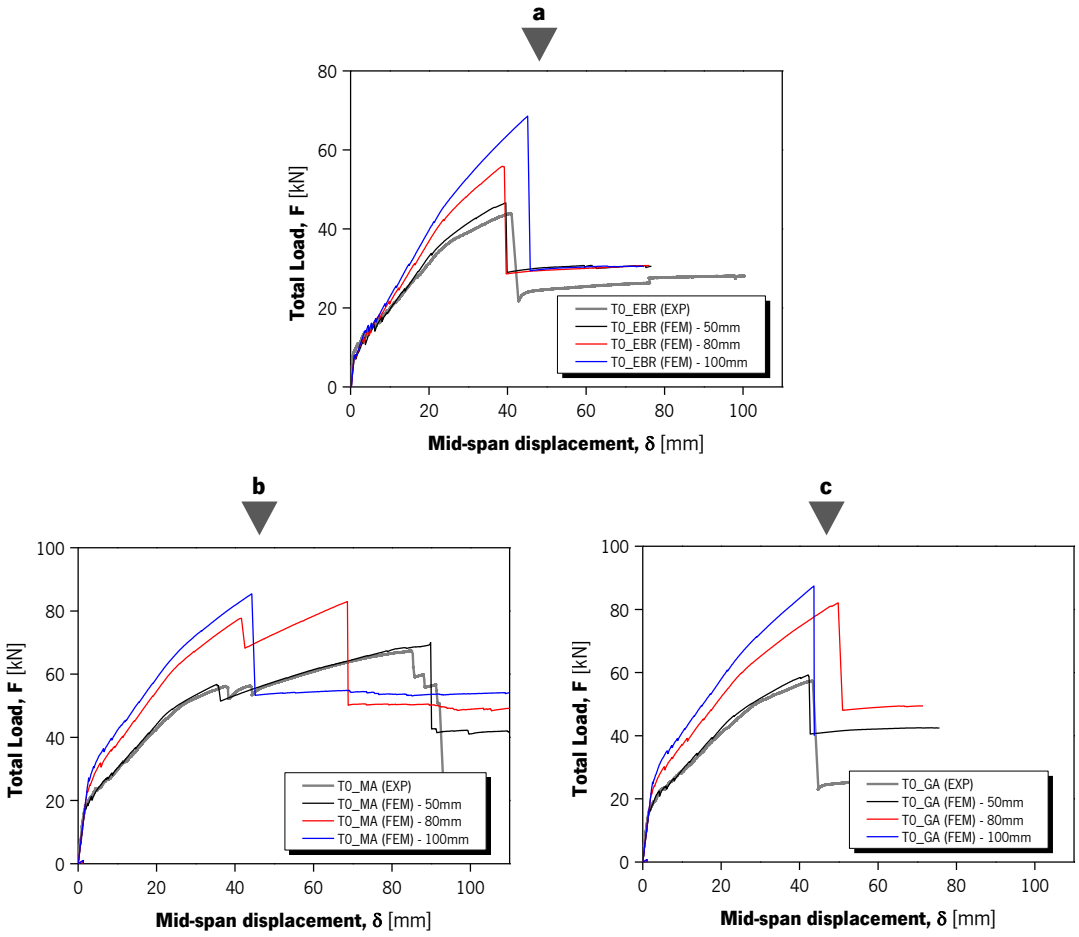

Figure 5.10: Influence of the laminate geometry on the relationship between the total load and mid-span displacement on slabs (a) EBR, (b) MA and (c) GA.

The failure mode observed in slabs with the mechanical anchorage system was CFRP rupture at its maximum tensile capacity. The slabs with the gradient anchorage presented debonding of the laminate as the dominant failure mode. However, the failure mode of slab T0_GA (FEM) – 100mm was CFRP rupture at its maximum tensile capacity.

The abovementioned observations point to the following remarks: (i) the increase on the CFRP cross-section improves the structural performance of all strengthened slabs (T0_EBR, T0_MA and T0_GA), with the delay of the crack initiation and steel yielding, and increase on the ultimate load; (ii) the increase on the CFRP cross-section and, consequently, prestress load, lead to the reduce on the structural ductility, which was higher on slabs with the MA anchorage system.

Table 5.8
Main Results obtained from the parametric study on the laminate geometry.

Specimen	Stiffness		Crack initiation		Yielding		Ultimate			Efficiency and ductility parameters		Failure Modes
	K_I	K_{II}	δ_{cr}	F_{cr}	δ_y	F_y	δ_{max}	F_{max}	ε_{max}	μ_F $\left(\frac{F_{max}}{F_y}\right)$	μ_δ $\left(\frac{\delta_{max}}{\delta_y}\right)$	
	[kN/mm]	[kN/mm]	[mm]	[kN]	[mm]	[kN]	[mm]	[kN]	[%]			
T0_EBR (EXP)	**12.5**	**1.2**	**0.68**	**8.49**	**25.87**	**37.05**	**40.69**	**43.98**	**0.76**	**1.19**	**1.57**	**D**
T0_EBR (FEM) – 50mm	8.0	1.3	0.98	7.86	23.61	36.65	39.54	46.61	0.73	1.27	1.67	D
T0_EBR (FEM) – 80mm	8.4	1.5	1.00	8.42	25.68	44.85	38.64	56.32	0.70	1.26	1.50	D
T0_EBR (FEM) – 100mm	9.9	1.6	0.87	8.64	27.86	51.51	45.03	69.20	0.80	1.34	1.62	D
T0_MA (EXP)	**9.8**	**1.3**	**1.87**	**17.87**	**26.88**	**50.58**	**84.78**	**67.46**	**1.48**	**1.33**	**3.15**	**F**
T0_MA (FEM) – 50mm	10.0	1.5	1.73	17.28	22.83	47.82	89.84	70.01	1.45	1.46	3.94	F
T0_MA (FEM) – 80mm	10.1	1.7	2.27	22.98	26.35	63.81	68.63	70.70	1.45	1.11	2.60	F
T0_MA (FEM) – 100mm	10.0	1.7	2.71	27.18	26.15	67.96	44.27	85.42	1.45	1.26	1.69	F
T0_GA (EXP)	**10.4**	**1.2**	**1.55**	**16.16**	**29.04**	**50.20**	**43.31**	**57.38**	**1.16**	**1.14**	**1.49**	**D**
T0_GA (FEM) – 50mm	10.1	1.4	1.62	16.31	24.71	47.57	42.21	59.24	1.16	1.25	1.71	D
T0_GA (FEM) – 80mm	10.1	1.6	2.17	21.91	28.12	63.15	49.85	82.10	1.29	1.30	1.77	D
T0_GA (FEM) – 100mm	10.2	1.8	2.49	25.29	26.79	68.46	43.64	87.43	1.45	1.28	1.63	F

Notes: D = Debonding; F = CFRP tensile failure.

5.6 Conclusion

The present chapter summarized the numerical modelling of RC slabs strengthened with prestressed CFRP laminates using two anchorage systems: the mechanical anchorage and the gradient anchorage. Two main parts composed this chapter: (i) the FE modelling of four slabs, previously tested under four-point bending tests (details of these slabs in Chapter 3); and (ii) a parametric study on the influence of prestress load and CFRP geometry. The obtained results allow to draw the following main conclusions:

- Good correlations have been found between the experimental results and numerical modelling, for the overall structural behaviour of slabs, including the debonding process and failure modes;
- Two parametric studies were carried out to assess the influence of the prestress level and of the CFRP laminate geometry on the slabs' structural performance. From the parametric study on the influence of the level of prestress, the following conclusions have been drawn:
  - The influence of the level of prestress was studied on the parametric study. A significant enhancement of load capacity at crack initiation, steel yielding, and failure was observed, for the slabs with the highest prestress load;
  - Regardless of the prestress load, slabs with the mechanical anchorage exhibit failure by CFRP rupture, whereas the failure mode observed in slabs with the gradient anchorage shifted from laminate debonding to CFRP rupture with the increase on the prestress level;
  - Higher levels of prestress yielded a decrease on the structural ductility, which is considerably higher on slabs with the MA anchorage system;
  - The mechanical anchorage prevented premature failure and, consequently, presented higher ductility than the non-prestressed slab.
- A second parametric study intended to study the influence of the CFRP laminate cross section. The results obtained allow drawing the following main conclusions:
  - The increase on the CFRP cross-section improved the structural performance of all strengthened slabs (T0_EBR, T0_MA and T0_GA), with the delay of the crack initiation and steel yielding, and increase on the ultimate load;

- Because the same level of prestrain (0.4%) was considered for all prestressed slabs, the increase on the CFRP cross-section lead to the increase of the prestress load and, consequently reduced the structural ductility.

5.7 References

[1] Manie J, editor. DIANA Finite Element Analysis Release Notes 10.2. Delftechpark: DIANA FEA BV; 2017.

[2] Hordijk D, Reinhardt H, Cornelissen H. Fracture mechanics parameters of concrete from uniaxial tests as influenced by specimen length. SEMRELIM Internaltional Conf. Fract. Concr. Rock, 1987, p. 138–49.

[3] CEB-FIP C. Model Code 1990. Com Euro-International Du Beton, Paris 1991. doi:10.1680/ceb-fipmc1990.35430.

[4] Sena-Cruz J. Strengthening of concrete structures with near-surface mounted CFRP laminate strips. University of Minho, 2004.

[5] S&P. CFRP laminates, technical datasheet. Seewen, Switzerland: 2014.

[6] Lu XZ, Teng JG, Ye LP, Jiang JJ. Bond-slip models for FRP sheets/plates bonded to concrete. Eng Struct 2005;27:920–37.

[7] Stevens N, Uzumeri S, Collins M. Analytical modelling of reinforced concrete subjected to monotonic and reversed loadings. Publ No 871 1987:University of Toronto, Toronto.

[8] Kim YJ, Shi C, Green MF. Ductility and Cracking Behavior of Prestressed Concrete Beams Strengthened with Prestressed CFRP Sheets. J Compos Constr 2008. doi:10.1061/(ASCE)1090-0268(2008)12:3(274).

[9] International C. Canadian highway bridge design code (CHBDC). Toronto: 2000.

[10] Rezazadeh M. Innovative Methodologies for the Enhancement of the Flexural Strengthening Performance of NSM CFRP Technique for RC Beams. University of Minho, 2015.

[11] El-Hacha R, Gaafar M. Flexural Strengthening of Reinforced Concrete Beams Using Prestressed Near-Surface-Mounted CFRP Bars. PCI J 2011.

[12] Badawi M, Soudki K. Flexural strengthening of RC beams with prestressed NSM CFRP rods - Experimental and analytical investigation. Constr Build Mater 2009. doi:10.1016/j.conbuildmat.2009.03.005.

[13] Hajihashemi A, Mostofinejad D, Azhari M. Investigation of RC Beams Strengthened with Prestressed NSM CFRP Laminates. J Compos Constr 2011. doi:10.1061/(ASCE)CC.1943-5614.0000225.

CHAPTER 6

MAIN CONCLUSIONS AND RECOMMENDATIONS FOR FUTURE WORKS

6.1 Conclusions

Externally-bonded carbon fibre reinforced polymer (EB-CFRP) composites are commonly employed to repair or to increase the flexural/shear resistance of RC structures. In some specific cases, the use of prestressed CFRP for strengthening RC structures is convenient or even required. This technique presents several positive aspects since it combines the benefits of passive EB-CFRP systems with the advantages associated with external prestressing. The durability and long-term behaviour of RC structures strengthened with prestressed CFRP laminates are still open issues, fundamental for the acceptance and recognition by the construction industry. The main objective of the research conducted in this thesis was to test, analyse and evaluate the durability, short and long-term structural behaviour of RC slabs strengthened in flexure with pre-stressed CFRP laminates under various specific environmental conditions, load conditions and chemical degradation. Two different types of anchorage systems were studied: (i) mechanical anchorage (MA) and, (ii) gradient anchorage (GA). The durability was studied by exposing strengthened RC specimens to the following environments, for approximately 8 months: (i) reference environment and specimens kept in a climatic chamber at 20 °C - REF; (ii) water immersion in tank at 20 °C of temperature - TW; (iii) water immersion in tank with 3.5% of dissolved chlorides at 20 °C of temperature - CW; and (iv) wet/dry cycles in a tank with a water temperature of 20 °C - WD. Simultaneously, several slabs were exposed to a sustained loading at a load level of 1/3 of the corresponding ultimate load, with the occurrence of cracking. In this chapter, the main conclusions of this work and the recommendations for future developments are presented.

6.1.1 Short-term behaviour of RC slabs strengthened with prestressed CFRP strips

Chapter 2 presented a preliminary experimental work composed of fourteen reinforced concrete (RC) slabs. Results show that, at service level, the strengthening improved the slabs performance with lower deflections, crack width delay and lower crack spacing. Prestress led to a greater use of the CFRP laminate strip, confirmed with the 74% - 132% increase on the ultimate strain on the CFRP laminate at the slab's failure, when compared with the non-prestressed strengthened slabs. Both anchorage techniques (MA and GA) presented similar response. Yet, the metallic anchors

composing the MA system prevented a premature failure by debonding and allowed the slabs to support higher ultimate loads and deflections. Strip intermediate debonding (confirmed through an analytical analysis based on the available literature) was the dominant failure mode of the strengthened slabs. However, one prestressed MA slab failed by FRP rupture at its maximum tensile capacity.

The influence of the laminate geometry was investigated in this preliminary study. The CFRP laminate width had a considerable influence on the general behaviour of the strengthened elements. The increase from 50 mm to 80 mm (50×1.2 [mm] → 80×1.2 [mm], 60% increase on the cross-section area) led to an increase on the stiffness (54%), cracking load (26%), steel yielding load (31%), and ultimate carrying capacity (23%). However, similar performance was observed for the strip with different thickness. Concrete surface preparation based on sand blasting yielded higher roughness and adherence than those grinded with a stone wheel. The performance improvement observed for each method of surface preparation fundaments this idea: series SB specimens (sand blasted) showed relative higher ultimate loads and they did fail with higher CFRP strains.

6.1.2 Durability and long-term behaviour of RC slabs strengthened with prestressed CFRP strips

The durability and long-term behaviour of sixteen RC slabs strengthened with prestressed CFRP strips was assessed and the obtained results were reported in Chapter 3. The short-term prestress losses were monitored, and both anchorage systems presented an average prestress loss of 2.5%. For the MA system, the short-term losses occurred when the system is blocked with the fixing screws, whereas in the GA system these prestress losses were observed at the release of the first 1/3 of force. As mentioned above, the durability was studied by exposing strengthened RC specimens to four distinct environmental actions and to a sustained loading for an ageing period of eight months. During the ageing period, the CFRP laminate strain increased when the specimens were immersed in water (environment TW and CW) due to, mainly the volumetric expansion. Also, the CFRP laminate strain readings were highly influenced with the temperature oscillations.

When the creep load was applied, the observed elastic deformations and CFRP strain variations were in agreement with the results obtained in the monotonic tests up to failure. In general, both anchorage systems (MA and GA) presented similar response during the creep loading. Yet, slabs with the gradient anchorage presented higher deformations than the MA slabs after the immersion on tap water, immersion on salt-water and wet-dry cycling. The highest vertical deflection due to creep occurred on specimens submitted to the wet-dry cycles and to the laboratory premises. An average creep coefficient for the test period (φ_{ult}) of 1.3 was computed and are in agreement with the expected values for reinforced concrete elements. Based on the test period, a long-term creep coefficient (φ_{t_∞}) was estimated and it did not exceed 1.9.

After the ageing, four-point bending tests were carried out to evaluate the ultimate behaviour of the strengthened RC slabs. Results showed that the exposure to water (series TW, CW and WD) improved the concrete strength and the corresponding modulus of elasticity, which increased the initial slabs' stiffness and delayed the crack initiation. Regardless of the anchorage systems, in all the slabs a reduction of the yielding and the failure loads was observed. The highest degradation observed on slabs with the MA and GA system, were reported for the environments TW and REF, respectively. The ductility of the prestress slabs was evaluated, and results showed that it was decreased after the environmental exposure. The ductility decrease was clearly higher on the MA slabs than on the GA slabs. However, similarly to the results obtained on the preliminary study (Chapter 2), the MA anchorage presented higher ductility mainly because it allowed the slab to carry additional load after the debonding of the strip.

6.1.3 Bond behaviour of transversely compressed mechanical anchorage system

In Chapter 4, an experimental program aimed at studying the effectiveness of a mechanical anchorage of CFRP laminates bonded to concrete structures was carried out. Twenty-two large scale pull-out specimens were tested, and the influence of three main parameters were studied: (i) laminate width – 50 mm, 80 mm and 100 mm; (ii) level of compressive stress measured through the applied torque level – 30 N·m, 100 N·m, 150 N·m and 200 mm; and (iii) temperature – 20 °C, 60 °C and 80 °C.

At room temperature (20 °C) the mechanical anchorage provides adequate compressive stress of the CFRP laminate to the concrete substrate, regardless of the level of compressive stress. The dominant failure mode was rupture of the CFRP laminate, however, for a laminate width of 100 mm, the lowest torque level (30 N·m) yielded to slippage of the CFRP laminate. Also, at room temperature, a typical cohesive failure in the concrete and interface failure between the concrete and epoxy was observed in the bonded length (EBR component). As expected, the debonding load increased with the laminate width. By removing the anchorage plate from the specimens tested at room temperature, an assessment of the visible damage was carried out and a relation Mohr-Coulomb between the compressive stress level and average shear stress at the maximum load was observed with a cohesion and friction angle of 5.26 MPa and 13.7°, respectively.

Steady-state and transient tests carried out at 60 °C and 80 °C showed that the temperature is a key factor on the behaviour of the pull-out specimens. Anchorage slippage was the failure mode observed in all specimens tested at elevated temperatures, including the steady state tests (60 °C, at 80 °C) and all the transient tests. In the transient tests, three different outcomes were observed: (i) the low load level of 80 kN (0.36% of CFRP strain) was not enough to result in failure for the defined temperature variation (from 30 °C to 80 °C); (ii) the medium load level of 100 kN (0.45% of CFRP strain) resulted in failure, but the confinement level worked as a relevant factor in the anchorage capacity; and (iii) the high load level of 120 kN (0.54% of CFRP strain) l to the anchorage failure shortly after the temperature reached the adhesive's T_g. In the steady-state tests carried out at elevated temperature (60 °C and 80 °C), a 43.9%-58.5% reduction of the ultimate load was observed when compared to the ones tested at room temperature.

The results obtained in the preliminary studies with slabs (Chapter 2) are in agreement with the results obtained with the pull-out tests carried out at room temperature, since the CFRP rupture was observed in similar conditions. As a final remark, it should be highlighted that the torque level was the tool used to control the confinement level of the anchorage and, based on the obtained results, it is a relevant factor to increase the anchorage capacity.

6.1.4 Numerical Simulations

Numerical simulations were developed to better understand the observations in the tests carried out on the main experimental campaign (Chapter 3). The performance of these simulations was compared with results in slabs submitted to monotonic tests up to failure. Good correlations have been found between the experimental results and numerical modelling, for the overall structural behaviour of slabs, including the debonding process and failure modes. Subsequently, these models were used on a parametric study that intended to investigate the influence of different parameters affecting the behaviour of the slabs, namely the prestress level and the CFRP geometry.

From the study on the influence of the prestress level (0.2%, 0.4%, 0.6% and 0.8% of CFRP strain), eight prestressed slabs were numerically simulated. Results showed that a significant enhancement of load capacity at crack initiation, steel yielding, and failure was observed, for the slabs with the highest prestress load. Regardless of the prestress load, slabs with the mechanical anchorage exhibit failure by CFRP rupture, whereas the failure mode observed in slabs with the gradient anchorage shifted from laminate debonding to CFRP rupture with the increase on the prestress level. This parametric study also included an analysis on the ductility of the slab. Higher levels of prestress yielded to a decrease on the structural ductility, which is considerable higher on slabs with the mechanical anchorage. Nonetheless, the MA system prevented premature failure and, consequently, presented higher ductility than the non-prestressed slab.

A second parametric study was developed in order to study the influence of the CFRP laminate cross section. Three commercially available geometries were selected: 50×1.2 [mm], 80×1.2 [mm], and 100×1.2 [mm]. The increase on the CFRP cross-section improved the structural performance of all strengthened slabs (non-prestressed and prestressed), with the delay of the crack initiation and steel yielding and increase on the ultimate load. The same level of prestrain (0.4%) was considered for all prestressed slabs and, consequently, the increase on the CFRP cross-section lead to the increase of the prestress load and reduction of the structural ductility.

6.2 Recommendations for future research developments

The research work conducted within this doctoral thesis gives new contributions for the knowledge on the durability, short and long-term behaviour of concrete structures strengthened with prestressed externally-bonded carbon FRP systems. However, the information about the areas treated in this document is still scarce and further investigation should be carried out. This section presents some recommendations for a deeper investigation on these subjects, mainly:

- In the developed experimental work, RC slabs strengthened with prestressed CFRP laminates have shown high levels durability and remarkable performance in terms of long-term behaviour. The processes used in this work have revealed great potential for the establishment of standardized procedures for durability assessment of prestressed CFRP strengthening systems. Based on the obtained results it is important to evaluate the influence of the same environmental actions for a longer period (e.g. 10 years) to fully understand the long-term and durability behaviour of prestressed EBR systems;
- The durability of RC slabs strengthened with prestressed CFRP laminates should also be investigated under the influence of high temperature cycles, freeze-thaw cycles and higher concentration of salts. On the same topic, an attempt to properly correlate the ageing carried out in laboratory (accelerated ageing) and the real exposure conditions should be included in future works;
- The study presented in Chapter 4 showed that the mechanical anchorage exhibits a flawless behaviour at room temperature. However, in the monotonic tests performed on MA slabs subjected to the long-term environmental exposures, a reduction on the anchorage resistance was observed, since the failure mode shifted from CFRP rupture to CFRP slippage at the mechanical anchorages. These observations indicate that durability of mechanical anchorages may be an important issue to be analysed. Thus, a study focused on the durability of these anchorages should be carried out;
- Good correlation between the numerically predicted slabs and the ones tested experimentally was obtained. An attempt to numerically simulate the long-term and durability behaviour of RC slabs strengthened with prestressed CFRP laminates should be included in future works. An effort to properly simulate the interface at the anchorage

region should be considered in future developments, when subjected to the effect of high temperatures or long-term exposure to an environmental ageing.